

NORTHWESTERN UNIVERSITY

Hydrogel Platforms for Investigating Microenvironmental Signaling Cues  
Influencing Human Glomerular Endothelial Cell and Podocyte Behavior

A DISSERTATION

SUBMITTED TO THE GRADUATE SCHOOL  
IN PARTIAL FULFILLMENT OF THE REQUIREMENTS

for the degree

DOCTOR OF PHILOSOPHY

Field of Biomedical Engineering

By

Jimmy Su

EVANSTON, ILLINOIS

September 2019

© Copyright by Jimmy Su, 2019

All Rights Reserved

## ABSTRACT

Hydrogel Platforms for Investigating Microenvironmental Signaling Cues  
Influencing Human Glomerular Endothelial Cell and Podocyte Behavior

Jimmy Su

End-stage renal disease, or kidney failure, can result from acute kidney injury or sustained kidney damage in the form of chronic kidney disease. As the prevalence of end-stage renal disease continues to rise, the gold-standard treatment—kidney transplantation—is increasingly restricted by the shortage of transplantable donor kidneys. Bioengineered kidney tissues may potentially alleviate these numbers by advancing understanding of kidney development and progression of diseases, improving the efficiency of drug discovery and toxicity testing, and eventually restoring or replacing lost kidney function in therapeutic applications. However, a number of obstacles remain before bioengineered kidney tissues reach clinical applications. One challenge in particular is the design and fabrication of biomaterial scaffolds or matrices that provide the necessary microenvironmental signaling cues to promote a functional cellular response or phenotype. Hydrogels are water-swollen, crosslinked polymer networks that mimic many of the properties of the native extracellular matrix and therefore may serve as ideal scaffolds or matrices for engineering complex tissues and organs. Here, I will present multiple hydrogel platforms for investigating interactions by the glomerular endothelial cells and podocytes that form the glomerular filtration barrier of the kidney nephron.

Hydrogels derived from tissue- and organ-specific decellularized extracellular matrix (dECM) may retain bioactive components from the native tissue or organ that could in turn modulate functional cell response. Therefore, the first hydrogel platform I will present is formulated from porcine kidney dECM that has been processed to form physically-crosslinked hydrogels suitable for cell culture and encapsulation investigations. Scanning electron micrographs of hydrogels demonstrated fibrous ultrastructures with interconnected pores, and rheological characterization revealed rapid gelation times with shear moduli dependent on the hydrogel polymer or protein concentration. Conditionally-immortalized human glomerular

endothelial cells (GEnCs) cultured on hydrogel substrates or encapsulated within hydrogel matrices exhibited high cell viability and proliferation over a one-week culture period. However, gene expression analysis of GEnCs encapsulated within kidney dECM hydrogels revealed significantly lower expression of several relevant genes of interest compared to those encapsulated within hydrogels composed of only purified type I collagen. These results were further supported by similar trends obtained through gene expression analysis of GEnCs cultured on the hydrogels as substrates.

Unfortunately, the complexity of dECM and limitations of naturally-derived materials hinder additional investigations that require the ability to adequately tailor or tune hydrogel properties. As a result, the second hydrogel platform I will present is a tunable hydrogel substrate with conjugated bioactive peptides to modulate cell binding and growth factor signaling. These hydrogels were formed by employing a poly(ethylene glycol) crosslinker to covalently crosslink gelatin polymers and simultaneously conjugate laminin-derived YIGSR peptides or vascular endothelial growth factor (VEGF)-mimetic QK peptides to the gelatin. Rheological characterization revealed rapid formation of hydrogels with similar stiffnesses across tested formulations, and swelling analysis demonstrated dependency on peptide and crosslinker concentrations in hydrogels. Levels of phosphorylated VEGF receptor 2 in cells cultured on hydrogel substrates illustrated that while human umbilical vein endothelial cells (HUVECs) responded to both soluble and conjugated forms of the QK peptide, GEnCs only responded to the conjugated presentation of the peptide. Furthermore, whereas HUVECs exhibited greatest upregulation in gene expression when cultured on YIGSR- and QK-conjugated hydrogel substrates after 5 days, GEnCs exhibited greatest upregulation when cultured on Matrigel control substrates at the same time point. These results indicate that conjugation of bioactive peptides to these hydrogel substrates significantly influenced endothelial cell behavior in cultures but with differential responses between HUVECs and GEnCs.

Within the glomerulus, both GEnCs and podocytes are necessary for the formation and function of the glomerular filtration barrier. Consequently, I will present investigations in which conditionally-immortalized human podocyte response to culture on hydrogel substrates or encapsulation within hydrogel matrices was evaluated. Interestingly, the results suggest that podocytes may be particularly sensitive to encapsulation within hydrogels, specifically type I collagen hydrogels and kidney dECM hydrogels.

Although podocytes exhibited enhanced podocyte-specific gene expression when cultured on soft Matrigel or poly(ethylene glycol)-crosslinked gelatin hydrogel substrates, cell survival appeared to be compromised at longer time points. In contrast, podocytes cultured on stiffer, 3D-printed gelatin hydrogel scaffolds maintained high cell viability, adhesion, and spreading even after extended culture. These results imply that hydrogel stiffness and 3D structure or architecture are two microenvironmental signaling cues that must be carefully considered when designing hydrogel platforms for maintaining healthy podocytes in a differentiated state. In summary, these hydrogel platforms and the subsequent evaluation of cell behavior will advance understanding of microenvironmental signaling cues integral for the development engineered kidney tissues.

## ACKNOWLEDGEMENTS

### Ph.D. Advisors

First and foremost, I would like to acknowledge my advisors for their support throughout this journey. Their mentorship has been crucial to my development as an independent scientist and engineer. Thank you both for believing in my abilities even as a young scientist, investing your time through hours of meetings and discussions, providing feedback on everything from experimental design to publications, allowing me to pursue interesting and new projects, and recognizing my growth into the researcher I am now.

Jason A. Wertheim, MD, PhD	Edward G. Elcock Professor of Surgical Research Associate Professor of Surgery - Organ Transplantation Vice Chair for Research, Department of Surgery Northwestern University
Ramille N. Shah, PhD	Associate Professor of Bioengineering University of Illinois at Chicago Co-Founder and Chief Scientific Officer Dimension Inx, LLC

### Dissertation Committee

I would also like to acknowledge the members of my dissertation committee. Thank you for your support in all of my endeavors, especially my fellowship applications, as well as the scientific and research guidance across multiple projects. The diverse expertise truly strengthened both my didactic knowledge of new areas as well as my research training towards becoming an independent scientist and engineer.

Guillermo A. Ameer, ScD	Daniel Hale Williams Professor of Biomedical Engineering Professor of Surgery Director, Center for Advanced Regenerative Engineering Northwestern University
Susan E. Quaggin, MD	Charles H. Mayo Professor of Medicine Chief of Nephrology and Hypertension, Department of Medicine Director, Feinberg Cardiovascular and Renal Research Institute Director, George M. O'Brien Kidney Research Core Center Northwestern University

### **Wertheim Organ Regeneration and Tissue Engineering Laboratory**

Impactful research rarely occurs in isolation, and as such I would like to acknowledge the other members and alumni of the Wertheim Laboratory for the scientific discussions, assistance in experimental studies, and general camaraderie in the work environment.

David Z. Ivancic	Research Technologist
Divya Rajendran, MS	Research Technologist
Jessica A. Hoch Brown, PhD	Postdoctoral Scholar
Michael D. DiVito, PhD	Postdoctoral Scholar
Katherine E. Hekman, MD, PhD	Postdoctoral Scholar
Bin Jiang, PhD	Postdoctoral Scholar
Kyle M. Koss, PhD	Postdoctoral Scholar
Yangxi Liu, PhD	Postdoctoral Scholar
Iman Sarami, MD	Postdoctoral Scholar
Joseph S. Uzarski, PhD	Postdoctoral Scholar
Bo Wang, DDS, PhD	Postdoctoral Scholar
Yuguo Wang, PhD	Postdoctoral Scholar
Adarsh S. Manjunath, MD	Resident, Urology
Andrew (Andy) Tully, MD	Resident, Surgery
Jennifer R. Ferrer, PhD	PhD Student
Bilal A. Naved	MD/PhD Student
Taeyil Son	MS Student
Mark Antkowiak	Visiting MD Student
Praneet Polineni	Visiting MD Student
Joseph M. Beggs	Undergraduate Student
Jeffrey C. Granados	Undergraduate Student
Christina Im	Undergraduate Student
Jacob Lissoos	Undergraduate Student
Angelin Matthew	Visiting High School Student
Melis Ozkan	Visiting High School Student
Maya Passman	Visiting High School Student

Special thanks to Joe Uzarski for providing hands-on mentorship as I was first adjusting to the lab and learning new techniques. And Jen Ferrer, thank you for being the other graduate student in the lab with whom I could celebrate with, commiserate with, and have frank discussions with about everything from diversity and inclusion to career advancement.

### Shah Tissue Engineering and Additive Manufacturing (TEAM) Laboratory

Similarly, I would like to acknowledge the other members and alumni of the Shah Laboratory for, again, the scientific discussions, assistance in experimental studies, and general camaraderie in the work environment.

Xin Li, MD, PhD	Research Technologist
Adam E. Jakus, PhD	Postdoctoral Scholar
Christoph Kenel, PhD	Postdoctoral Scholar
Danielle O. Duggins	PhD Student
Emma S. Gargus	MD/PhD Student
Nicholas R. Geisendorfer	PhD Student
Phillip L. Lewis, PhD	PhD Student
Kelly A. Parker	PhD Student
Alexandra L. Rutz, PhD	PhD Student
Shannon L. Taylor, PhD	PhD Student
Linda M. Guiney, PhD	Collaborating PhD Student
Nikhita D. Mansukhani, PhD	Collaborating PhD Student
William E. Reyna	Collaborating PhD Student
Seth R. Feder, MS	MS Student
Max H. Greenberg, MS	MS Student
Margaret A. Hammersley, MS	MS Student
Lazura (Lizzie) K. Krasteva, MS	MS Student
Clayton H. Rische, MS	MS Student
Jonathan Rosini, MS	MS Student
Ming Yan, MS	MS Student
Hui (Winnie) Yang, MS	MS Student
William J. Jeang	Undergraduate Student
John Jeevarajan	Undergraduate Student
Chris Lee	Undergraduate Student
Kelly Hyland	Undergraduate Student
Christina Robinson	Undergraduate Student
Akash Setty	Visiting High School Student

Special thanks to Alex Rutz whose hard work and creativity laid much of the groundwork for my dissertation research. And Phillip Lewis, thank you for the mentorship, the collaborations, and the friendship, all of which have truly helped me throughout my time in graduate school.

### Research Collaborators

I would like to acknowledge our collaborators who have been gracious enough to share the conditionally-immortalized cell lines with us, which enabled the focus of my research on the glomerular filtration barrier, and their guidance in experimental design and analysis of results.

Moin A. Saleem, MBBS, PhD	Professor of Paediatric Renal Medicine University of Bristol
Simon C. Satchell, MBBS, PhD	Reader & Consultant in Renal Medicine University of Bristol
Lindsay S. Keir, MBChB, PhD	Previously Research Associate Northwestern University
Lan Ni	Research Associate University of Bristol

### Northwestern University Department of Biomedical Engineering

I would like to acknowledge, of course, the Department of Biomedical Engineering at Northwestern University, which allowed me to pursue graduate studies and research. Thank you to the current and previous administrative faculty and staff for supporting the graduate students while also challenging us to make strides in research progress across the broad field of biomedical engineering.

Eric J. Perreault, PhD	Chair of Biomedical Engineering
Suzanne Olds, PhD	Assistant Chair of Biomedical Engineering
Wendy Murray, PhD	Director of Graduate Studies
Hao Zhang, PhD	Director of Graduate Studies
Erin McElhenie	Program Assistant
Jonathan T. Parker	Program Assistant
Amanda Peterson	Program Assistant
Nakendra A. Jackson	Graduate Program Assistant
Ian Magenta	Graduate Program Assistant
Kristine (Kristi) A. Yamaoka	Graduate Program Assistant

Additionally, thank you to the Biomedical Engineering Graduate Students (BMEGS) organization for easing the transition to graduate school, facilitating departmental interactions, and bringing some cohesiveness to the graduate program. I would also like to thank all of the other graduate students in the department who I have interacted with during my time at the university--it has been a pleasure and an

honor to work alongside you all, to be able to consider several of you friends, and to now be professional colleagues.

### **Northwestern University Comprehensive Transplant Center (CTC)**

I would like to acknowledge the current and previous administrative staff of the Comprehensive Transplant Center who have been absolutely essential in running the day-to-day operations for personnel, ensuring proper execution and submission of grant and fellowship applications, and scheduling meetings with busy faculty.

Kelly A. Memmer	Assistant Director of Research & Finance
Rasika Ranganathan	Associate Research Administrator
John Scofic	Financial Specialist
Bernedette (Bernie) Malone	Administrator
Nancy D. Herrera, MS	Laboratory Manager
Alexandra (Ali) Bowersock	Administrative Coordinator
Meghan Jones	Administrative Coordinator
Stephanie R. East	Administrative Coordinator Feinberg Cardiovascular and Renal Research Institute

### **Northwestern University Simpson Querrey Institute (SQI)**

I would also like to acknowledge the administrative staff of the Simpson Querrey Institute whose critical efforts maintained a safe and efficient lab space for everyone to work in the most productive manner.

Alexandra Kolot	Assistant Director of Research Facilities
Maura Walsh	Executive Coordinator

### **Northwestern University (NU) Core Facilities**

Core facilities at the university contribute in innumerable ways to the research environment, and I would like to acknowledge the core facilities that have enabled me to conduct my dissertation research.

Analytical bioNanoTechnology Equipment Core (ANTEC)

Center for Advanced Microscopy (CAM)

Electron Probe Instrumentation Center (EPIC) of the  
NU Atomic and Nanoscale Characterization Experimental Center (NUANCE)

George M. O'Brien Kidney Research Core Center (NU GoKidney)  
 Mouse Histology & Phenotyping Laboratory (MHPL)  
 NUSeq Core

## **Fellowships**

Fellowships truly enable trainees to pursue independent research and gain expertise in new areas. Therefore, I would like to acknowledge my fellowship funding as well as the current and previous administrative faculty and staff affiliated with the fellowship programs for granting me access to so many resources that have allowed me to become the scientist and engineer I am now.

### *Ruth L. Kirschstein National Research Service Award (NRSA) Individual Predoctoral Fellowship (F31)*

F31 DK108544	National Institute of Diabetes and Digestive and Kidney Diseases
Tracy Rankin, PhD, MPH	Program Director

### *Northwestern University Predoctoral Biotechnology Training Program (BTP)*

T32 GM008449	National Institute of General Medical Sciences
William M. Miller, PhD	Director
Joshua Leonard, PhD	Director
Eric Weiss, PhD	Director
Jennifer K. Hardney	Associate Research Administrator
Emily J. Kocevar	Program Coordinator

Additionally, thank you to the other BTP trainees who worked to guide the professional and community goals of the training program and from whom I have learned so much—together, the events and people made the numerous commutes to Evanston worthwhile.

## **Funding Sources**

Unfortunately, research is not always accessible in that it requires specific lab space, consumables, and expensive instrumentation. As a result, I would like to acknowledge the funding sources awarded to my advisors (*i.e.*, the principal investigators of the labs) that allowed me to perform and conduct the research presented in my dissertation.

R01 DK113168	National Institute of Diabetes and Digestive and Kidney Diseases (J.A.W.)
I01 BX002660	United States Department of Veterans Affairs Biomedical Laboratory Research and Development Service Merit Review (J.A.W.)

American Society of Transplantation Research Network (J.A.W.)  
 Chicago Biomedical Consortium (J.A.W.)  
 McCormick Foundation (J.A.W.)  
 National Kidney Foundation of Illinois (J.A.W.)  
 Zell Family Foundation (J.A.W.)  
 U01 DK107350 (Re)Building a Kidney Consortium  
 K01 DK099454 National Institute of Diabetes and Digestive and Kidney Diseases (R.N.S.)  
 Google Foundation (R.N.S.)

The contents presented do not represent the view of the United States Department of Veterans Affairs, the National Institutes of Health, or the United States Government. Funding sources had no involvement in study design; collection, analysis, or interpretation of data; or in writing of this dissertation.

### **Previous Research Mentors and Collaborators**

My career in research and path to receiving a PhD did not begin once I was accepted into the program at Northwestern University but rather much earlier. For that reason, I would like to acknowledge all of the previous research mentors and collaborators I have worked with. While my experiences have encompassed a breadth of different fields and areas, my mentors have always pushed me to become an independent and creative thinker with attention to detail and experimental design. And they have continued to support me beyond the time I spent in the lab to reach my full potential as a research scientist and engineer.

Héctor D. Martínez Ávila, PhD	Co-Founder and Chief Technology Officer CELLINK AB
Patrick S. Thayer, PhD	Chief Applications Officer Previously Bioink Officer CELLINK, LLC
Zhizhong Yin, PhD	Previously Chief Executive Officer Euveda Biosciences, Inc.
Lei Zheng, MD, PhD	Associate Professor of Oncology and Surgery The Johns Hopkins University
Jiaojiao Zhou, MD, PhD	Zhejiang University Previously Visiting Research Scholar The Johns Hopkins University
Thomas M. Hyde, MD, PhD	Chief Medical Officer Director, Section on Neuropathology Previously Chief Operating Officer and Investigator Lieber Institute for Brain Development

Ran Tao, PhD	Lead Research Scientist Lieber Institute for Brain Development
Chao Li, PhD	Staff Scientist Lieber Institute for Brain Development
Jung-Chi Liao, PhD	Associate Research Fellow, Institute of Atomic and Molecular Sciences Academia Sinica Previously Assistant Professor of Mechanical Engineering Columbia University
T. Tony Yang, PhD	Postdoctoral Scholar, Institute of Atomic and Molecular Sciences Academia Sinica Previously Ph.D. Student in Mechanical Engineering Columbia University
Sharon Gerecht, PhD	Professor of Chemical and Biomolecular Engineering Director, Institute for NanoBioTechnology The Johns Hopkins University
Abigail (Abby) Hielscher, PhD	Assistant Professor of Anatomy Philadelphia College of Osteopathic Medicine - Georgia Previously Postdoctoral Scholar The Johns Hopkins University
Michael A. Beer, PhD	Associate Professor of Biomedical Engineering The Johns Hopkins University
Timothy C. Wang, MD	Dorothy L. and Daniel H. Silberberg Professor of Medicine Chief, Division of Digestive and Liver Diseases Columbia University
C. Benedikt (Ben) Westphalen, MD	Coordinator, Clinical & Translational Research CCC München - Comprehensive Cancer Center Ludwig-Maximilians-Universität München (University of Munich) Previously Postdoctoral Scholar Columbia University
Josephine P. Blaha, PhD	Teacher Holmdel High School

An extra special thank you to Dr. Blaha, who has undoubtedly made the greatest impact on my education. Thank you for always caring about your students, fostering a supportive learning environment, teaching with passion, overseeing Science Olympiad, and being prepared with Oreos! I truly appreciate the opportunities you created for me to advance my education, your recognition of my achievements, and the confidence you had in the places I (and my classmates) would go.

## Family

Thank you to my family for being supportive of me throughout not only my graduate education but also my personal growth and development as we continue this journey through life.

Chung-Jey Su, PhD	Father
Melissa (Ming-Huey) Su, MD, PhD	Mother
Jody E. Su	Sister
Jennifer I. Su Thompson, MD	Sister
David C. Thompson, PhD	Brother-in-Law
Chloë A. Thompson	Niece
Annabelle M. Thompson	Niece
Extended Family	

## Organizations

Outside of the academy, I would like to acknowledge the organizations that have been instrumental in my growth and development at the intersection of race as an Asian American and queerness as part of the LGBTQ+ community. In addition, I would like to recognize these organizations for their continued work in community-based organizing and advocacy. Thank you so much to all the wonderful people I have met through these organizations as well who have become a part of my chosen family.

National Queer Asian Pacific Islander Alliance (NQAPIA)

Invisible 2 Invincible: Asian Pacific Islander Pride of Chicago (i2i)

Trikone Chicago

## Friends

To all of my friends from all periods of my life, thank you for your company and support that helped me thrive and mature during both the pleasant and rough times. Friendship truly is a wondrous thing. Although there are too many people to list, I want to express special gratitude to the following friends:

Emily Fu, MD

Coral Jane Fung Shek, MSE

Emily, you are the best friend I have known the longest. We have seen each other grow immensely, and I am so proud of your accomplishments as I know you are of mine. Thank you for always listening, especially during times of intense emotion, and keeping me grounded throughout. Coral, I cannot imagine what my life would be like had I not met you. You helped me navigate through so many challenges during our time as undergraduates and beyond. Thank you for sharing so many interests and experiences with me and continuing to be such a supportive friend as we continue to grow as people.

**Partner**

Finally, I would like to acknowledge my partner and significant other:

Natawut Monaikul, MS

Natawut, thank you for being my best friend. It is unfathomable how lucky I am to share my life with you. Your love has supported me throughout this extremely stressful period of life, pushed me to continue working on myself towards becoming a better person, and motivated me to continue pursuing new and exciting challenges. Words cannot truly express my gratitude. Thank you to your family as well for welcoming me as part of the family.

## LIST OF ABBREVIATIONS

### Biological

<b>BM</b>	basement membrane
<b>cDNA</b>	complementary deoxyribonucleic acid
<b>dECM</b>	decellularized extracellular matrix
<b>DNA</b>	deoxyribonucleic acid
<b>dsDNA</b>	double-stranded deoxyribonucleic acid
<b>ECM</b>	extracellular matrix
<b>FBS</b>	fetal bovine serum
<b>GAG</b>	glycosaminoglycan
<b>GBM</b>	glomerular basement membrane
<b>HSPG</b>	heparan sulfate proteoglycan
<b>PECAM1</b>	platelet endothelial cell adhesion molecule 1
<b>RNA</b>	ribonucleic acid
<b>sGAG</b>	sulfated glycosaminoglycan
<b>VEGF</b>	vascular endothelial growth factor
<b>VEGFR</b>	vascular endothelial growth factor receptor

### Cells

<b>GEnC</b>	glomerular endothelial cell
<b>HKMEC</b>	human kidney microvascular endothelial cell
<b>HUVEC</b>	human umbilical vein endothelial cell
<b>MDCK</b>	Madin-Darby canine kidney

### Chemicals and Reagents

<b>DAPI</b>	4',6-diamidino-2-phenylindole
-------------	-------------------------------

<b>DMMB</b>	1,9-dimethylmethylene blue
<b>DPBS</b>	Dulbecco's phosphate-buffered saline
<b>H&amp;E</b>	hematoxylin and eosin
<b>PBS</b>	phosphate-buffered saline
<b>PEG</b>	poly(ethylene glycol)
<b>PEGX</b>	poly(ethylene glycol) crosslinker
<b>SVA</b>	succinimidyl valerate
<b>TNBS</b>	2,4,6-trinitrobenzenesulfonic acid

#### Engineering and Devices

<b>2D</b>	two-dimensional
<b>3D</b>	three-dimensional
<b>BioMEMS</b>	biological and biomedical microelectromechanical systems
<b>BRECS</b>	bioartificial renal epithelial cell system
<b>IAK</b>	implantable artificial kidney
<b>MEMS</b>	microelectromechanical systems
<b>RAD</b>	renal assist device
<b>RRT</b>	renal replacement therapy
<b>SCD</b>	selective cytopheretic device

#### Other

<b>ESRD</b>	end-stage renal disease
<b>OPTN</b>	Organ Procurement and Transplantation Network
<b>RPM</b>	revolutions per minute
<b>SEM</b>	scanning electron microscope or microscopy
<b>TEM</b>	transmission electron microscope or microscopy

## TABLE OF CONTENTS

ABSTRACT .....	3
ACKNOWLEDGEMENTS .....	6
LIST OF ABBREVIATIONS.....	16
TABLE OF CONTENTS.....	18
LIST OF TABLES AND FIGURES.....	24
<b><u>CHAPTER I:</u> An Introduction to Bioengineering Strategies for Modeling Kidney Function and Future</b>	
Renal Replacement Therapies.....	27
1.1. Kidney Structural and Functional Complexity .....	28
1.1.1. Overview of the Nephron and Associated Vasculature.....	28
1.1.2. The Glomerulus and the Glomerular Filtration Barrier .....	30
1.1.3. Glomerular Disease .....	33
1.2. Bioengineering Strategies for Modeling Kidney Function and Future Renal Replacement Therapies.....	34
1.2.1. Current Renal Replacement Therapies and the Clinical Need.....	34
1.2.2. The Bioartificial Kidney and Implantable Artificial Kidney .....	37
1.2.3. Biological and Biomedical Microelectromechanical Systems (BioMEMS).....	39
1.2.4. Whole-Kidney Decellularization and Bioengineering .....	41
1.2.5. Kidney Organoids .....	42
1.3. Hydrogels as Extracellular Matrix Mimics for Bioengineered Kidney Tissues .....	44
1.3.1. Properties of Hydrogels.....	45
1.3.2. Crosslinking Methods for Hydrogel Network Formation.....	45
1.3.3. Materials for Hydrogels .....	46
1.3.4. Review of Hydrogel Platforms for Modeling Kidney Function Towards Engineered Kidney Tissues .....	47

	19
1.4. Conclusion .....	50
<b>CHAPTER II: Development and Characterization of Kidney Decellularized Extracellular Matrix</b>	
Hydrogels and Evaluation as a Platform for Glomerular Endothelial Cell Culture and	
Encapsulation.....	52
2.1. Introduction .....	53
2.2. Materials & Methods.....	55
2.2.1. Kidney Decellularization .....	55
2.2.2. Evaluation and Characterization of Decellularized Kidney Tissues.....	56
2.2.3. Preparation and Characterization of Hydrogels from Kidney Decellularized Extracellular Matrix .....	57
2.2.4. Cell Culture and Cell Experimental Studies .....	58
2.2.5. Cell Viability and Proliferation.....	60
2.2.6. Histological, Transmission Electron Microscopy (TEM), and Gene Expression Analysis and Immunofluorescence Staining .....	61
2.2.7. Statistical Analysis .....	63
2.3. Results.....	63
2.3.1. Kidney Decellularization .....	64
2.3.2. Macroscopic and Ultrastructural Characterization of Hydrogels.....	64
2.3.3. Rheological Characterization of Hydrogels .....	67
2.3.4. Cell Viability and Proliferation on Hydrogel Substrates.....	69
2.3.5. Cellular Encapsulation Within Hydrogels .....	71
2.3.6. Gene Expression and Immunofluorescence .....	75
2.4. Discussion.....	81
2.5. Conclusion .....	85
<b>CHAPTER III: Poly(Ethylene Glycol)-Crosslinked Gelatin Hydrogel Substrates with Conjugated</b>	
Bioactive Peptides Influence Endothelial Behavior .....	
3.1. Introduction .....	88

	20
3.2. Material & Methods.....	90
3.2.1. Peptide Synthesis and Determination of Peptide Concentrations for Experiments .....	90
3.2.2. Preparation of Hydrogels and Phase Analysis .....	91
3.2.3. Quantification of Free Amine Content.....	92
3.2.4. Rheological Characterization and pH Measurement .....	93
3.2.5. Scanning Electron Microscopy (SEM).....	93
3.2.6. Swelling Analysis .....	93
3.2.7. Cell Culture.....	94
3.2.8. Cell Experimental Studies .....	95
3.2.9. VEGFR2/KDR Phosphorylation Assay.....	95
3.2.10. Gene Expression Analysis.....	96
3.2.11. Immunofluorescence Staining .....	97
3.2.12. Statistical Analysis .....	98
3.3. Results.....	99
3.3.1. Optimization of Peptide and PEGX Concentrations .....	100
3.3.2. Quantification of Free Amine Content.....	103
3.3.3. Rheological Characterization and pH Measurements.....	105
3.3.4. Scanning Electron Micrographs and Swelling Analysis of Hydrogels.....	107
3.3.5. QK Peptide Bioactivity and Phosphorylation of VEGFR2 in HUVECs and GEnCs .....	109
3.3.6. HUVEC Culture, Gene Expression Analysis, and Immunofluorescence .....	110
3.3.7. GEnC Culture and Gene Expression Analysis .....	114
3.4. Discussion.....	117
3.5. Conclusion .....	123
<b>CHAPTER IV: Challenges with <i>In Vitro</i> Cultures of Podocytes and Evaluation of Hydrogel Platforms to Preserve or Enhance Mature Podocyte Phenotype .....</b>	<b>125</b>

	21
4.1. Introduction .....	126
4.2. Materials & Methods.....	128
4.2.1. Culture of Conditionally-Immortalized Human Podocytes.....	128
4.2.2. Kidney Decellularization and Preparation of Hydrogels from Kidney Decellularized Extracellular Matrix .....	128
4.2.3. Preparation of PEG-Crosslinked Gelatin Hydrogels with Conjugated Peptides...	129
4.2.4. Preparation of 3D-Printed Gelatin Hydrogel Scaffolds.....	130
4.2.5. Cell Experimental Studies .....	131
4.2.6. Evaluation of Cell Response .....	132
4.2.7. Statistical Analysis .....	135
4.3. Results.....	135
4.3.1. Gene Expression Analysis of Podocytes Cultured on Conventional Tissue Culture Polystyrene .....	135
4.3.2. Podocyte Culture on Kidney dECM Hydrogel Substrates and Encapsulation within Kidney dECM Hydrogels.....	137
4.3.3. Podocyte Culture on Matrigel and PEG-Crosslinked Gelatin Hydrogel Substrates and Gene Expression Analysis.....	141
4.3.4. Podocyte Culture on 3D-Printed Gelatin Scaffolds.....	144
4.4. Discussion.....	148
4.5. Conclusion .....	154
<b>CHAPTER V: Conclusion &amp; Future Directions .....</b>	<b>155</b>
5.1. Significance & Impact of Findings .....	156
5.2. Future Directions .....	160
5.2.1. Kidney Decellularized Extracellular Matrix Hydrogels for Cell Culture and Encapsulation.....	160
5.2.2. Poly(Ethylene Glycol)-Crosslinked Hydrogels With Conjugated Peptides to Enhance Bioactivity .....	162

5.2.3. Hydrogel Platforms to Preserve or Enhance Podocyte Phenotype in In Vitro Culture Towards a Model of the Glomerular Filtration Barrier .....	165
REFERENCES .....	169
<u>CHAPTER VI: Appendices</u> .....	200
6.1. Appendix A: Dose-Dependent Cytotoxicity of Gentamicin and Cisplatin on Madin-Darby Canine Kidney (MDCK) Cells Measured by the Resazurin Reduction Assay .....	201
6.1.1. Introduction .....	201
6.1.2. Materials & Methods .....	201
6.1.3. Results & Discussion .....	203
6.2. Appendix B: Evaluation of Madin-Darby Canine Kidney (MDCK) Cells Cultured on Kidney Decellularized Extracellular Matrix Scaffolds .....	206
6.2.1. Introduction .....	206
6.2.2. Materials & Methods .....	206
6.2.3. Results & Discussion .....	209
6.3. Appendix C: Evaluation of Conditionally-Immortalized Human Podocytes Cultured on Kidney Decellularized Extracellular Matrix Scaffolds .....	211
6.3.1. Introduction .....	211
6.3.2. Materials & Methods .....	211
6.3.3. Results & Discussion .....	214
6.4. Appendix D: Viability Staining of Madin-Darby Canine Kidney (MDCK) Cells Encapsulated Within Kidney Decellularized Extracellular Matrix (dECM) Hydrogels .....	216
6.4.1. Introduction .....	216
6.4.2. Materials & Methods .....	216
6.4.3. Results & Discussion .....	218
6.5. Appendix E: Rheological Characterization of Various Tissue- and Organ-Specific Decellularized Extracellular Matrix Hydrogels .....	221
6.5.1. Introduction .....	221

6.5.2. Materials & Methods .....	221
6.5.3. Results & Discussion .....	223
CURRICULUM VITAE .....	228

## LIST OF TABLES AND FIGURES

Figure 1-1: Schematics of the kidney, the nephron, and the glomerular filtration barrier. ....	29
Figure 1-2: Kidney Organ Procurement and Transplantation Network (OPTN) data by year.....	37
Figure 1-3: Schematics of the extracellular matrix (ECM) and hydrogel crosslinking. ....	44
Table 2-1: Primer sequences for gene expression analysis via quantitative real-time polymerase chain reaction (qPCR). ....	62
Figure 2-1: Process to form kidney decellularized extracellular matrix hydrogels. ....	63
Figure 2-2: Evaluation and characterization of decellularized kidney tissues.....	65
Figure 2-3: Scanning electron micrographs, macroscopic images, and rheological time sweeps of hydrogels. ....	66
Figure 2-4: Rheological frequency and strain sweeps of hydrogels.....	68
Table 2-2: Rheological characterization of hydrogels.....	69
Figure 2-5: Viability and proliferation of GEnCs cultured hydrogel substrates or encapsulated within hydrogels. ....	70
Figure 2-6: Histological analysis of GEnCs encapsulated within hydrogels (1 million cells/mL) after 7 days in culture.....	72
Figure 2-7: Histological analysis and TEM of GEnCs encapsulated within hydrogels (1 million cells/mL) after 12 days in culture. ....	73
Figure 2-8: Histological analysis of GEnCs encapsulated within hydrogels (5 million cells/mL). ....	74
Figure 2-9: Gene expression analysis of GEnCs cultured on hydrogel substrates.....	76
Figure 2-10: Gene expression analysis of GEnCs encapsulated within hydrogels (1 million cells/mL). ....	77
Figure 2-11: Gene expression analysis of GEnCs encapsulated within hydrogels (5 million cells/mL). ....	78
Figure 2-12: Additional gene expression analysis of GEnCs encapsulated within hydrogels (5 million cells/mL).....	79
Figure 2-13: Immunofluorescence staining for PECAM-1 in GEnCs encapsulated within hydrogels. ....	80

Table 3-1: Peptide sequences.....	91
Table 3-2: Main hydrogel formulations tested.....	92
Table 3-3: Primer sequences for gene expression analysis via quantitative real-time polymerase chain reaction (qPCR).....	97
Figure 3-1: Preparation of PEG-crosslinked gelatin hydrogels and conjugation of peptides.....	99
Figure 3-2: Phase plot of varying YIGSR peptide concentrations with varying PEGX concentration. ....	101
Figure 3-3: Photomicrographs of GEnCs cultured on hydrogel substrates of varying combinations and concentrations of YIGSR and QK peptides. ....	102
Table 3-4: Free amine content of hydrogel precursor polymer solutions and crosslinked hydrogels. ....	103
Figure 3-4: Quantification of free amine content and rheological time sweeps of hydrogel formulations. ....	104
Table 3-5: pH and rheological characterization of hydrogels.....	105
Figure 3-5: Rheological frequency and strain sweeps of hydrogels.....	106
Figure 3-6: Low-magnification scanning electron micrographs of hydrogels.....	107
Figure 3-7: Scanning electron micrographs and swelling analysis of hydrogels.....	108
Figure 3-8: Cellular levels of phosphorylated VEGFR2 measured by an ELISA. ....	110
Figure 3-9: Photomicrographs of HUVECs cultured on hydrogel substrates.....	112
Figure 3-10: Gene expression analysis and immunofluorescence staining of HUVECs cultured on hydrogel substrates.....	113
Figure 3-11: Photomicrographs of GEnCs cultured on hydrogel substrates. ....	115
Figure 3-12: Gene expression analysis of GEnCs cultured on hydrogel substrates.....	116
Table 4-1: Primer sequences for gene expression analysis via quantitative real-time polymerase chain reaction (qPCR).....	135
Figure 4-1: Gene expression analysis of conditionally-immortalized human podocytes cultured on conventional tissue culture polystyrene.....	136
Figure 4-2: Proliferation and viability staining of podocytes cultured on type I collagen hydrogels or kidney dECM hydrogels.....	138

Figure 4-3: Viability staining of podocytes encapsulated within type I collagen hydrogels or kidney dECM hydrogels of varying concentration.....	139
Figure 4-4: Viability staining of podocytes encapsulated within type I collagen and kidney dECM hydrogel mixtures.....	140
Figure 4-5: Photomicrographs of podocytes cultured on Matrigel or PEG-crosslinked gelatin hydrogel substrates.....	142
Figure 4-6: Gene expression analysis of podocytes cultured on Matrigel or PEG-crosslinked gelatin hydrogel substrates.....	143
Figure 4-7: Photomicrographs of podocytes cultured on 3D-printed gelatin scaffolds.....	145
Figure 4-8: Viability staining of podocytes cultured on 3D-printed gelatin scaffolds.....	146
Figure 4-9: Scanning electron micrographs of podocytes cultured on 3D-printed gelatin scaffolds.....	147
Figure 5-1: Schematics of heterofunctional PEGX reactions for independent crosslinking of polymers and conjugation of peptides.....	164
Figure 5-2: Potential <i>in vitro</i> models of the glomerular filtration barrier enabled by 3D printing and bioprinting technologies.....	168
Figure 6-1: Estimated MDCK cell number after continuous treatment with gentamicin.....	203
Figure 6-2: Estimated MDCK cell number after continuous treatment with cisplatin.....	204
Figure 6-3: Histological analysis and immunofluorescence staining of MDCK cells cultured on kidney dECM scaffold disks.....	209
Figure 6-4: Viability staining, histological analysis, and transmission electron micrographs of human podocytes cultured on kidney dECM scaffold disks.....	215
Figure 6-5: Viability staining of MDCK cells encapsulated within type I collagen hydrogels or kidney dECM hydrogels of varying concentrations.....	220
Figure 6-6: Rheological time sweeps of tissue and organ dECM hydrogels.....	225
Figure 6-7: Rheological frequency sweeps of tissue and organ dECM hydrogels.....	226
Figure 6-8: Rheological strain or amplitude sweeps of tissue and organ dECM hydrogels.....	227

**CHAPTER I:**

**An Introduction to Bioengineering Strategies  
for Modeling Kidney Function and Future Renal Replacement Therapies**

## 1.1. Kidney Structural and Functional Complexity

The primary function of the kidneys is fluid and electrolyte balance, that is, homeostatic regulation of water and salts in the body. More specifically, according to Dee Unglaub Silverthorn's *Human Physiology*, kidney function can be categorized into six general areas: 1.) regulation of extracellular fluid volume and blood pressure, 2.) regulation of osmolarity, 3.) maintenance of ion balance, 4.) homeostatic regulation of pH, 5.) excretion of wastes, and 6.) production of hormones<sup>[1]</sup>. To achieve this, the kidneys filter approximately 180 L of blood plasma per day in the adult human, requiring 20-25% of the total cardiac output.

### 1.1.1. Overview of the Nephron and Associated Vasculature

Kidney function is achieved by the combined activity of approximately one million nephrons in each human kidney<sup>[2]</sup> (**Figure 1-1 A**). The nephron is the functional unit of the kidney, and a single nephron can be further divided into segments each with unique properties (**Figure 1-1 B**). The nephron begins at the glomerulus where the Bowman's capsule surrounds a specialized capillary bed, and combined this structure is referred to as the renal corpuscle. The glomerulus is where blood plasma filtration and ultrafiltrate formation occurs in the nephron. The Bowman's capsule then leads into the proximal and distal tubules where reabsorption and secretion of water and solutes occur. Finally, the distal tubules of multiple nephrons connect into collecting ducts where additional reabsorption of water occurs after which the remaining fluid is drained into the renal pelvis, and the fluid, now referred to as urine, exits the kidney through the ureter. The outer region of the kidney containing the glomeruli and the majority of the tubular structures is referred to as the kidney cortex, and the inner region containing the collecting ducts and where the tubules dip to form the loop of Henle is referred to as the kidney medulla<sup>[1, 3]</sup>.

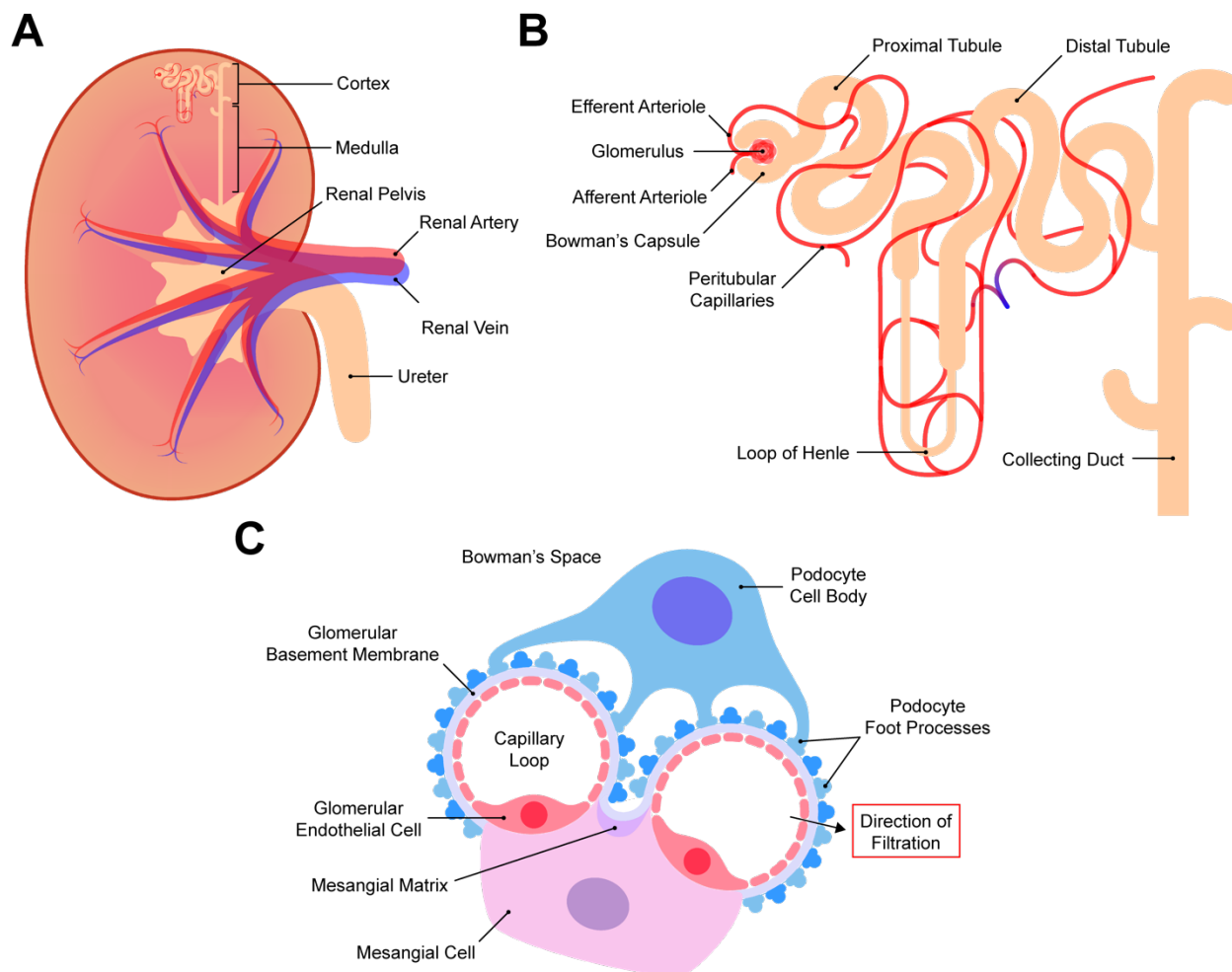


**Figure 1-1: Schematics of the kidney, the nephron, and the glomerular filtration barrier.**

(A) Cross section (sagittal plane) of a normal human kidney. The kidney may be divided into the outer cortex region, inner medulla region, and the renal pelvis that leads to the ureter through which urine exits the kidneys. Vasculature enters the kidney as the renal artery and exits as the renal vein. (B) The nephron begins at the glomerulus where blood plasma filtration occurs. The glomerulus is encased by the Bowman's capsule that leads into the tubules where reabsorption and secretion of water and solutes occur. The tubules may be subdivided into the proximal tubule, loop of Henle, and distal tubule. The end of the distal tubule connects to the collecting duct where additional reabsorption of water may occur before the resulting urine is drained into the renal pelvis. The associated vasculature enters the glomerulus as the afferent arteriole, forms the glomerular capillaries, exits the glomerulus as the efferent arteriole, and then forms the peritubular capillaries. (C) Cross section of the glomerular filtration barrier. The glomerular capillary loops are formed by glomerular endothelial cells (GECs) that exhibit transcytoplasmic nanopores known as fenestrations. The glomerular capillaries are supported by a central stock formed by mesangial cells that secrete extracellular matrix molecules to form the mesangial matrix. Podocytes, also known as visceral epithelial cells, intricately wrap around the capillary loops by extending foot processes from their main cell body. The glomerular basement membrane (GBM) is positioned in between the GECs and podocyte foot processes. As blood flows through the glomerular capillaries, filtrate moves outward passing through the tri-layer structure of GEC fenestrations, the GBM, and filtration slits between podocyte foot processes before reaching the Bowman's space.

The vasculature is an additional and particularly important component of the kidney distinct from the nephron as the kidney is dependent on the vasculature for movement of blood and plasma not only to and from the kidney but also throughout the organ. Vasculature enters the kidney as the renal artery before forming smaller arteries and then arterioles that permeate throughout the kidney cortex. Eventually, these arterioles become the specialized capillary beds referred to as glomerular capillaries that form the basis of the glomerulus. The arteriole leading into a glomerulus is referred to as the afferent arteriole, and the arteriole leading out of the glomerulus is referred to as the efferent arteriole. Beyond the efferent arteriole lie the peritubular capillaries and, for the juxtamedullary nephrons that dip further into the kidney medulla, the vasa recta that intricately surround the nephron tubules. Finally, the peritubular capillaries join back together to form venules and small veins before exiting the kidney as the renal vein<sup>[1]</sup>.

### **1.1.2. The Glomerulus and the Glomerular Filtration Barrier**

The glomerulus and the glomerular filtration barrier acts as a size- and charge-selective sieve<sup>[4-6]</sup> (**Figure 1-1 C**). In humans, the glomerulus is approximately 100-200  $\mu\text{m}$  in diameter<sup>[7, 8]</sup>. The main components of the glomerular filtration barrier include: glomerular endothelial cells (GEnCs), podocytes, and the intervening glomerular basement membrane (GBM).

GEnCs form the capillary loops or tufts of the glomerulus. A single capillary in the human glomerulus is approximately 6-8  $\mu\text{m}$  in diameter<sup>[9]</sup>. GEnCs are unique from other endothelial cells in the body in that they are unusually flattened being approximately 50-150 nm in height<sup>[10]</sup>. Furthermore, GEnCs exhibit transcytoplasmic nanopores approximately 60-80  $\mu\text{m}$  in diameter known as fenestrations<sup>[11]</sup>. Fenestrations are present in a variety of capillary beds, but GEnC fenestrations are unique in that they lack a diaphragm and expression of plasmalemmal vesicle-associated protein-1 (PLVAP) when mature<sup>[11]</sup>. In addition, GEnCs possess an endothelial surface layer thought to be 200-400 nm thick that forms from the combination of the endothelial glycocalyx and the endothelial cell coat<sup>[4-6, 11, 12]</sup>. The glycocalyx is composed of membrane-bound proteoglycans and sialoproteins, whereas the endothelial cell coat is composed of a mixture of plasma proteins adsorbed to the glycocalyx. Although it has been technically challenging to visualize and measure the thickness of these structures, it has been reported that the glycocalyx is about

50-100 nm thick<sup>[13]</sup> and that the endothelial cell coat is about 200-300 nm thick<sup>[14]</sup>, both in rodents. Ultimately, both GEnC fenestrations and the endothelial surface layer are thought to play important roles in determining and maintaining the permeability properties of the glomerular filtration barrier.

Podocytes, sometimes referred to as visceral epithelial cells, are highly-differentiated cells that wrap around and intimately interact with GEnCs. It has been estimated that there are approximately 500-600 podocytes per glomerulus in the average white, American male<sup>[15, 16]</sup>. Podocytes also exhibit a unique and impressive cellular morphology characterized by a large, central cell body and multiple cytoplasmic extensions termed major or primary processes that subdivide into secondary processes and end in finer pedicels or foot processes<sup>[17, 18]</sup>. These larger processes are composed predominantly of microtubules and intermediate filaments, whereas foot processes are composed of bundles of parallel actin filaments<sup>[19, 20]</sup>. Podocyte foot processes regularly interdigitate with neighboring podocytes creating filtration slits approximately 30-40 nm wide<sup>[21]</sup>. These filtration slits are traversed by unique cellular junctions known as slit diaphragms. During development and in the mature state, podocyte slit diaphragms and the surrounding area contain proteins traditionally associated with tight junctions, adherens junctions, gap junctions, and neuronal junctions<sup>[22]</sup>. The slit diaphragms are intrinsically linked to podocyte function, including: contribution to the permeability properties of the glomerular filtration barrier, coupling of these intercellular junctions to the podocyte actin skeleton and involvement in signal transduction, and regulation of foot process plasticity<sup>[22]</sup>. Podocytes also express a glycocalyx composed primarily of podocalyxin and syndecans<sup>[5]</sup>, which imparts a negative charge to the podocyte cell surface and plays an essential role in the formation and maintenance of podocyte foot processes<sup>[23]</sup>. In the event of podocyte injury and disruption of the glomerular filtration barrier, there is often the loss of podocyte slit diaphragms and effacement of foot processes<sup>[24, 25]</sup>. Whether this process marks the onset of disease or is the result of disease progression is unclear<sup>[26]</sup>, although it likely depends on the etiology of the disease in question.

The final component of the glomerular filtration barrier is the GBM. In humans, the GBM is approximately 300-400 nm thick<sup>[3, 27-29]</sup>, which is unusually thick as the basement membranes in most microvascular beds is only 50-100 nm thick<sup>[30, 31]</sup>. Ultrastructural studies have revealed that the GBM results from the fusion of basement membrane components secreted by both glomerular endothelial cells and

podocytes<sup>[32]</sup>. These components are primarily type IV collagen, laminin, nidogens (formerly known as entactins), and heparan sulfate proteoglycans (HSPGs)<sup>[33-35]</sup>. Type IV collagen and laminin are the most abundant components of basement membranes and are necessary for basement membrane formation and stability<sup>[31, 36]</sup>. Multiple isoforms of both type IV collagen and laminin have been identified and expressed throughout basement membranes in the body, and specific isoforms for each have been identified in the GBM. Interestingly, during glomerulogenesis developmental transitions occur resulting in differences in the predominant isoforms of type IV collagen and laminin present in the developing versus mature GBM<sup>[33-35]</sup>. These developmental transitions are critical as mutations in genes encoding specific isoforms of these proteins result in GBM defects and kidney disease<sup>[34]</sup>. Nidogens contain binding sites for both type IV collagen as well as laminin, thus acting as a protein crosslinker between type IV collagen and laminin networks<sup>[37]</sup>. HSPGs, which consist of a protein core with covalently conjugated glycosaminoglycan side chains, impart a significant anionic charge to the GBM. While this was previously thought to be the main driver for the permselectivity of the glomerular filtration barrier<sup>[38, 39]</sup>, more recent evidence suggests that this may not actually be the case<sup>[6, 31, 35]</sup>. However, many growth factors contain heparin-binding domains, therefore the presence of HSPGs in the basement membrane may aid in sequestration and presentation of these factors for improved cell signaling<sup>[6, 31, 40]</sup>. Agrin is the predominant HSPG present in the mature GBM, although perlecan is initially also present in the developing GBM<sup>[33-35]</sup>. The GBM ultimately unites GEnCs and podocytes by providing the underlying matrix substrate that both of these unique cell populations may bind to and together form the glomerular filtration barrier.

Although they do not directly contribute to the glomerular filtration barrier, the mesangial cells and parietal epithelial cells are two additional cell types that reside in the glomerulus and should be discussed. Mesangial cells and the extracellular matrix they secrete to form the mesangial matrix, collectively referred to as the mesangium, provide structural support of the glomerular tuft<sup>[3, 41]</sup>. These cells are responsible for splitting of the initial glomerular vessel into multiple capillary loops<sup>[42]</sup> and also maintenance of the capillary loop structures by extending contractile processes that bind to and maintain the infoldings of the GBM<sup>[43-45]</sup>. Furthermore, the contractile nature of mesangial cells enable the fine regulation of glomerular capillary flow and ultrafiltration area<sup>[1, 41, 46, 47]</sup> and detection of changes in capillary stretch<sup>[41]</sup>. Finally, mesangial cells

participate in cellular crosstalk via secreted signaling factors with GEnCs and podocytes, and this crosstalk is necessary for the development and maintenance of healthy glomeruli<sup>[41, 48, 49]</sup>. Parietal epithelial cells and the underlying parietal basement membrane form the Bowman's capsule that encases the glomerular capillaries<sup>[3]</sup>. Parietal epithelial cells and podocytes arise from the same progenitor cells during development but later diverge<sup>[50]</sup>, and parietal epithelial cells in the mature kidney resemble squamous epithelial cells<sup>[3, 5]</sup>. At the urinary pole, these cells exhibit a graded expression of markers as the Bowman's capsule leads to the proximal tubule<sup>[3, 51]</sup>. At the vascular pole, a unique population of peripolar or "transitional" cells that exhibit an intermediate phenotype between parietal epithelial cells and podocytes have been identified<sup>[51]</sup>. Parietal epithelial cells have recently received more attention in order to better define the normal phenotype of these cells and their potential for reparative or regenerative roles as a podocyte stem or progenitor cell<sup>[51, 52]</sup>.

### **1.1.3. Glomerular Disease**

Glomerular disease or damage to the glomerular filtration barrier typically manifests as increased leakage of protein content or even red blood cells into the urine, referred to as nephrotic and nephritic syndromes, respectively, and thus interferes with the clearance of waste products and toxins from the bloodstream<sup>[53]</sup>. Progression of glomerular disease toward nephron loss can be grouped into dysregulative, degenerative, and inflammatory mechanisms with regard to pathological manifestations<sup>[54]</sup>, although the etiology of these diseases may be either genetic, environmental, or a combination of both<sup>[24]</sup>. Damage to the glomerular filtration barrier may occur as injury to any of the three components of the filtration barrier, for example as: thrombotic events in the glomerular microvasculature, thinning or thickening of the GBM, or loss of podocyte slit diaphragms and foot process effacement<sup>[55, 56]</sup>. In some instances, the mesangium may also play a role in glomerular disease. For example, the mesangium may be the target of immunoglobulin deposits or dysregulation may lead to mesangial cell proliferation and increased accumulation of mesangial matrix<sup>[55, 56]</sup>. Ultimately, this reduction in kidney function due to glomerular disease and nephron loss may lead to acute kidney injury or the development of chronic kidney disease.

## 1.2. Bioengineering Strategies for Modeling Kidney Function and Future Renal Replacement

### Therapies

End-stage renal disease (ESRD), or kidney failure, can result from acute kidney injury or sustained kidney damage in the form of chronic kidney disease. In 2016, there were more than 124,000 newly reported cases of ESRD in the United States resulting in over 726,000 cases total with Medicare spending for beneficiaries rising to \$35.4 billion<sup>[57]</sup>. In particular, between 2012 and 2016, glomerular disease was the leading cause of ESRD in pediatric patients at 22.3% of the affected population<sup>[57]</sup>. The onset of ESRD requires renal replacement therapy to restore lost kidney function.

#### 1.2.1. Current Renal Replacement Therapies and the Clinical Need

Artificial replacement of organ function has been investigated since early times, and advancements have only progressed, especially since the beginning of the 20th century. Modern dialysis, a common and the most widely-known form of artificial renal replacement therapy (RRT), was initially developed in the early 1900s<sup>[58]</sup>. Broadly, RRTs aim to replace the normal filtration function of the kidneys, and current indications by physicians for RRT in patients include renal failure, acid-base abnormalities, electrolyte imbalances, and accumulation of toxins or poisons<sup>[58]</sup>. Artificial RRTs can be categorized by the guiding transport phenomena for solute clearance: dialysis relies on diffusion whereas hemofiltration relies on convection, although both processes rely on the use of a semipermeable membrane<sup>[58]</sup>. Dialysis may be additionally separated into hemodialysis and peritoneal dialysis setups. Hemodialysis is an extracorporeal method whereby the patient's blood is removed from the circulatory system and pumped through a dialyzer to be filtered before being returned to the patient's body. In the dialyzer, blood is forced through thin, hollow fibers composed of a semipermeable membrane while dialysate is passed outside of the fibers in a countercurrent fashion to allow for efficient diffusion of solutes across the membrane due to a concentration gradient<sup>[58-60]</sup>. In the past, hemodialysis was restricted to dialysis centers and strict visit schedules, but advancements and miniaturization of technologies now allow for home hemodialysis<sup>[59]</sup>. Peritoneal dialysis is a paracorporeal method that utilizes the patient's peritoneum as a natural semipermeable membrane<sup>[58]</sup>. Dialysate is placed in the peritoneal cavity, and diffusion of solutes and fluid occurs over the course of

several hours due to a concentration gradient. Multiple exchanges with fresh dialysate are required to ensure efficient filtration and can be performed manually during the daytime as in the case of continuous ambulatory peritoneal dialysis or automatically during the evening as in the case of automated peritoneal dialysis<sup>[59]</sup>. Hemodialysis is often the preferred setup for patients on dialysis<sup>[61]</sup>, but this decision results from a combination of the patient characteristics, indication for RRT, location (within or outside of the hospital), and resources<sup>[58]</sup>. In contrast to dialysis, hemofiltration utilizes a pressure gradient to force water movement across a semipermeable membrane and thus “pull” or “drag” solutes along<sup>[58, 60]</sup>. Hemofiltration delivery is limited to continuous RRT in the hospital. Continuous RRTs utilize hemodialysis, hemofiltration, or a combination thereof to achieve volume removal and solute clearance and are typically reserved for patients placed in intensive care units with acute kidney injury. The rationale is that a more gradual clearance of solutes and removal of fluids over prolonged periods is safer for hemodynamically unstable or vasopressor-dependent patients such as those confined to intensive care units<sup>[60, 62]</sup>.

Since its inception, the fundamentals behind artificial RRTs have remained the same. The most significant changes in RRT delivery have focused on equipment technology to automate many processes and enhance usability<sup>[58]</sup>. Advances in other aspects include improved water purity (enabled by the development of reverse osmosis technology)<sup>[58, 63]</sup> and adoption of superior synthetic polysulfone, polyacrylonitrile, or polymethylmethacrylate membranes over natural cellulose membranes<sup>[64]</sup>. However, while artificial RRTs are life-saving, they are unable to replace all of the functions of the kidney such as production of hormones. Ultimately, the optimal RRT and the current gold standard for treatment of ESRD and kidney failure is kidney transplantation. In a kidney transplant, a healthy kidney from a deceased or living donor is placed in the abdomen of the patient and connected to the respective blood vessels and the bladder. The transplanted kidney is then able to perform all of the functions now lost from the patient’s original kidneys<sup>[59]</sup>. Kidney transplantation significantly improves long-term patient survival and increases overall quality of life in comparison to artificial RRTs<sup>[65-67]</sup>.

Unfortunately, with the increasing prevalence of ESRD and advances in healthcare practices and technologies that enable longer patient survival on artificial RRTs, the number of patients on the waiting list for a kidney transplant continues to rise. According to the United States Organ Procurement and

Transplantation Network, at the end of 2018 there were over 95,000 patients on the waiting list for a kidney transplant (**Figure 1-2**)<sup>[68]</sup>. Although the number of kidney transplants performed each year continues to rise as well, the increase is only a fraction of the increase in the number of patients on the waiting list. In 2018, only about 21,000 kidney transplants were performed (**Figure 1-2**)<sup>[69]</sup> [OPTN], and this number is ultimately limited by the availability of donor kidneys. Furthermore, patients who are fortunate enough to receive a donor kidney transplant are required to maintain a strict, lifelong regimen of expensive immunosuppressants to decrease the likelihood of transplant rejection<sup>[69, 70]</sup>. Therefore, there is a compelling need for bioengineered kidney tissues as: 1.) models for understanding development and disease progression, 2.) models to bridge the gap between pre-clinical studies using *in vitro* cell culture or animal models and clinical testing in humans for more efficient drug discovery and development, and 3.) eventual therapies for restoring lost kidney function<sup>[71]</sup>. Recognizing the urgency of the situation, the National Institute of Diabetes and Digestive and Kidney Diseases recently formed the (Re)Building a Kidney consortium to bring together experts from diverse scientific backgrounds in kidney research with the ultimate goals of devising strategies to stimulate regeneration of nephrons *in situ* to restore kidney function and developing and implementing strategies for *in vitro* engineering of replacement kidney tissue<sup>[72]</sup>. Here we will review some of the most notable bioengineering strategies currently being pursued for modeling kidney function.

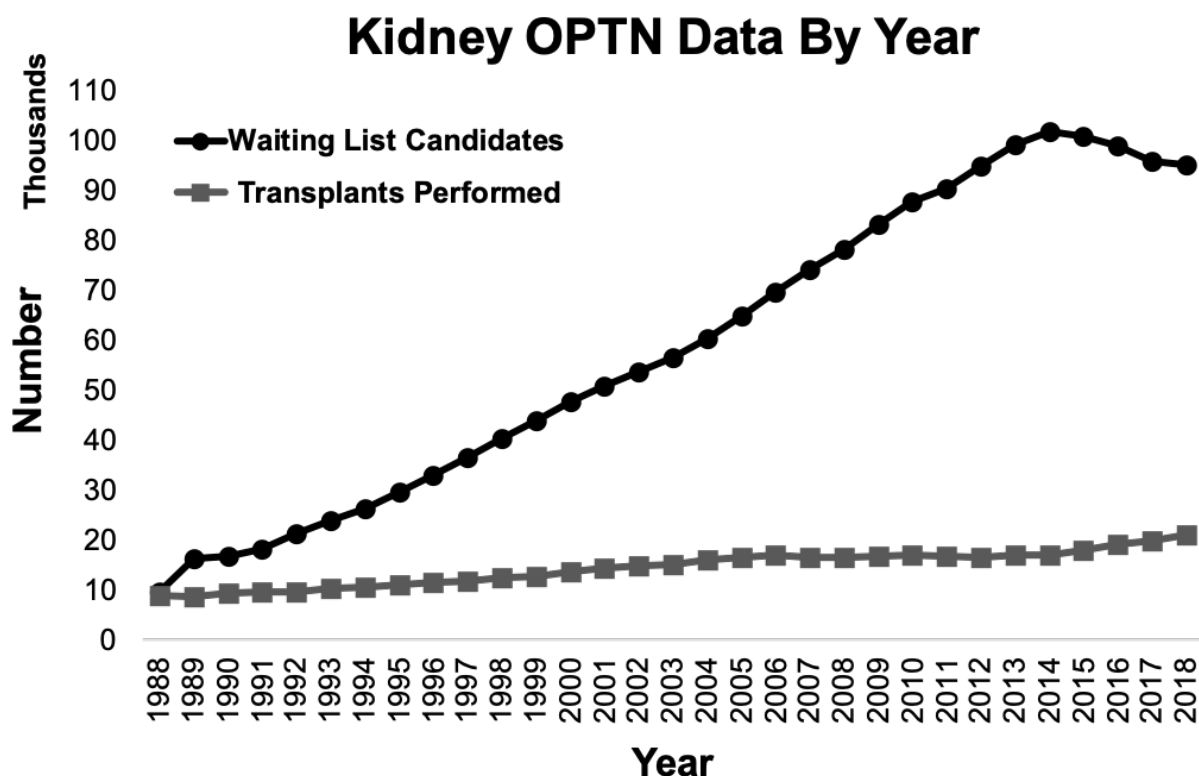


**Figure 1-2: Kidney Organ Procurement and Transplantation Network (OPTN) data by year.** Number of patients on the waiting list for a kidney transplant and number of kidney transplants performed each year from 1988 to 2018. Based on OPTN data as of January 1st, 2019.<sup>[68]</sup>

### 1.2.2. The Bioartificial Kidney and Implantable Artificial Kidney

The concept of the bioartificial kidney and subsequent research in its development was initially pioneered by H. David Humes<sup>[73-76]</sup>. In its original conception, the bioartificial kidney was designed as an extracorporeal device composed of a conventional synthetic hemofilter in series with a renal tubule assist device (RAD). The hemofilter would provide the filtration function of the kidney while the RAD would provide the metabolic function of the kidney (*i.e.*, reabsorption and secretion of solutes that typically occurs in the kidney tubules). To achieve this function, the RAD consisted of a standard hemofiltration cartridge in which tubular epithelial cells were cultured on the inner surfaces of the semipermeable, hollow fiber membranes and allowed to form a confluent monolayer<sup>[74-76]</sup>. This was first achieved in a single fiber system using Madin-Darby canine kidney (MDCK) cells<sup>[77]</sup> before being scaled up to a multi-fiber system using porcine proximal tubule epithelial cells<sup>[78, 79]</sup> with demonstration of the desired metabolic processes. Large-animal

studies further demonstrated that the bioartificial kidney resulted in partial restoration of kidney function in acutely uremic dogs<sup>[80, 81]</sup> and improved cardiovascular performance associated with changes in cytokine profiles and conferred significant survival advantages in uremic dogs with septic shock<sup>[82, 83]</sup> and pigs with septic shock<sup>[84]</sup>.

While phase I and phase II clinical trials with the RAD utilizing human proximal tubule epithelial cells were initially encouraging demonstrating safety and efficacy with regard to increased survival in patients receiving continuous RRT due to acute renal failure<sup>[85, 86]</sup>, a phase IIb study was not completed due to difficulties with the manufacturing process and an unanticipated high survival rate of patients treated with sham control RADs without cells<sup>[87]</sup>. This underscored some of the hurdles that researchers continue to face in commercializing medical devices with cells: 1.) identifying a reliable and consistent cell source with sufficient numbers and 2.) devising economical strategies in manufacturing, storage, and distribution of the devices<sup>[75]</sup>. In light of these results, development of the bioartificial kidney diverged into two separate strategies: the selective cytopheretic device (SCD) and the bioartificial renal epithelial cell system (BRECS)<sup>[88]</sup>.

In contrast to the RAD, the SCD does not contain cells but instead is simply an extracorporeal device containing a bundled collection of polysulfone membrane fibers. The SCD is placed in series after a hemofilter, and as blood treated with citrate is passed around the membrane fibers activated leukocytes bind and are sequestered resulting in immunomodulatory effects<sup>[89]</sup>. The SCD has been tested in animal models for a variety of conditions typically associated with inflammation<sup>[90-93]</sup> as well as in clinical trials for treatment of acute kidney injury and chronic hemodialysis patients<sup>[94-98]</sup>. Taking into consideration the challenges in manufacturing the RAD, the BRECS utilizes an enhanced propagation method for expanding primary renal epithelial cells from adult renal epithelial progenitor cells<sup>[99]</sup> to overcome limitations in cell source and numbers and cultured on porous, niobium-coated carbon disks housed in a perfusable unit<sup>[100]</sup>. The system was specifically designed to be cryopreserved for storage and reconstituted to meet on-demand clinical need<sup>[100]</sup>. The BRECS was demonstrated to confer survival advantage in a porcine model of septic shock<sup>[101]</sup>, and improvements in the design of the system have led to a more-economical, wearable system for clinical translation<sup>[102, 103]</sup>. In addition to the SCD and the BRECS, a few other groups have also delved

into the development of a bioartificial kidney, although most of these investigations have been limited to exploring different membrane compositions<sup>[104-107]</sup>, membrane coatings<sup>[108]</sup>, and cell sources<sup>[109, 110]</sup>.

With the progression of science and engineering, there has been the trend of the miniaturization of technologies. Building upon the body of knowledge surrounding the bioartificial kidney, Shuvo Roy and William H. Fissell have been accelerating the development of an implantable artificial kidney (IAK)<sup>[111-113]</sup>. The IAK is composed of a high-efficiency filter, the HemoCartridge that recapitulates the functions of the glomerulus, and a microfluidic bioreactor containing renal tubule epithelial cells, the BioCartridge that recapitulates the functions of the tubules<sup>[113]</sup>. Manufacture of the HemoCartridge has been enabled by advances in micromachining and microfabrication techniques utilized in the development of microelectromechanical systems (MEMS). The HemoCartridge contains silicon nanopore membranes with slit-shaped pores and coated with polymers to prevent biofouling demonstrated in hemocompatibility and implantation studies<sup>[114-120]</sup>. The superior slit-pore geometry has been empirically- and computationally- validated for ultrafiltration<sup>[121-123]</sup>, and the membranes have also been evaluated for use in hemodialysis applications (though requiring a few design changes)<sup>[124, 125]</sup>. For the BioCartridge, renal tubular epithelial cells may be cultured on the same silicon nanopore membranes and form confluent monolayers with tight junctions<sup>[126]</sup>, although more recent bioreactor designs have utilized optically-transparent polycarbonate membranes for more facile imaging<sup>[127-129]</sup>. As an implantable device, the IAK comes with new challenges including maintenance of cell phenotype and other failure assessments over extended periods, but the IAK as the potential to truly revolutionize current artificial RRTs.

### **1.2.3. Biological and Biomedical Microelectromechanical Systems (BioMEMS)**

Microelectromechanical systems (MEMS) refer to devices manufactured using similar microfabrication and micromachining techniques traditionally employed for integrated circuits. MEMS technologies convert real-world signals from one form of energy to another thus enabling construction of sensors, actuators, and other systems but scaled down to the micro-scale to increase performance and reduce costs<sup>[130]</sup>. BioMEMS is therefore the application of MEMS to biological and biomedical applications<sup>[131]</sup>, including the “delivery, manipulation, analysis, or construction of biological and chemical

entities”<sup>[132]</sup>. BioMEMS broadly encompasses systems of similar principles that are sometimes referred to by other names, including microfluidic devices<sup>[133]</sup>, micro total analysis systems ( $\mu$ TAS)<sup>[134]</sup>, lab-on-a-chip<sup>[135]</sup> or organs-on-chips<sup>[136]</sup>, and microphysiological systems<sup>[137]</sup>. Applications of BioMEMS are numerous and range from diagnostic applications and toxicity testing to drug delivery systems and medical devices<sup>[131, 132]</sup>, including the IAK discussed in the previous section.

BioMEMS technology has found itself in a variety of applications related to kidney research and bioengineering. For example, the nephron may be conceptualized as a single albeit somewhat complex microfluidic system, and this has actually been designed and computationally modelled in a system incorporating cells<sup>[138]</sup> and in a system utilizing a smart membrane without cells<sup>[139]</sup>. In practice, recapitulating the filtration function of the glomerulus is much simpler than recapitulating the transport functions of the tubules, and this is exemplified by current artificial RRTs available. BioMEMS may achieve the separation of solutes by employing the unique diffusive transport that occurs across microfluidic channels<sup>[140]</sup> or convective or diffusive transport across semipermeable membranes such as in the IAK<sup>[114, 124, 125]</sup>.

However, BioMEMS and kidney-on-a-chip technologies have demonstrated the potential to transform how researchers study biological systems by incorporating physiologically-relevant fluid flow which imparts a shear stress on cells that may be cultured within these systems<sup>[141]</sup>. Furthermore, these technologies may be scaled for greater throughput, include multi-compartmental setups, or in the future incorporate patient-derived cells for development of therapeutics or nephrotoxicity testing<sup>[142-144]</sup>. Towards this goal, a number of investigators have developed systems with human cells for modeling specific segments of the nephron, including the glomerular filtration barrier<sup>[145, 146]</sup>, the proximal tubule<sup>[127, 147-152]</sup>, and the peritubular capillaries<sup>[153, 154]</sup>. Investigators have also delved into multi-compartmental setups for modeling interactions across multiple segments of the nephron, including glomerular-tubular interactions<sup>[155]</sup> and tubular-vascular interactions<sup>[156]</sup>, as well as across multiple organ systems<sup>[157-159]</sup>. Beyond traditional BioMEMS fabrication techniques, investigators have begun to apply additive manufacturing technologies such as 3D printing for BioMEMS fabrication<sup>[160, 161]</sup> and modeling of the proximal tubule<sup>[162]</sup> and tubular-vascular interactions<sup>[163]</sup>. Despite rapid and exciting advances in the field, BioMEMS still face challenges

that must be addressed for future translational applications and commercialization. Biological challenges include the need for superior biocompatible materials, validation of assays, and *in vitro* to *in vivo* extrapolation<sup>[142]</sup>, whereas engineering challenges include systems integration, standardization, and the overall economics of the proposed application<sup>[164]</sup>.

#### **1.2.4. Whole-Kidney Decellularization and Bioengineering**

In contrast to BioMEMS technologies and the miniaturization of systems, the goal of whole-organ decellularization and bioengineering is to preserve the extracellular matrix (ECM) in its native architecture for use as a biologic scaffold<sup>[165-167]</sup>. Composed of proteins, polysaccharides, and other biological molecules secreted by resident cells, the ECM presents biophysical and biochemical signaling cues that results in dynamic and reciprocal interactions between the ECM and cells, thus regulating the development and maintenance of tissues and organs<sup>[168, 169]</sup> (**Figure 1-3 A**). Tissue- and organ-specific ECM may be isolated through a process known as decellularization in which the tissue or organ of interest is treated with physical processes (*e.g.*, freeze-thaw), chemical agents (*e.g.*, detergents), or biological agents (*e.g.*, enzymes) to remove the native cells<sup>[170-172]</sup>. For the purposes of whole-organ bioengineering, solid organs such as the kidney are perfused through the native vasculature with the desired decellularization agents in order to preserve the 3D structure and architecture of the ECM<sup>[171, 172]</sup>. The resulting decellularized ECM (dECM) scaffold may then be recellularized or repopulated with the desired cells and maintained in a bioreactor to enhance maturation. This process has been successfully demonstrated in a number of organs, including hearts from rats<sup>[173]</sup> and pigs<sup>[174]</sup>, livers from rats<sup>[175, 176]</sup> and pigs<sup>[177]</sup>, and lungs from rats<sup>[178, 179]</sup> and humans<sup>[180]</sup>.

This strategy is thought to be particularly appropriate for the kidney due to the spatial heterogeneity and specific structural features of the organ<sup>[181]</sup>. A number of investigations have focused on establishing optimal perfusion decellularization protocols to produce kidney dECM scaffolds from rodents<sup>[182, 183]</sup>, pigs<sup>[184-188]</sup>, and humans (specifically discarded kidneys deemed unsuitable for transplant purposes)<sup>[189, 190]</sup>. Additional investigations have demonstrated recellularization of scaffolds with various cell types with some evidence of kidney function, including: human umbilical vein endothelial cells and rat neonatal kidney cells

in rat-derived scaffolds<sup>[191]</sup>, induced-pluripotent stem cell-derived endothelial cells or Madin-Darby canine kidney cells in rat-derived scaffolds<sup>[182]</sup>, rat primary renal cells and mesenchymal stromal cells in rat-derived scaffolds<sup>[183]</sup>, and primary porcine renal cells in pig-derived scaffolds<sup>[192]</sup>. There is also significant interest in understanding how kidney dECM scaffolds may influence the response and differentiation of pluripotent stem cells and renal or nephron progenitor cells, and examples of such investigations include mouse embryonic stem cells in rat-derived scaffolds<sup>[193-196]</sup> and human renal progenitor cells in mouse-derived scaffolds<sup>[197]</sup>. However, challenges regarding whole-organ bioengineering still remain before these strategies can be translated to clinical applications. Some outstanding questions include organ source and immunogenicity, standardization of decellularization protocols and scaffolds, identification and expansion of cells (and of various types), and complete recellularization or repopulation of scaffolds including endothelial lining of the vasculature to prevent a thrombogenic response after implantation<sup>[165-167]</sup>.

### **1.2.5. Kidney Organoids**

The term organoid first gained popularity from 1965 to 1985 when it was used to describe classic cell dissociation and reaggregation experiments towards understanding organogenesis and developmental biology<sup>[198]</sup>. The word has recently made a resurgence in scientific literature, although it now refers to a 3D structure derived exclusively from stem cells that 1.) consists of multiple, organ-specific cell types, 2.) is capable of self-organization resembling said organ, and 3.) exhibits some functional capacity of that organ<sup>[198-200]</sup>. The self-renewable stem cells employed may either be pluripotent stem cells (PSCs), which include embryonic stem cells (ESCs) and induced-pluripotent stem cells (iPSCs) that can give rise to all lineages of the body (*i.e.*, endoderm, mesoderm, and ectoderm)<sup>[201]</sup>, or multipotent adult stem cells that can give rise to multiple cell types of one lineage<sup>[198]</sup>. Differentiation of stem cells and generation of organoids generally involves driving stem cell fate towards the desired lineage through exposure with specific soluble signals as informed by developmental biology and then further specification with additional soluble signals and often 3D culture strategies in a matrix environment (*e.g.*, Matrigel) to promote self-organization<sup>[198-200]</sup>. Organoid cultures for numerous tissues and organs have recently been developed, but the most notable examples include gut and intestinal<sup>[202, 203]</sup>, brain<sup>[204]</sup>, and retinal<sup>[205, 206]</sup> organoids.

Researchers were quick to apply these strategies towards the development of kidney organoids, and multiple groups have described the differentiation of pluripotent stem cells into nephron progenitor cells of metanephric mesenchyme origin<sup>[207, 208]</sup> and ureteric bud-committed progenitor cells<sup>[209]</sup> that give rise to the tubules and collecting duct, respectively. However, Takasato *et al.*, were able to successfully induce both metanephric mesenchyme and ureteric bud progenitor populations simultaneously and generate kidney organoids with both tubular and collecting duct structures<sup>[210-212]</sup>. Currently, many researchers refer to aggregates of metanephric mesenchyme-derived nephron progenitor cells that result in the formation of tubular structures expressing markers for podocytes, proximal tubules, and distal tubules as “kidney organoids”, despite the lack of expression for ureteric bud-derived cell markers, *i.e.*, collecting duct markers<sup>[213, 214]</sup>; however, for the purposes of this review, this distinction will be disregarded. Interestingly, it has been shown that co-culture of independently differentiated metanephric mesenchyme-derived nephron progenitor cells and ureteric bud-committed progenitor cells results in self-organized kidney organoids with a branching collecting duct system<sup>[215]</sup>. Since the establishment of kidney organoid differentiation protocols, several investigations have been published demonstrating the potential of kidney organoids in modeling kidney injury and disease<sup>[216-219]</sup>. More recently, there have been efforts to scale-up the production of kidney organoids to facilitate high-throughput screening processes and production of kidney cell types for other biomedical applications<sup>[220, 221]</sup>. Future challenges in kidney organoid research include vascularization of organoids, necessary for filtration function as well as supplying nutrients to thicker and denser organoids, and coalescence of collecting ducts into a single ureter for drainage<sup>[222]</sup>. On the issue of vascularization, a few investigations have demonstrated the ability of kidney organoids to induce invasion of host vasculature when implanted beneath mouse kidney capsules<sup>[223]</sup> or into chick chorioallantoic membranes<sup>[224]</sup>. Additional investigations have revealed the importance of fluid flow and shear stress in promoting vascularization and maturation of kidney organoids using a microfluidic system<sup>[225]</sup>. These results suggest that in moving forward bioengineering strategies may be pivotal in translation of kidney organoid technologies into patient therapies.

### 1.3. Hydrogels as Extracellular Matrix Mimics for Bioengineered Kidney Tissues

Although examples of hydrogels may be found in many different fields and applications, there is particular interest in hydrogels for biomedical applications<sup>[226]</sup>, including regenerative engineering<sup>[227-229]</sup> and drug delivery<sup>[230, 231]</sup>.

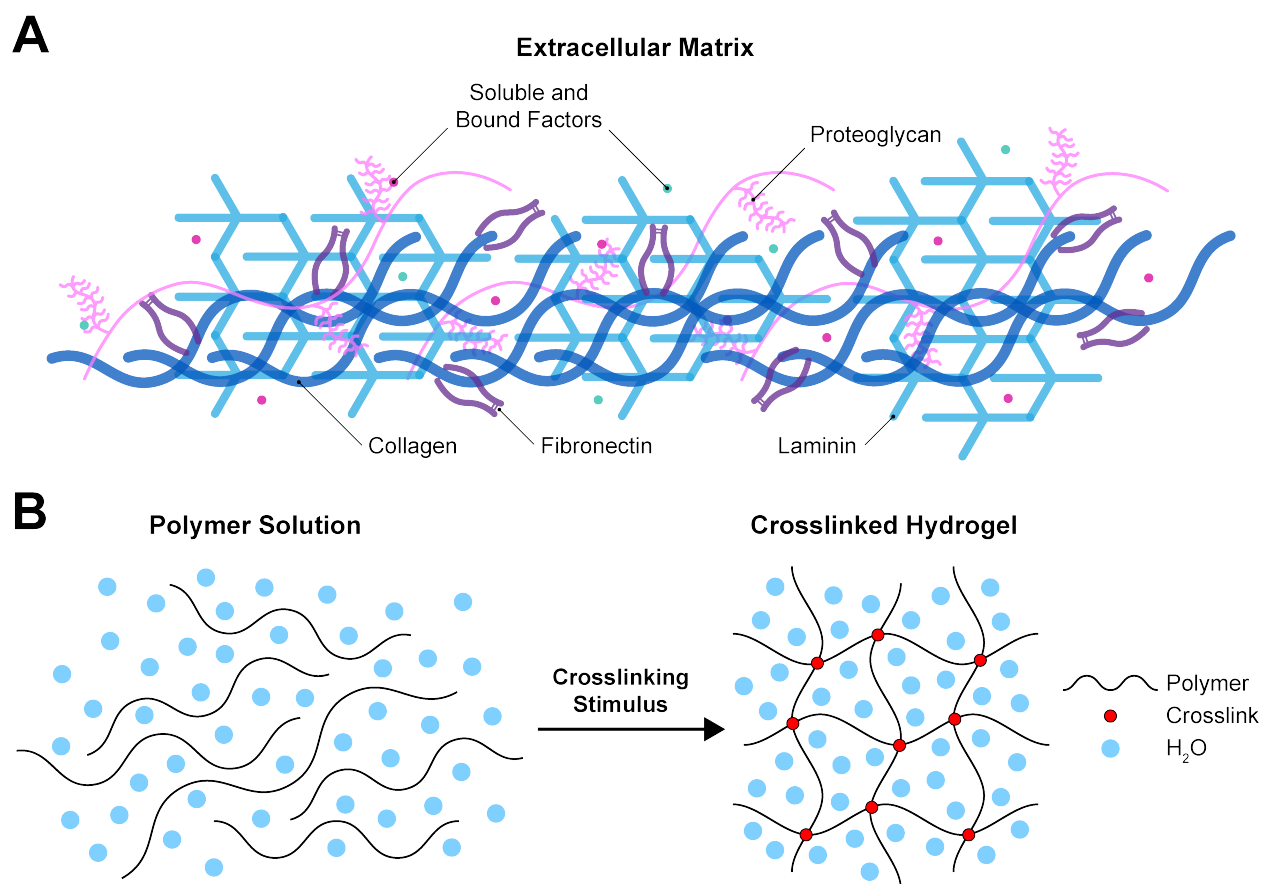


**Figure 1-3: Schematics of the extracellular matrix (ECM) and hydrogel crosslinking.**

(A) The ECM is composed of a variety of proteins, polysaccharides, and other molecules secreted by cells. While ECM composition varies widely throughout the body, typical components include collagens, fibronectins, laminins, and proteoglycans. The ECM may also bind to and sequester growth factors and other signaling molecules that can influence cell response. (B) Crosslinking of polymer solution results in the formation of a swollen hydrogel network. Possible crosslinking stimuli include temperature, pH, light, small molecules or enzymes, etc.

### 1.3.1. Properties of Hydrogels

Hydrogels are crosslinked or interconnected polymer networks with the ability to absorb generous amounts of water, generally 70% or greater by weight (**Figure 1-3 B**). The swelling behavior and stiffness of a hydrogel are influenced by its network structure, which may be quantitatively described by structural or molecular parameters, specifically: the polymer volume fraction in the swollen state ( $v_{2,s}$ ), the average molecular weight between crosslinks ( $\overline{M}_c$ ), and the correlation length ( $\xi$ ) or the related measure of distance between crosslinks (*i.e.*, mesh or pore size)<sup>[232]</sup>. These structural parameters may be tuned during polymer synthesis or crosslinking, thus allowing for tight control of the resulting hydrogel properties. In addition, the highly-hydrated environment of hydrogels enables facile transport of nutrients and waste throughout the network, making hydrogels the only materials permissible for cell encapsulation<sup>[233]</sup>. Furthermore, hydrogels may be specifically designed and engineered to mimic the native ECM by tailoring the network's physical and chemical properties<sup>[234-236]</sup>. And with continued advances in chemistry, materials science, and engineering, there will be a continued movement towards the development of hydrogels able to truly recapitulate the dynamic nature of the ECM<sup>[237, 238]</sup>.

### 1.3.2. Crosslinking Methods for Hydrogel Network Formation

Crosslinking methods for formation of hydrogels may be broadly categorized into physical and chemical methods. Physically-crosslinked hydrogels rely on physical interactions between polymer chains that result in network formation. These physical interactions may include polymer chain entanglements, ionic interactions, hydrogen bonds, or hydrophobic interactions<sup>[239]</sup>. Shear-thinning and self-healing hydrogels are examples of hydrogels that rely on physical interactions for their unique behavior<sup>[240]</sup>. These types of hydrogels are particularly useful for specific applications such as injectable systems or direct extrusion-based 3D printing<sup>[240-242]</sup>. Furthermore, physically-crosslinked hydrogels generally do not require chemical modifications or addition of crosslinking initiators *in situ*. However, it is difficult to tune hydrogel properties such as gelation time, network structure, stiffness, and degradation rate independently, and degradation rates of physically-crosslinked hydrogels are often much more rapid due to the nature of transient physical interactions<sup>[231]</sup>.

Chemically-crosslinked hydrogels, on the other hand, rely on covalent interactions between polymer chains resulting in a more permanent network structure. In the past, formation of chemical crosslinks have relied on the use of small molecules or enzymes to catalyze reactions between available side groups, radical polymerization reactions, or reactions between pre-functionalized polymer chains<sup>[231, 239]</sup>. While these methods of crosslinking enable greater tunability in hydrogel design and properties in comparison to physically-crosslinked hydrogels, they are often detrimental to cell viability or result in toxic byproducts that must be removed<sup>[231]</sup>, thus limiting their versatility in application. However, with the rapid expansion and utilization of click chemistries, there has been a push towards engineering truly bioorthogonal hydrogel systems<sup>[243-246]</sup>. Of course, hydrogel networks are not limited to physical or chemical crosslinks only, and a combination of crosslinking methods are often desirable and may depend on the materials and applications.

### **1.3.3. Materials for Hydrogels**

Biocompatible materials, or biomaterials, for hydrogels may be broadly categorized into natural and synthetic materials based on their source of origin. Natural materials are derived from renewable resources found in nature, including animals and plants, or may be produced recombinantly. The use of natural materials for hydrogels is befitting because many natural materials are components of the native ECM, which means that they are biocompatible, biodegradable, and bioactive (*i.e.*, inherently promote cell interactions such as binding and degradation). Natural materials also present functional groups for additional chemical modifications, if desired, and many natural materials may be crosslinked through physical interactions which are generally cytocompatible<sup>[228, 247]</sup>. Natural materials commonly utilized for hydrogels may be further subdivided into proteins and polysaccharides. Proteins may be considered polymer chains composed of amino acids, and example proteins for hydrogels include collagen<sup>[248]</sup> and its derivative gelatin<sup>[249]</sup>, fibrin/fibrinogen<sup>[250]</sup>, elastin<sup>[251]</sup>, keratin<sup>[252]</sup>, silk fibroin<sup>[253]</sup>, and soy<sup>[254]</sup> and other plant-based proteins<sup>[255]</sup>. Polysaccharides are polymeric carbohydrate structures, and example polysaccharides for hydrogels include alginate<sup>[256]</sup>, agarose<sup>[257]</sup>, chitosan/chitin<sup>[258]</sup>, dextran<sup>[259]</sup>, hyaluronic acid/hyaluronan<sup>[260]</sup> and other glycosaminoglycans<sup>[261]</sup>, cellulose<sup>[262]</sup>, and starch<sup>[263]</sup>. In addition to purified

materials, methods have also been developed to process tissue- and organ-specific dECM into hydrogels containing a combination of proteins, polysaccharides, and other molecules present in the native ECM<sup>[264]</sup>. While there are numerous options available for natural material-based hydrogels, they face disadvantages such as possible batch-to-batch variability based on the source, limitations in processing (due to possible denaturation or degradation), and the inability to independently control hydrogel stiffness and degradation for those that rely on physical crosslinking mechanisms<sup>[247]</sup>.

In contrast to natural materials, synthetic materials can be synthesized reproducibly and with controlled molecular structures (e.g., molecular weight, copolymers, linear versus multi-arm versus grafted structures). This allows for greater tunability of the resulting network and hydrogel properties, such as mechanical properties, rate of degradation, and the ability for biofunctionalization<sup>[228, 247]</sup>. A variety of synthetic materials have been developed and utilized for hydrogels, and some examples include poly(ethylene oxide) or poly(ethylene glycol), poly(acrylic acid) and polyacrylamide, and poly(vinyl alcohol)<sup>[226-229, 247]</sup>. However, due to their inherent lack of bioactive sites for cell interaction, it is technically challenging to replicate the complexity of the native ECM through the use of only synthetic materials<sup>[247]</sup>. Semi-synthetic hydrogels produced through molecular or protein engineering systems<sup>[234]</sup>, semi-synthetic hydrogels composed of or including natural materials but produced through synthetic processes such as peptide- or polypeptide-based hydrogels<sup>[265]</sup>, self-assembling peptide amphiphile hydrogels<sup>[266]</sup>, and nucleic acid-based hydrogels<sup>[267]</sup>, and natural-synthetic hydrogel blends<sup>[268]</sup> are promising methods to bridge this gap<sup>[247]</sup>.

#### **1.3.4. Review of Hydrogel Platforms for Modeling Kidney Function Towards Engineered Kidney**

##### ***Tissues***

Hydrogels exhibit ideal properties that mimic the nature of the native ECM, and with the variety of methods for crosslinking, materials available, and capacity for modifications and tailorability, hydrogel platforms have been readily employed in a number of regenerative engineering and modeling applications, including those focused on the kidney. For example, because of these properties, White and Deen investigated the permeability of agarose-dextran hydrogels as analogs of the glomerular basement

membrane<sup>[269]</sup>. But in order to better design hydrogel platforms for engineering kidney tissue models, it is important to understand hydrogel biophysical and biochemical properties that influence cell response. In particular, it has become well established that substrate stiffness contributes to the regulation of cell adhesion and spreading<sup>[270]</sup> and even stem cell differentiation<sup>[271]</sup>. Recent studies have demonstrated that this is no exception for cell types of the kidneys. Human renal proximal tubular epithelial cells exhibited increased spreading and proliferation when cultured on type IV collagen-conjugated poly(ethylene glycol) diacrylate hydrogel substrates of increasing stiffness<sup>[272]</sup>, although human renal epithelial cells showed increased expression of key transporters when cultured on softer, Geltrex-coated polyacrylamide hydrogel substrates for extended periods<sup>[273]</sup>. Similarly, human podocytes exhibited enhanced gene and protein expression when cultured on transglutaminase-crosslinked gelatin hydrogel substrates of an optimal stiffness<sup>[274]</sup>. In addition, it was recently demonstrated that kidney organoids undergo enhanced differentiation when cultured on softer, vitronectin-coated polyacrylamide hydrogel substrates<sup>[224]</sup>. These investigations may inform future ones, especially in applications in which hydrogels are utilized as substrates for cell culture.

Hydrogel substrates may serve as models of the basement membrane<sup>[36]</sup>, and specifically Matrigel or Geltrex are often employed as a commercially-available basement membrane matrix source<sup>[275]</sup>. As an example, Kitahara *et al.* utilized Matrigel as a substrate to investigate the influence of human mesangial cells on capillary-like network formation by human umbilical vein endothelial cells<sup>[276]</sup>. However, as a natural material derived from murine carcinoma, Matrigel is limited by its complex and poorly-defined composition as well as its lack of tunability. Furthermore, even within the kidney, basement membrane structures may vary in composition and properties based on the overlying cell populations<sup>[277]</sup>, which highlights the importance of targeted hydrogel design. For example, O'Neill *et al.* demonstrated that regional specificity (*i.e.*, cortical, medullary, papillary) of kidney dECM hydrogel substrates regulated mouse kidney papilla-derived stem cell growth and metabolism<sup>[278]</sup>. Magno *et al.* further illustrated that the fibrillar architecture of kidney dECM hydrogels may be modulated through incorporation of macromolecular crowders, leading to changes in morphogenesis by human umbilical vein endothelial cells and by mouse kidney papilla-derived stem cells<sup>[279]</sup>. A more recent investigation by Su *et al.* demonstrated that conjugation of bioactive peptides

to poly(ethylene glycol)-crosslinked gelatin hydrogel substrates influenced gene expression of both human umbilical vein endothelial cells as well as GEnCs, although the responses of these endothelial cell types was distinctly different from each other<sup>[280]</sup>. Bruggeman *et al.* specifically designed hydrogel membranes by horseradish peroxidase-catalyzed crosslinking of tyramine-substituted gelatin for mimicking capillary walls and demonstrated coculture of mouse GEnCs and podocytes as a model of the glomerular filtration barrier<sup>[281]</sup>.

Hydrogel substrates have also become more common for the construction of BioMEMS as researchers move from the traditional polydimethylsiloxane-based devices. Construction of these devices have included injection of type I collagen into polydimethylsiloxane chambers and subsequent collagen polymerization<sup>[149-151]</sup>, molding of type I collagen and kidney cortical dECM hydrogels<sup>[154, 156, 282]</sup>, and casting of a fibrinogen-gelatin thrombin- and transglutaminase-crosslinked hydrogels for modeling proximal tubules and tubular-vasculature interactions<sup>[162, 163]</sup>. Interestingly, additional studies verified that the fibrinogen-gelatin thrombin- and transglutaminase-crosslinked hydrogel formulation promoted the desired adhesion of immature kidney organoids for construction of a millifluidic chip whereas glass, tissue culture polystyrene, fibrin hydrogels, and fibrin-type I collagen hydrogels were deemed unsuitable<sup>[225]</sup>.

As mentioned previously, hydrogels are the only class of materials permissible to cell encapsulation. These truly three-dimensional microenvironments can alter cell behavior and function, resulting in cell responses not observed in traditional 2D cultures. For example, there have been numerous investigations surrounding epithelial and endothelial cell morphogenesis within type I collagen hydrogels, such as the formation of cysts by Madin-Darby canine kidney cells<sup>[283]</sup> and capillary-like structures by human umbilical vein endothelial cells<sup>[284]</sup>. Because hydrogels recapitulate the nature of the native ECM, these 3D cultures represent superior models for investigations of developmental and cell biology and further advance the path towards engineering complex tissues and organs<sup>[235]</sup>. Beyond investigations utilizing readily-available Madin-Darby canine kidney cells, Astashkina *et al.* established a kidney tubule-based model from primary mouse proximal tubule epithelial cells encapsulated within hyaluronic acid-poly(ethylene glycol) diacrylate hydrogels for toxicity assays of nephrotoxic agents<sup>[285]</sup> and dendrimer and gold nanoparticles<sup>[286]</sup>. Similarly, DesRochers *et al.* developed a kidney tissue model for nephrotoxicity evaluation using

immortalized human renal cortical epithelial cells encapsulated within combination hydrogels of Matrigel and type I collagen<sup>[287]</sup>. On the other side focusing on the glomerulus, Su *et al.* investigated the response of human GEnCs to encapsulation within hydrogels and interestingly observed superior gene expression by cells encapsulated in control type I collagen hydrogels in comparison to cells encapsulated in kidney dECM hydrogels<sup>[288]</sup>. Towards understanding disease progression, Waters *et al.* developed a tri-culture system including human glomerular endothelial cells, mesangial cells, and podocytes encapsulated within type I collagen hydrogels to model glomerulosclerosis<sup>[289]</sup>. These studies are compelling but are still limited in modeling truly functional kidney tissues. Future studies will certainly follow that continue to advance hydrogel design and development towards engineering complex kidney tissues.

#### **1.4. Conclusion**

Research and development within the interdisciplinary field of biological and biomedical engineering offer potential solutions to develop superior renal replacement therapies, treatments to prevent or even reverse disease progression, and hopefully eliminate the donor kidney shortage and transplant waitlist. However, to reach such a significant goal will require the coalescence of well-defined and characterized cell populations, advanced biomaterials, and microenvironmental signaling cues to promote and maintain desired cell phenotypes. Future advanced biomaterials, including biomaterial hydrogel systems or platforms, will likely include bioorthogonal and stimuli-responsive strategies for comprehensive and dynamic tunability to enable precise spatial and temporal control of biophysical and biochemical signaling cues. Concurrent cell-based studies will reveal cell-material or cell-matrix and cell-cell interactions, thus informing future design needs and parameters for modulating cell response. Finally, in combination with advances in stem cell technologies and increasing adoption of advanced biomanufacturing techniques, there will be the progression towards dense, multicellular constructs fabricated with controlled structures and architectures. Future obstacles will then include proper maturation of engineered constructs, if necessary, and evaluation of engineered tissue or organ function. Although challenges still remain, research investigations and discoveries over the past several decades have created

a strong foundation and expansive toolkit for engineering of complex and functional tissues and organs, including the kidney.

**CHAPTER II:**

**Development and Characterization of Kidney Decellularized Extracellular Matrix Hydrogels  
and Evaluation as a Platform for Glomerular Endothelial Cell Culture and Encapsulation**

Chapter 2, in part, has been published elsewhere: <sup>[288]</sup> Su J, Satchell SC, Shah RN, and Wertheim JA. "Kidney decellularized extracellular matrix hydrogels: Rheological characterization and human glomerular endothelial cell response to encapsulation." *Journal of Biomedical Materials Research Part A* **106A** (2018): 2448-2462.

## 2.1. Introduction

Approximately 15% of the adult population in the United States is affected by chronic kidney disease<sup>[290]</sup>, and this percentage is expected to increase both in the United States and worldwide, especially in countries with aging populations and increasing prevalence of hypertension and diabetes mellitus<sup>[291]</sup>. Current approaches to modeling kidney development and disease progression include cell culture, animal models, and stem cell-derived organoids<sup>[72]</sup>. Traditional cell culture using two-dimensional (2D), monolayer systems are still widely utilized though they lack critical structural signaling cues found in the native three-dimensional (3D) microenvironment<sup>[292, 293]</sup>. In comparison, animal models, specifically transgenic mouse models, enable superior correlation between genotype and phenotype with the added capacity to directly measure renal function<sup>[294-296]</sup>; however, animal models lack utility in efficient, high-throughput drug screening and have inherent limitations in recapitulating human disease<sup>[297]</sup>. More recently, advances in stem cell research have led to the development of organoids for a variety of organ systems<sup>[198-200]</sup>, including the kidney<sup>[208, 211, 213]</sup>. However, organoid research is still evolving and additional investigation is required before organoids reach translational potential. Therefore, there is a compelling need for bioengineered kidney tissues as models of development, disease progression, or drug discovery to better understand and prevent the onset of chronic kidney disease and the progression to end-stage renal disease.

Traditional tissue engineering strategies rely on biocompatible materials processed into porous scaffolds for cell seeding and attachment<sup>[298-300]</sup>; however, many of the early materials utilized such as poly-lactic-*co*-glycolic acid or poly- $\epsilon$ -caprolactone only provide mechanical support and structure for cell-seeded constructs<sup>[301]</sup>. Within the *in vivo* physiological environment, cells are surrounded by cell-secreted products collectively referred to as the extracellular matrix (ECM). The ECM is well-known for its role as a support structure and imparting mechanical integrity to tissues and organs; however, the ECM also presents

bioactive signals to cells that regulate development and maintenance<sup>[168, 302, 303]</sup>. By design, the ECM acts as a natural, inductive scaffold that in many ways is analogous to a composite and stimulus-responsive hydrogel<sup>[235, 236]</sup>.

Hydrogels are crosslinked networks of polymers that have demonstrated considerable potential as a 3D cell culture platform<sup>[226-228, 235, 236]</sup>. The polymeric network and highly hydrated environment of hydrogels mimic the microstructure and mechanical properties of ECM and enable diffusion of oxygen, nutrients, and waste through the network<sup>[235, 236]</sup>. Furthermore, many hydrogels can be formed under mild, cytocompatible conditions amenable to cell encapsulation<sup>[227, 228]</sup>. Hydrogels derived from isolated components of the ECM such as collagen or gelatin are utilized in drug delivery, cell transplantation, and tissue engineering applications<sup>[304, 305]</sup>. These single- or even multi-component hydrogels, however, lack the full biochemical complexity of the entire ECM milieu. As research regarding tissue- and organ-derived decellularized ECM (dECM) has gained popularity, investigators have developed methods to process a variety of dECM materials into hydrogels for cell culture applications and minimally-invasive injectable therapies<sup>[264]</sup>. While dECM hydrogels derived from some tissue and organ systems, such as the heart<sup>[306-309]</sup>, liver<sup>[310-312]</sup>, and skeletal muscle<sup>[308, 313-315]</sup> have been the focus of several publications, other tissues and organs, for example the kidney, have received little investigation.

The objective of this study was to develop kidney dECM hydrogels as a cell culture platform for bioengineered kidney tissue models and compare cell response to traditional biomaterials such as collagen hydrogels. Here, we present a method to process kidney dECM into physically crosslinked hydrogels as a substrate for cell culture or a 3D matrix for cell encapsulation. Routine histology (hematoxylin and eosin staining) and DNA quantification demonstrated the efficacy of the kidney decellularization process while immunofluorescence staining revealed retention of key ECM proteins. Rheological characterization of the hydrogels illustrated the time to gelation and measured the plateau shear moduli.

To evaluate the utility of these kidney dECM hydrogels for studies employing kidney-specific cell populations, we investigated the cell response of conditionally-immortalized glomerular endothelial cells (GEnCs) cultured on top of and encapsulated within hydrogels. The conditionally-immortalized GEnCs are a cell line generated from endothelial cells specifically isolated from kidney glomeruli<sup>[316]</sup>. These endothelial

cells form the capillary loops through which blood flows and is filtered, forming the first layer of the glomerular filtration barrier responsible for the filtering function of the kidney<sup>[11]</sup>. Primary GEnCs are difficult to isolate and expand in culture due to the loss of important phenotypic features with increasing passage number<sup>[316]</sup>. However, the conditionally-immortalized cell line utilized in this study combines the advantage of continuous cell expansion and passaging when cultured at the permissive temperature while retaining the ability to acquire a mature phenotype when thermoswitched to the non-permissive temperature.

Culture of GEnCs on top of hydrogel substrates confirmed favorable cell viability and proliferation over a twelve-day culture period. Encapsulation of GEnCs within these hydrogel matrices, which has not been previously investigated by others, resulted in favorable cell viability and proliferation during a week in culture, but evaluation of gene expression demonstrated lower fold-change expression for cells encapsulated in kidney dECM hydrogels compared to type I collagen hydrogels.

## **2.2. Materials & Methods**

### **2.2.1. Kidney Decellularization**

Female Yorkshire pig (3-4 months in age) kidneys were obtained fresh from Northwestern Simulation (Northwestern University Feinberg School of Medicine) following approval by the Northwestern Institutional Animal Care and Use Committee (IACUC) and stored at -80 °C until decellularization. Prior to decellularization, kidneys were thawed for several hours in warm water and then minced into pieces approximately 0.5 cm × 0.5 cm × 0.25 cm in size with a clean razor blade. During this process, the majority of the renal pelvis and perirenal fat was removed. Kidney tissue pieces were then rinsed with deionized H<sub>2</sub>O under constant stirring for one day at room temperature with intermittent H<sub>2</sub>O changes. After rinsing, kidney pieces were treated with 0.1% (m/v) sodium dodecyl sulfate (Sigma-Aldrich, #L3771) under constant stirring for two days. Afterwards, decellularized kidney pieces were rinsed with deionized H<sub>2</sub>O under constant stirring for one day with intermittent H<sub>2</sub>O changes to ensure removal of residual detergent from the tissue. The resulting kidney dECM was frozen at -80 °C until further processing.

## **2.2.2. Evaluation and Characterization of Decellularized Kidney Tissues**

*Histological Analysis.* Fresh native and decellularized kidney tissues were fixed in 10% neutral-buffered formalin (Thermo Scientific, #5701) for at least 48 hours before paraffin embedding and sectioning. For histological analysis, sections were deparaffinized in xylene (Fisher Scientific, #X3P) and rehydrated prior to staining with Mayer's hematoxylin solution (Sigma-Aldrich, #MHS) and eoson Y solution (Sigma-Aldrich, #HT110132) (H&E). After staining, #1 glass coverslips (Fisher Scientific, #12-542B or #12-545D) were mounted with Richard-Allan Scientific Cytoseal XYL (Thermo Scientific, #8312-4). Slides were imaged on a Zeiss Axioskop upright microscope mounted with a Zeiss AxioCam MRc5 camera using AxioVision 4.8.3 software.

*DNA Quantification.* Native and decellularized kidney tissue pieces were lyophilized for at least two days on a VirTis advantage Plus EL-85, and the dry weight of samples was recorded. Tissue samples were digested with Proteinase K (Sigma-Aldrich, #P2308) in digestion buffer composed of 0.05 M Tris base (Sigma-Aldrich, T#1503), 1 mM CaCl<sub>2</sub> (Sigma-Aldrich, #C5670), pH 8 at 60 °C overnight. DNA was quantified with the Quant-iT PicoGreen dsDNA Assay Kit (Invitrogen, #P7589) following the manufacturer's protocol and a dsDNA standard included in the kit to generate a standard curve. Fluorescence was measured on a BioTek Cytation 3 Cell-Imaging Multi-Mode Reader with an excitation wavelength of 480 nm and emission wavelength of 520 nm. Biological replicates were run in triplicate ( $n = 3$ ) with technical replicates in triplicate. DNA content was normalized to the dry weight of the sample, and data is presented as a percentage of native kidney tissue DNA content.

*Immunofluorescence Staining.* Paraffin-embedded sections were deparaffinized and rehydrated before antigen retrieval in a BioCare Medical Decloaking Chamber™ NxGen (model no. DC2012) at 95 °C for 40 min. with antigen retrieval buffer (Abcam, #ab94674). Sections were rinsed with 1× Phosphate-Buffered Saline (PBS, Mediatech, #21-040), permeabilized with 0.05% TWEEN-20 (Sigma-Aldrich, #P9416) for 10 min., and then blocked with SEA BLOCK Blocking Buffer (Thermo Scientific, #37527) for 30 min. before incubation with primary antibodies. Primary antibodies were diluted in blocking buffer as follows: rabbit anti-collagen I at 1:100 (Abcam, #ab34710), rabbit anti-collagen IV at 1:500 (Abcam, #ab6586), and rabbit anti-laminin at 1:200 (Abcam, #ab11575). Sections were incubated with primary

antibodies for 1 h at room temperature, rinsed, and then incubated with secondary antibodies for 1 h at 37 °C (goat anti-rabbit Alexa Fluor 488, Invitrogen, #A-11034, diluted 1:300 in blocking buffer). After secondary antibody incubation, sections were rinsed and coverslips were mounted with Mowiol mounting medium composed of Mowiol 4-88 Reagent (Calbiochem, #475904), glycerol (EMD Millipore, #137028), and 0.2 M Tris buffer (pH 8.5, Fisher Scientific, #BP152) containing 4',6-diamidino-2-phenylindole (DAPI, Invitrogen, #D1306) to stain for cell nuclei. Slides were imaged on a Nikon A1 Confocal Laser Microscope System.

*Sulfated Glycosaminoglycan Quantification.* Sulfated glycosaminoglycan (sGAG) content was quantified using the 1,9-dimethyl-methylene blue (DMMB) dye assay. Tissue samples were digested with Proteinase K as described previously in section 2.2.2. – *DNA Quantification.* DMMB dye solution was prepared by dissolving 8.0 mg DMMB dye (Sigma-Aldrich, #341088), 1.52 g glycine (Sigma-Aldrich, #G-8898), and 1.19 g NaCl (Fisher Scientific, #S642) in 500 mL ultrapure water and adjusting the pH to 3.0. Samples were diluted as necessary in 1× Tris-EDTA buffer (Invitrogen, #T1493), and 20 µL of sample was mixed with 200 µL of DMMB dye solution in clear, 96-well plates. Absorbance was measured on a BioTek Cytation 3 Cell-Imaging Multi-Mode Reader at 530 nm ( $A_{530}$ ). Biological replicates were run in triplicate ( $n = 3$ ) with technical replicates in duplicates, compared to a standard curve of chondroitin sulfate (Biocolor, #B1010), and normalized to dry weight of samples.

### **2.2.3. Preparation and Characterization of Hydrogels from Kidney Decellularized Extracellular**

#### ***Matrix***

*Preparation of Kidney dECM Hydrogels.* Kidney dECM hydrogels were prepared similarly to previously described protocols for other decellularized tissues<sup>[317]</sup>. Briefly, frozen kidney dECM was lyophilized for two days, snap frozen, and milled with a Thomas Wiley Mini-Mill Cutting Mill. Milled dECM was enzymatically digested at 10 mg/mL kidney dECM, 1 mg/mL pepsin (Sigma-Aldrich, #P7000), and 0.01 M HCl (Sigma-Aldrich, #H9892) for 48 h. The resulting pepsin digest was aliquoted and frozen at -80 °C. Aliquots were thawed overnight at 4 °C as needed for experiments. Hydrogel precursor polymer solutions were prepared by neutralizing the pepsin digest with one-hundredth the volume of 1.0 M NaOH (Sigma-

Aldrich, #S2770), adding one-tenth of the total volume desired of 10× phosphate-buffered saline (PBS, Mediatech, #46-013-CM) to achieve a final concentration of 1×, and diluting the mixture with sterile MilliQ H<sub>2</sub>O. The final hydrogel was formed after incubating the precursor polymer solution at 37 °C for at least one hour. Collagen hydrogels were prepared similarly from purified porcine type I atelo-collagen (Advanced BioMatrix, #5169-100ML) as controls for experimental studies.

*Rheological Characterization.* Rheological characterization of hydrogels was performed following a protocol suggested for hydrogels for tissue engineering applications<sup>[318]</sup>. Testing was performed using an Anton Paar MCR 302 rheometer with a 25-mm parallel-plate fixture under strain-controlled conditions. All samples were prepared fresh, and the lower Peltier cell was set to 4 °C for sample loading. After the hydrogel precursor polymer solution was loaded onto the instrument, the measuring system was lowered, and mineral oil (Amresco, #J217) was applied to the edges of the sample and fixture, and the system was enclosed within a solvent trap to prevent sample dehydration. For frequency and strain sweeps, samples were incubated on the instrument stage at 37 °C for 30-45 min to allow hydrogel formation before testing. Final time sweeps were performed for 120 min at 37 °C, 0.1% strain, and 10 rad/s. All sweeps were run in triplicate ( $n = 3$ ).

*Scanning Electron Microscopy (SEM).* Hydrogels were fixed in 2% (v/v) glutaraldehyde (Sigma-Aldrich, #G5882) and 3% (m/v) sucrose (Sigma-Aldrich, #S7903) in MilliQ H<sub>2</sub>O for 1 h. Samples were dehydrated in a graded ethanol series (30-100% in MilliQ H<sub>2</sub>O, Decon Laboratories, #2701) of 15 min intervals, critical-point dried in a Tousimis SAMDRI-790 Critical Point Dryer, sputter coated with ~5 nm of Au using a Baltec MED-020 Coating System, and imaged on a JEOL NeoScope JCM-6000PLUS.

#### **2.2.4. Cell Culture and Cell Experimental Studies**

*Cell Culture.* Human conditionally-immortalized GEnCs were cultured as described previously<sup>[316]</sup>. These are primary cells that have been transfected with a temperature-sensitive *SV40-T* antigen and the essential catalytic subunit of human telomerase (*hTERT*) to avoid replicative senescence<sup>[319]</sup>. When cultured at the permissive temperature of 33 °C at which expression of these transgenes is active, the cells maintain an immature state and are able to proliferate. When thermoswitched to the non-permissive

temperature of 37 °C, the cells become quiescent and adopt a more mature phenotype that is comparable to freshly isolated GEnCs. Conditionally-immortalized GEnCs were cultured in Microvascular Endothelial Growth Medium 2 (EGM-2 MV BulletKit, Lonza, #CC-3202) containing 5% fetal bovine serum (FBS) and growth factors as supplied with the exception of vascular endothelial growth factor (VEGF). Growth factor supplements: epidermal growth factor, R3-insulin-like growth factor-1, fibroblast growth factor  $\beta$ , ascorbic acid, hydrocortisone, and gentamicin and amphotericin-B. Media was exchanged every other day for GEnCs, and cells were used at passage 30 or below. GEnCs were cultured for at least five days after thermoswitching to the non-permissive temperature to ensure complete inactivation of the transgenes.

*Culture on Hydrogel Substrates.* Hydrogel precursor polymer solutions were mixed, cast into well-plates, and incubated at 37 °C for 1 h. Cells were then prepared for cell seeding: the cells were rinsed once with 1× Dulbecco's Phosphate-Buffered Saline (DPBS, Mediatech, #21-030), incubated with TrypLE Express (Gibco, #12605-028) for 5 min at 33 °C, collected and counted via the trypan blue exclusion method using Trypan Blue solution (Sigma-Aldrich, #T8154), centrifuged at 1100 RPM for 5 min, and resuspended at a concentration of 50,000 cells/mL. Cells were then seeded on top of hydrogel substrates and cultured for one week at 33 °C plus an additional five days at 37 °C.

*Cell Encapsulation Within Hydrogels.* Well-plates were coated with poly(2-hydroxyethylmethacrylate) (poly(2-HEMA); Sigma-Aldrich, #P3932) at least one day prior following established protocols to prevent cell attachment to the well-plate surface<sup>[320, 321]</sup>. Briefly, poly(2-HEMA) was added to 95% (v/v) ethanol at a concentration of 30 mg/mL at 40-60 °C under constant stirring until dissolved and then sterile filtered through a polyethersulfone mesh with a pore size of 0.22  $\mu\text{m}$  (EMD Millipore, #SCGP00525). Sufficient volume of the poly(2-HEMA) solution was added to cover the well surface, and the solution was allowed to evaporate overnight in a biosafety cabinet. To encapsulate cells, cells were dissociated as described previously and counted. The appropriate volume of cell suspension was aliquoted to obtain the necessary number of cells for encapsulation at the desired cell density or concentration. The cell suspension was then centrifuged, and pellets were resuspended in a minimal volume of media. Hydrogel precursor polymer solutions were then prepared and mixed, and concentrated cell suspensions were added and mixed in with the precursor polymer solutions to achieve the desired final

concentration. Solutions with encapsulated cells were then cast into well-plates and incubated at 37 °C for at least 1 h before media was added on top of hydrogels and plates were transferred to 33 °C. GEnCs encapsulated at an initial concentration of 1 million cells/mL were cultured in complete EGM-2 MV media with the exception of the VEGF supplement whereas cells encapsulated at 5 million cells/mL were cultured in Endothelial Basal Medium 2 (EBM-2, Lonza, #CC-3156) supplemented with 5% FBS, gentamicin, and amphotericin-B.

### **2.2.5. Cell Viability and Proliferation**

*Cell Viability Imaging.* Cell viability was assessed with the LIVE/DEAD Assay Viability/Cytotoxicity Kit for Mammalian Cells (Molecular Probes, #L3224) following the manufacturer's protocol. Briefly, samples were rinsed once with 1× DPBS and incubated with 4.0 μM ethidium homodimer and 2.0 μM calcein in 1× DPBS for 30 min at 33 or 37 °C. Samples were rinsed once more with 1× DPBS and immediately imaged on a Nikon A1R+ Confocal Laser Microscope System.

*Quantification of Cell Viability.* Live/dead images were separated by channel and images were analyzed in MATLAB R2017a (Mathworks) to quantify cell viability. Image pairs were loaded into the software and converted to grayscale, and objects in the images were counted using a fast two-dimensional peak finder function available on the Mathworks File Exchange website (fastpeakfind.m) that locates local maxima in arrays after applying a threshold. Quantification of cell viability was calculated as follows:

$$\% \text{ viable cells} = \frac{\text{live cell count}}{(\text{live cell count}) + (\text{dead cell count})} * 100\%$$

Four independent samples ( $n = 4$ ) were stained for each experimental group and time point, and three fields-of-view were imaged per sample for a total of twelve images per experimental group per time point.

*Cell Proliferation.* Samples were digested with Proteinase K digestion buffer as described previously in section 2.2.2. – *DNA Quantification.* DNA was quantified with the Quant-iT PicoGreen dsDNA Assay Kit (Invitrogen, #P7589) following the manufacturer's protocol and a dsDNA standard included in the kit to generate a standard curve. Samples for cell proliferation studies were run in quadruplicate ( $n = 4$ ). Double-stranded DNA content was quantified from cell pellets of 50,000 cells as counted using the trypan

blue exclusion method to determine the amount of dsDNA per cell ( $n = 3$ ) to calculate the total cell number from dsDNA content. Proliferation is presented as the total cell number and cell number normalized to the number of cells initially seeded or encapsulated.

## **2.2.6. Histological, Transmission Electron Microscopy (TEM), and Gene Expression Analysis and Immunofluorescence Staining**

*Histology.* Samples were fixed, sectioned, stained, and mounted as described previously in section 2.2.2. – *Histological Analysis.* Slides were imaged on a Zeiss Axioskop upright microscope mounted with a CRi Nuance camera using CRi Nuance 3.0.0 software.

*Transmission Electron Microscopy (TEM).* Samples were fixed in 2.5% (v/v) glutaraldehyde (Sigma-Aldrich, #G7776) and 1.6% (v/v) paraformaldehyde (Alfa Aesar, #43368) in 0.1 M cacodylate buffer (Ted Pella, #18851), pH 7.4 for several days at 4 °C. Samples were subsequently post-fixed with 1% osmium tetroxide for 1 h then 1% uranyl acetate in maleate buffer for 1 h, dehydrated in a graded ethanol and propylene oxide series, and embedded in Epon (polymerized at 60 °C for 48 hours). Ultrathin sections were visualized with a FEI Tecnai Spirit G2 TEM.

*Gene Expression Analysis.* RNA was isolated from samples and cell pellets using TRIzol Reagent (Invitrogen, #15596018) following the manufacturer's protocol, and isolated RNA was treated with DNA-free DNA Removal Kit (Ambion, #AM1906) to remove contaminating genomic DNA from samples. RNA concentration was measured using a NanoDrop 1000 Spectrophotometer (Thermo Scientific). Reverse transcription and cDNA synthesis was performed using iScript Reverse Transcription Supermix for RT-qPCR (Bio-Rad, #170-8841) with an Applied Biosystems GeneAMP PCR System 9700 following the manufacturer's protocol. Quantitative real-time polymerase chain reaction was performed using SsoAdvanced Universal SYBR Green Supermix (Bio-Rad, #170-5270) with 300 nM each of forward and reverse primers and 0.10 ng/μL cDNA on an Applied Biosystems QuantStudio 7 Flex Real-Time PCR System. Primer sequences for genes of interest are listed in **Table 2-1**. The thermal profile used included an initial polymerase activation step at 95 °C for 30 sec, followed by 40 amplification cycles of denaturation at 95 °C for 15 sec and annealing and extension at 60 °C for 60 sec. Expression of each gene of interest

was normalized to expression of the housekeeping gene *cyclophilin A (PPIA)*, and the relative degree of gene amplification was calculated using the  $\Delta\Delta C_T$  method:  $2^{[(C_T \text{ gene 2} - C_T \text{ PPIA 2}) - (C_T \text{ gene 1} - C_T \text{ PPIA 1})]}$ . “ $C_T$  gene 1” represents the threshold cycle ( $C_T$ ) of the target gene of the reference population, cells cultured on tissue culture polystyrene, and “ $C_T$  gene 2” the target gene of the sample of interest. Biological replicates were run in quadruplicate ( $n = 4$ ) with technical replicates in triplicate.

<b>Gene</b>	<b>Forward Primer (5' to 3')</b>	<b>Reverse Primer (5' to 3')</b>
<b>PPIA</b>	CCC ACC GTG TTC TTC GAC ATT	GGA CCC GTA TGC TTT AGG ATG A
<b>PECAM1</b>	TAT GAT GCC CAG TTT GAG GT	GAA TAC CGC AGG ATC ATT TG
<b>CDH5</b>	TTG GAA CCA GAT GCA CAT TGA T	TCT TGC GAC TCA CGC TTG AC
<b>ICAM2</b>	CGG ATG AGA AGG TAT TCG AGG T	CAC CCA CTT CAG GCT GGT TAC
<b>MMP14</b>	CAT CTG TGA CGG GAA CTT TGA	GGC AGT GTT GAT GGA CGC A
<b>KDR</b>	GTG ATC GGA AAT GAC ACT GGA G	CAT GTT GGT CAC TAA CAG AAG CA
<b>TEK</b>	TCC GCT GGA AGT TAC TCA AGA	GAA CTC GCC CTT CAC AGA AAT AA
<b>TIE1</b>	AAG CAG ACA GAC GTG ATC TGG	GCA CGA TGA GCC GAA AGA AG
<b>PTPRB</b>	GGG CTC ACC CTG TAA CTT TAG C	TCT ATC CGA AAG GTA GGG CAC
<b>VWF</b>	TGC CTC CAA AGG GCT GTA TC	CAC CAC TGT TCT CCA CTG CTC
<b>PLVAP</b>	CTC TTC ATG GTC TAT GGC AAC G	GCG AGC ATT CAG CCA CAT C
<b>EHD3</b>	TGC TCT TCG ATG CCC ACA AA	CTT GTC CTC GTG GTT CTT GAG
<b>EHD4</b>	CCT TCA TCG CCG TGA TGT ATG	AGC GAC TGA GCT TTC TAA ACG
<b>ITGA3</b>	GGA GCG AGA TCC CTC CAA AAT	GGC TGT TGT CAT ACT TCT CAT GG
<b>ITGB1</b>	CCC ACC GTG TTC TTC GAC ATT	GGA CCC GTA TGC TTT AGG ATG A

*Immunofluorescence Staining.* Fixed and paraffin-embedded sections were processed as described previously in section 2.2.2 – *Immunofluorescence Staining*. Primary antibodies were diluted in blocking buffer as follows: mouse anti-PECAM-1 at 1:100 (Abcam, #ab187377) and rabbit anti-collagen I at 1:100 (Abcam, #ab24710). Secondary antibodies were diluted in blocking buffer as follows: goat anti-mouse Alexa Fluor 488 at 1:500 (Invitrogen, #A-11029) and goat anti-rabbit Alexa Fluor 555 at 1:500 (Invitrogen, #A-21429). Slides were mounted with Mowiol mounting medium containing DAPI to stain for cell nuclei and imaged on a Nikon A1 Confocal Laser Microscope System.

### 2.2.7. Statistical Analysis

All quantitative data is represented as the mean  $\pm$  standard error of the mean. Statistical significance was determined using an unpaired, two-tailed Student's *t*-test assuming equal variance with Microsoft Excel (Microsoft). Significance for all statistical analyses was defined as  $p < 0.05$ .

### 2.3. Results

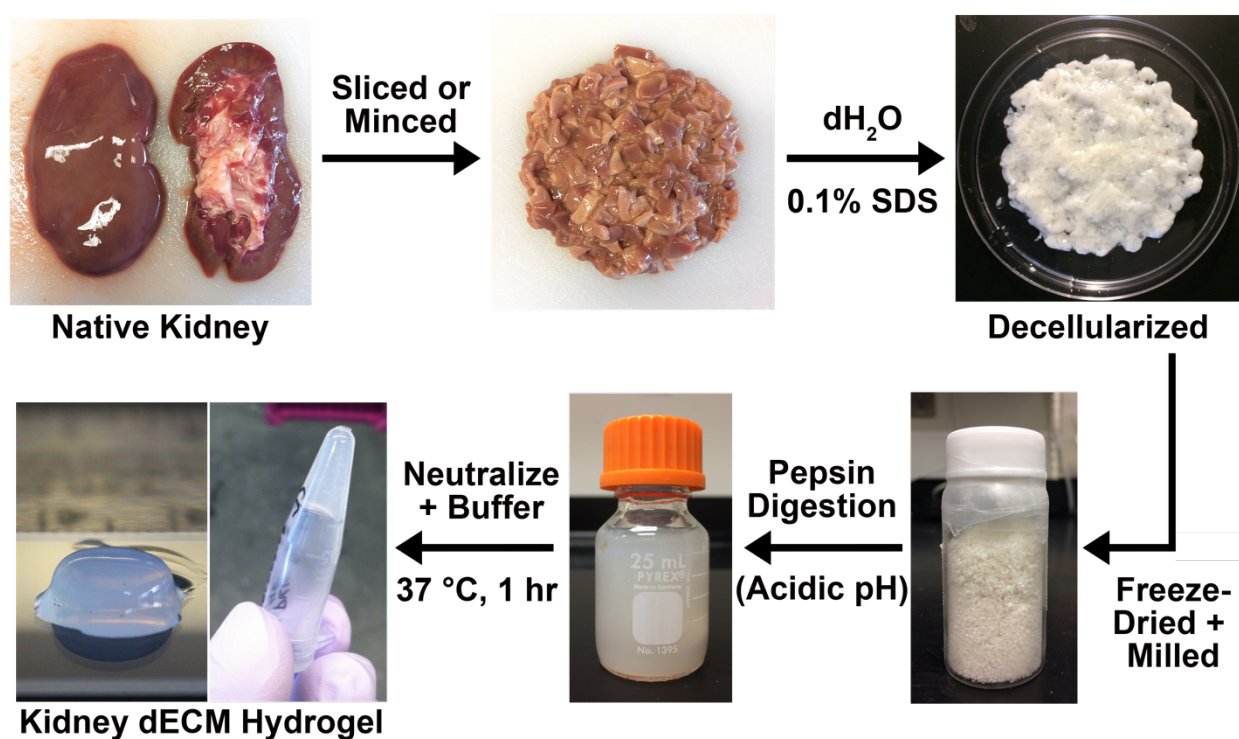


**Figure 2-1: Process to form kidney decellularized extracellular matrix hydrogels.**

The native porcine kidney is minced into pieces approximately  $0.5 \text{ cm} \times 0.5 \text{ cm} \times 0.25 \text{ cm}$  in size and treated with 0.1% (w/v) sodium dodecyl sulfate to remove all of the cellular material. The resulting decellularized extracellular matrix is lyophilized and milled into a fine powder before being subjected to a pepsin digestion at acidic pH (0.01 M HCl) to disrupt collagen fibril aggregates and solubilize the material. To form a hydrogel, the pepsin digest is kept on ice, neutralized with 1.0 M NaOH, buffered to pH 7.4, and incubated at 37 °C for about one hour.

### **2.3.1. Kidney Decellularization**

Minced kidney tissue began to lose color during the initial rinse step with deionized H<sub>2</sub>O as blood was removed. After several hours in detergent, the edges of tissue pieces became white, and after two days, all kidney tissue acquired a blanched appearance (**Figure 2-1**). After decellularization, hematoxylin and eosin staining revealed removal of cell nuclei as evidenced by the lack of dark hematoxylin nucleic counterstain present, and glomerular and tubular ECM structures remained identifiable (**Figure 2-2 A**). Quantification of the amount of double-stranded DNA present within native and decellularized tissues demonstrated that  $\geq 98\%$  of the DNA content (by dry weight) was removed during the decellularization process (**Figure 2-2 B**). Immunofluorescence staining for key ECM proteins including type I collagen, type IV collagen, and laminin revealed the presence of these proteins in decellularized tissues, particularly in glomerular structures for type IV collagen and laminin (**Figure 2-2C**). In addition, results from the DMMB dye assay indicated retention of approximately half of the sGAG content in decellularized tissues in comparison to native tissues when normalized to the lyophilized masses of the samples (**Figure 2-2 D**).

### **2.3.2. Macroscopic and Ultrastructural Characterization of Hydrogels**

Kidney dECM hydrogels formed at concentrations of 2.5 mg/mL and 5.0 mg/mL retained the cylindrical shape of the mold in which they were cast and were robust enough to be handled with a spatula. Kidney dECM hydrogels at 1.0 mg/mL and collagen hydrogels 2.5 mg/mL concentrations retained the circular shape but did not meet the height of the original mold. The reduced volume of these hydrogels was likely due to the greater exclusion of water during hydrogel formation which necessitated careful handling of these fragile hydrogels (**Figure 2-3 A-D, insets**). Ultrastructural imaging via scanning electron microscopy revealed fibrous morphologies of all hydrogels with randomly-oriented fibrils and interconnected pores (**Figure 2-3 A-D**).

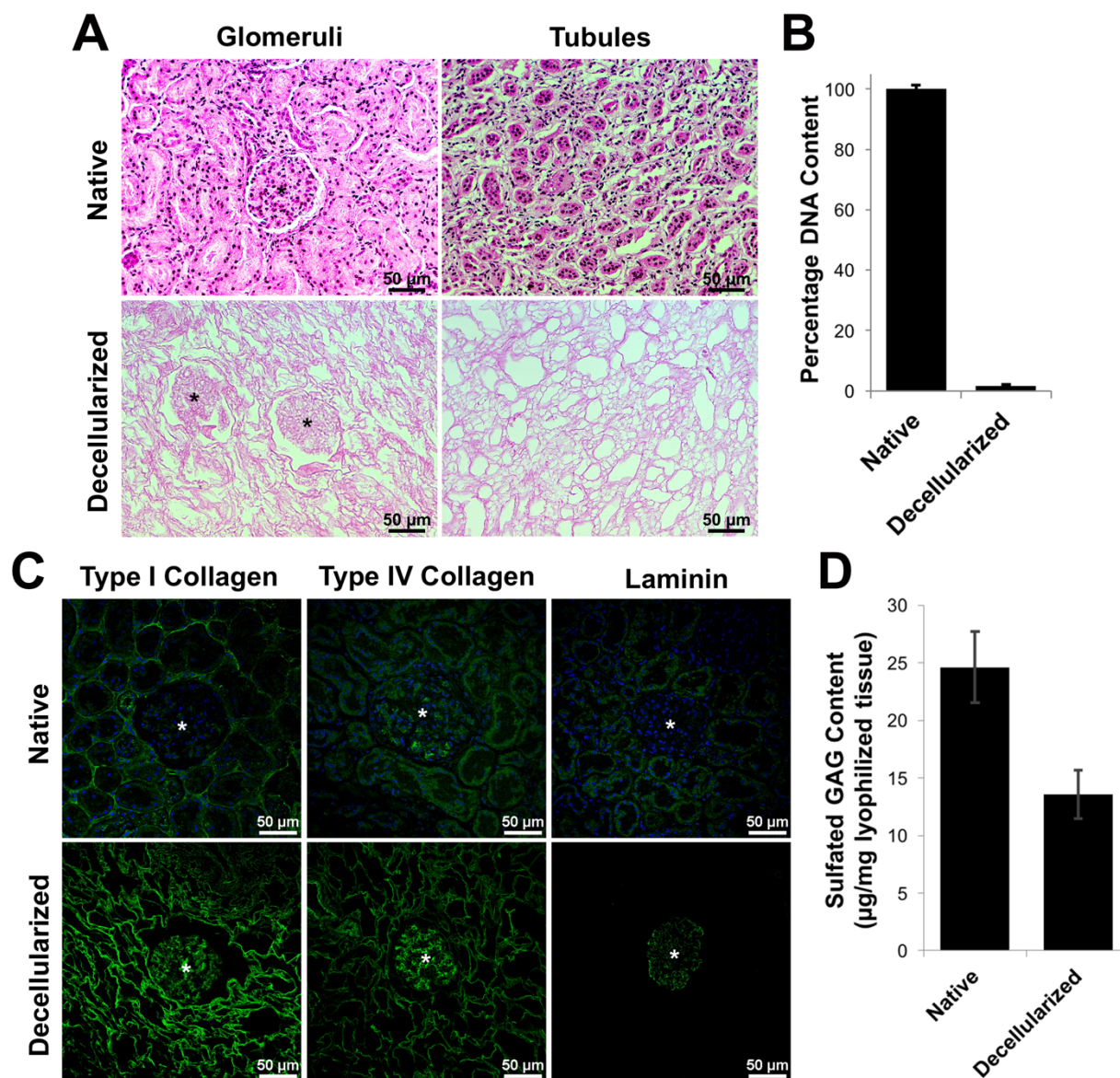


**Figure 2-2: Evaluation and characterization of decellularized kidney tissues.**

(A) Routine hematoxylin and eosin staining of native and decellularized kidney sections demonstrating removal of cellular nuclei (dark spots) and preservation of the ECM architecture, including glomeruli (\*) and tubule structures. (B) Quantification of double-stranded DNA content in native and decellularized kidney tissue. DNA content was normalized to the dry weight of each sample, and data is presented as a percentage of native kidney tissue DNA content ( $n = 3$ ). (C) Immunofluorescence staining of native and decellularized kidney sections demonstrating retention of type I collagen I, type IV collagen, and laminin in decellularized tissues; glomerular structures indicated by (\*). (D) Quantification of sulfated glycosaminoglycan content in native and decellularized kidney tissue. sGAG content was normalized to the dry mass of each sample with samples run in triplicate ( $n = 3$ ).

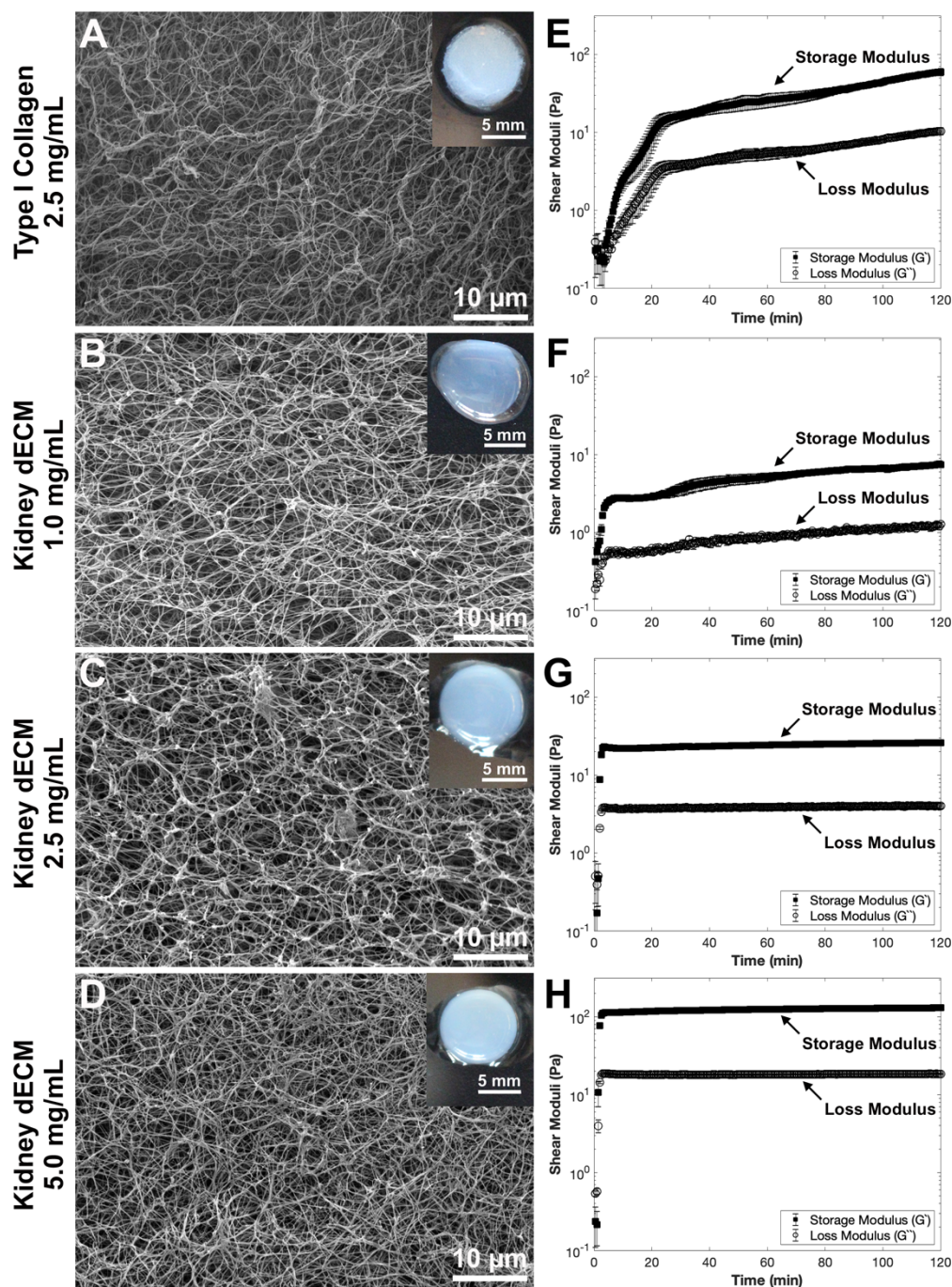


**Figure 2-3: Scanning electron micrographs, macroscopic images, and rheological time sweeps of hydrogels.**

SEM and macroscopic images (insets) of (A) collagen hydrogel at 2.5 mg/mL, (B) kidney dECM hydrogel at 1.0 mg/mL, (C) kidney dECM hydrogel at 2.5 mg/mL, and (D) kidney dECM hydrogel at 5.0 mg/mL. Rheological characterization of hydrogel formation over time with measured shear moduli plotted on a logarithmic scale of (E) collagen hydrogels at 2.5 mg/mL, (F) kidney dECM hydrogels at 1.0 mg/mL, (G) kidney dECM hydrogels at 2.5 mg/mL, and (H) kidney dECM hydrogels at 5.0 mg/mL.

### 2.3.3. Rheological Characterization of Hydrogels

Rheological testing was performed to measure the change in shear moduli ( $G'$ ,  $G''$ ) over time and rate of gelation, and values are reported in **Table 2-2**. The gelation point is reported as the time at which the shear moduli are equal in value<sup>[318]</sup>. The time to plateau is reported as the time at which the storage modulus ( $G'$ ) is approximately an order of magnitude larger than the loss modulus ( $G''$ ) and both moduli have reached the plateau phase indicating that a stable hydrogel has formed. The shear moduli of all hydrogels (**Figure 2-3 E-H**) were characterized by sigmoidal curves with rapid onset of gelation upon ramping the temperature up to 37 °C. Collagen hydrogels (2.5 mg/mL, **Figure 2-3 E**) presented the longest time to plateau at 25 min. with an equilibrium  $G'$  value of 15 Pa. The  $G'$  continued to increase to 60 Pa after 120 min. Kidney dECM hydrogels at 1.0 mg/mL (**Figure 2-3 F**) formed stable hydrogels much more rapidly with the time to plateau being 3.5 min. and an equilibrium  $G'$  value of 2.0-7.5 Pa. Kidney dECM hydrogels at 2.5 mg/mL and 5.0 mg/mL (**Figure 2-3 G, H**) formed stable hydrogels after just 3 min. with equilibrium  $G'$  values of 22-26 Pa and 110-130 Pa, respectively. To confirm formation of a hydrogel, samples were subject to frequency (**Figure 2-4 A-D**) and strain (**Figure 2-4 E-H**) sweeps. The  $G'$  of all samples was independent at frequencies of 25 rad/s and below, and the angular frequency value used for time sweeps was verified to be in the low-frequency plateau region for all samples. Strain sweeps demonstrated the presence of a linear viscoelastic region for all samples, confirming the formation of hydrogels, and the strain value used for time sweeps was within the linear viscoelastic region for all samples. Additionally, all samples exhibited decreasing  $G'$  values after approximately 70% strain with catastrophic failure occurring within the range of 300-500% strain.

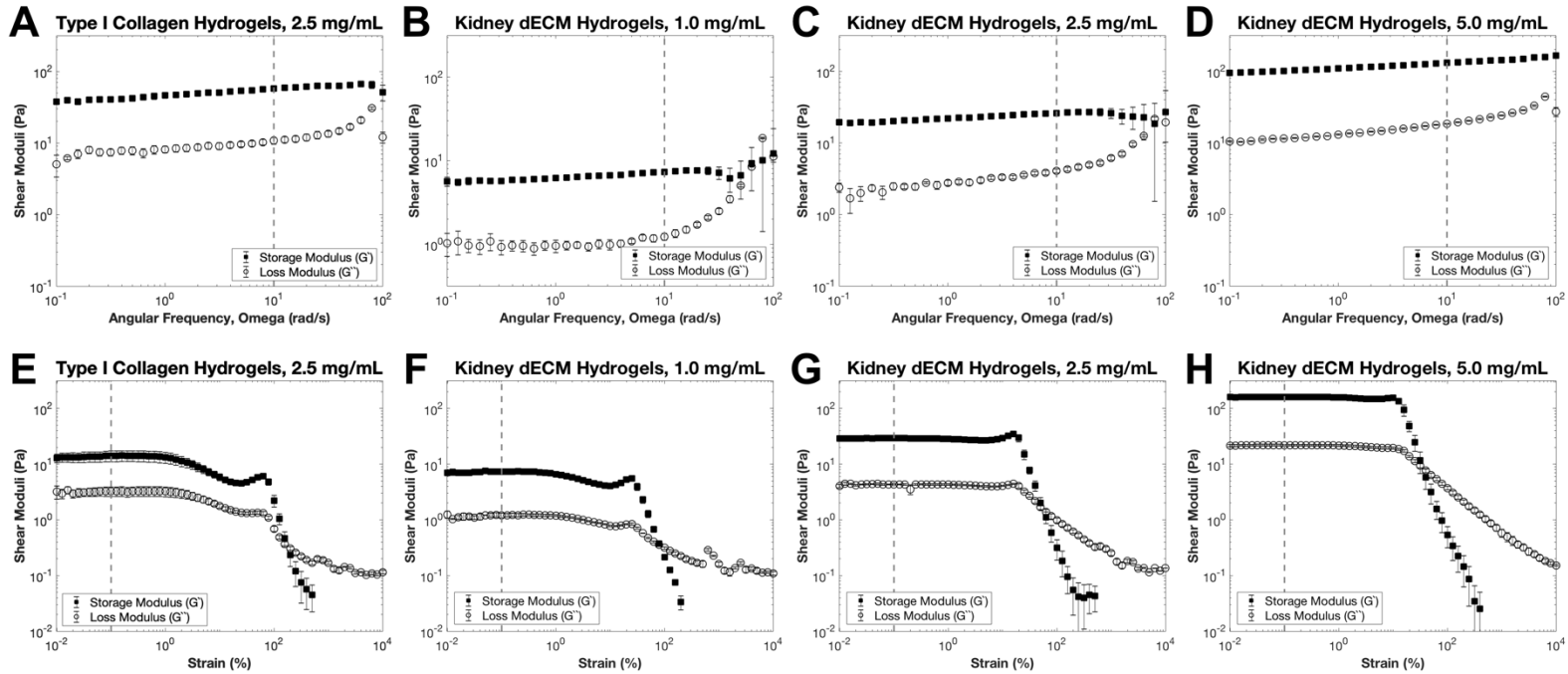


**Figure 2-4: Rheological frequency and strain sweeps of hydrogels.**

Shear moduli versus angular frequency plotted on logarithmic axes for (A) collagen hydrogels at 2.5 mg/mL, (B) kidney dECM hydrogels at 1.0 mg/mL, (C) kidney dECM hydrogels at 2.5 mg/mL, and (D) kidney dECM hydrogels at 5.0 mg/mL. Dashed lines represent the angular frequency at which time sweeps were performed: 10 rad/s. Shear moduli versus strain plotted on logarithmic axes for (E) collagen hydrogels at 2.5 mg/mL, (F) kidney dECM hydrogels at 1.0 mg/mL, (G) kidney dECM hydrogels at 2.5 mg/mL, and (H) kidney dECM hydrogels at 5.0 mg/mL. Dashed lines represent the strain percent at which time sweeps were performed: 0.1% strain.

	<b>Type I Collagen Hydrogels</b>	<b>Kidney dECM Hydrogels</b>		
<b>Concentration (mg/mL)</b>	2.5	1.0	2.5	5.0
<b>Gelation Point (min)</b>	5.0	1.0	2.0	1.5
<b>Time to Plateau Phase (min)</b>	25.0	3.5	3.0	3.0
<b>Equilibrium Storage Modulus, G' (Pa)</b>	15.0-60.0	2.0-7.5	22.0-26.0	110.0-130.0
<b>Average Strain Range of Strain Stiffening Behavior</b>	25.0-70.0%	12.5-25.0%	5.0-15.0%	5.0-10.0%

#### **2.3.4. Cell Viability and Proliferation on Hydrogel Substrates**

Live/dead staining and image analysis revealed high viability (85-98%) of human conditionally-immortalized GEnCs cultured on type I collagen hydrogels (2.5 mg/mL) and kidney dECM hydrogels (2.5 mg/mL) substrates at days 1 and 12 (**Figure 2-5 A, B**). Quantification of DNA content of samples over time indicated proliferation of GEnCs cultured on both collagen and kidney dECM hydrogels with cells increasing over six-fold in number during the seven-day culture period at the permissive temperature. Cell proliferation after thermoswitching and culture at the non-permissive temperature between days 7 and 12 decreased, as expected (**Figure 2-5 C**).

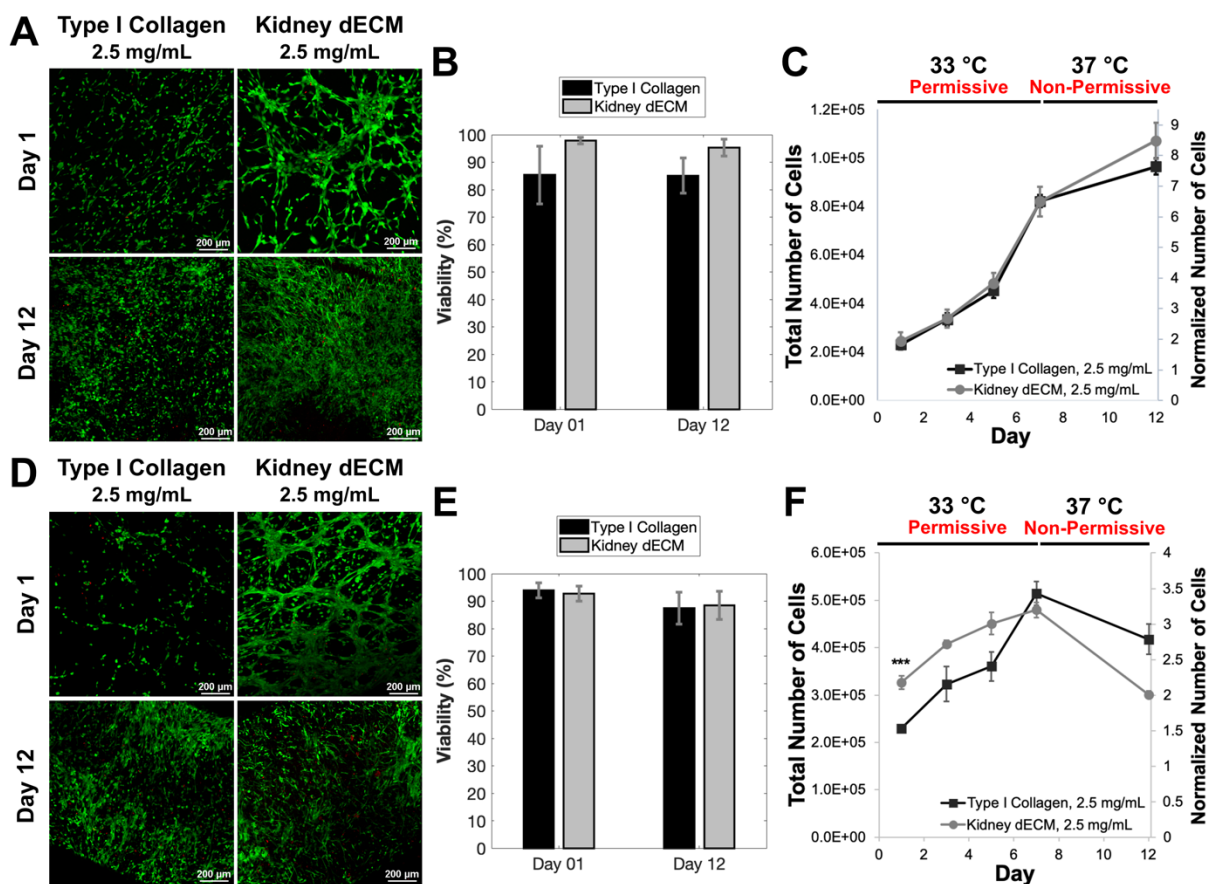


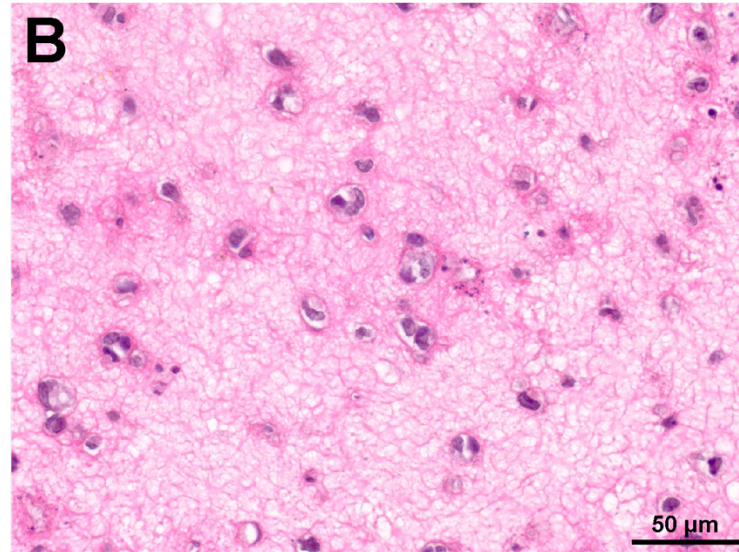
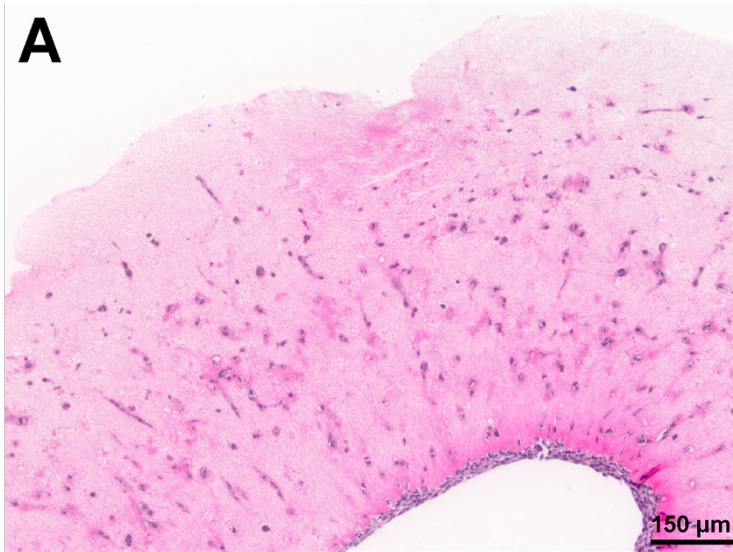
**Figure 2-5: Viability and proliferation of GEnCs cultured hydrogel substrates or encapsulated within hydrogels.**

(A) Live/dead staining and confocal imaging of GEnCs cultured on collagen I hydrogels or kidney dECM hydrogels at days 1 and 12. (B) Quantification of viability of cells cultured on top of hydrogel substrates presented as the percentage live cells from image analysis. (C) Quantification of cultured GEnC proliferation over twelve days using a Quant-iT PicoGreen dsDNA Assay Kit. Normalized values (right axis) were normalized to the number of cells seeded per sample on day 0. Samples initially seeded with 12,500 cells per sample (50,000 cells/mL). Number of independent measurements,  $n = 4$ . (D) Live/dead staining and confocal imaging of GEnCs encapsulated within collagen hydrogels or kidney dECM hydrogels at days 1 and 12. (E) Quantification of viability of cells encapsulated within hydrogels presented as the percentage live cells from image analysis. (F) Quantification of encapsulated GEnC proliferation over twelve days using a Quant-iT PicoGreen dsDNA Assay Kit. Normalized values (right axis) were normalized to the number of cells encapsulated per sample on day 0. Samples initially seeded with 150,000 cells per sample (1 million cells/mL). Number of independent measurements:  $n = 4$ . \*\*\*  $p < 0.005$ .

### **2.3.5. Cellular Encapsulation Within Hydrogels**

Live/dead staining and image analysis revealed high cell viability of GEnCs encapsulated within both collagen hydrogels (2.5 mg/mL) and kidney dECM hydrogels (2.5 mg/mL) at days 1 (92-94%) and 12 (86-88%) (**Figure 2-5 D, E**). Hydrogels encapsulating cells began to contract after three days in culture and resembled compacted disks after twelve days. Encapsulated GEnCs proliferated during the first seven days when cultured at the permissive temperature, approximately tripling in number for both experimental groups. The cell number was significantly greater ( $p < 0.005$ ) for cells encapsulated in kidney dECM hydrogels than cells encapsulated in collagen hydrogels on day 1 with 100,000 more cells present in kidney dECM hydrogels; however, there was no significant difference in cell number between the groups at time points beyond day 1 (**Figure 2-5 F**). Histological analysis of encapsulated GEnCs at an initial concentration of 1 million cells/mL cultured for 7 (**Figure 2-6**) and 12 days (**Figure 2-7**) showed cell distribution throughout hydrogels and settling of cells during hydrogel formation towards the bottom edge of samples. Samples from both groups demonstrated some cell spreading between days 7 and 12 but little presence of cell-cell contacts and no tube formation, which was also confirmed by TEM (**Figure 2-7 C, F**).

Type I Collagen



Kidney dECM

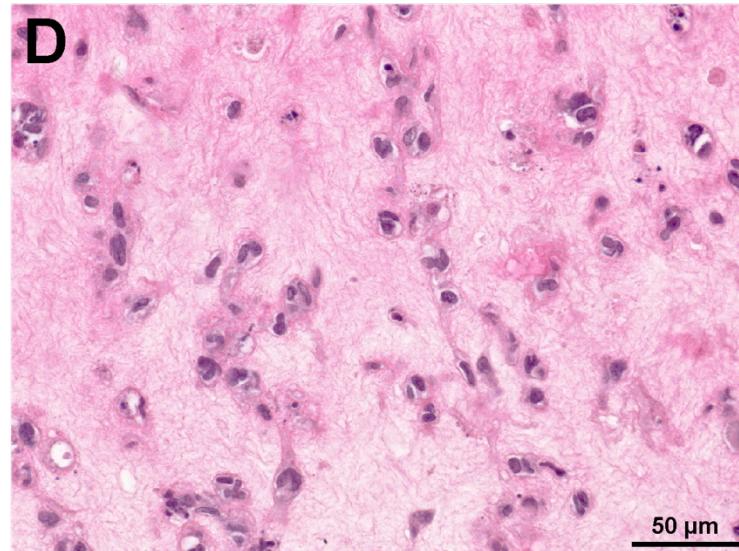
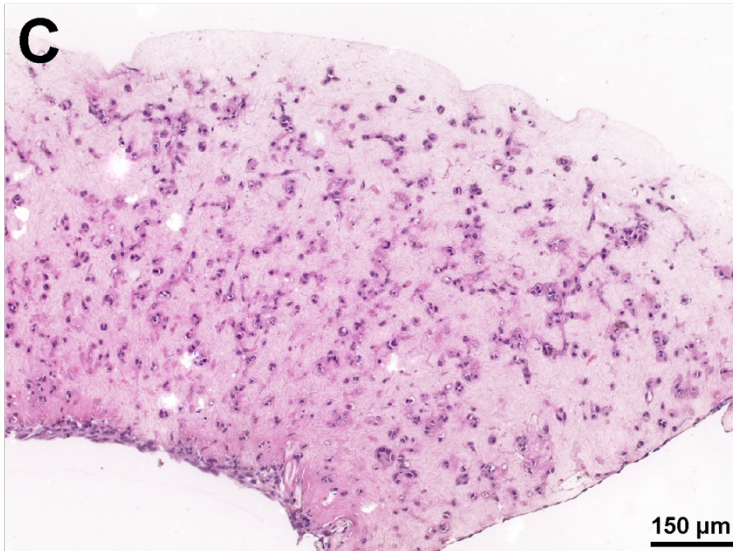


**Figure 2-6: Histological analysis of GEnCs encapsulated within hydrogels (1 million cells/mL) after 7 days in culture.** (A, B) H&E-stained sections of GEnCs encapsulated within collagen hydrogels. (C, D) H&E-stained sections of GEnCs encapsulated within kidney dECM hydrogels.

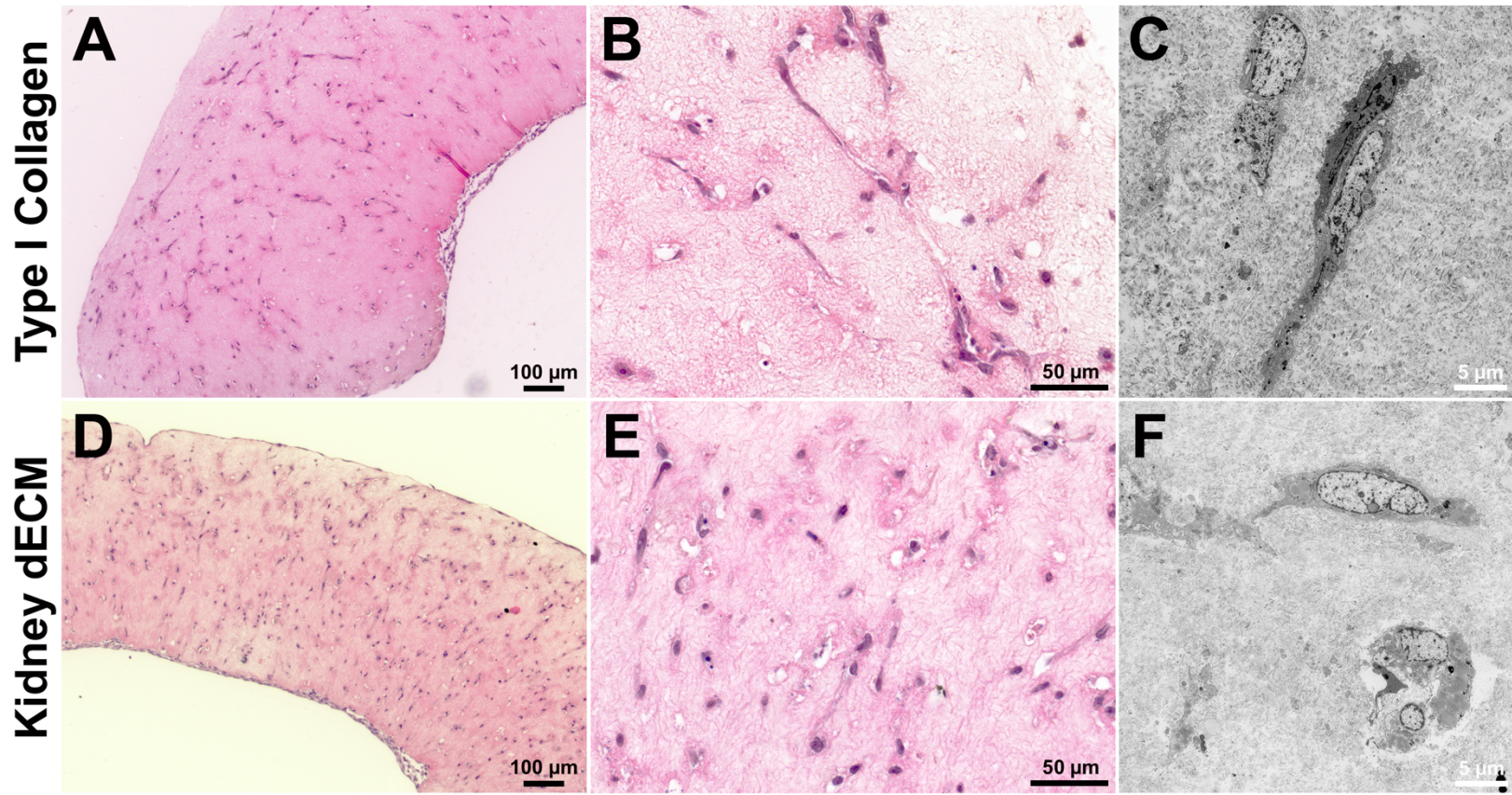


**Figure 2-7: Histological analysis and TEM of GEnCs encapsulated within hydrogels (1 million cells/mL) after 12 days in culture. (A, B) H&E-stained sections and (C) TEM micrograph of GEnCs encapsulated within collagen hydrogels. (D, E) H&E-stained sections and (F) TEM micrograph of GEnCs encapsulated within kidney dECM hydrogels.**

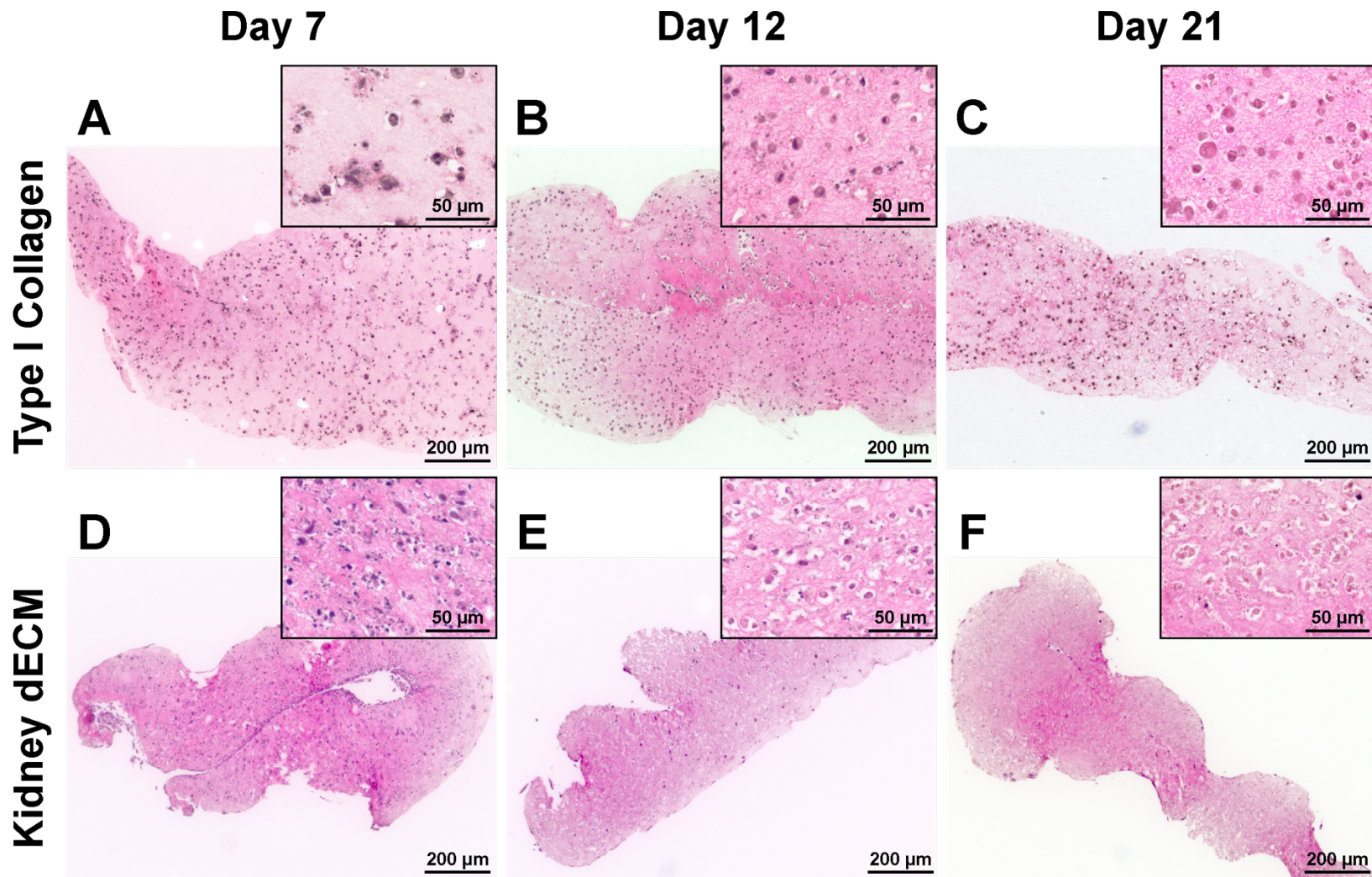


**Figure 2-8: Histological analysis of GEnCs encapsulated within hydrogels (5 million cells/mL).**

(A-C) H&E-stained sections of GEnCs encapsulated within type I collagen hydrogels after 7, 12, and 21 days in culture, respectively. (D-F) H&E-stained sections of GEnCs encapsulated within kidney dECM hydrogels after 7, 12, and 21 days in culture, respectively.

GEnCs were also encapsulated at a higher initial concentration of 5 million cells/mL, and hydrogels began to contract after just one day in culture due to the greater density of cells. Histological analysis of collagen hydrogel samples from days 7, 12, and 21 revealed homogeneous cell distribution throughout the hydrogels; however, cells retained a rounded morphology at all time points (**Figure 2-8 A-C**). Kidney dECM hydrogel samples revealed similarly homogeneous cell distribution throughout the hydrogels on day 7, but fewer cell nuclei were visible on days 12 and 21 (**Figure 2-8 D-F**). Cells also retained a rounded morphology at all time points when encapsulated within kidney dECM hydrogels.

### **2.3.6. Gene Expression and Immunofluorescence**

Gene expression analysis revealed greater expression of relevant genes of interest by GEnCs cultured on collagen hydrogel substrates compared to expression by cells cultured on kidney dECM hydrogel substrates at almost all time points (**Figure 2-9**). Specifically, whereas cells cultured on collagen hydrogel substrates exhibited upregulation of gene expression when normalized to the reference population, cells cultured on kidney dECM hydrogel substrates exhibited reduced upregulation or downregulation of gene expression. Genes analyzed are involved in cell-cell interactions (**Figure 2-9 A-C**: *PECAM1*, *CDH5*, *ICAM2*), signaling pathways (**Figure 2-9 D, E**: *KDR*, *TEK*), and endothelial function (**Figure 2-9 F, G**: *VWF*, *PLVAP*).

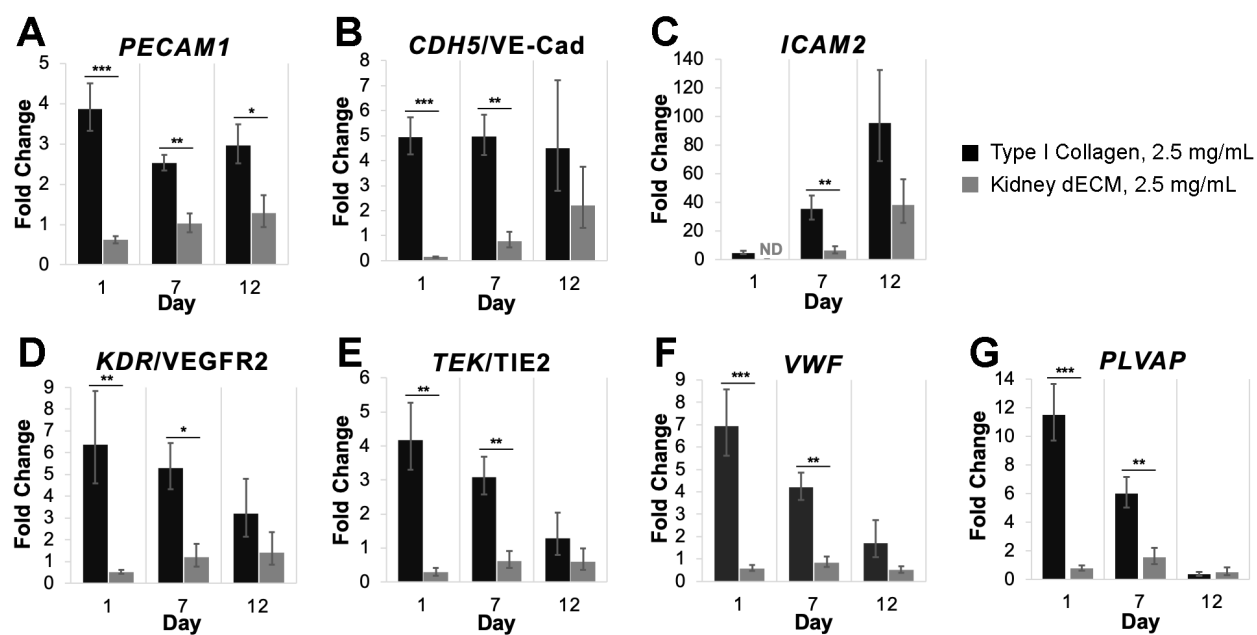


**Figure 2-9: Gene expression analysis of GEnCs cultured on hydrogel substrates.**

Gene expression analysis of samples after 1, 7, and 12 days in culture. (A) *PECAM1* encoding for platelet endothelial cell adhesion molecule 1 or CD31. (B) *CDH5* encoding for cadherin 5 or vascular endothelial cadherin. (C) *ICAM2* encoding for intercellular adhesion molecule 2 or CD102. (D) *KDR* encoding for kinase insert domain receptor or vascular endothelial growth factor receptor 2. (E) *TEK* encoding for tyrosine kinase with immunoglobulin-like and EGF-like domains 2 or TIE2. (F) *VWF* encoding for von Willebrand factor. (G) *PLVAP* encoding for plasmalemma vesicle-associated protein. Values expressed as fold-change expression normalized to gene expression of cells cultured on tissue culture polystyrene at day 0 ( $n = 4$ ). Statistical significance denoted by: \*  $p < 0.05$ , \*\*  $p < 0.01$ , and \*\*\*  $p < 0.001$ .

Gene expression analysis of GEnCs encapsulated at an initial concentration of 1 million cells/mL (Figure 2-10) revealed higher fold-change expression of cells encapsulated in collagen hydrogels compared to cells encapsulated in kidney dECM hydrogels on days 1 and 7 for all of the genes analyzed except *ITGB1*. Genes analyzed included those described previously (Figure 2-9) as well as additional genes involved in cell-matrix remodeling (Figure 2-10 D: *MMP14*), signaling pathways (Figure 2-10 G, H: *TIE1*, *PTPRB*), endothelial function (Figure 2-10 K, L: *EHD3*, *EHD4*), and cell-matrix binding interactions (Figure 2-10 M, N: *ITGA3*, *ITGB1*). Gene expression for both experimental groups was typically highest on day 12, with a few exceptions: *PLVAP*, *TIE1*, *ITGA3* and *ITGB1* for collagen hydrogels and *ITGB1* for kidney dECM hydrogels.

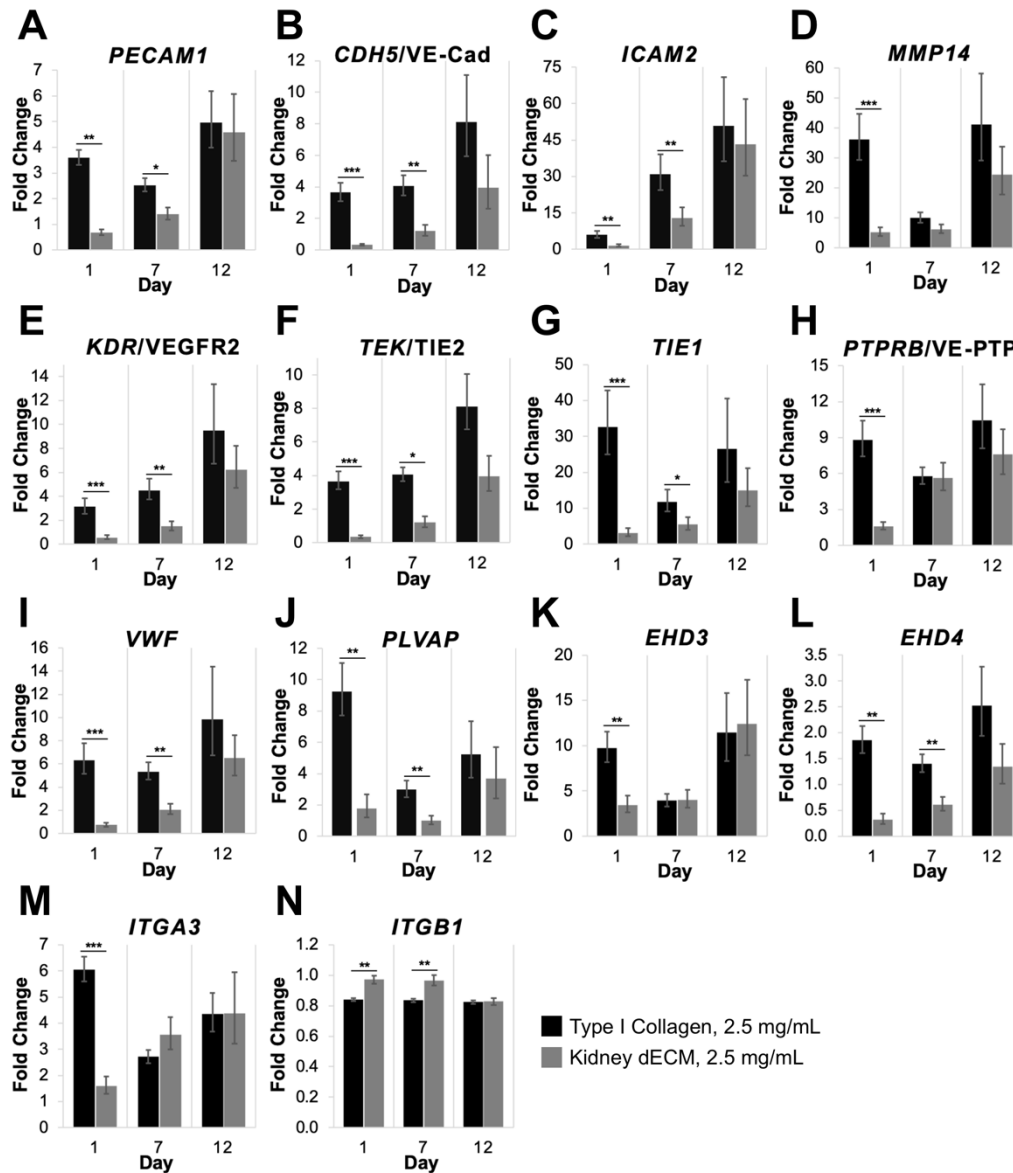


**Figure 2-10: Gene expression analysis of GEnCs encapsulated within hydrogels (1 million cells/mL).**

Gene expression analysis of samples after 1, 7, and 12 days in culture. (A) *PECAM1* encoding for platelet endothelial cell adhesion molecule or CD31. (B) *CDH5* encoding for cadherin 5 or vascular endothelial cadherin. (C) *ICAM2* encoding for intercellular adhesion molecule 2 or CD102. (D) *MMP14* encoding for matrix metalloproteinase 14 or MT1-MMP. (E) *KDR* encoding for kinase insert domain receptor or vascular endothelial growth factor receptor 2. (F) *TEK* encoding for tyrosine kinase with immunoglobulin-like and EGF-like domains 2 or TIE2. (G) *TIE1* encoding for tyrosine kinase with immunoglobulin-like and EGF-like domains 1 or TIE1. (H) *PTPRB* encoding for receptor-type tyrosine-protein phosphatase beta or VE-PTP. (I) *VWF* encoding for von Willebrand Factor. (J) *PLVAP* encoding for plasmalemma vesicle-associated protein. (K) *EHD3* encoding for Eps15 homology domain-containing protein 3. (L) *EHD4* encoding for EH domain-containing protein 4. (M) *ITGA3* encoding for integrin subunit alpha 3. (N) *ITGB1* encoding for integrin subunit beta 1. Values expressed as fold-change expression normalized to gene expression of cells cultured on tissue culture polystyrene at day 0 ( $n = 4$ ). Statistical significance denoted by: \*  $p < 0.05$ , \*\*  $p < 0.01$ , and \*\*\*  $p < 0.001$ .

Similar trends in gene expression were observed for GEnCs encapsulated at a higher initial concentration of 5 million cells/mL (Figures 2-11 and 2-12). Interestingly, this increased cell density seemed to extend the disparity in gene expression such that cells encapsulated within collagen hydrogels continued to exhibit higher fold-change expression than cells encapsulated within kidney dECM hydrogels at day 12 (Figures 2-11 and 2-12). However, for a subset of genes additionally analyzed at day 21 (Figure 2-11), expression between experimental groups were similar as expression by GEnCs encapsulated within collagen hydrogels decreased.

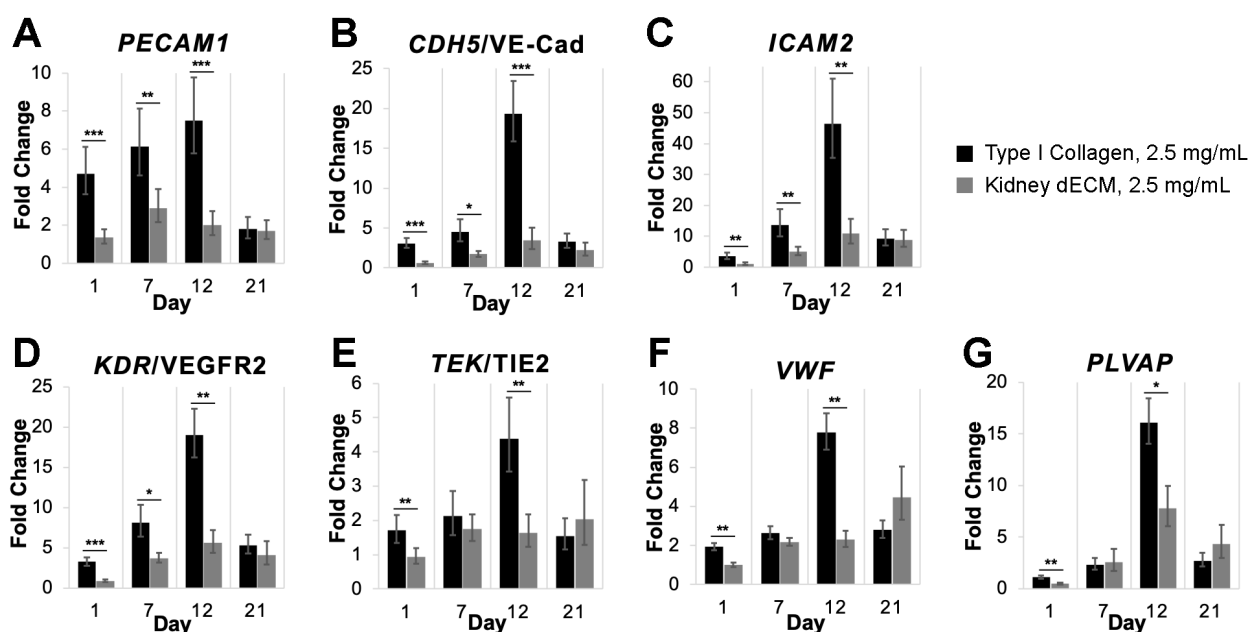


**Figure 2-11: Gene expression analysis of GEnCs encapsulated within hydrogels (5 million cells/mL).** Gene expression analysis of samples after 1, 7, 12, and 21 days in culture. (A) *PECAM1* encoding for platelet endothelial cell adhesion molecule 1 or CD31. (B) *CDH5* encoding for cadherin 5 or vascular endothelial cadherin. (C) *ICAM2* encoding for intercellular adhesion molecule 2 or CD102. (D) *KDR* encoding for kinase insert domain receptor or vascular endothelial growth factor receptor 2. (E) *TEK* encoding for tyrosine kinase with immunoglobulin-like and EGF-like domains 2 or TIE2. (F) *VWF* encoding for von Willebrand factor. (G) *PLVAP* encoding for plasmalemma vesicle-associated protein. Values expressed as fold-change expression normalized to gene expression of cells cultured on tissue culture polystyrene at day 0 ( $n = 4$ ). Statistical significance denoted by: \*  $p < 0.05$ , \*\*  $p < 0.01$ , and \*\*\*  $p < 0.001$ .

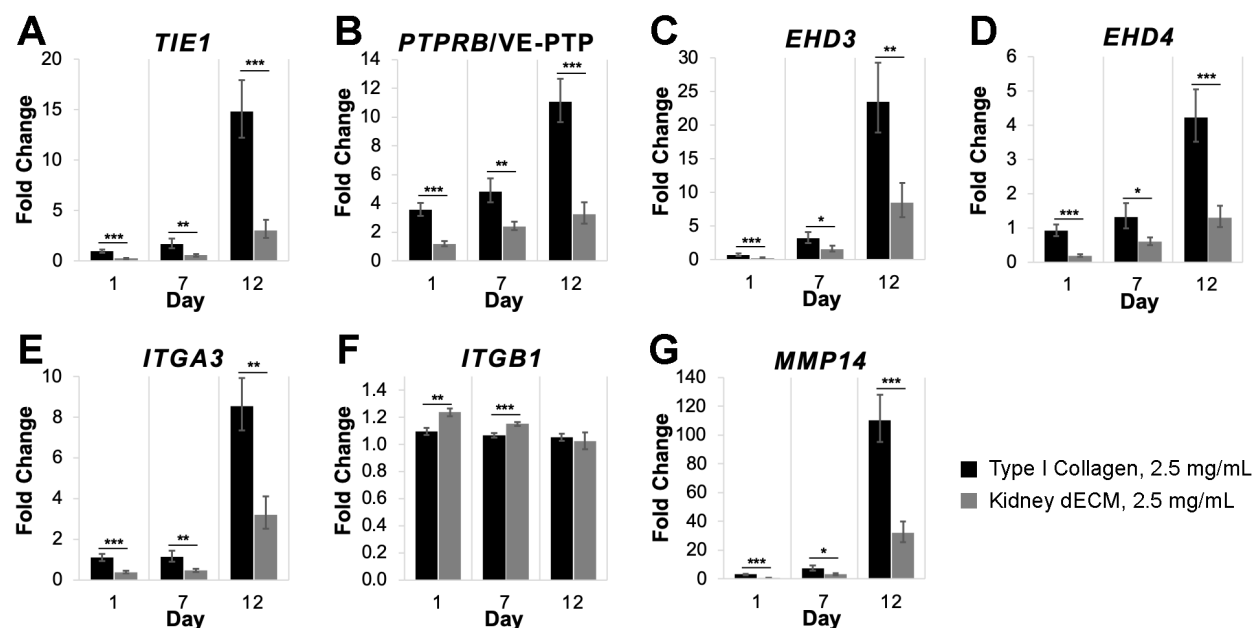


**Figure 2-12: Additional gene expression analysis of GEnCs encapsulated within hydrogels (5 million cells/mL).**

Gene expression analysis of samples after 1, 7, and 12 days in culture. (A) *TIE1* encoding for tyrosine kinase with immunoglobulin-like and EGF-like domains 1 or TIE1. (B) *PTPRB* encoding for receptor-type tyrosine-protein phosphatase beta or VE-PTP. (C) *EHD3* encoding for Eps15 homology domain-containing protein 3. (D) *EHD4* encoding for EH domain-containing protein 4. (E) *MMP14* encoding for matrix metalloproteinase 14 or MT1-MMP. (F) *ITGA3* encoding for integrin subunit  $\alpha$  3. (G) *ITGB1* encoding for integrin subunit  $\beta$  1. Values expressed as fold-change expression normalized to gene expression of cells cultured on tissue culture polystyrene at day 0 ( $n = 4$ ). Statistical significance denoted by: \*  $p < 0.05$ , \*\*  $p < 0.01$ , and \*\*\*  $p < 0.001$ .

Finally, immunofluorescence staining confirmed expression of platelet endothelial cell adhesion molecule (PECAM-1 or CD31 encoded by *PECAM1*) by GEnCs encapsulated within either collagen hydrogels or kidney dECM hydrogels on days 7 and 12 (Figure 2-13).

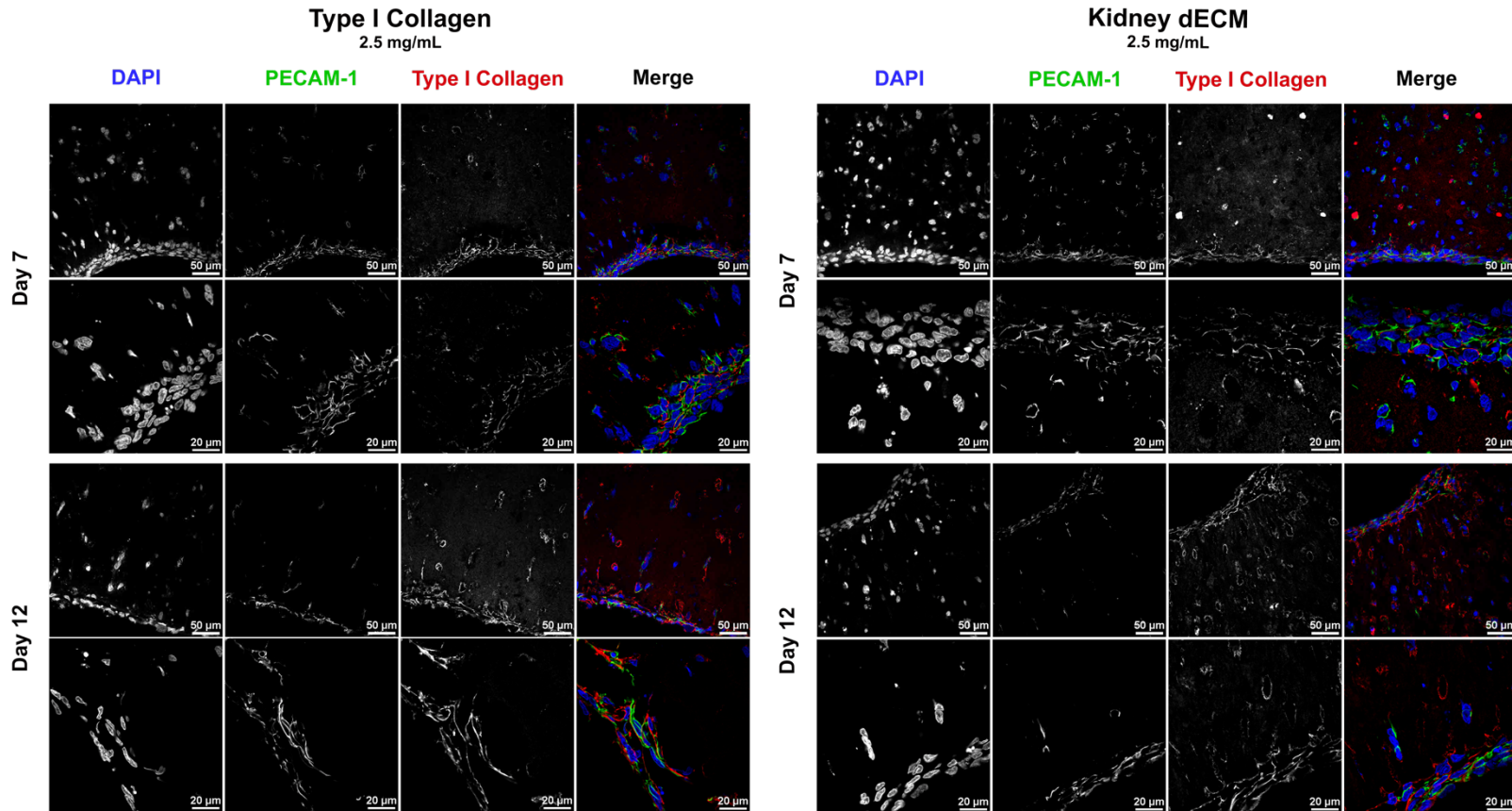


**Figure 2-13: Immunofluorescence staining for PECAM-1 in GEnCs encapsulated within hydrogels.**

Platelet endothelial cell adhesion molecule 1 (PECAM-1) expression by GEnCs encapsulated within type I collagen or kidney dECM hydrogels at an initial concentration of 1 million cells/mL after 7 or 12 days in culture. Merged images: DAPI (blue), PECAM-1 (green), and type I collagen (red).

## 2.4. Discussion

Decellularized ECM is a versatile material that has been utilized in a number of applications over the years ranging from biological wound dressings<sup>[322]</sup> to coatings for cell culture<sup>[323, 324]</sup>. Although the native architecture of the dECM is lost during processing to form hydrogels, the complex tissue- and organ-specific biochemical signals of the native source are thought to be retained<sup>[264]</sup>. As a result, hydrogels derived from dECM, as opposed to those derived from synthetic or purified natural sources, have inherent cell-interactive motifs and bioactive factors. We have demonstrated that porcine kidney dECM can be solubilized and processed to form a mechanically stable hydrogel that supports cell viability and proliferation. Kidney dECM hydrogels were evaluated by rheological characterization and *in vitro* studies were performed for comparison with purified type I collagen hydrogels.

The enzymatic digestion method adopted in this study allows for the solubilization of dECM material without additional purification steps that may result in the removal of desired biochemical components<sup>[317]</sup>. The digestion occurs as pepsin, an enzyme that is active only at very acidic pH, cleaves collagen telopeptide bonds and disrupts collagen fibril aggregates<sup>[325]</sup>. Once the digest is neutralized, thus inactivating the enzyme, and brought to physiological temperature and salt concentration, the collagen and other matrix peptides self-assemble in an entropy-driven process<sup>[325, 326]</sup>. The resulting kidney dECM hydrogels possess a loosely organized fibrous organization with an interconnected pore structure as visualized under SEM (**Figure 2-3 A-D**) that is comparable to collagen hydrogels and various dECM hydrogels characterized by other groups<sup>[264]</sup>.

Gelation kinetics and shear moduli ( $G'$ ,  $G''$ ) of kidney dECM hydrogels were analyzed by parallel-plate rheology. Time sweeps revealed that kidney dECM hydrogels at all the concentrations tested exhibited a decreased lag phase (time of nucleation) and an increased rate of self-assembly in comparison to collagen hydrogels (**Figure 2-3 E-H**). This observation agrees with previous time-lapse confocal reflection microscopy studies, which reinforces the idea that additional components present in dECM, such as proteoglycans and glycosaminoglycans, increase the polymerization kinetics of collagen self-assembly<sup>[327]</sup>. Evaluation of steady-state  $G'$  values of kidney dECM hydrogels also revealed that increasing dECM

concentration led to an increase in  $G'$  value or hydrogel stiffness. This observation agrees with rheological or mechanical characterization of various dECM hydrogels investigated by other groups<sup>[264]</sup>, such as liver<sup>[311]</sup> and skeletal muscle<sup>[314]</sup>.

Strain sweeps demonstrated that the hydrogels undergo a strain-stiffening behavior (**Figure 2-4 E-H**). This nonlinear elastic property is common among biological materials such as fibrin and is thought to prevent damage to tissues caused by large deformations<sup>[328]</sup>. Kidney dECM hydrogels of all concentrations tested exhibited strain-stiffening behavior anywhere between 5-25% strain; however, strain stiffening was much more apparent in lower concentration kidney dECM hydrogels (1.0 and 2.5 mg/mL) as opposed to 5.0 mg/mL hydrogels. Type I collagen hydrogels, on the other hand, exhibited strain-stiffening behavior between 25-70% strain. Strain-stiffening behavior is correlated with a material's network structure<sup>[329]</sup>. For physically crosslinked networks, such as the hydrogels examined in this work, strain stiffening is dependent on the flexibility of the polymers or protein filaments. More flexible filaments result in networks that stiffen at higher strains whereas less flexible filaments result in networks that stiffen at lower strains<sup>[328]</sup>. This suggests that the collagen fibrils present in the kidney dECM hydrogels are less flexible than those present in the purified type I collagen hydrogels. This may be a result of the processing procedure (*i.e.*, pepsin digestion) in combination with the presence of other ECM components that may alter collagen fibril stiffness and overall network structure.

The network structure and overall matrix stiffness act in concert with the matrix components to influence the response of cells exposed to the matrix microenvironment<sup>[168, 271, 330, 331]</sup>. Kidney dECM and collagen hydrogels of similar concentration (2.5 mg/mL) exhibited similar  $G'$  values based on rheological characterization and were thus employed in cell studies to avoid introducing hydrogel stiffness as a confounding variable during analysis. The concentration for collagen hydrogels was limited to a maximum of 2.5 mg/mL due to the low concentration of the material supplied by the vendor (a solution of 2.9 mg/mL).

Human conditionally-immortalized GEnCs were employed as a model cell type for investigating the cell response to interactions with kidney dECM hydrogels. This cell line is derived from endothelial cells isolated from kidney glomeruli. Unlike primary cells that are difficult to expand in culture and lose important phenotypic characteristics over time, the conditionally-immortalized GEnCs maintain the capacity to be

expanded in culture when cultured at the permissive temperature, but when thermoswitched to the non-permissive temperature become quiescent and adopt a progressively mature phenotype. The *in vitro* cell studies presented here demonstrate that kidney dECM hydrogels may serve as a biocompatible substrate to support attachment, viability, and proliferation of human GEnCs with results similar to those of collagen hydrogels (**Figure 2-5 A-C**). In addition, because these hydrogels are formed under mild conditions and at physiological temperature, they are permissive for cell encapsulation. The cell encapsulation studies presented here demonstrate that human GEnCs exhibit high viability when encapsulated within kidney dECM hydrogels (**Figure 2-5 D, E**). However, as the cells began to exert contractile forces on the relatively weak mechanical properties of the collagen and kidney dECM hydrogels in an effort to spread or migrate<sup>[270]</sup>, the hydrogels contracted. Moreover, despite increasing gene expression over the twelve-day culture period of cell-cell interaction proteins *PECAM1*, *CDH5*, and *ICAM2* (**Figure 2-10 A-C** and **2-11 A-C**) as well as *MMP14* (**Figure 2-10 D** and **2-12 G**) involved in ECM breakdown<sup>[332]</sup>, strong cell-cell interactions were not observed in H&E-stained sections (**Figures 2-6 to 2-8**).

In addition to the weak mechanical properties of the hydrogels, it is possible that the biochemical composition of the kidney dECM hydrogels developed in this investigation were not ideal for encapsulation of the GEnCs utilized. Biochemical characterization of decellularized kidney tissues presented in this work was performed, demonstrating retention of key ECM proteins such as type I collagen, type IV collagen, laminin, and sulfated GAGs. However, decellularized ECM hydrogels are complex and may contain any combination of proteins, cryptic peptides and bioactive motifs, sequestered growth factors, cytokines, chemokines, and even matrix-bound nanovesicles<sup>[264]</sup>. Any of these additional bioactive components may present negative or undesired signaling cues to specific cell types. Alternatively, despite increasing gene expression of several growth factor receptors over the culture period, including *KDR*, *TEK*, *TIE1*, and *PTPRB* (**Figures 2-10 E-H**, **2-11 D-E**, and **2-12 A-B**), critical bioactive factors may be lost or rendered inactive during decellularization or hydrogel processing<sup>[170]</sup>, resulting in poor cell response. For example, VEGF was deliberately excluded from the culture media in these studies following previous investigations utilizing this conditionally-immortalized cell line<sup>[316, 333, 334]</sup>; however, the lack of active and bioavailable VEGF may explain the deficiency of cell-cell contacts formed. Similar trends in gene expression by cells

cultured on hydrogel substrates (**Figure 2-9**) further support the possibility that the biochemical composition of kidney dECM hydrogels was suboptimal in comparison to control collagen hydrogels. Future studies will aim to tune the hydrogel mechanical properties and composition by modifying the processing procedures to include covalent crosslinking methods and strategies to restore critical signaling cues thought to be lost.

The work presented here is the first to explore the use of kidney dECM hydrogels for direct encapsulation of GEnCs; however, this is not the first study to investigate the potential of kidney dECM hydrogels in general. O'Neill, *et al.* explored the regional specificity of kidney dECM in solubilized, hydrogel, and sheet forms on modulating mouse papilla-derived kidney stem cell growth and metabolism<sup>[278]</sup>. The rheological or mechanical properties of the region-specific kidney dECM hydrogels were not investigated in the O'Neill, *et al.* study; however, the authors demonstrated that kidney stem cells adopted a significantly more proliferative and metabolically active phenotype when cultured in the presence of kidney dECM as opposed to heart or bladder dECM. Furthermore, they also demonstrated that kidney stem cells cultured in the presence of kidney papillae-derived dECM in any form resulted in lower cell proliferation, higher metabolic activity, and altered cell morphology in comparison to cortex- and medulla-derived dECM<sup>[278]</sup>. It is thought that the renal papilla represents the native kidney stem cell niche<sup>[335, 336]</sup>, therefore, it follows that dECM derived from the papillae would maintain a stem cell phenotype as suggested by the results. Furthermore, the authors propose that cortical- and medullary-derived dECM may show potential in directing differentiation of kidney stem cells towards specific renal lineages<sup>[278]</sup>.

Nagao, *et al.* examined the influence of human kidney cortex-derived dECM hydrogels on human kidney peritubular microvascular endothelial cell (HKMEC) phenotype<sup>[282]</sup>. Proteomics analysis of the decellularized kidney cortex revealed that type IV collagen was present in the highest abundance; however, rheological testing indicated that the complex modulus of the corresponding hydrogel at a concentration of 7.5 mg/mL only reached 15 Pa. This is much weaker than the 110-130 Pa measured for the kidney dECM hydrogels at a concentration of 5.0 mg/mL presented in this study. Nagao, *et al.* further demonstrated that HKMECs cultured on these hydrogel substrates exhibited a more quiescent and mature phenotype. The addition of type I collagen to increase the hydrogel mechanical properties (up to 250 Pa) led to a more activated HKMEC state<sup>[282]</sup>. The data presented by the authors coincides with *in vivo* evidence that an

increased collagen content in the kidney ECM is associated with fibrosclerosis and the development of chronic kidney disease<sup>[337-339]</sup>.

Most recently, Magno, *et al.* investigated the ability to utilize macromolecular crowding as a method for tailoring the fibrillar architecture of kidney dECM hydrogels<sup>[279]</sup>. The incorporation of increasing concentrations of a macromolecular crowder, Ficoll400, resulted in faster rates of fibrillogenesis as measured by turbidimetric analysis, generation of thicker fibrils and greater fibril alignment, and reduced hydrogel stiffness. Interestingly, this effect is the opposite of those previously observed for pure type I collagen hydrogels where increasing concentrations of macromolecular crowders resulted in a decrease in fibril thickness and reduced fiber alignment<sup>[340]</sup>. In addition, the researchers found that the inclusion of Ficoll400 resulted in greater network formation by human umbilical vein endothelial cells (in the presence of VEGF) and morphogenesis of mouse kidney stem cells when cultured on kidney dECM hydrogels<sup>[279]</sup>.

Together, this and previous studies demonstrate that kidney-derived dECM hydrogels are able to support cell attachment, viability, and proliferation. Furthermore, region-specific kidney-derived dECM hydrogel substrates have already been shown to modulate cell response and either maintain an immature, stem cell-like phenotype<sup>[278]</sup> or a more mature, quiescent phenotype<sup>[282]</sup>. Future studies may thoroughly investigate region-specific kidney-derived dECM composition or the ability to tailor such hydrogels with additives, the corresponding gelation kinetics, and the ultrastructure and rheological characteristics of the resulting hydrogel. Such investigations will continue to delineate some of the factors that influence the response of different cell types or stem cells directly encapsulated within tissue- and organ-specific 3D cell culture microenvironments.

## 2.5. Conclusion

Kidney dECM can be digested and processed to form hydrogels that retain biochemical signaling cues of the kidney dECM microenvironment. The kidney dECM hydrogels presented in this study exhibit fibrous ultrastructural networks similar to other dECM hydrogels previously presented by others but unique rheological characteristics from other tissue- and organ-derived dECM hydrogels and from purified type I collagen hydrogels. These kidney dECM hydrogels may act as a substrate for cell culture or for

encapsulation of cells as a 3D cell culture microenvironment. While only human glomerular endothelial cells were presented in this study, it is anticipated that the hydrogels may serve as a culture environment for any cell type, kidney-specific, stem cell, or otherwise with potential in developing a kidney tissue model for developmental studies and pharmaceutical screening applications.

**CHAPTER III:**

**Poly(Ethylene Glycol)-Crosslinked Gelatin Hydrogel Substrates  
with Conjugated Bioactive Peptides Influence Endothelial Behavior**

Chapter 3, in part, has been published elsewhere: <sup>[280]</sup> Su J, Satchell SC, Wertheim JA, and Shah RN. "Poly(ethylene glycol)-crosslinked gelatin hydrogel substrates with conjugated bioactive peptides influence endothelial cell behavior." *Biomaterials* **201** (2019): 99-112.

### 3.1. Introduction

The extracellular matrix (ECM) is composed of proteins, polysaccharides, and other biological molecules secreted by resident cells. These components together act as a natural scaffolding material that imparts mechanical integrity to tissues and organs as well as presents bioactive signals essential for cell and tissue development and maintenance<sup>[169, 303]</sup>. The ECM is a dynamic and highly-hydrated network akin to a stimulus-responsive hydrogel that is tailored to the microenvironmental needs of the inhabiting cells<sup>[235, 236]</sup>. In particular, the basement membrane (BM) is a specialized ECM substrate that lies beneath epithelial and endothelial cell populations and provides structural support, spatial organization, and bioactive signaling cues to the overlying cells<sup>[31]</sup>. Despite the popularity of naturally-derived materials such as basement membrane extracts (e.g., Matrigel) for studying complex cell-cell and cell-matrix interactions, often times these materials are limited by lot-to-lot variability and the inability to precisely tune material properties<sup>[36]</sup>.

The objective of this investigation was to engineer a hydrogel substrate capable of mimicking properties of the BM specifically to explore endothelial cell-cell and cell-matrix interactions. To accomplish this, we employed a versatile approach for generating hydrogels from both synthetic and natural polymer sources with tunable stiffness, termed the PEGX method<sup>[341]</sup>. The method utilizes a poly(ethylene glycol) (PEG) crosslinker, or PEGX, to form covalent crosslinks between available reactive groups on the polymers resulting in a stable network and hydrogel formation. Hydrogel stiffness may be modulated by varying the polymer concentration or the amount of crosslinker added, and the crosslinking method can be extended to a variety of different physical and chemical PEGX variants<sup>[341]</sup>.

Gelatin was chosen as the base polymer for the hydrogels. Though not generally considered a BM component, gelatin is an accessible and economical biomaterial that has been employed in numerous biomedical applications, such as vehicles for drug delivery, scaffolds for tissue engineering, and hydrogels

for 3D matrix cultures<sup>[305, 342, 343]</sup>. Because gelatin is derived from collagen, it retains key bioactive peptide sequences such as cell-binding sites (*e.g.*, RGD) and matrix metalloproteinase-sensitive degradation motifs. To specifically tailor the bioactivity of these hydrogel substrates to better mimic the BM of endothelial cells, we sought to incorporate peptide sequences known to modulate endothelial cell behavior. We further hypothesized that the desired peptides could be conjugated to the gelatin polymer through the use of additional PEGX, resulting in a covalent link that would lead to prolonged residence time, as opposed to simple encapsulation of the peptides within the hydrogels, and therefore extend availability for signaling pathway activation. Two peptides of significant interest for examining the effects on endothelial cells are the laminin-derived YIGSR peptide and the vascular endothelial growth factor (VEGF)-mimetic QK peptide.

The YIGSR peptide is derived from the  $\beta$ 1 chain of laminin, a major component of the BM<sup>[31]</sup>, and was discovered to mediate cell adhesion and migration through binding of the 67-kDa laminin receptor<sup>[344, 345]</sup>. Research by other groups demonstrated that modification of polyurethaneurea films and scaffolds with YIGSR peptides enhanced endothelial attachment and reduced platelet adhesion<sup>[346-348]</sup>. Interestingly, in combination with RGD peptides, YIGSR peptides inhibited endothelial growth on self-assembled peptide hydrogels<sup>[349]</sup>. However, additional investigations showed that covalent attachment of RGD and YIGSR peptides to PEG acrylate/diacrylate hydrogels enhanced endothelial cell migration<sup>[350]</sup> and tubulogenesis<sup>[351]</sup>.

The QK peptide is a VEGF-mimetic peptide first designed by D'Andrea, *et al.* and confirmed to bind and activate VEGF Receptor 1 (VEGFR1 or Flt-1) and VEGF Receptor 2 (VEGFR2 or KDR)<sup>[352]</sup>. VEGF signaling is important in a variety of physiological contexts, but it is especially critical in the development of new blood vessels and maintenance of healthy vasculature and endothelial function<sup>[353]</sup>. Furthermore, heparan sulfate proteoglycans, another major component of the BM, are known to bind and sequester growth factors including specific VEGF isoforms<sup>[31]</sup>. However, in contrast to large growth factors such as recombinant VEGF, the use of short, bioactive peptide mimetics is advantageous due to their smaller size, decreased chemical complexity, and reduced production costs<sup>[354]</sup>. The QK peptide consists of 15 natural amino acids and is likely named for the first and last residues that constitute the peptide's helical region (the sequence between residues 4 and 12 of the peptide) and correspond to the  $\alpha$ -helix region of VEGF<sup>[352]</sup>.

Research by other groups demonstrated that the QK peptide stimulated endothelial growth when tethered to elastin-like peptide hydrogels<sup>[355]</sup>, promoted endothelial network formation when incorporated into type I collagen coatings<sup>[356]</sup>, and enhanced endothelial tube-like structure formation when conjugated to PEG diacrylate<sup>[357]</sup> and gelatin methacrylate<sup>[358]</sup> hydrogels.

In this work, we developed crosslinked gelatin hydrogels with conjugated YIGSR and QK peptides using the PEGX method and evaluated these hydrogels as BM-like substrates for endothelial cell culture. Successful crosslinking of the gelatin polymers and conjugation of the YIGSR and QK peptides was determined by measuring the available reactive groups remaining after the crosslinking reaction. Rheology was performed to observe hydrogel crosslinking kinetics and measure the rheological properties (*i.e.*, shear moduli) of the hydrogels. Scanning electron microscopy and swelling analysis revealed the ultrastructural and swelling characteristics of the hydrogels, respectively. For cell culture studies, we employed human umbilical vein endothelial cells (HUVECs) and conditionally-immortalized human glomerular endothelial cells (GEnCs). Intracellular levels of phosphorylated VEGFR2 in response to treatment with soluble QK peptide or culture on QK-conjugated hydrogels was measured to assess the bioactivity of the peptide. Finally, gene expression of cells cultured on hydrogel substrates was evaluated at multiple timepoints.

## **3.2. Material & Methods**

### **3.2.1. Peptide Synthesis and Determination of Peptide Concentrations for Experiments**

QK, YIGSR, and RYGS (scrambled YIGSR peptide control) peptides were purchased through custom peptide synthesis from ABI Scientific and confirmed to have a purity of >95% by high-performance liquid chromatography. Peptide sequences are listed in **Table 3-1**. Lysine  $\epsilon$ -amino groups were acetylated to prevent cross-reactivity with the amine-reactive PEGX. C-termini of peptides were amidated to enhance stability, but N-termini were left unmodified. Peptides were solubilized in 1 $\times$  phosphate-buffered saline solution (PBS, pH 7.4, Gibco, #10010) as concentrated stock solutions and frozen in aliquots at -20 °C. Aliquots were thawed and diluted as necessary for hydrogel preparation. Hydrogel formulations containing a range of peptide concentrations (QK and/or YIGSR) were devised based on evaluations of literature investigations. Previous studies exploring the bioactivity of the QK peptide and incorporation of the QK

peptide into other hydrogel systems tested concentrations ranging from 1  $\mu\text{M}$  to 100  $\mu\text{M}$  and greater<sup>[352, 356-358]</sup>. Therefore, we selected QK peptide concentrations of 0, 1, 10, and 100  $\mu\text{M}$  to evaluate its effect on endothelial cells when conjugated to hydrogels using the PEGX method. A study investigating conjugation of the YIGSR peptide into PEG diacrylate hydrogels used a concentration of 3.5 mM<sup>[351]</sup>. Another study incorporating the YIGSR peptide into self-assembling peptide hydrogels found optimal HUVEC growth at a concentration of 6 mM<sup>[349]</sup>. Therefore, we selected YIGSR concentrations of 0, 3, 6, and 12 mM to evaluate its effect on endothelial cells when conjugated to hydrogels using the PEGX method.

Peptide	Sequence (N-terminal to C-terminal)	Theoretical MW (g/mol)
<b>QK</b>	(K-Ac)LTWQELYQL(K-Ac)Y(K-Ac)GI where (K-Ac) indicates acetylation of the lysine $\epsilon$ -amino group	2036.31
<b>YIGSR</b>	YIGSR	593.68
<b>RYGSI</b>	RYGSI	593.68

### **3.2.2. Preparation of Hydrogels and Phase Analysis**

The general strategy for the preparation of PEG-crosslinked gelatin hydrogels with conjugated peptides is outlined in **Figure3-1**. Gelatin type A (Sigma-Aldrich, #G1890) was solubilized in PBS at 37 °C at a stock concentration of 10% (m/v). Hydrogel precursor polymer solutions were prepared by mixing the following in order: PBS for dilution, 1 M NaOH (Sigma-Aldrich, #S2770) to buffer solutions to an approximate final pH of 6 for optimal crosslinking kinetics, peptides (if desired), and gelatin stock solution. Polymer solutions were held at 37 °C prior to crosslinking to ensure solution phase and thoroughly vortexed before the addition of crosslinker. Homobifunctional poly(ethylene glycol) succinimidyl valerate (SVA) (MW 5000 g/mol, Laysan Bio), referred to as simply PEG crosslinker or PEGX, was prepared as a concentrated stock solution at 40 mM in PBS just prior to crosslinking of polymer solutions. Immediately after adding PEGX to hydrogel precursor polymer solutions, solutions were vortexed, pipetted into well plates or molds as necessary, and incubated at 37 °C for 2 hrs. Main hydrogel formulations investigated are listed in **Table 3-2**. For phase analysis and phase plot generation, hydrogel formulations were prepared in microcentrifuge

tubes. After the 2 h incubation period, phase of formulations, either solution (sol) or hydrogel (gel), was determined by tube inversion, and those determined to be gel phase were manipulated with a spatula to qualitatively gauge hydrogel stiffness. Hydrogels that could be easily spread were designated as “soft”, and those that retained their shape were designated as “robust”<sup>[341]</sup>.

**Table 3-2: Main hydrogel formulations tested.**

Sample	No Peptides	QK	YIGSR	YIGSR/QK	RYGSI (Scrambled YIGSR Control)
Gelatin, % (m/v)	5.0	5.0	5.0	5.0	5.0
QK ( $\mu$ M)	0.0	100.0	0.0	100.0	0.0
YIGSR (mM)	0.0	0.0	12.0	12.0	0.0
RYGSI (mM)	0.0	0.0	0.0	0.0	12.0
PEGX (mM)	1.55	1.60	7.95	8.00	7.95
PEGX:Gelatin (m:m)	0.155	0.160	0.795	0.800	0.795

### 3.2.3. Quantification of Free Amine Content

Free amine content of hydrogel precursor polymer solutions and crosslinked hydrogels were quantified by the 2,4,6-trinitrobenzenesulfonic acid (TNBS) assay and performed according to previously published studies<sup>[341, 359, 360]</sup>. TNBS working solution was prepared fresh by diluting stock solution (picrylsulfonic acid solution, Sigma-Aldrich, #P2297) to a concentration of 0.01 M with a 4% (m/v) sodium bicarbonate solution (Sigma-Aldrich, #S5761), pH 8.5 prepared in deionized H<sub>2</sub>O. A volume of 500  $\mu$ L TNBS working solution was added to freshly-prepared 50- $\mu$ L hydrogel precursor polymer solutions and crosslinked hydrogels, and samples were incubated at 37 °C for 2 h. To stop reactions, 500  $\mu$ L of 10% (m/v) sodium dodecyl sulfate (Sigma-Aldrich, #L3771) prepared in deionized H<sub>2</sub>O and 250  $\mu$ L of 1 M HCl (Sigma-Aldrich, #H9892) were added to samples. Samples were then allowed to hydrolyze overnight at 37 °C. Samples were diluted as necessary in deionized H<sub>2</sub>O, and 200  $\mu$ L per sample was transferred to a clear 96-well plate. Absorbance at 335 nm ( $A_{335}$ ) was measured on a BioTek Cytation 3 Cell-Imaging Multi-Mode Reader. Samples were tested in triplicate ( $n = 3$ ) with technical replicates in duplicate, compared to

a standard curve of L-leucine (Sigma-Aldrich, #L8000), and normalized to the uncrosslinked control group of 5% (m/v) gelatin solution with no peptides.

### **3.2.4. Rheological Characterization and pH Measurement**

Rheological characterization of hydrogels was performed following a recommended protocol for hydrogels for tissue engineering applications<sup>[318]</sup>. Testing was performed using an Anton Paar MCR 302 rheometer with a 25-mm 2°-angle cone-plate fixture under strain-controlled conditions. The lower Peltier cell was set to 37 °C and allowed to equilibrate prior to sample loading. All samples were prepared fresh and immediately loaded onto the rheometer stage. Once the measuring system was lowered, mineral oil (Amresco, #J217) was applied to the edges of the fixture and sample, and the entire system was enclosed within a solvent trap to prevent sample dehydration. Time sweeps were performed for 2 h at 37 °C, 1% strain, and 10 rad/s. Frequency and strain sweeps were performed immediately following under the same conditions. After sample loading, the pH of excess sample volume remaining was measured using a VWR sympHony SB70P pH meter with a Thermo Scientific Orion PerpHecT ROSS Combination pH Micro Electrode. All samples were tested in triplicate ( $n = 3$ ).

### **3.2.5. Scanning Electron Microscopy (SEM)**

Hydrogels were fixed in 2% (v/v) glutaraldehyde (Sigma-Aldrich, #G7776) and 3% (m/v) sucrose (J. T. Baker, #4072) in 1× PBS, pH 7.4 for 1 h at 4 °C. Samples were dehydrated in a graded ethanol series (30-100% in MilliQ H<sub>2</sub>O, Decon Laboratories, #2701) of 15 min intervals and critical-point dried in a Tousimis SAMDRI-790 Critical Point Dryer. For low-magnification SEM, samples were sputter coated with ~10 nm of Au using a Baltec MED-020 Coating System and imaged on a JEOL NeoScope JCM-6000PLUS. For high-magnification SEM, samples were coated with ~9 nm of Os using an SPI Supplies Osmium Plasma Coater OPC-60A and imaged on a Hitachi S-4800 Type II field emission SEM.

### **3.2.6. Swelling Analysis**

Hydrogel precursor polymer solutions plus PEGX were prepared, and 100 µL of polymer solution was cast into 8-mm diameter cylindrical silicone molds (Grace Bio-Labs). After the 2 h incubation period,

crosslinked hydrogels were carefully removed from molds, and the initial weights ( $W_{initial}$ ) of samples were recorded. Samples were then allowed to equilibrate in 3 mL PBS per sample for 24 h at 37 °C. After equilibration, samples were removed from PBS, lightly blotted with filter paper, and weighed. The new equilibrated or swollen wet weights ( $W_{wet}$ ) of samples were recorded. Samples were then frozen at -80 °C and lyophilized overnight on a VirTis adVantage Plus EL-85, and the dry weights ( $W_{dry}$ ) of samples were recorded. The percent weight increase and swelling ratio of hydrogels were calculated as follows:

$$\% \text{ weight increase} = \frac{W_{wet} - W_{initial}}{W_{initial}} * 100\%$$

$$\text{swelling ratio, } Q_s = \frac{W_{wet}}{W_{dry}}$$

All samples were weighed on a Mettler Toledo XP105DR Excellence Plus analytical balance, and the sample size was six hydrogels for each group ( $n = 6$ ).

### 3.2.7. Cell Culture

Human umbilical vein endothelial cells (HUVECs) were purchased from Lifeline Cell Technology (normal primary, #FC-0003) and cultured in Endothelial Growth Medium-2 (EGM-2 BulletKit, Lonza, #CC-3162) containing 2% fetal bovine serum (FBS) and growth factors as supplied with the exception of VEGF. Growth factor supplements: epidermal growth factor, fibroblast growth factor  $\beta$ , R3-insulin-like growth factor-1, ascorbic acid, hydrocortisone, heparin, and gentamicin and amphotericin-B. Cells were cultured at 37 °C and 5% CO<sub>2</sub>, media was exchanged every other day, and cells were used between passages 3 and 5 for experimental studies. Conditionally-immortalized human glomerular endothelial cells (GEnCs) were cultured as described previously<sup>[316]</sup>. These are primary cells that have been transfected with a temperature-sensitive *SV40-T* antigen and the essential catalytic subunit of human telomerase (*hTERT*) to prevent replicative senescence<sup>[316, 319]</sup>. Culture at the permissive temperature of 33 °C results in active expression of the transgenes to maintain an immature cell state and allow proliferation of the cells. Thermoswitching to the non-permissive temperature of 37 °C results in inactivation of the transgenes, causing the cells to become quiescent and adopt a more mature phenotype that is comparable to freshly isolated GEnCs<sup>[316]</sup>. GEnCs were cultured in Microvascular Endothelial Growth Medium-2 (EGM-2 MV

BulletKit, Lonza, #CC-3202) containing 5% FBS and growth factors as supplied with the exception of VEGF. Growth factor supplements: epidermal growth factor, fibroblast growth factor  $\beta$ , R3-insulin-like growth factor-1, ascorbic acid, hydrocortisone, and gentamicin and amphotericin-B. Media was exchanged every other day, and cells were used at passage 30 or below for experimental studies.

### **3.2.8. Cell Experimental Studies**

Experimental studies involving cell culture on hydrogel substrates were performed in a similar manner as previously-established endothelial cell tube formation assays<sup>[361, 362]</sup>. Hydrogel precursor polymer solutions plus PEGX were prepared and cast in well plates, 165  $\mu\text{L}/\text{cm}^2$ , and allowed to incubate for 2 h at 37 °C prior to plating of cells. Matrigel Basement Membrane Matrix (Phenol Red-Free, Corning, #356237) served as an additional control for cell experimental studies. Matrigel was thawed on ice, cast in well plates, and incubated alongside experimental groups. Cells were then prepared for plating: cells were rinsed once with 1 $\times$  Dulbecco's phosphate-buffered saline (DPBS, Mediatech, #21-030), lifted with TrypLE Express (Gibco, #12605) at 37 °C, collected and counted via the trypan blue exclusion method using Trypan Blue solution (Sigma-Aldrich, #T8154), centrifuged at 1100 RPM for 5 min, and resuspended in complete media. Cells were plated on substrates at an approximate final density of 48,000 cells/ $\text{cm}^2$ , and well plates were transferred to a 37 °C incubator at 5%  $\text{CO}_2$ . At designated time points, photomicrographs of samples were captured on a Lumenera INFINITY1-3C microscopy camera mounted on a Nikon Eclipse TS100 using Lumenera *INFINITY ANALYZE* 6.5 software.

### **3.2.9. VEGFR2/KDR Phosphorylation Assay**

Phosphorylated VEGFR2 was quantified with the Human Phospho-VEGF R2/KDR DuoSet IC ELISA (R&D Systems, #DYC1766) kit. GEnCs were expanded at 33 °C, plated on culture substrates three days prior to treatment, and cultured at 37 °C after plating. HUVECs were plated on culture substrates two days prior to treatment and cultured at 37 °C. Both HUVECs and GEnCs were fully confluent prior to treatment and sample collection. Cells were serum deprived overnight in Endothelial Basal Medium-2 (EBM-2, Lonza, #CC-3156) plus 1% FBS (Gibco, #16000) and 1% penicillin-streptomycin (Gibco, #15140) prior to treatment and then serum starved in EBM-2 plus 1% penicillin-streptomycin for 5 h prior to

treatment. Cells were treated with one of the following soluble factors for 5 min at 37 °C: no treatment (negative control), 100 ng/mL recombinant human VEGF-165 (~5.2 μM, R&D Systems, #293-VE-010/CF) (positive control), 1 μM soluble QK peptide, or no treatment for cells cultured on QK hydrogels (hydrogels conjugated with 100 μM of QK peptide). After treatment, cells were rinsed twice with DPBS and collected with Lysis Buffer #9 composed of Sample Diluent Concentrate 2 (R&D Systems, #DYC002), 10 μg/mL aprotinin (Tocris, #4139), and 10 μg/mL leupeptin (Tocris, #1167) following the kit recommendations. Cell lysates were frozen at -80 °C until assayed following the manufacturer's protocol, and sample absorbance at 450 nm ( $A_{450}$ ) corrected by absorbance at 540 nm ( $A_{540}$ ) was measured on a BioTek Synergy 2 Multi-Mode Microplate Reader. Biological replicates were tested in quadruplicate ( $n = 4$ ) with technical replicates in duplicate. Samples were compared to a standard curve of Human Phospho-VEGF R2/KDR Control provided by the manufacturer and normalized to negative (no treatment, tissue culture polystyrene substrates) control groups for each cell type.

### **3.2.10. Gene Expression Analysis**

RNA was isolated from samples and cell pellets using TRIzol Reagent (Invitrogen, #15596) following the manufacturer's protocol. Isolated RNA was treated with DNA-free DNA Removal Kit (Ambion, #1906) to remove contaminating genomic DNA from samples. RNA concentration was measured using a NanoDrop 1000 Spectrophotometer (Thermo Scientific). Reverse transcription and cDNA synthesis was performed using iScript Reverse Transcription Supermix for RT-qPCR (Bio-Rad, #170-8841) with an Applied Biosystems GeneAMP PCR System 9700 following the manufacturer's protocol. Quantitative real-time polymerase chain reaction was performed using SsoAdvanced Universal SYBR Green Supermix (Bio-Rad, #170-5270) with 300 nM each of forward and reverse primers and 0.10 ng/μL DNA on an Applied Biosystems QuantStudio 7 Flex Real-Time PCR System. Primer sequences for genes of interest are listed in **Table 3-3**. The thermal profile used included an initial polymerase activation step at 95 °C for 30 sec followed by 40 amplification cycles of denaturation at 95 °C for 15 sec and annealing and extension at 60 °C for 60 sec. The expression of each gene of interest was normalized to expression of the housekeeping gene *cyclophilin A (PPIA)*, and the relative degree of gene amplification was calculated using the  $\Delta\Delta C_T$

method:  $2^{[(C_T \text{ GOI } 2 - C_T \text{ PPIA } 2) - (C_T \text{ GOI } 1 - C_T \text{ PPIA } 1)]}$ . “C<sub>T</sub> GOI 1” represents the threshold cycle (C<sub>T</sub>) of the gene of interest of the reference population, and “C<sub>T</sub> GOI 2” represents the gene of interest of the experimental sample. Day 0 HUVECs cultured on tissue culture polystyrene served as the reference population for HUVEC samples, and day 0 GEnCs cultured on tissue culture polystyrene served as the reference population for GEnC samples. Biological replicates were tested in quadruplicate ( $n = 4$ ) with technical replicates in triplicate.

**Table 3-3: Primer sequences for gene expression analysis via quantitative real-time polymerase chain reaction (qPCR).**

Gene	Forward Primer (5' to 3')	Reverse Primer (5' to 3')
<b>PPIA</b>	TCG CTC TCT GCT CCT CCT GTT CGA	GGC GCC CAA TAC GAC CAA ATC C
<b>PECAM1</b>	TAT GAT GCC CAG TTT GAG GT	GAA TAC CGC AGG ATC ATT TG
<b>CDH5</b>	TTG GAA CCA GAT GCA CAT TGA T	TCT TGC GAC TCA CGC TTG AC
<b>ITGB1</b>	CCC ACC GTG TTC TTC GAC ATT	GGA CCC GTA TGC TTT AGG ATG A
<b>ITGB3</b>	GTG ACC TGA AGG AGA ATC TGC	CCG GAG TGC AAT CCT CTG G
<b>KDR</b>	GTG ATC GGA AAT GAC ACT GGA G	CAT GTT GGT CAC TAA CAG AAG CA
<b>TEK</b>	TCC GCT GGA AGT TAC TCA AGA	GAA CTC GCC CTT CAC AGA AAT AA
<b>VWF</b>	TGC CTC CAA AGG GCT GTA TC	CAC CAC TGT TCT CCA CTG CTC
<b>NOS3</b>	TGA TGG CGA AGC GAG TGA AG	ACT CAT CCA TAC ACA GGA CCC
<b>PLVAP</b>	CTC TTC ATG GTC TAT GGC AAC G	GCG AGC ATT CAG CCA CAT C

### 3.2.11. Immunofluorescence Staining

Samples were rinsed once with DPBS and fixed with 4% paraformaldehyde (Alfa Aesar, #43368) in DPBS for 12 min at room temperature after which fixative was replaced with fresh DPBS, and samples were stored at 4 °C until staining. To perform whole-mount immunofluorescence staining, fixed samples were carefully removed from well plates and transferred to microcentrifuge tubes. Samples were rinsed once with PBS, permeabilized with 0.1% Triton X-100 (Amresco, #0694) in PBS (PBST) for 10 min., and then blocked with SEA BLOCK Blocking Buffer (Thermo Scientific, #37527) for 30 min to 1 h. Primary antibodies were diluted in blocking buffer as follows: mouse anti-PECAM-1 at 1:100 (Abcam, #ab187377) and rabbit anti-VEGF Receptor 2 at 1:200 (Cell Signaling Technology, #2479). Samples were incubated with primary antibodies for 1 h at room temperature, rinsed three times with PBST, blocked with blocking

buffer for an additional 5 min, and then incubated with secondary antibodies for 1 h at 37 °C. Secondary antibodies were diluted in blocking buffer as follows: goat anti-mouse Alexa Fluor 488 at 1:300 (Invitrogen, #A-11029) and goat anti-rabbit Alexa Fluor 555 at 1:300 (Invitrogen, #A-21429). After secondary antibody incubation, samples were rinsed three times with PBST, rinsed once with PBS, and mounted between #1.0 glass coverslips (Fisher Scientific, #12-542-B) with Mowiol mounting medium composed of Mowiol 4-88 Reagent (Calbiochem, #475904), glycerol (EMD Millipore, #137028), and 0.2 M Tris buffer (pH 8.5, Fisher Scientific, #BP152) containing 4',6-diamidino-2-phenylindole (DAPI, Invitrogen, #D1306) to stain for cell nuclei. Whole-mount samples were imaged on a Nikon A1 Confocal Laser Microscope System.

### **3.2.12. Statistical Analysis**

All quantitative data is represented as the mean  $\pm$  standard error of the mean. Statistical significance was determined using an unpaired, two-tailed Student's *t*-test assuming equal variance with Microsoft Excel (Microsoft). Significance for all statistical analyses was defined as  $p < 0.05$ .

### 3.3. Results

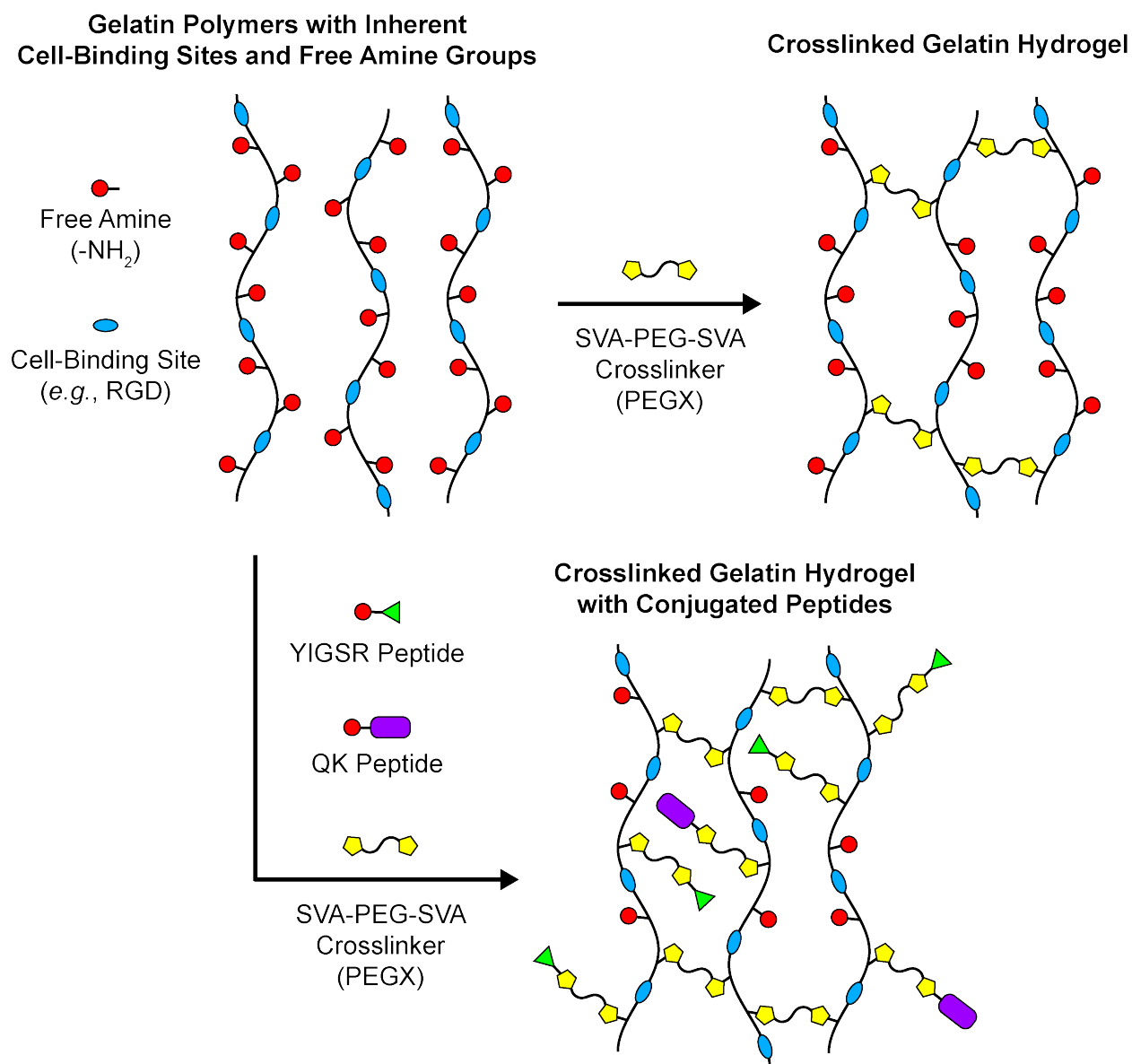


**Figure 3-1: Preparation of PEG-crosslinked gelatin hydrogels and conjugation of peptides.**

Gelatin possesses inherent cell-binding sites and free amine reactive groups. When PEGX is added to a gelatin solution, the SVA functional groups react with the free amines, forming crosslinks between gelatin polymers that results in hydrogel formation. Bioactive peptides presenting free amines, such as the YIGSR and QK peptides, can be added to the precursor polymer solution and with additional PEGX become conjugated to the gelatin polymers during hydrogel formation.

### **3.3.1. Optimization of Peptide and PEGX Concentrations**

A higher concentration of PEGX was required to adequately conjugate YIGSR peptides to the gelatin polymers at millimolar concentrations and ensure formation of stable hydrogel substrates that would not rapidly degrade in cell culture conditions. Phase analysis of formulations and the resulting phase plot depicts the necessary PEGX concentrations to generate increasingly stiffer hydrogels with conjugated YIGSR concentrations of interest (**Figure 3-2**). Rheological characterization of specific formulations aided in selecting precise PEGX concentrations to generate robust hydrogels of similar stiffness. Hydrogel formulations selected for the following initial cell experiment possessed final storage moduli of ~200-250 Pa.

Hydrogel substrates with varying combinations and concentrations of YIGSR and QK peptides (total of sixteen combinations) were prepared for cell culture to determine optimal peptide concentrations that elicited a discernible cell response. Matrigel was included as an additional group for comparison. GEnCs were plated on hydrogel substrates, and cells were observed in culture over time by optical microscopy. Cells cultured on hydrogels conjugated with 12 mM YIGSR peptide began to form cord-like structures after several hours. After 24 h in culture, cells cultured on YIGSR-conjugated hydrogels exhibited cord-like structure formation with branching structures occurring more frequently on hydrogels conjugated with 6 or 12 mM YIGSR peptide (**Figure 3-3**). At the same time, GEnCs also formed smaller yet distinctively apparent cord-like structures on hydrogels conjugated with 10 and 100  $\mu$ M QK peptide with consistently larger structures forming on hydrogels conjugated with 100  $\mu$ M QK peptide in comparison to those conjugated with only 10  $\mu$ M QK peptide (**Figure 3-3**). Therefore, in subsequent investigations, the maximum tested peptide concentrations were chosen, that is 100  $\mu$ M QK peptide and 12 mM YIGSR peptide (**Table 3-2**), as these concentrations elicited the greatest and most rapid cell response in this initial experiment.

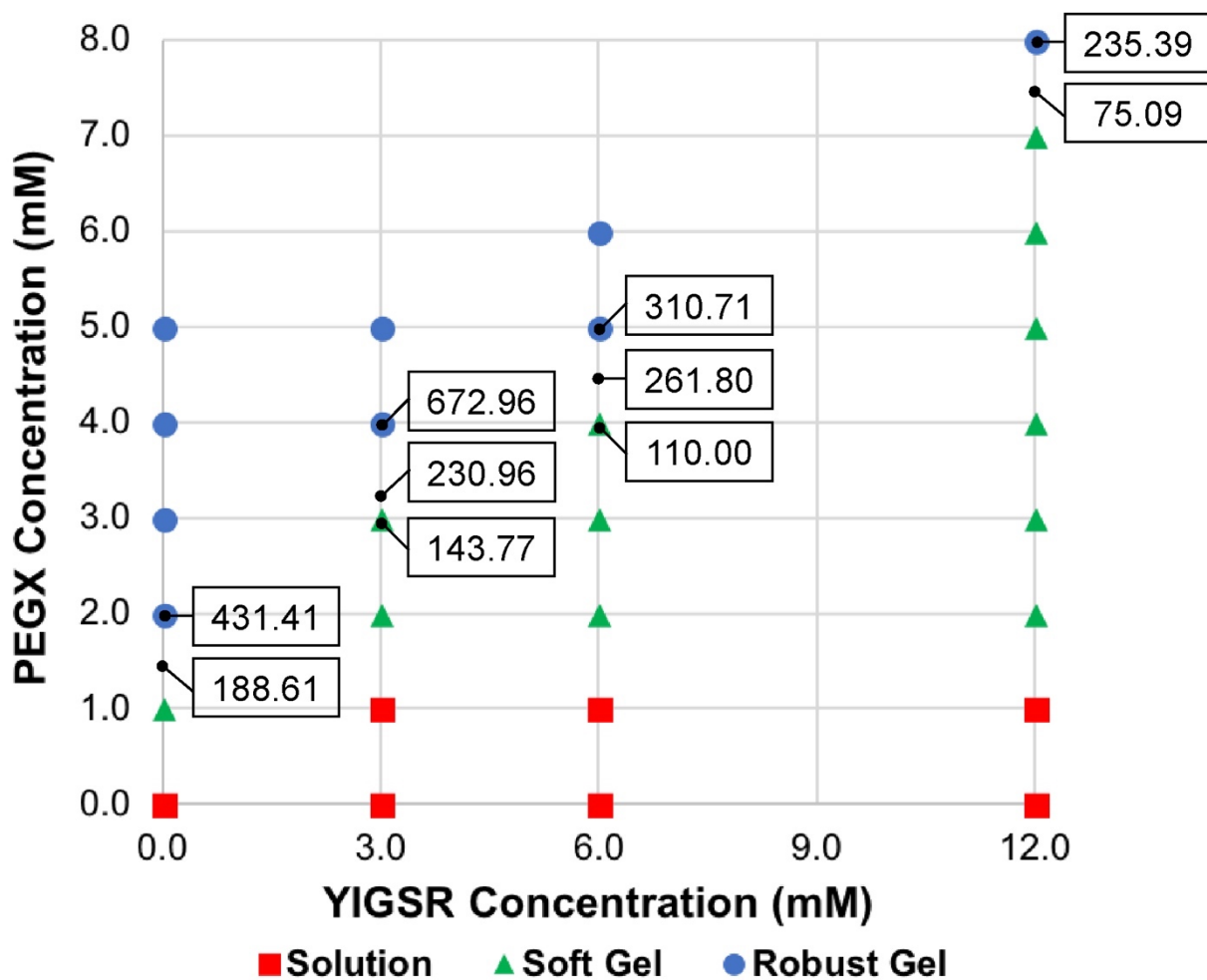


**Figure 3-2: Phase plot of varying YIGSR peptide concentrations with varying PEGX concentration.** The gelatin concentration is held constant at 5% (m/v). Values in boxes are the final storage moduli (in Pa) of indicated formulations as measured by two-hour time sweeps on a rheometer.

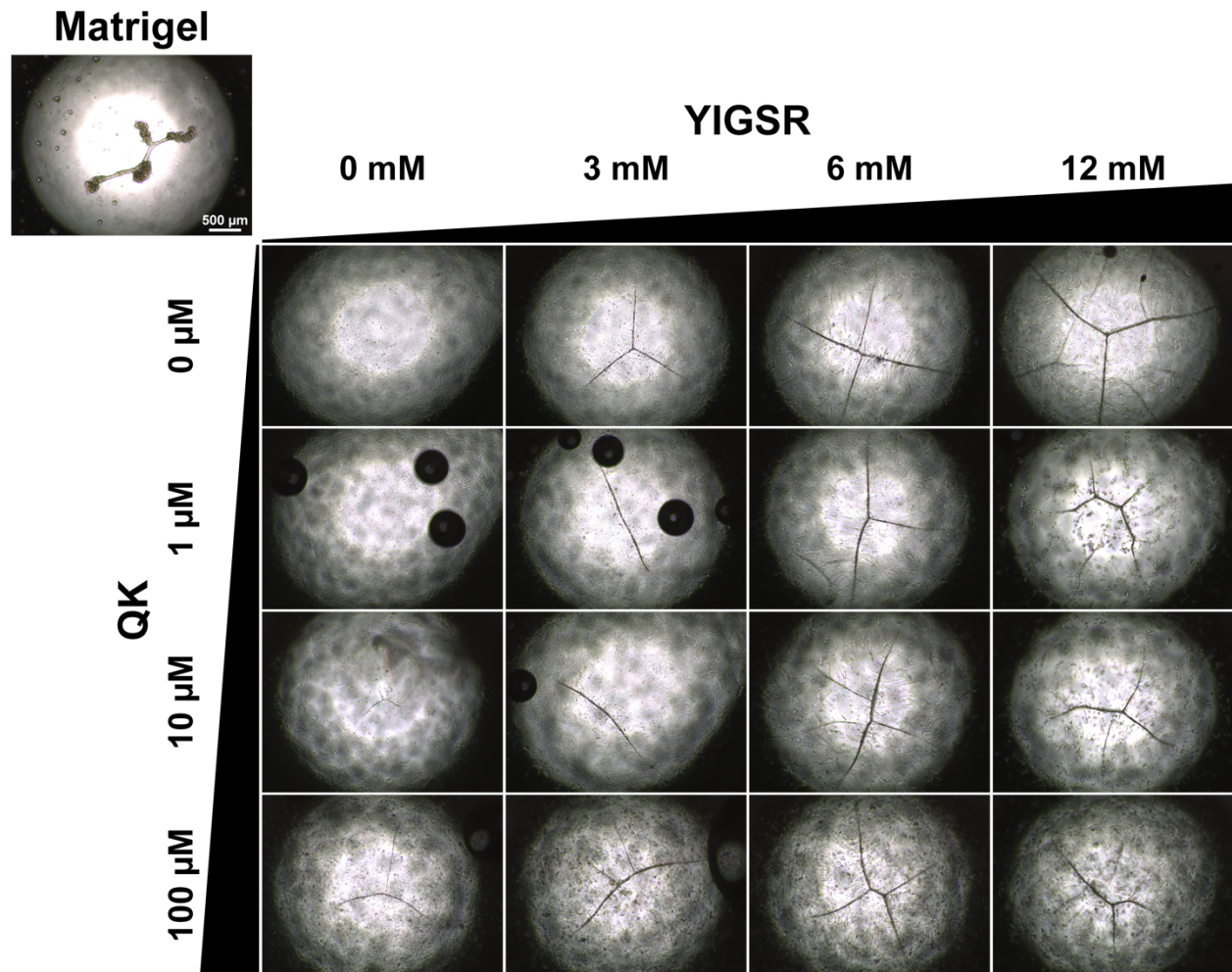


**Figure 3-3: Photomicrographs of GEnCs cultured on hydrogel substrates of varying combinations and concentrations of YIGSR and QK peptides.**  
Cultures after 24 h. Matrigel was included as an additional control group.

### 3.3.2. Quantification of Free Amine Content

<b>Sample</b>	<b>No Peptides</b>	<b>QK</b>	<b>YIGSR</b>	<b>YIGSR/QK</b>
<b>Uncrosslinked</b>				
<b>Normalized Free Amine Content</b>	1.00 ± 0.03	1.03 ± 0.04	1.50 ± 0.03	1.52 ± 0.06
<b>Plus PEGX</b>				
<b>Normalized Free Amine Content</b>	0.77 ± 0.03	0.79 ± 0.09	0.63 ± 0.02	0.70 ± 0.07
<b>% Reacted Amines</b>	23.30 ± 3.06	23.52 ± 8.58	57.84 ± 0.49	54.17 ± 4.94

Quantification of free amine content of hydrogel precursor polymer solutions via the TNBS assay demonstrated that, compared to hydrogel formulations with no peptides, addition of 100  $\mu$ M QK peptide resulted in only a slight increase of free amine content whereas addition of 12 mM YIGSR peptide resulted in a larger increase of 50% in free amine content (**Table 3-4** and **Figure 3-4 A**). The addition of the amine-reactive PEGX to crosslink polymer solutions and form hydrogels resulted in a reduction of free amine content for all groups. This reduction corresponded to 20-25% reacted amines for hydrogels with no peptides and QK hydrogels and 50-60% reacted amines for YIGSR and YIGSR/QK hydrogels (**Table 3-4** and **Figure 3-4 A**).

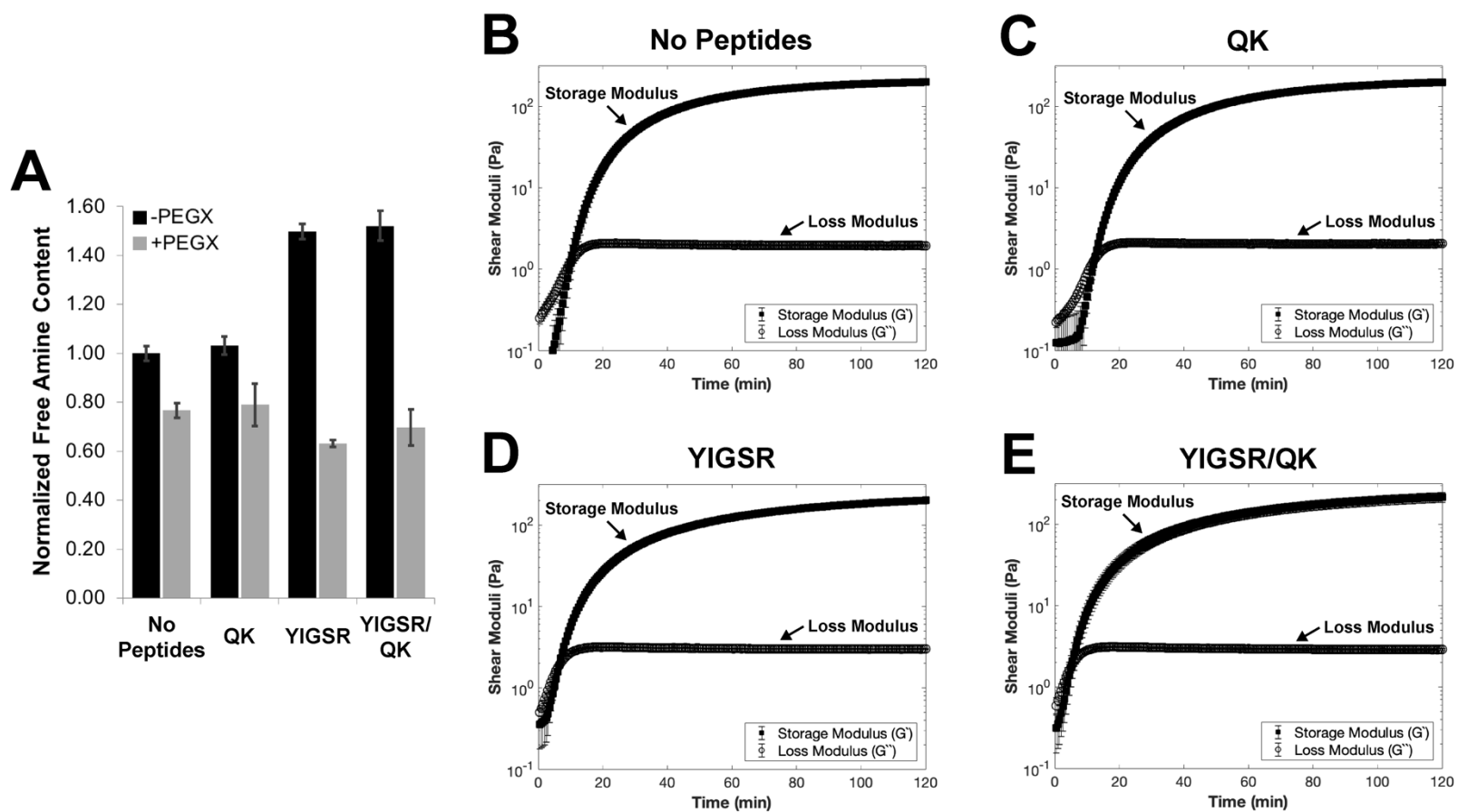


**Figure 3-4: Quantification of free amine content and rheological time sweeps of hydrogel formulations.**

(A) Free amine content of uncrosslinked hydrogel precursor polymer solutions and crosslinked hydrogels quantified by the TNBS assay. Sample groups were normalized to the uncrosslinked hydrogel precursor polymer solution with no peptides group ( $n = 3$ ). Rheological characterization of hydrogel formation over time with shear moduli ( $G'$ ,  $G''$ ) plotted on semi-log plots: (B) hydrogels with no peptides, (C) QK, (D) YIGSR, and (E) YIGSR/QK hydrogels. Samples run in triplicate ( $n = 3$ ).

### 3.3.3. Rheological Characterization and pH Measurements

<b>Sample</b>	<b>No Peptides</b>	<b>QK</b>	<b>YIGSR</b>	<b>YIGSR/QK</b>
<b>pH</b>	6.13 ± 0.01	6.08 ± 0.01	5.87 ± 0.01	5.85 ± 0.01
<b>G'-G'' Crossover (min)</b>	10.5 ± 0.60	12.3 ± 0.31	6.5 ± 0.18	4.7 ± 0.24
<b>Storage Modulus, G' at 2 h (Pa)</b>	198.65 ± 3.57	197.68 ± 15.68	201.02 ± 8.36	214.47 ± 28.89
<b>Loss Modulus, G'' at 2 h (Pa)</b>	1.95 ± 0.05	2.05 ± 0.08	3.00 ± 0.03	2.88 ± 0.09
<b>Complex Shear Modulus, G at 2 h (Pa)</b>	198.66 ± 3.57	197.69 ± 15.68	201.04 ± 8.36	214.49 ± 28.89

Rheological characterization revealed changes in shear moduli ( $G'$ ,  $G''$ ) during hydrogel formation. Shear moduli measurements are listed in **Table 3-5** and include the storage modulus ( $G'$ ) and loss modulus ( $G''$ ) crossover point and the storage, loss, and complex shear moduli at 2 h. In addition, pH measurement of formulations immediately after addition of PEGX indicate that all formulations fell within a pH range from 5.85 to 6.15 (**Table 3-5**). Time sweeps demonstrate sigmoidal gelation profiles for all hydrogel formulations (**Figure 3-4 B-E**) with  $G'$ - $G''$  crossover points between 4.5 and 12.5 min (**Table 3-5**) indicating rapid formation of hydrogels after the addition of PEGX. Shear moduli began to stabilize around 1 h, and final storage and complex shear moduli at 2 h for all hydrogels ranged between 195 and 215 Pa (**Table 3-5**). Frequency sweeps revealed that the  $G'$  of all hydrogels were relatively independent of the frequencies tested, and the angular frequency value employed for time sweeps was verified to be in the low-frequency plateau region for all formulations (**Figure 3-5 A-D**). Strain or amplitude sweeps revealed that the shear moduli of all hydrogels were independent of strain up until 100% strain (the linear viscoelastic region) after which hydrogels exhibited strain-stiffening behavior and catastrophic failure at approximately 1000% strain (**Figure 3-5 E-H**).

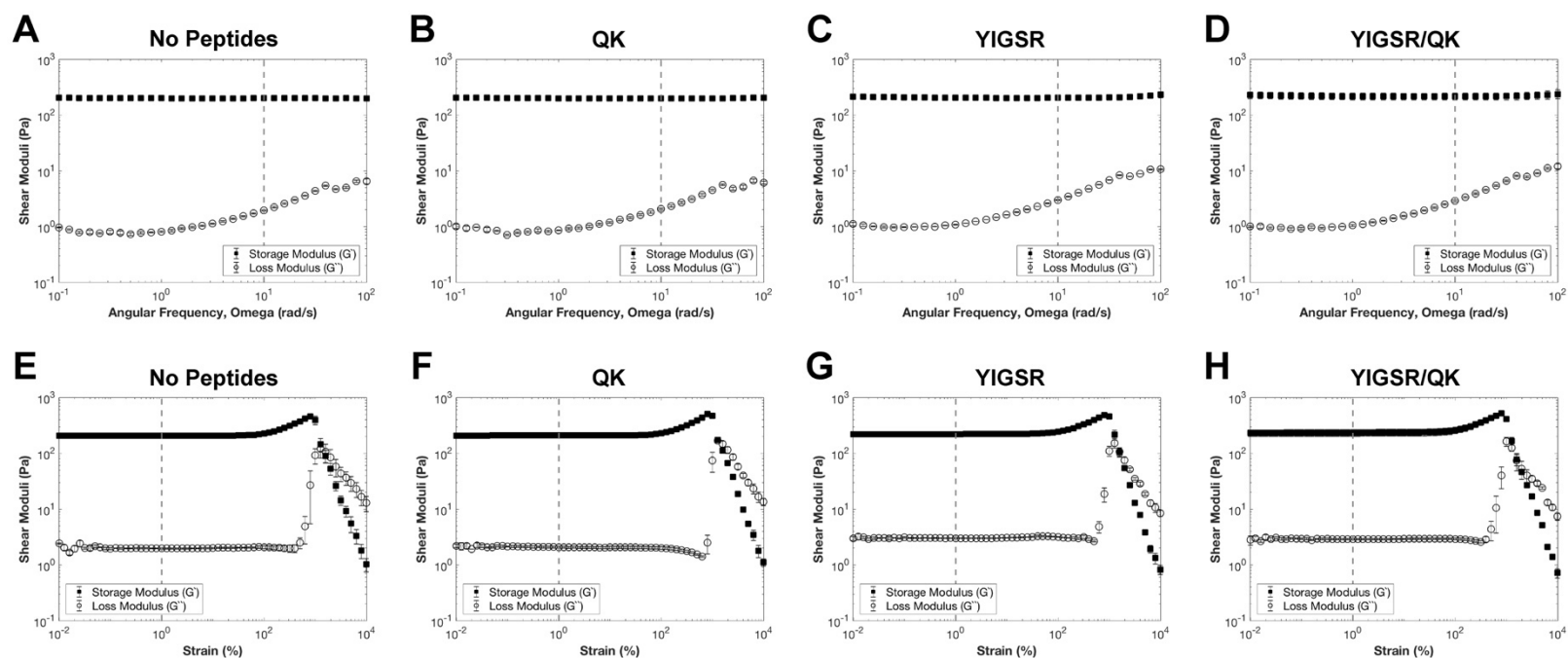


**Figure 3-5: Rheological frequency and strain sweeps of hydrogels.**

Shear moduli ( $G'$ ,  $G''$ ) versus angular frequency plotted on log-log plots: (A) hydrogels with no peptides, (B) QK, (C) YIGSR, and (D) YIGSR/QK hydrogels. Dashed lines represent the angular frequency at which time sweeps were performed: 10 rad/s. Shear moduli versus strain plotted on log-log plots: (E) hydrogels with no peptides, (F) QK, (G) YIGSR, and (H) YIGSR/QK hydrogels. Dashed lines represent the strain percent at which time sweeps were performed: 1% strain.

### 3.3.4. Scanning Electron Micrographs and Swelling Analysis of Hydrogels

At low magnifications, scanning electron microscopy revealed relatively flat, homogeneous surfaces for all hydrogels (**Figure 3-6**). At higher magnifications, hydrogels exhibited a porous yet relatively unstructured and amorphous ultrastructure (as opposed to a fibrillar one) (**Figure 3-7 A-D**). Analysis of hydrogels between initial and swollen states demonstrated that hydrogels with no peptides and QK hydrogels exhibited similar percent weight increases of  $115.42 \pm 4.94$  and  $120.98 \pm 1.49$ , respectively, whereas YIGSR and YIGSR/QK hydrogels exhibited much greater percent weight increases of  $209.30 \pm 5.42$  and  $220.94 \pm 2.18$ , respectively (**Figure 3-7 E**). However, analysis of swelling ratios, that is the ratio of wet to dry weight of samples, revealed that all of the hydrogels exhibited similar swelling ratios between 32 and 35 (**Figure 3-7 F**).

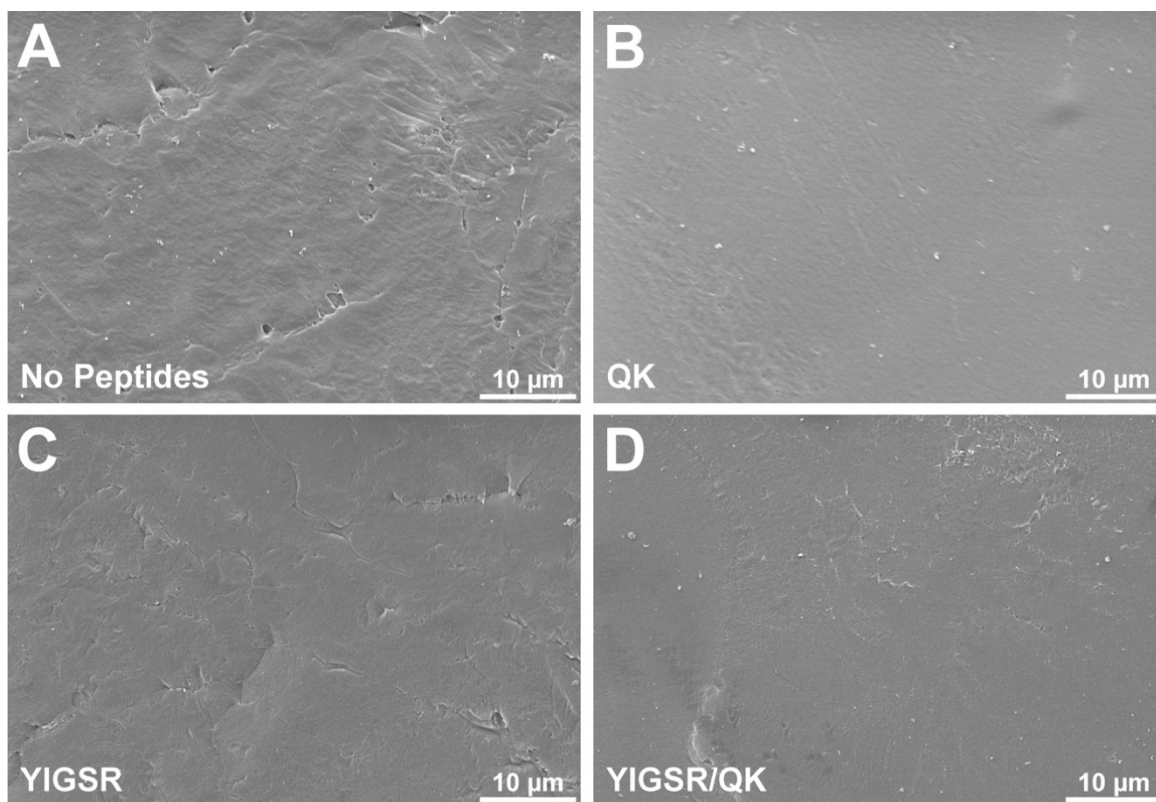


**Figure 3-6: Low-magnification scanning electron micrographs of hydrogels.**

Scanning electron micrographs of (A) hydrogels with no peptides, (B) QK, (C) YIGSR, and (D) YIGSR/QK hydrogels.

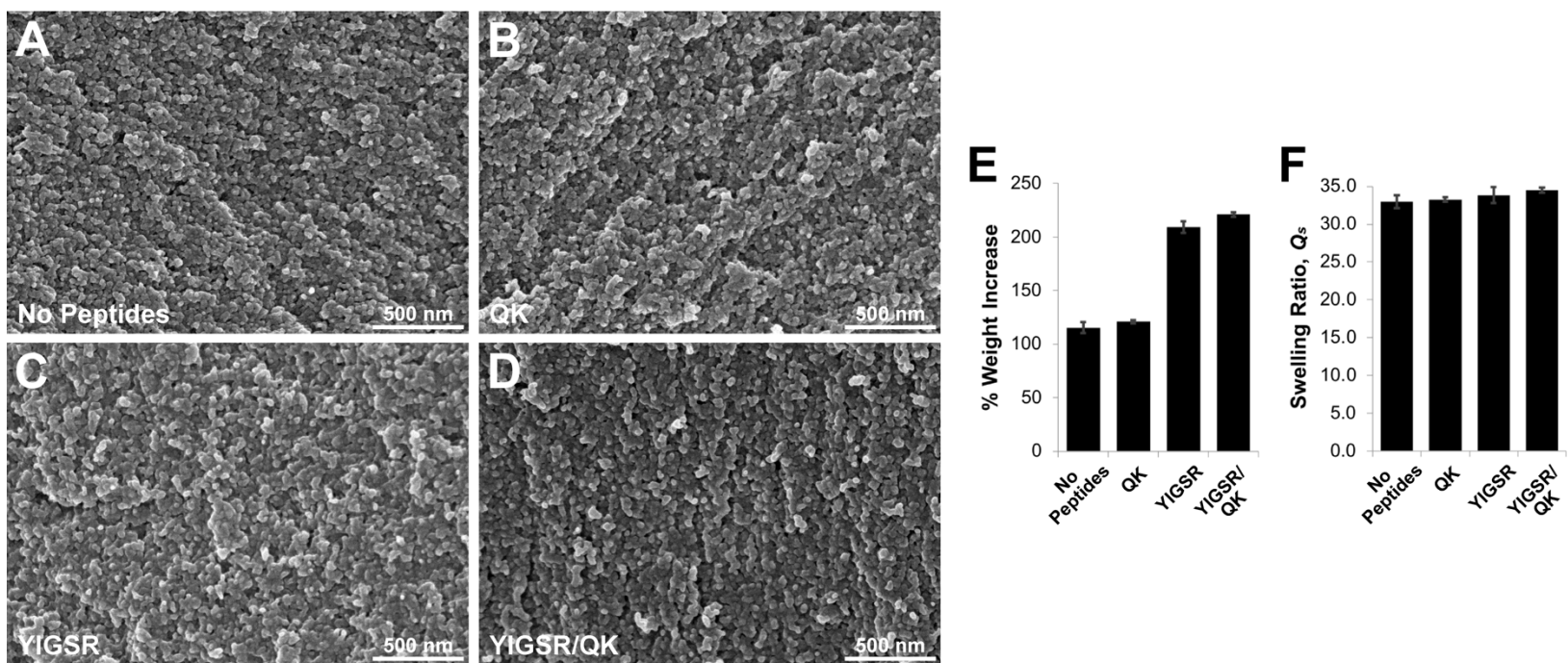


**Figure 3-7: Scanning electron micrographs and swelling analysis of hydrogels.**

High-magnification scanning electron micrographs of (A) hydrogels with no peptides, (B) QK, (C) YIGSR, and (D) YIGSR/QK hydrogels. (E) Percent weight increases from initial to swollen hydrogel states, and (F) swelling ratios of swollen hydrogels to dry polymer weights ( $n = 6$ ).

### **3.3.5. QK Peptide Bioactivity and Phosphorylation of VEGFR2 in HUVECs and GEnCs**

To ensure that the QK peptide was indeed bioactive in the soluble form and that this bioactivity was preserved after conjugation, an ELISA specific to phosphorylated VEGFR2 was used to measure cellular levels of activated and phosphorylated VEGFR2 in response to the QK peptide. Treatment of HUVECs with either soluble VEGF<sub>165</sub> or soluble QK peptide resulted in significantly increased levels of phosphorylated VEGFR2 relative to untreated controls for HUVECs cultured on tissue culture polystyrene or on hydrogels with no peptides (**Figure 3-8 A**). HUVECs cultured on QK hydrogels also resulted in significantly increased levels of phosphorylated VEGFR2 relative to HUVECs cultured on hydrogels with no peptides (**Figure 3-8 A**). Surprisingly, treatment of GEnCs with either soluble VEGF<sub>165</sub> or soluble QK peptide did not result in significant changes in levels of phosphorylated VEGFR2 relative to untreated controls, and this was consistent for both GEnCs cultured on tissue culture polystyrene or on hydrogels with no peptides (**Figure 3-8 B**). In contrast, however, GEnCs cultured on QK hydrogels resulted in significantly increased levels of phosphorylated VEGFR2 relative to GEnCs cultured on hydrogels with no peptides (**Figure 3-8 B**).

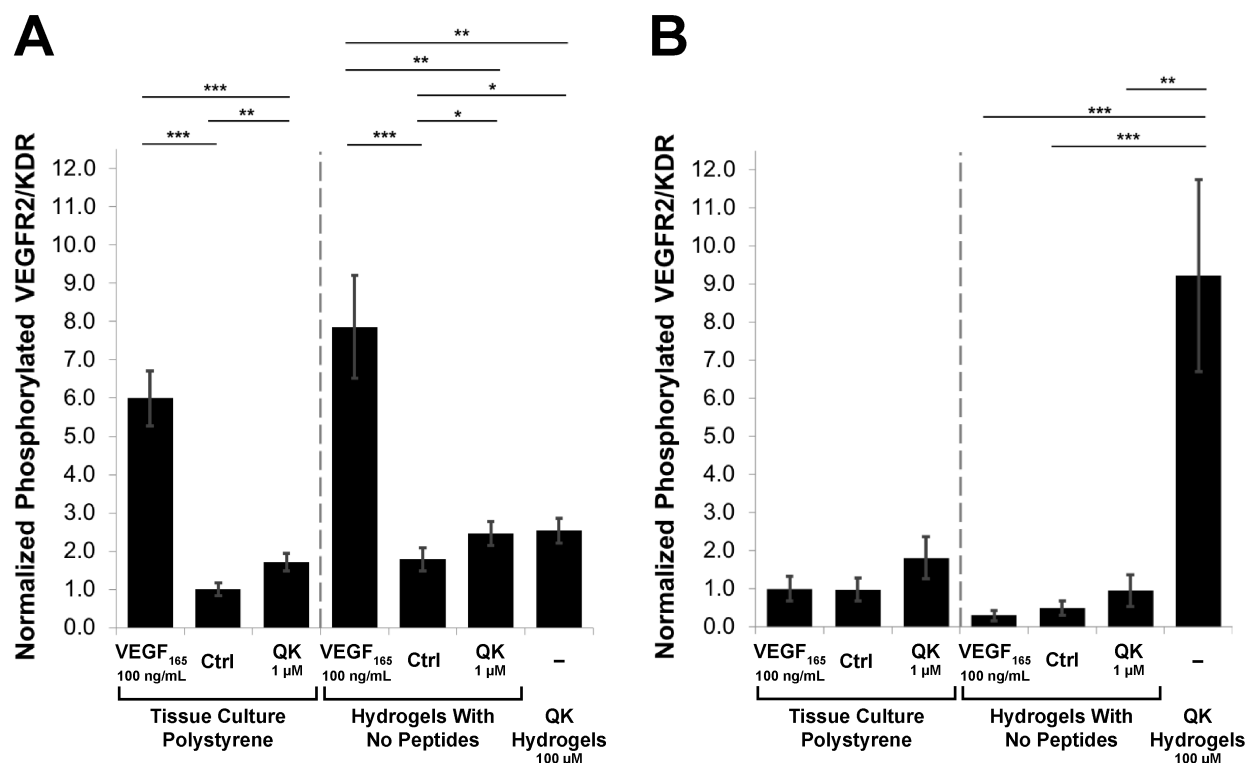


**Figure 3-8: Cellular levels of phosphorylated VEGFR2 measured by an ELISA.**

Phosphorylated VEGFR2 in (A) HUVECs and (B) GEnCs following treatment with 100 ng/mL VEGF<sub>165</sub> (positive control), no treatment (“Ctrl”, negative control), or treatment with 1 μM soluble QK peptide for cells cultured on tissue culture polystyrene or hydrogels with no peptides, or no treatment for cells cultured on QK hydrogels. Quantification was normalized to the no treatment groups on tissue culture polystyrene for each cell type ( $n = 4$ ). Statistical significance denoted by: \*  $p < 0.05$ , \*\*  $p < 0.01$ , and \*\*\*  $p < 0.001$ .

### 3.3.6. HUVEC Culture, Gene Expression Analysis, and Immunofluorescence

HUVECs were plated on hydrogel substrates and cultured for up to 5 days (Figure 3-9). For cell culture experiments, Matrigel served as positive control because it is commonly utilized in endothelial cell tube formation and angiogenesis assays<sup>[361, 362]</sup>. RYGS1 hydrogels served as an additional scrambled YIGSR peptide control to account for the increased concentration of PEGX necessary in YIGSR and YIGSR/QK hydrogel formulations. On Matrigel, HUVECs underwent rapid morphogenesis and formed an interconnected network within 6 h that began to regress by 24 h and was completely absent after 3 days though cell aggregates could be observed at the sides of wells. On hydrogels with no peptides, HUVECs proliferated to form a monolayer approximately 60-70% confluent by 24 h, and cells continued to proliferate

resulting in the cord-like structures observed at day 3 and beyond. On QK hydrogels, a similar response was observed as HUVECs cultured on hydrogels with no peptides. On YIGSR hydrogels, HUVECs began to form cord-like structures by 6 h that increased in size and connections by 24 h, but cells did not form a confluent monolayer by day 5, and instead the network formed by the cord-like structures appeared to tighten. On YIGSR/QK hydrogels, a similar response was observed as HUVECs cultured on YIGSR hydrogels. On RYGSI hydrogels, HUVECs began to form cord-like structures by 6 h in a similar manner as on YIGSR and YIGSR/QK hydrogels; however, cells continued to proliferate and formed a confluent monolayer by day 3 with cord-like structures still present.

Genes of interest included in gene expression analysis are involved in cell-cell interactions (*PECAM1*, *CDH5/VE-Cad*), cell-matrix interactions via integrins (*ITGB1*, *ITGB3*), signaling pathways via cell surface receptors (*KDR/VEGFR2*, *TEK/TIE2*), and endothelial function (*VWF*, *NOS3*, *PLVAP*) (**Figure 3-10**). In general, gene expression analysis revealed highest fold-change expression by HUVECs cultured on YIGSR/QK hydrogels at day 5 (**Figure 3-10 A-I**). This is true for *CDH5* (**Figure 3-10 B**), *ITGB3* (**Figure 3-10 D**), *KDR* (**Figure 3-10 E**), *TEK* (**Figure 5F**), *VWF* (**Figure 3-10 G**), and *NOS3* (**Figure 3-10 H**). For *PECAM1* (**Figure 3-10 A**) and *ITGB1* (**Figure 3-10 C**), HUVECs exhibited greatest upregulation on QK hydrogels at 24 h, and for *PLVAP* (**Figure 3-10 I**), HUVECs exhibited greatest upregulation on Matrigel at 24 h. HUVECs cultured on RYGSI hydrogels generally exhibited the lowest fold-change expression of genes compared to other groups at all time points. Immunofluorescence staining confirmed the expression of platelet endothelial cell adhesion molecule (PECAM-1 or CD31 encoded by *PECAM1*) and of VEGFR2 (encoded by *KDR*) by HUVECs cultured on no peptide, QK, YIGSR, and YIGSR/QK hydrogels at 6 and 24 h (**Figure 3-10 J**).

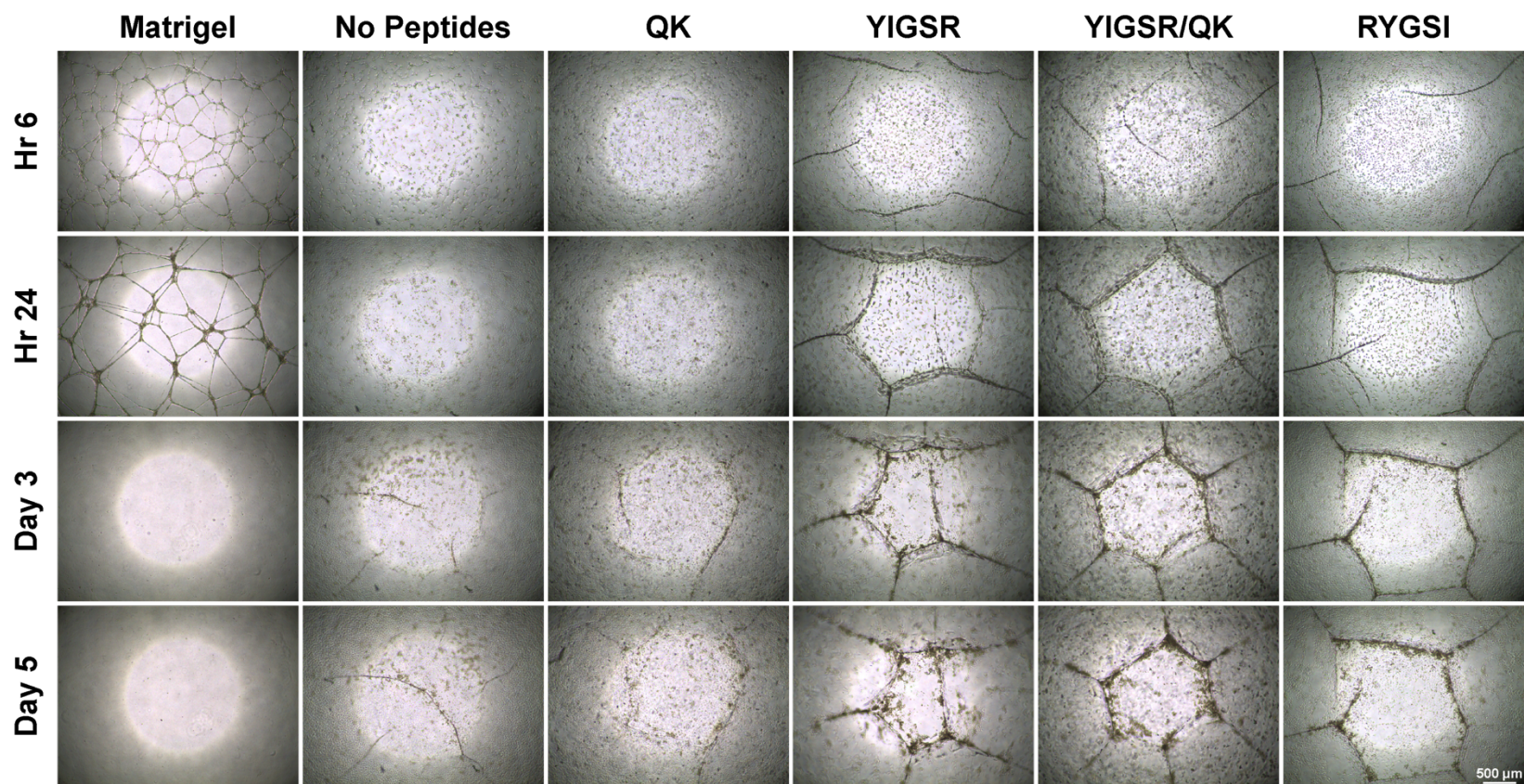


**Figure 3-9: Photomicrographs of HUVECs cultured on hydrogel substrates.**

Photomicrographs at designated time points showing formation of cord-like structures that vary with hydrogel formulations.

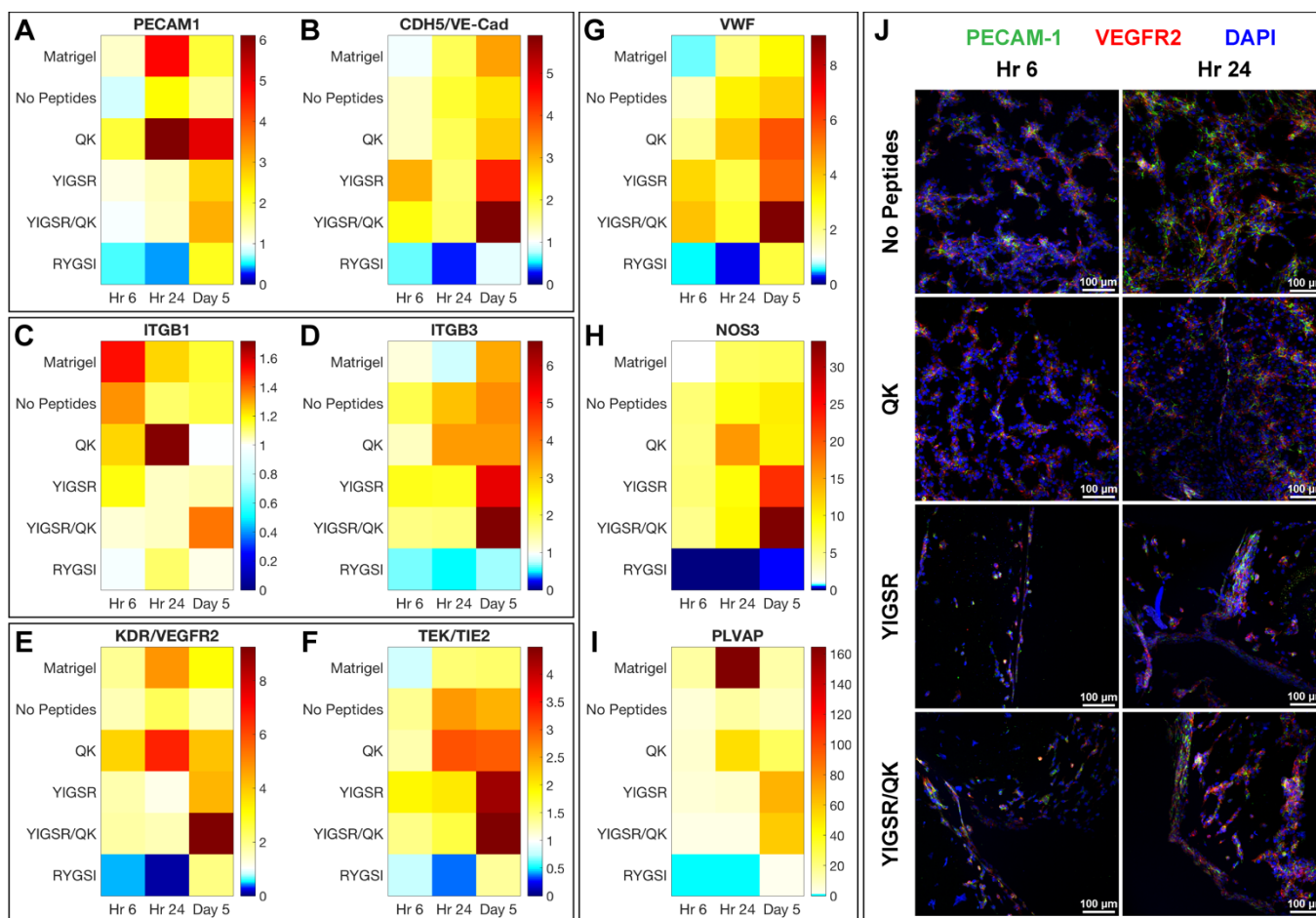


**Figure 3-10: Gene expression analysis and immunofluorescence staining of HUVECs cultured on hydrogel substrates.**

Gene expression analysis of cultures at 6 h, 24 h, and 5 days. (A) *PECAM1* encoding for platelet endothelial cell adhesion molecule or CD31. (B) *CDH5* encoding for cadherin 5 or vascular endothelial cadherin, also known as CD144. (C) *ITGB1* encoding for integrin subunit  $\beta 1$ . (D) *ITGB3* encoding for integrin subunit  $\beta 3$ . (E) *KDR* encoding for kinase insert domain receptor or vascular endothelial growth factor receptor 2. (F) *TEK* encoding for tyrosine kinase with immunoglobulin-like and EGF-like domains 2 or TIE2. (G) *VWF* encoding for von Willebrand factor. (H) *NOS3* encoding for nitric oxide synthase 3. (I) *PLVAP* encoding for plasmalemma vesicle-associated protein. Values presented as fold-change expression normalized to gene expression of HUVECs cultured on tissue culture polystyrene at day 0 ( $n = 4$ ). (J) Whole-mount immunofluorescence staining of HUVECs cultured on hydrogel substrates at 6 and 24 h. Merged images: PECAM-1 (green), VEGFR2 (red), and DAPI (blue).

### 3.3.7. GEnC Culture and Gene Expression Analysis

GEnCs were similarly plated on hydrogel substrates and cultured for up to 5 days at the non-permissive temperature (**Figure 3-11**). On Matrigel, GEnCs underwent rapid morphogenesis and formed an interconnected network within 6 h that rapidly regressed by 24 h, and by 3 days only large cell aggregates remained. On hydrogels with no peptides, GEnCs proliferated slowly as the transgenes began to degrade resulting in a fully confluent and stable monolayer on days 3 and 5. On QK hydrogels, GEnCs proliferated in a similar manner as on hydrogels with no peptides; however, this proliferation resulted in the formation of cord-like structures not seen on hydrogels with no peptides at day 5. On YIGSR hydrogels, GEnCs began to form cord-like structures by 6 h that continued to form connections over the culture period; however, the cells did not form a confluent monolayer by day 5 and appear morphologically distinct compared to the cord-like structures formed by HUVECs on the same hydrogels (**Figure 3-9**). On YIGSR/QK hydrogels, a similar response was observed as GEnCs cultured on YIGSR hydrogels. On RYGSI hydrogels, GEnCs began to form cord-like structures by 6 h in a similar manner as on YIGSR and YIGSR/QK hydrogels; however, cells were not homogeneously distributed across the hydrogel and instead clustered towards the center of the well, which resulted in the formation of a confluent monolayer in the center of the well by day 5 and cord-like structures that present as denser in appearance.

Gene expression analysis results of GEnC cultures were generally more varied than results from HUVEC cultures, and fold-change expression by GEnCs was generally lower than by HUVECs (**Figure 3-12**). GEnCs exhibited greatest fold-change expression on Matrigel at day 5 for *PECAM1* (**Figure 3-12 A**), *CDH5* (**Figure 3-12 B**), *KDR* (**Figure 3-12 E**), *TEK* (**Figure 3-12 F**), *VWF* (**Figure 3-12 G**), and *PLVAP* (**Figure 3-12 I**). In addition, GEnCs cultured on RYGSI hydrogels exhibited high fold-change expression of genes such as *PECAM1*, *CDH5*, and *ITGB3* (**Figure 3-12 D**) at day 5 and *ITGB1* (**Figure 3-12 C**) and *TEK* at 6 h.

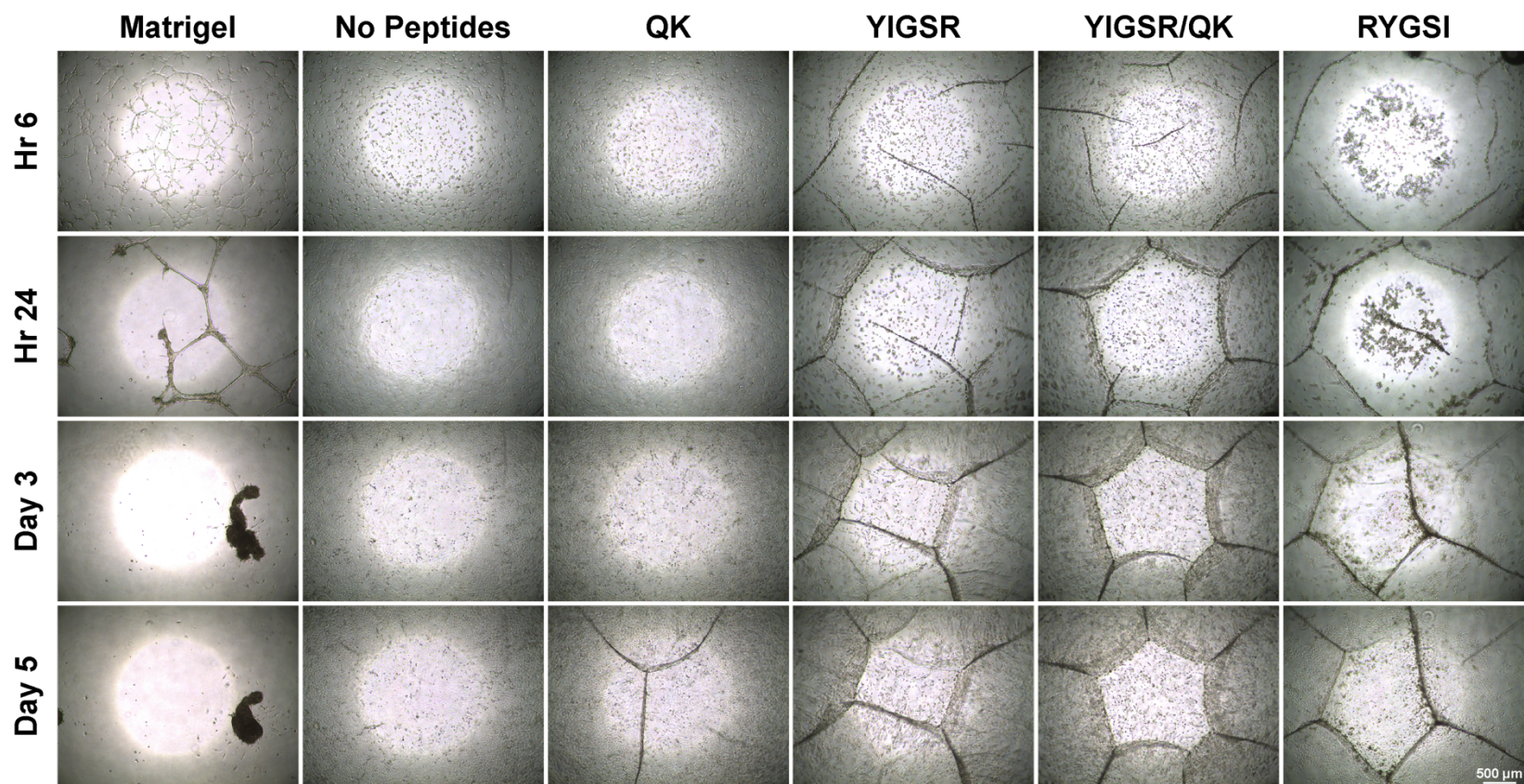


**Figure 3-11: Photomicrographs of GEnCs cultured on hydrogel substrates.**  
 Photomicrographs at designated time points showing formation of cord-like structures that vary with hydrogel formulations.

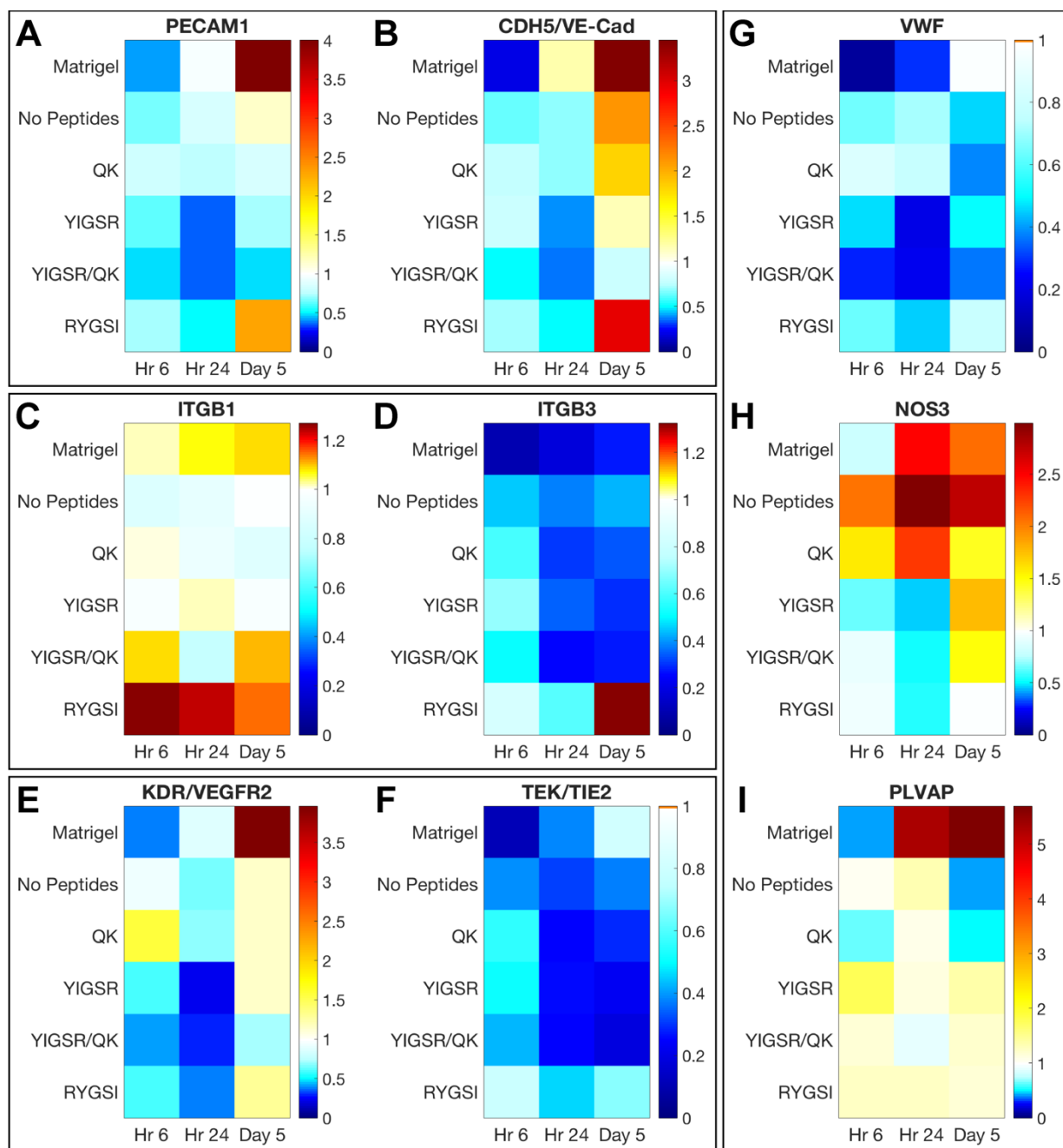


**Figure 3-12: Gene expression analysis of GEnCs cultured on hydrogel substrates.**

Gene expression analysis of cultures at 6 h, 24 h, and 5 days. (A) *PECAM1* encoding for platelet endothelial cell adhesion molecule or CD31. (B) *CDH5* encoding for cadherin 5 or vascular endothelial cadherin, also known as CD144. (C) *ITGB1* encoding for integrin subunit  $\beta$ 1. (D) *ITGB3* encoding for integrin subunit  $\beta$ 3. (E) *KDR* encoding for kinase insert domain receptor or vascular endothelial growth factor receptor 2. (F) *TEK* encoding for tyrosine kinase with immunoglobulin-like and EGF-like domains 2 or TIE2. (G) *VWF* encoding for von Willebrand factor. (H) *NOS3* encoding for nitric oxide synthase 3. (I) *PLVAP* encoding for plasmalemma vesicle-associated protein. Values presented as fold-change expression normalized to gene expression of GEnCs cultured on tissue culture polystyrene at day 0 ( $n = 4$ ).

### 3.4. Discussion

The BM, a structure composed of layered ECM molecules, underlies epithelial and endothelial cell populations and provides a dynamic interface between these cells and the surrounding parenchyma<sup>[31]</sup>. Recapitulating the unique properties of the BM using synthetic biomaterial systems such as hydrogel matrices requires careful modulation of the system's physicochemical properties<sup>[36]</sup>. In this work, we employed a versatile chemical crosslinking strategy, the PEGX method, to generate stable gelatin hydrogels for cell culture while simultaneously conjugating synthetic peptides to the gelatin polymer backbone to impart additional bioactivity. The two peptides of interest for these investigations were the laminin-derived YIGSR peptide<sup>[344, 345]</sup> and the VEGF-mimetic QK peptide<sup>[352]</sup>. Material characterization of the hydrogel formulations included rheological, ultrastructural, and swelling analyses, and *in vitro* studies with HUVECs and GEnCs were performed to evaluate performance of the hydrogels as a BM mimic for endothelial cell culture.

Hydrogels are highly hydrated, crosslinked networks of polymers. In the current investigation, the formation of a hydrogel from a precursor polymer solution occurs when the PEGX SVA functional groups react with free amines present on the gelatin polymers resulting in a covalently-crosslinked gelatin network (**Figure 3-1**). Using this system, hydrogels can be additionally functionalized with bioactive molecules containing free amine groups such as synthetic peptides. Quantification of the free amine content of hydrogel precursor polymer solutions and crosslinked hydrogels via the TNBS assay confirmed that crosslinking occurs as a result of the PEGX reacting with free amine groups (**Figure 3-4 A**). As expected, the percentage of reacted amines for the hydrogels with no peptides (**Table 3-4**) was similar in range to results presented in a previously published investigation demonstrating the utility the PEGX method<sup>[341]</sup>. Furthermore, the addition of the YIGSR peptide at a concentration of 12 mM increased the free amine content of the respective hydrogel precursor polymer solutions to approximately 1.5 times that of polymer solutions with no peptides, and addition of PEGX resulted in normalized free amine content values below that of crosslinked hydrogels with no peptides. This indicates that both successful crosslinking between gelatin polymers as well as conjugation of the YIGSR peptide to the gelatin polymer network occurred. It is possible that other products will result from the crosslinking reaction, such as the reaction of a single PEGX

molecule with two peptides; however, we expect these products to occur at a much lower frequency than the desired conjugation of peptides to the gelatin polymers due to the greater availability of free amines on the gelatin.

Successful crosslinking of the hydrogel precursor polymer solutions was further confirmed by rheological characterization. Time sweeps and shear moduli measurements revealed rapid crosslinking of formulations and  $G'$ - $G''$  crossovers (that is, the time at which the elastic or solid-like properties matched the viscous or liquid-like properties of the sample) within several minutes after the addition of PEGX (**Table 3-5**). Shear moduli were mostly stable by 2 h, indicating the crosslinking reaction was nearly complete by this time (**Figure 3-4 B-E**). Final storage and complex shear moduli of hydrogels were of similar magnitudes and within the range of 195 to 215 Pa (**Table 3-5**).

This narrow range of storage moduli was intended to eliminate hydrogel stiffness as a possible confounding factor that could influence cellular response. It has been well-documented that cells respond to the mechanical properties of their microenvironment through mechanotransduction<sup>[270, 330]</sup>. Substrate stiffness will not only influence endothelial cell morphology and actin stress fiber formation<sup>[363, 364]</sup> but also modulate expression of growth factors and receptor proteins<sup>[365]</sup>. Ultimately, these factors influence endothelial morphogenesis and capillary network formation<sup>[363, 366-368]</sup>. In these investigations, storage moduli of approximately 200 Pa were desired as the BM-like archetype Matrigel control has a reported storage modulus of 55 to 90 Pa<sup>[318, 369]</sup>; however, “soft” hydrogel formulations crosslinked via the PEGX method (those with storage moduli below 150 Pa) previously were shown to degrade rapidly in cell culture conditions<sup>[341]</sup>, so a balance between substrate stiffness and rate of degradation was necessary.

Additional frequency and strain sweeps confirmed the formation of elastic hydrogels after crosslinking (**Figure 3-5**). Interestingly, the hydrogels exhibited strain stiffening when exposed to strains between 100% and 1000%. Strain stiffening is a common behavior among biological materials, such as fibrin, type I collagen, and kidney decellularized extracellular matrix hydrogels, but is typically difficult to recapitulate with synthetic polymer networks<sup>[288, 328, 329]</sup>. Although these hydrogels are formed through covalent crosslinks using a synthetic crosslinker, the strain-stiffening behavior suggests that interactions

between the gelatin polymers such as physical associations may still influence the resulting network structure.

Ultrastructural analysis of hydrogel surfaces via SEM did not demonstrate any considerable variation across groups (**Figure 3-7 A-D**). Swelling analysis of hydrogels, however, revealed a distinction between hydrogels without conjugated YIGSR peptide and YIGSR-conjugated hydrogels. Investigating the percent weight increase between initial and swollen hydrogel states, we found that YIGSR and YIGSR/QK hydrogels tripled in weight (~200% increase) whereas hydrogels with no peptides and QK hydrogels only doubled in weight (~100% increase) (**Figure 3-7 E**). However, the swelling ratios between swollen hydrogel and dry polymer states was relatively similar across groups (**Figure 3-7 F**). This indicates that this distinction was a result of the increased dry polymer weight of YIGSR-conjugated hydrogels, which not only have the addition of the YIGSR peptide but also higher concentrations of PEGX (**Table 3-2**). To account for this additional variable, a scrambled YIGSR peptide control (the RYGSI peptide) previously shown to lack the cell-binding activity of the YIGSR peptide<sup>[349]</sup> was included in later cell studies.

The VEGF-mimetic QK peptide has been reported to bind VEGF receptors resulting in activation of downstream intracellular signaling pathways in endothelial cells, and in particular pathways downstream of VEGFR2<sup>[352, 370]</sup>. Activation of VEGFR2 leads to dimerization of receptors and autophosphorylation of intracellular tyrosine residues<sup>[371]</sup>. After activation, VEGFR2 is internalized during which signaling continues until the receptor is degraded or undergoes desphosphorylation and recycling<sup>[372]</sup>. Importantly, studies suggest that internalization of VEGF itself is not necessary for phosphorylation of VEGFR2 and downstream signaling<sup>[373]</sup>. Therefore, utilizing a commercially-available intracellular ELISA kit, we demonstrated that soluble QK peptide indeed resulted in significantly elevated levels of phosphorylated VEGFR2 in HUVECs, and this activity was preserved even after conjugation to crosslinked gelatin hydrogel substrates using PEGX (**Figure 3-8 A**).

Surprisingly, this activity did not appear to be consistent between cell types as treatment with soluble QK peptide did not result in significant changes in levels of phosphorylated VEGFR2 in GEnCs (**Figure 3-8 B**). In addition, although the treatment of HUVECs with soluble VEGF<sub>165</sub> resulted in significantly elevated levels of phosphorylated VEGFR2 as expected, this was not the case for GEnCs treated for the

same duration and with the same concentration of VEGF<sub>165</sub>. In contrast, GEnCs cultured on QK hydrogels exhibited significantly elevated levels of phosphorylated VEGFR2. This is particularly intriguing as matrix-bound VEGF has been found to preferentially activate VEGFR2 signaling pathways involved in cell migration<sup>[374]</sup> and result in endothelial vessels that are smaller in diameter and contain more branching points in a tumor model<sup>[375]</sup>. As a specialized microvascular endothelial cell population, it is possible that the GEnCs are more responsive to matrix-bound VEGF (or in this case, matrix-bound QK peptide) as this would result in endothelial structures more reminiscent of microvascular beds. This is further supported by knowledge that heparan sulfate proteoglycans within the glomerular basement membrane<sup>[35]</sup> may sequester growth factors with heparin-binding domains, including VEGF<sub>165</sub><sup>[376, 377]</sup>. VEGF<sub>165</sub> is the predominant VEGF isoform secreted by podocytes<sup>[378]</sup>, the specialized perivascular cells that form the external layer of the glomerular filtration barrier, and this VEGF secretion by podocytes is crucial in the formation and maintenance of the glomerular filtration barrier<sup>[6, 377]</sup>. Therefore, these results may help tie together the unique physical path and regulation of VEGF within the glomerulus: from secretion by podocytes, to sequestration within the glomerular basement membrane, and finally presentation to GEnCs.

HUVECs were employed as readily-available and prototypical cells for investigating endothelial cell response to culture on our hydrogel substrates (**Figure 3-9**). HUVECs cultured on Matrigel rapidly assembled into multicellular, tube-like networks that later regressed into cell aggregates, as expected<sup>[361, 362]</sup>. While HUVECs cultured on hydrogels with no peptides and QK hydrogels formed confluent monolayers, HUVECs cultured on YIGSR and YIGSR/QK hydrogels formed cord-like structures that persisted throughout the culture period. To our surprise, however, HUVECs cultured on RYGSI hydrogel responded in a similar manner forming cord-like structures. This suggests that the cord-like structure formation observed was not a result of the bioactivity of the YIGSR peptide but instead due to some other factor. Swelling analysis, discussed previously, revealed that YIGSR-conjugated hydrogels exhibited greater percent weight increases relative to hydrogels with no peptides and QK hydrogels, which is likely an effect of the increased dry polymer content of these formulations (**Figure 3-7 E-F** and **Table 3-2**). Therefore, when confined to the well dimensions in a cell culture plate, YIGSR-conjugated and similarly RYGSI hydrogels swell to a greater extent than hydrogels with no peptides and QK hydrogels, resulting in an

uneven culture surface or regions of tension and compression that may influence local cellular adhesion and migration.

Gene expression analysis of cultures, however, demonstrated that the addition of conjugated bioactive peptides led to changes in expression of many genes of interest in HUVECs (**Figure 3-10**). In several instances, these changes were upregulation in comparison to culture on hydrogels with no peptides, and ultimately the combined synergistic effects of the peptides in YIGSR/QK hydrogels resulted in the highest fold-change expression by day 5. On the other hand, although HUVECs formed similar cord-like structures on RYGSI hydrogels, gene expression analysis demonstrated that conjugation of the inactive peptide resulted in downregulation of most of the genes of interest. This downregulation was often even below expression levels of cells cultured on hydrogels with no peptides, which is likely an effect of the increased PEG content of RYGSI hydrogels that would alter both the density of available cell-binding sites as well as the swelling properties and thus surface topography of the hydrogel substrates.

Conditionally-immortalized human GEnCs were also employed as an additional cell type for investigating endothelial cell response to culture on our hydrogel substrates (**Figure 3-11**). GEnCs cultured on hydrogels with no peptides formed confluent monolayers, and addition of conjugated QK peptide resulted in some cord-like structure formation by cells. While GEnCs cultured on YIGSR and YIGSR/QK hydrogels also seemed to form cord-like structures, these structures appeared less dense than those formed by HUVECs on the same hydrogel substrates. Interestingly, structures formed on RYGSI hydrogels by GEnCs and HUVECs appear more similar to each other, which again suggests that the bioactivity of the YIGSR peptide plays an important role in modulating cell response.

Gene expression analysis of cultures likewise demonstrated quite different trends between GEnCs and HUVECs (**Figure 3-12**). For many genes of interest, the conjugation of bioactive peptides did not lead to significant changes in gene expression. Instead, GEnCs exhibited the highest fold-change expression on Matrigel and RYGSI hydrogels, typically at day 5. Correlating these results with images of the cultures, GEnCs seem to prefer extensive cell-cell interactions that form during cell aggregation over cell-matrix interactions. This corresponded to upregulation of genes involved in cell-cell interactions such as *PECAM1* and *CDH5*, cell surface receptors involved in signaling pathways such as *KDR* and *TEK*, and endothelial

function such as *VWF* and *PVLAP*. These results reinforce findings from a previous investigation in which GEnCs encapsulated within kidney decellularized extracellular matrix hydrogels exhibited lower fold-change expression of many of the same genes of interest in comparison to cells encapsulated within type I collagen hydrogels in part due to an inability to form strong cell-cell interactions<sup>[288]</sup>.

The differences in cell response by HUVECs and GEnCs is ultimately not unexpected. Endothelial vessels and vascular beds in the body are phenotypically heterogeneous and occupy a diverse range of physiological microenvironments<sup>[379, 380]</sup>. It is not surprising that when isolated from an *in vivo* setting and cultured *in vitro* these various cell populations will respond differently. For example, Ligresti, *et al.* isolated human kidney peritubular microvascular endothelial cells (HKMECs) and through functional and molecular assays found that these cells lack intrinsic regenerative growth capacity and angiogenic potential, which is in contrast to the proliferative nature of HUVECs<sup>[154]</sup>. Further investigations by the same group additionally highlighted the distinct responses HKMECs exhibited in comparison to HUVECs when cells were cultured on hydrogel substrates composed of type I collagen, kidney cortex decellularized extracellular matrix, or a combination of both materials<sup>[282]</sup>. Similar to these HKMECs, GEnCs are a specialized microvascular endothelial cell population isolated from a specific region of the kidney. Therefore, it follows that the GEnCs will invariably respond in a much different manner in comparison to HUVECs as we have seen from our results.

Altogether, we have demonstrated the use of the PEGX method to generate stable, crosslinked gelatin hydrogels suitable for cell culture. Furthermore, this versatile crosslinking method permits the additional conjugation of bioactive peptides to the polymer backbone as a strategy to modulate cell response. Several groups have previously demonstrated a variety of methods for generating peptide-modified PEG hydrogels or PEG-peptide composite hydrogels, including mixed mode thiol-acrylate photopolymerization using PEG diacrylate<sup>[381]</sup>, PEG-peptide macromers for subsequent photopolymerization using PEG acrylate<sup>[382]</sup> or PEG diacrylate<sup>[383]</sup>, thiol-ene photocoupling using PEG-norbornene<sup>[384, 385]</sup>, and self-assembled peptide amphiphile and photopolymerizable PEG dimethacrylate composite hydrogels<sup>[386]</sup>. However, in comparison, the synthetic-natural PEG-gelatin composite hydrogels investigated here promote cell adhesion and permit cell-mediated degradation even in the absence of

additional peptides. This again demonstrates the versatility of the PEGX method as demonstrated here and elsewhere<sup>[341]</sup>.

Furthermore, unlike the above referenced investigations, the PEGX chemistry utilized in this work does not require a photo-mediated reaction and thus eliminates the need for a photoinitiator. However, using the specific single SVA-PEG-SVA crosslinker explored in this study, polymer crosslinking and conjugation of additional bioactive molecules necessitates increasing the total polymer weight of formulations depending on the concentrations of the molecules of interest. This can lead to confounding variables such as changes in hydrogel swelling and cell-binding ligand densities. Future investigations may opt to explore PEGX physical and chemical variants, such as multi-arm PEG crosslinkers<sup>[341]</sup> or bioorthogonal “click” chemistries<sup>[245, 246]</sup>, to crosslink polymers and conjugate multiple bioactive molecules using orthogonal reactions for greater control of hydrogel properties. Ultimately, advances in engineering BM-like hydrogel substrates will not only enhance physiological understanding of cell-cell and cell-matrix interactions but also accelerate the development of tissue models for drug testing and novel strategies for regenerative therapies.

### **3.5. Conclusion**

The PEGX method is a versatile crosslinking strategy that, in this study, was used to simultaneously generate stable, crosslinked gelatin hydrogels as well as conjugate bioactive peptides onto the gelatin polymers. Hydrogels formed from precursor polymer solutions within several minutes after the addition of PEGX, but differential swelling properties occurred as a result of adjusting peptide and PEGX concentrations. These peptide-conjugated hydrogels were investigated as cell culture substrates for two human endothelial cell types, human umbilical vein endothelial cells and human glomerular endothelial cells, that exhibited uniquely different cell behavior evaluated by measuring levels of phosphorylated VEGFR2 and changes in gene expression. Future investigations may explore additional PEGX variants for crosslinking and conjugation reactions, a variety of polymers or bioactive molecules for biofunctionalization, or other cells types to evaluate cellular response. Ultimately, these studies contribute to the growing interest

in developing basement membrane-like hydrogels for delineating complex epithelial and endothelial cell-cell and cell-matrix interactions.

**CHAPTER IV:****Challenges with *In Vitro* Cultures of Podocytes  
and Evaluation of Hydrogel Platforms to Preserve or Enhance Mature Podocyte Phenotype**

#### 4.1. Introduction

The glomerular filtration barrier is responsible for selective passage of water and small solutes and restriction of large molecules and proteins from the vasculature into the kidney tubules during renal filtration [4-6]. This barrier is composed of the glomerular endothelial cells that form the glomerular capillaries, the glomerular basement membrane, and the podocytes. Podocytes, also known as visceral epithelial cells, constitute the outermost and final component of the glomerular filtration barrier. These terminally differentiated cells exhibit a unique morphology with a main cell body and projections that extend and envelop the glomerular capillaries before ending in fine foot processes or pedicels. Although the foot processes are the only point of contact podocytes maintain with the underlying glomerular basement membrane, foot processes of adjacent podocytes interdigitate resulting in an intricate organization<sup>[17, 18]</sup>. Furthermore, the gaps between interdigitating foot processes known as filtration slits are spanned by specialized cell-cell junctions known as slit diaphragms, which together form a flexible sieve important in maintaining the properties of the glomerular filtration barrier<sup>[22]</sup>.

Damage to the glomerular filtration barrier or glomerular disease may present clinically as proteinuria or hematuria, increased protein content or presence of blood in the urine, respectively<sup>[53]</sup>. Often this is accompanied by or leads to podocyte injury in the form of foot process effacement or even podocyte loss and denudement of the glomerular basement membrane. Continued loss of podocytes beyond a critical level results in glomerulosclerosis and reduced filtration function<sup>[24, 26]</sup>. Loss of podocytes is further exacerbated by the post-mitotic state of these singular cells preventing functional replacement of cell numbers<sup>[17, 387]</sup>. Animal models, specifically transgenic mouse models, have enabled fantastic insight into the development and progression of kidney diseases and podocyte injury<sup>[294]</sup>; however, animal models do not completely emulate human physiology and disease<sup>[297]</sup>. Consequently, there is a distinct need for human podocyte culture models to advance understanding of podocyte cell biology and response to injury.

Isolation and primary culture of podocytes from a variety of species was initially described in the 1970s<sup>[388-390]</sup>. These protocols involve the dissection of kidney cortical tissue, sieving of the tissue through meshes to obtain glomeruli, and enzymatic dissociation of glomeruli to obtain the podocytes or subsequent culture of the glomeruli to obtain podocyte outgrowths<sup>[391, 392]</sup>. While primary cells are thought to be most

representative of cells in the *in vivo* state, standard primary podocyte cultures are limited by their lack of proliferative capacity<sup>[392]</sup> and rapid dedifferentiation from a highly “arborized” morphology to a “cobblestone” morphology<sup>[391]</sup>. Primary podocytes may be immortalized for continual expansion by insertion of the simian virus 40 large tumor antigen (*SV40-T*) via transfection<sup>[393]</sup>; however, this is expected to alter the natural cell state, especially of the terminally-differentiated podocyte<sup>[392]</sup>. This led researchers to take advantage of the Immortomouse and develop temperature-sensitive transgenes for culture of conditionally-immortalized mouse and human podocyte cell lines<sup>[394-397]</sup>. However, while these cell lines are now considered the gold standard cell culture models for podocytes, there is significant variation amongst different lines<sup>[398]</sup> and often significantly reduced or lost phenotypic expression<sup>[219]</sup>. In addition, improper culture technique can result in dedifferentiation or non-differentiation sub-populations in cultures, resulting in poor reproducibility<sup>[391]</sup>.

Maintaining a differentiated podocyte phenotype *in vitro* is likely difficult due to the pervasiveness of traditional cell culture techniques where cells are cultured on rigid, 2D substrates that in no way or form mimic the *in vivo* microenvironment<sup>[399]</sup>. In the body, cells not only interact with other cells in a 3D environment, but they also produce and are surrounded by extracellular matrix (ECM). The ECM provides mechanical support and organization to tissues and organs in addition to presenting biophysical and biochemical signaling cues that influence cellular response and behavior<sup>[168, 169]</sup>. Biomaterial platforms such as hydrogels have gained increasing attention as ECM mimics for 3D cell culture and regenerative engineering<sup>[235, 236]</sup>. Hydrogels as water-swollen, crosslinked polymer networks may be tailored or tuned to exhibit biophysical and biochemical properties desired for specific applications.

The objective of these investigations was to evaluate podocyte response to culture on specific hydrogel substrates or encapsulation within hydrogel matrices and correlate these results with microenvironmental signaling cues necessary for preserving or enhancing podocyte phenotype *in vitro*. The hydrogel platforms surveyed include kidney decellularized extracellular matrix (dECM) hydrogels for cell culture and encapsulation investigated in Chapter 2 and elsewhere<sup>[288]</sup>, poly(ethylene glycol) (PEG)-crosslinked gelatin hydrogel substrates with and without conjugated vascular endothelial growth factor-mimetic peptides investigated in Chapter 3 and elsewhere<sup>[280]</sup>, and 3D-printed gelatin hydrogel scaffolds investigated by others<sup>[400, 401]</sup>. Response by conditionally-immortalized human podocytes was evaluated by

measuring cell proliferation, microscopy and viability staining, and gene expression analysis, when available.

## **4.2. Materials & Methods**

### **4.2.1. Culture of Conditionally-Immortalized Human Podocytes**

Conditionally-immortalized human podocytes were cultured as described previously<sup>[396]</sup>. These are primary cells that have been transfected with a temperature-sensitive *SV40-T* antigen and the essential catalytic subunit of human telomerase (*hTERT*) to prevent replicative senescence<sup>[319, 396]</sup>. Culture at the permissive temperature of 33 °C results in active expression of the transgenes to maintain an immature cell state and allow proliferation of the cells. Thermoswitching to the non-permissive temperature of 37 °C results in inactivation of the transgenes, causing the cells to become quiescent and adopt a more mature phenotype [2002 Saleem]. Podocytes were expanded in RPMI 1640 (Gibco, #11875) supplemented with 10% fetal bovine serum (FBS, Gibco, #16000), 1% penicillin-streptomycin (Gibco, #15140), and 1% insulin-transferrin-sodium selenite (ITS Liquid Media Supplement, Sigma-Aldrich, #I3146) at 33 °C and 5% CO<sub>2</sub>. During experimental studies, cells were thermoswitched as indicated to 37 °C and 5% CO<sub>2</sub> in RPMI 1640 supplemented with 10% FBS and 1% penicillin-streptomycin. Media was exchanged every two to three days, and cells were used at passage 24 or below for experimental studies.

### **4.2.2. Kidney Decellularization and Preparation of Hydrogels from Kidney Decellularized**

#### ***Extracellular Matrix***

Hydrogels were prepared from kidney dECM as described previously in Chapter 2 and published elsewhere<sup>[288]</sup>. Female Yorkshire pig (3-4 months in age) kidneys were obtained fresh from Northwestern Simulation (Northwestern University Feinberg School of Medicine) following approval by the Northwestern Institutional Animal Care and Use Committee (IACUC) and stored at -80 °C until decellularization. Prior to decellularization, kidneys were thawed for several hours in warm water and then minced into pieces approximately 0.5 × 0.5 × 0.25 cm in size with a clean razor blade. During this process, the majority of the renal pelvis and perirenal fat was removed. Kidney tissue pieces were then rinsed with deionized H<sub>2</sub>O under

constant stirring for one day at room temperature with intermittent H<sub>2</sub>O changes. After rinsing, kidney pieces were treated with 0.1% (m/v) sodium dodecyl sulfate (Sigma-Aldrich, #L3771) under constant stirring for two days. Afterwards, decellularized kidney pieces were rinsed with deionized H<sub>2</sub>O under constant stirring for one day with intermittent H<sub>2</sub>O changes to ensure removal of residual detergent from the tissue. The resulting kidney dECM was frozen at -80 °C until further processing.

Kidney dECM hydrogels were prepared similarly to previously described protocols for other decellularized tissues<sup>[317]</sup>. Briefly, frozen kidney dECM was lyophilized for two days using a Labconco FreeZone 6 Plus, snap frozen in liquid N<sub>2</sub>, and milled with a Thomas Wiley Mini-Mill Cutting Mill. Milled dECM was enzymatically digested at 10 mg/mL kidney dECM in 1 mg/mL pepsin (Sigma-Aldrich, #P7000) and 0.01 M HCl (Sigma-Aldrich, #H9892) for 48 h. The resulting pepsin digest was aliquoted and frozen at -80 °C. Aliquots were thawed overnight at 4 °C as needed for experiments. Hydrogel precursor polymer solutions were prepared by neutralizing the pepsin digest with one-hundredth the volume of 1.0 M NaOH (Sigma-Aldrich, #S2770), adding one-tenth of the total volume desired of 10× PBS (Mediatech, #46-013) to achieve a final concentration of 1×, and diluting the mixture with sterile MilliQ H<sub>2</sub>O. Hydrogels were formed after incubation of precursor polymer solutions at 37 °C for at least 1 h. Type I Collagen hydrogels were prepared similarly from purified porcine type I atelo-collagen (Advanced BioMatrix, #5169-100ML).

#### **4.2.3. Preparation of PEG-Crosslinked Gelatin Hydrogels with Conjugated Peptides**

PEG-crosslinked gelatin hydrogels with conjugated peptides were prepared as described previously in Chapter 3 and published elsewhere<sup>[280]</sup>. Vascular endothelial growth factor-mimetic QK peptides were purchased through custom peptide synthesis from ABI Scientific and confirmed to have a purity of >95% by high-performance liquid chromatography. QK peptide sequence from N- to C-terminal: KLTWQELYQLKYKGI, and a theoretical molecular weight of 2036.31 g/mol<sup>[352]</sup>. Lysine ε-amino groups were acetylated to prevent cross-reactivity with the amine-reactive PEG crosslinker (PEGX). C-termini of peptides were amidated to enhance stability, but N-termini were left unmodified. Peptides were solubilized in 1× phosphate-buffered saline solution (PBS, pH 7.4, Gibco, #10010) as concentrated stock solutions and frozen in aliquots at -20 °C. Aliquots were thawed and diluted as necessary for hydrogel preparation.

Gelatin type A (Sigma-Aldrich, #G1890) was solubilized in PBS at 37 °C at a stock concentration of 10% (m/v). Hydrogel precursor polymer solutions were prepared by mixing the following in order: PBS for dilution, 1.0 M NaOH to buffer solutions to an approximate final pH of 6 for optimal crosslinking kinetics, QK peptide to a final concentration of 100  $\mu$ M (if desired), and gelatin stock solution to a final concentration of 5% (m/v). Polymer solutions were held at 37 °C prior to crosslinking to ensure solution phase and thoroughly vortexed before the addition of crosslinker. Homobifunctional poly(ethylene glycol) succinimidyl valerate (SVA) (MW 5000 g/mol, Laysan Bio), referred to as simply PEG crosslinker or PEGX, was prepared as a concentrated stock solution at 40 mM in PBS just prior to crosslinking of polymer solutions. PEGX was added to hydrogel precursor polymer solutions to a final concentration of 1.55 mM for hydrogels with no peptides (referred to as “no peptides”) and 1.60 mM for QK-conjugated hydrogels (referred to as “QK”). Immediately after addition of PEGX, solutions were vortexed, pipetted into well plates, and incubated at 37 °C for 2 h. As an additional control group, Matrigel Basement Membrane Matrix (Phenol Red-Free, Corning, #356237) was thawed on ice, cast in well plates, and incubated alongside experimental groups.

#### **4.2.4. Preparation of 3D-Printed Gelatin Hydrogel Scaffolds**

3D-printed gelatin scaffolds were prepared as described previously<sup>[400, 401]</sup>. Briefly, gelatin type A was solubilized in PBS at a concentration of 10% (m/v) at 37 °C. The gelatin solution was transferred to a printer cartridge and 3D printed using a pneumatic-based, piston-driven direct extrusion 3D printer: the EnvisionTEC 3D-Bioplotter Manufacturer Series. The gelatin solution was maintained at a constant temperature of 30 °C within a high-temperature printhead and extruded through a stainless steel luer lock needle tip with an inner diameter of 200  $\mu$ m and needle length of 2 mm (EnvisionTEC) at pressures between 1.8 and 2.2 bar. Gelatin was printed at a speed of 10 mm/s onto glass microscope slides placed on the print stage cooled to 10 °C. Boxes 15  $\times$  15 mm in length and width were printed with four layers in height. Strut spacing and layer slicing were defined as 800  $\mu$ m and 156  $\mu$ m, respectively. The advancing angle or angle of orientation of printed struts between subsequent layers was adjusted as desired to fabricate scaffolds of varying pore geometries. Specifically, scaffolds were fabricated with 30° (0, 30, 60, and 90°), 60° (0, 60, 120, 180°), and 90° (0, 90, 180, 270°) advancing angles with 90° advancing-angle scaffolds

printed with struts offset slightly to avoid scaffold through-pores. Printed scaffolds were kept chilled on ice to prevent melting.

After printing, scaffolds were immediately crosslinked with a solution of 15 mM *N*-(3-dimethylaminopropyl)-*N'*-ethylcarbodiimide hydrochloride (Sigma-Aldrich, #E1769) and 6 M *N*-hydroxysuccinimide (Sigma-Aldrich, #130672) prepared in sterile MilliQ H<sub>2</sub>O for 1 h on ice. Scaffolds were then rinsed three times with excess sterile MilliQ H<sub>2</sub>O to remove residual crosslinker, sterilized overnight in 70% (v/v) ethanol (Decon Laboratories, #2701) at 4 °C followed by irradiation under ultraviolet light for 1 h, and stored in PBS supplemented with 1% penicillin-streptomycin at 4 °C until use. Immediately prior to cell seeding, scaffolds were removed from glass slides with sterile razor blades and biopsy punched using 6 mm biopsy punches (Integra Miltex, #33-36) to create circular scaffold disks.

#### **4.2.5. Cell Experimental Studies**

*Preparation of Cells for Culture or Encapsulation.* Cells were rinsed once with 1× Dulbecco's phosphate-buffered saline (DPBS, Mediatech, #21-030) and incubated with TrypLE Express (Gibco, #12605) at 33 °C for 5 min to lift cells. TrypLE Express was deactivated with excess cell culture media, and detached cells were collected and counted via the trypan blue exclusion method using Trypan Blue solution (Sigma-Aldrich, #T8154). Cells were centrifuged at 1200 RPM for 5 min and resuspended in complete media at the desired cell concentration.

*Culture on Hydrogel Substrates.* Culture studies on hydrogel substrates were performed in a similar manner as previously-established endothelial cell tube formation assays<sup>[361, 362]</sup>. For type I collagen and kidney dECM hydrogel substrates, hydrogel precursor polymer solutions were prepared and cast into well plates, 200 μL/cm<sup>2</sup>, and incubated at 37 °C for 1 h. Cells were seeded on top of hydrogel substrates at a final density of 12,500 cells/cm<sup>2</sup>, and cultures were maintained for one week at 33 °C and 5% CO<sub>2</sub> before being thermoswitched to 37 °C for the remaining 14 days (21-day culture period total). For Matrigel and PEG-crosslinked gelatin hydrogel substrates, hydrogel precursor polymer solutions were prepared and cast in well plates, 165 μL/cm<sup>2</sup>, and incubated at 37 °C for 2 h. Cells were seeded on hydrogel substrates at a final density of 48,000 cells/cm<sup>2</sup>, and cultures were maintained at 37 °C and 5% CO<sub>2</sub> for the 14-day culture

period. For 3D-printed gelatin scaffolds, scaffolds were carefully placed within wells of custom silicone isolators of the same diameter (Grace Bio-Labs) attached to glass microscope slides and autoclaved. Concentrated cell suspensions of 50,000 cells/scaffold were seeded onto scaffolds, and cells were allowed to attach for 1.5 h before careful addition of additional media. After overnight incubation at 33 °C and 5% CO<sub>2</sub>, scaffolds with cells were carefully transferred to wells of Costar Clear Flat Bottom Ultra-Low Attachment 24-Well Plates (Corning, #3473) using a sterile microspatula. Cells were maintained at 33 °C and 5% CO<sub>2</sub> for three days before being thermoswitched to 37 °C for the remaining 18 days (21-day culture period total).

*Cell Encapsulation within Type I Collagen and Kidney dECM Hydrogels.* Well plates were coated with poly(2-hydroxyethylmethacrylate) [poly(2-HEMA)] at least one day prior to cell encapsulation within hydrogels to prevent cell attachment to well plate surfaces following established protocols<sup>[320, 321]</sup>. Briefly, poly(2-HEMA) (Sigma-Aldrich, #P3932) was dissolved in 95% (v/v) ethanol at a concentration of 30 mg/mL under constant stirring at 40-60 °C and then sterile filtered through a polyethersulfone mesh with a pore size of 0.22 µm (EMD Millipore, #SCGP00525). Sufficient volume of the poly(2-HEMA) solution was added to each well to cover the well surface, and the solution was allowed to evaporate overnight in a biosafety cabinet. Cells were counted as described previously and aliquoted to obtain the necessary number of cells for encapsulation at the desired concentrations: 1 million cells/mL or 5 million cells/mL. The cell suspension was centrifuged, and pellets were resuspended in a minimal volume of complete media. Concentrated cell suspensions were added to hydrogel precursor polymer solutions, gently pipetted to mix, and cast into wells (200 µL/cm<sup>2</sup>). Hydrogel precursor polymer solutions with cells were incubated at 37 °C for at least 1 h to ensure hydrogel formation and cell encapsulation before complete media was added to wells and plates were transferred to 33 °C and 5% CO<sub>2</sub>.

#### **4.2.6. Evaluation of Cell Response**

*Cell Proliferation.* Samples were collected at designated time points and stored at -80 °C until analysis. Samples were digested with Proteinase K (Sigma-Aldrich, #P2308) in digestion buffer composed of 0.05 M Tris (Sigma-Aldrich, #T1503) and 1 mM CaCl<sub>2</sub> (Sigma-Aldrich, #C5670) in deionized H<sub>2</sub>O at pH

8 at 60 °C overnight. DNA content of digested samples was quantified with the Quant-iT PicoGreen dsDNA Assay Kit (Invitrogen, #P7589) following the manufacturer's protocol and compared to a standard curve generated using the dsDNA standard included in the kit. Fluorescence intensity was measured using a BioTek Cytation 3 Cell-Imaging Multi-Mode Reader with an excitation wavelength of 480 nm and an emission wavelength of 520 nm. Four biological replicates were analyzed at each time point ( $n = 4$ ). DNA content was similarly quantified from cell pellets of counted cells using the Trypan Blue exclusion method to determine the amount of DNA per cell ( $n = 3$ ). Proliferation is presented as the total cell number as well as cell number normalized to the number of cells initially seeded or encapsulated.

*Cell Viability Imaging.* Cell viability was evaluated using the LIVE/DEAD Assay Viability/Cytotoxicity Kit for Mammalian Cells (Invitrogen, #L3224) following the manufacturer's protocol. Briefly, samples were rinsed once with  $1\times$  DPBS, incubated with 4  $\mu$ M ethidium homodimer and 2  $\mu$ M calcein in DPBS for 30 min at 33 or 37 °C, and then rinsed once more with DPBS before imaging on a Nikon C2+ confocal microscope.

*Microscopy.* Photomicrographs of samples were captured on a Lumenera INFINITY1-3C microscopy camera mounted on a Nikon Eclipse TS100 using Lumenera INFINITY ANALYZE 6.5 software. For scanning electron microscopy (SEM), samples were fixed in 1.6% paraformaldehyde (Alfa Aesar, #43368) and 2.5% glutaraldehyde (Sigma-Aldrich, #G5882) in 0.1 M sodium cacodylate buffer (Ted Pella, #18851), pH 7.4 at 4 °C for several days, dehydrated in a graded ethanol series (30-100% in MilliQ H<sub>2</sub>O), critical-point dried in a Tousimis SAMDRI-795 Critical Point Dryer, coated with Os using an SPI Supplies Osmium Plasma Coater OPC-60A, and imaged on a Hitachi SU8030 cold-source field emission SEM.

*Gene Expression Analysis.* RNA was isolated from samples using TRIzol Reagent (Invitrogen, #15596) following the manufacturer's protocol, and isolated RNA was treated with DNA-free DNA Removal Kit (Ambion, #AM1906) to remove contaminating genomic DNA from samples. RNA concentration was measured using a NanoDrop 1000 Spectrophotometer (Thermo Scientific). Reverse transcription and cDNA synthesis was performed using iScript Reverse Transcription Supermix for RT-qPCR (Bio-Rad, #170-8841) with an Applied Biosystems GeneAMP PCR System 9700 following the manufacturer's protocol. Real-time quantitative polymerase chain reaction was performed using SsoAdvanced Universal SYBR Green Supermix (Bio-Rad, #170-5270) with 300 nM each of forward and reverse primers and 0.10 ng/ $\mu$ L

cDNA on an Applied Biosystems QuantStudio 7 Flex Real-Time PCR System. Primer sequences for genes of interest are listed in **Table 4-1**. The thermal profile used included an initial polymerase activation step at 95 °C for 30 sec followed by 40 amplification cycles of denaturation at 95 °C for 15 sec and annealing and extension at 60 °C for 60 sec. The expression of each gene of interest was normalized to expression of the housekeeping gene *cyclophilin A (PPIA)*, and relative degree of gene amplification was calculated using the  $\Delta\Delta C_T$  method:  $2^{[(C_T \text{ GOI } 2 - C_T \text{ PPIA } 2) - (C_T \text{ GOI } 1 - C_T \text{ PPIA } 1)]}$ . “C<sub>T</sub> GOI 1” represents the threshold cycle (C<sub>T</sub>) of the gene of interest for the reference population, and “C<sub>T</sub> GOI 2” represents the C<sub>T</sub> of the gene of interest for the experimental sample. Human kidney total RNA (Invitrogen, #AM7976) served as the reference population for gene expression analysis of podocytes cultured on tissue culture polystyrene, and podocytes cultured on tissue culture polystyrene at the permissive temperature on day 0 served as the reference population for gene expression analysis of hydrogel culture and encapsulation studies. Biological replicates were tested in triplicate ( $n = 3$ ) for podocytes cultured on tissue culture polystyrene or quadruplicate ( $n = 4$ ) for hydrogel culture and encapsulation samples with technical replicates in triplicate.

**Table 4-1: Primer sequences for gene expression analysis via quantitative real-time polymerase chain reaction (qPCR).**

<b>Gene</b>	<b>Forward Primer (5' to 3')</b>	<b>Reverse Primer (5' to 3')</b>
<b>PPIA</b>	CCC ACC GTG TTC TTC GAC ATT	GGA CCC GTA TGC TTT AGG ATG A
<b>WT1</b>	GGC ATC TGA GAC CAG TGA GAA	GAG AGT CAG ACT TGA AAG CAG T
<b>MAFB</b>	GAC GCA GCT CAT TCA GCA G	CTC GCA CTT GAC CTT GTA GGC
<b>TCF21</b>	TCC TGG CTA ACG ACA AAT ACG A	TTT CCC GGC CAC CAT AAA GG
<b>NPHS1</b>	CGC AGG AGG AGG TGT CTT ATT C	CGG GTT CCA GAG TGT CCA AG
<b>NPHS2</b>	GGG AAT CAA AGT GGA GAG AAT AG'	CAG AGA CTG AAG GGT GTG GAG
<b>KIRREL1</b>	GCC ATC TAC TCG TCG TTT AAG	GCA CGG TAG TCA GCA TAG AG
<b>CD2AP</b>	TGT GAA ACT TCG GAC AAG AAC A	AGT GAC TGT AGG ATT AAG GGC T
<b>SYNPO</b>	GCC CAA CTC CCA TCT AAT GGC	GGG ATG AGC GTA GCT TCT CTG
<b>PODXL</b>	TCC CAG AAT GCA ACC CAG AC	GGT GAG TCA CTG GAT ACA CCA A
<b>VEGFA</b>	GTC CAA CAT CAC CAT GCA GAT TA	GCT GTA GGA AGC TCA TCT CTC
<b>FLT1</b>	GAA AAC GCA TAA TCT GGG ACA GT	GCG TGG TGT GCT TAT TTG GA
<b>KDR</b>	GTG ATC GGA AAT GAC ACT GGA G	CAT GTT GGT CAC TAA CAG AAG CA
<b>FLT4</b>	ATC CGA GGA GCT ACT AGA GGG	AGC GCA GAT GCT CGT ACT TG
<b>COL4A4</b>	GTG CCG TTA AAG GTA TTC AGG G	GTG GCT CTA CCA ACA GGG T
<b>LAMB2</b>	GGA CGA AAA GAA GTG CTT CCT	GCA GGG ATA CCA TTC TCT GAC T

#### **4.2.7. Statistical Analysis**

All quantitative data is represented as the mean  $\pm$  standard error of the mean. Statistical significance was determined using an unpaired two-tailed Student's *t*-test assuming equal variance with Microsoft Excel (Microsoft). Significance for all statistical analyses was defined as  $p < 0.05$ .

### **4.3. Results**

#### **4.3.1. Gene Expression Analysis of Podocytes Cultured on Conventional Tissue Culture**

##### ***Polystyrene***

As a benchmark for podocyte phenotype in conventional culture conditions, gene expression from conditionally-immortalized human podocytes cultured on tissue culture polystyrene at both the permissive and non-permissive temperatures was analyzed (**Figure 4-1**). Several podocyte-specific genes of interest

were tested and compared with total RNA isolated from human kidney. The results revealed relatively low expression of several genes of interest with expression of some genes not detected at all. These included genes encoding transcription factors (*WT1*, *MAFB*, *TCF21*), slit diaphragm proteins (*NPHS1*, *NPHS2*), and glycocalyx markers (*PODXL*). The remaining genes encoding secreted growth factors (*VEGFA*) and slit diaphragm and actin-associated proteins (*KIRREL1*, *CD2AP*, *SYNPO*) only exhibited moderate expression. Interestingly, most gene expression declined after the recommended two-week culture at the non-permissive temperature, which is counter to the supposed advantage of conditional immortalization.

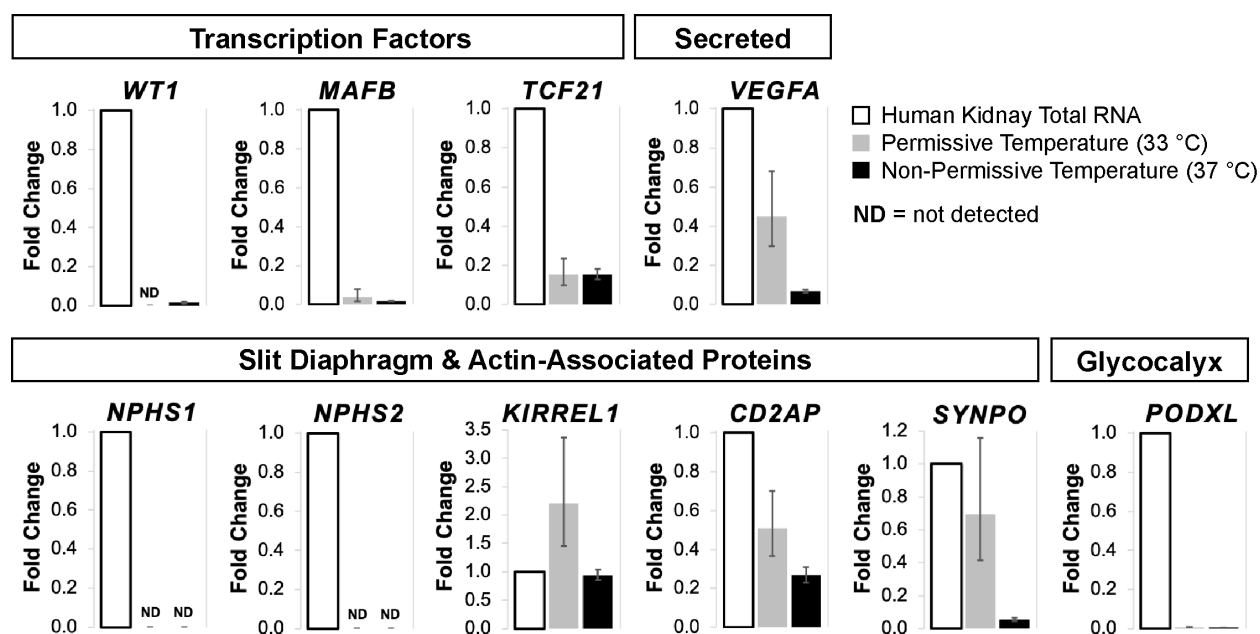


**Figure 4-1: Gene expression analysis of conditionally-immortalized human podocytes cultured on conventional tissue culture polystyrene.**

RNA was isolated from cells cultured at the permissive temperature of 33 °C or cells cultured for two weeks at the non-permissive temperature of 37 °C. Genes of interest include genes encoding transcription factors (*WT1* for Wilms tumor protein, *MAFB* for MAF bZIP transcription factor B, *TCF21* for transcription factor 21), secreted factors (*VEGFA* for vascular endothelial growth factor A), slit diaphragm and actin-associated proteins (*NPHS1* for nephrin, *NPHS2* for podocin, *KIRREL1* for Neph1, *CD2AP* for CD2-associated protein, *SYNPO* for synaptopodin), and glycocalyx markers (*PODXL* for podocalyxin). Values presented as fold-change expression normalized to human kidney total RNA ( $n = 3$ ).

### **4.3.2. Podocyte Culture on Kidney dECM Hydrogel Substrates and Encapsulation within Kidney**

#### **dECM Hydrogels**

Podocytes demonstrated moderate proliferation when initially cultured on kidney dECM hydrogels for one week at the permissive temperature (**Figure 4-2 A**). Surprisingly, this proliferation was not observed for podocytes cultured on collagen hydrogels under the same conditions. These results correspond with live/dead staining indicating high cell viability of cells cultured on either hydrogel substrate at day 1 but greater cell viability and substrate coverage of cells cultured on kidney dECM hydrogels on day 7 (**Figure 4-2 B**). After thermoswitching cells to the non-permissive temperature, however, cell number continued to decrease on both hydrogel substrates over the remaining culture period (**Figure 4-2 A**), which similarly corresponded with live/dead staining indicating reduced cell viability and decreased substrate coverage (**Figure 4-2 B**).

Podocytes were successfully encapsulated within collagen and kidney dECM hydrogels of varying concentrations (**Figure 4-3**). Live/dead staining indicated adequate preservation of cell viability after encapsulation; however, encapsulation within lower concentration hydrogels resulted in increased settling of cells and inhomogeneous cell distribution resulting in the appearance of a monolayer in confocal images. As encapsulated cells were maintained in culture, cell viability did not improve and in some cases appeared to decline. This decline in cell viability was more pronounced in collagen hydrogels and kidney dECM hydrogels of higher concentrations (2.5 and 5.0 mg/mL). In particular, although some cells encapsulated in kidney dECM hydrogels of 5.0 mg/mL appeared to adopt more spread morphologies at day 1, by day 7 and beyond only rounded cell morphologies were observed. More cells with spread morphologies were apparent in collagen hydrogels and kidney dECM hydrogels of 2.5 mg/mL, but many cells still exhibited rounded morphologies and compromised cell viability. Cell viability and morphologies appeared best by cells encapsulated within kidney dECM hydrogels of 1.0 mg/mL. Notably, contraction of hydrogels was observed as early as day 1 with greater contraction apparent in hydrogels of lower concentrations. Similar results were observed for podocytes encapsulated within type I collagen and kidney dECM blend hydrogels (**Figure 4-4**), although these samples were only maintained over a shorter 7-day culture.

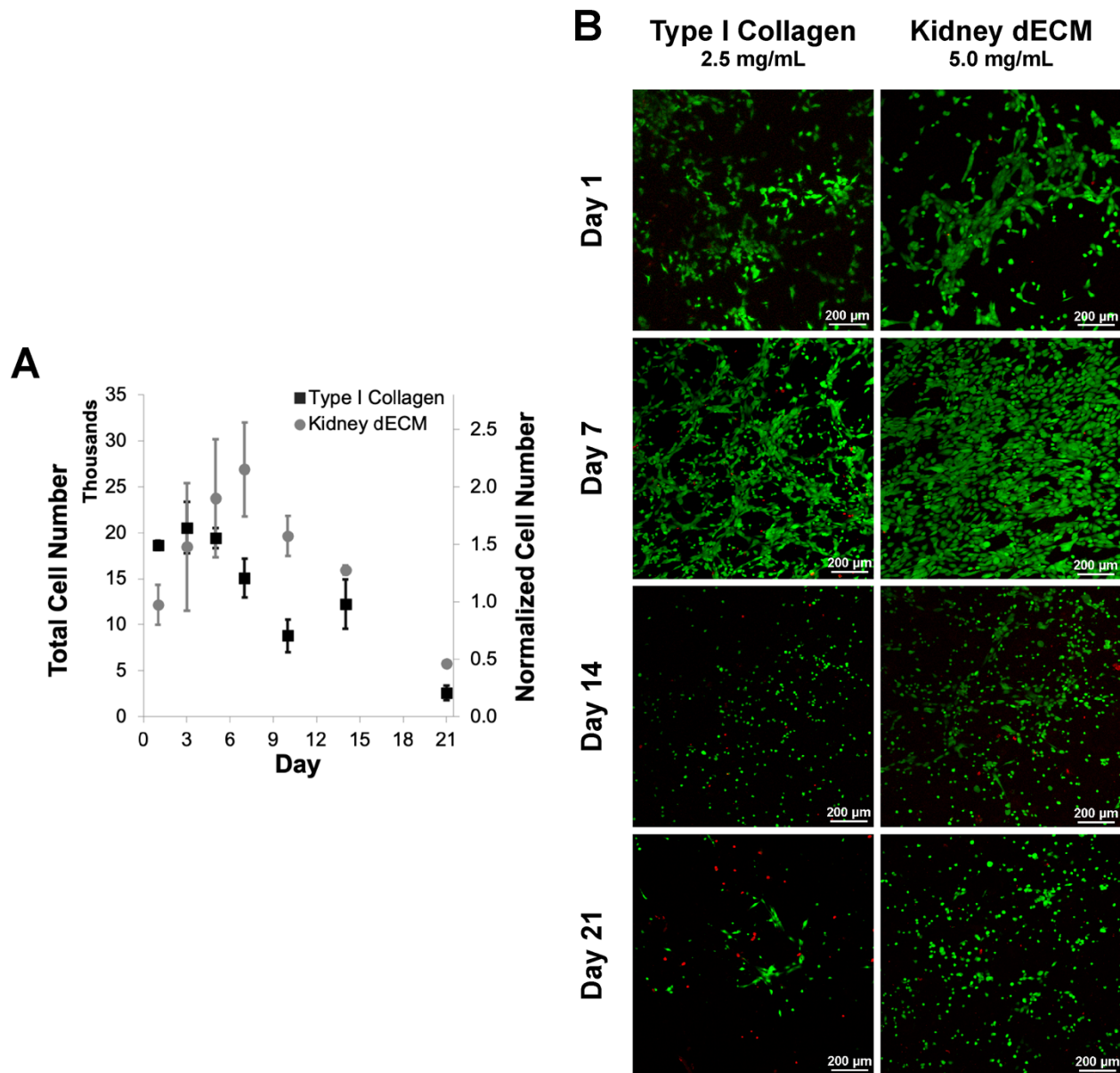


**Figure 4-2: Proliferation and viability staining of podocytes cultured on type I collagen hydrogels or kidney dECM hydrogels.**

Cells were thermoswitched from the permissive to the non-permissive temperature at day 7. (A) Quantification of podocyte proliferation over 21 days. Normalized values (right axis) were normalized to the number of cells initially seeded per sample on day 0. Number of biological replicates,  $n = 3$ . (B) Live (green) and dead (red) viability staining and confocal imaging of podocytes at indicated time points over a 21-day culture period.

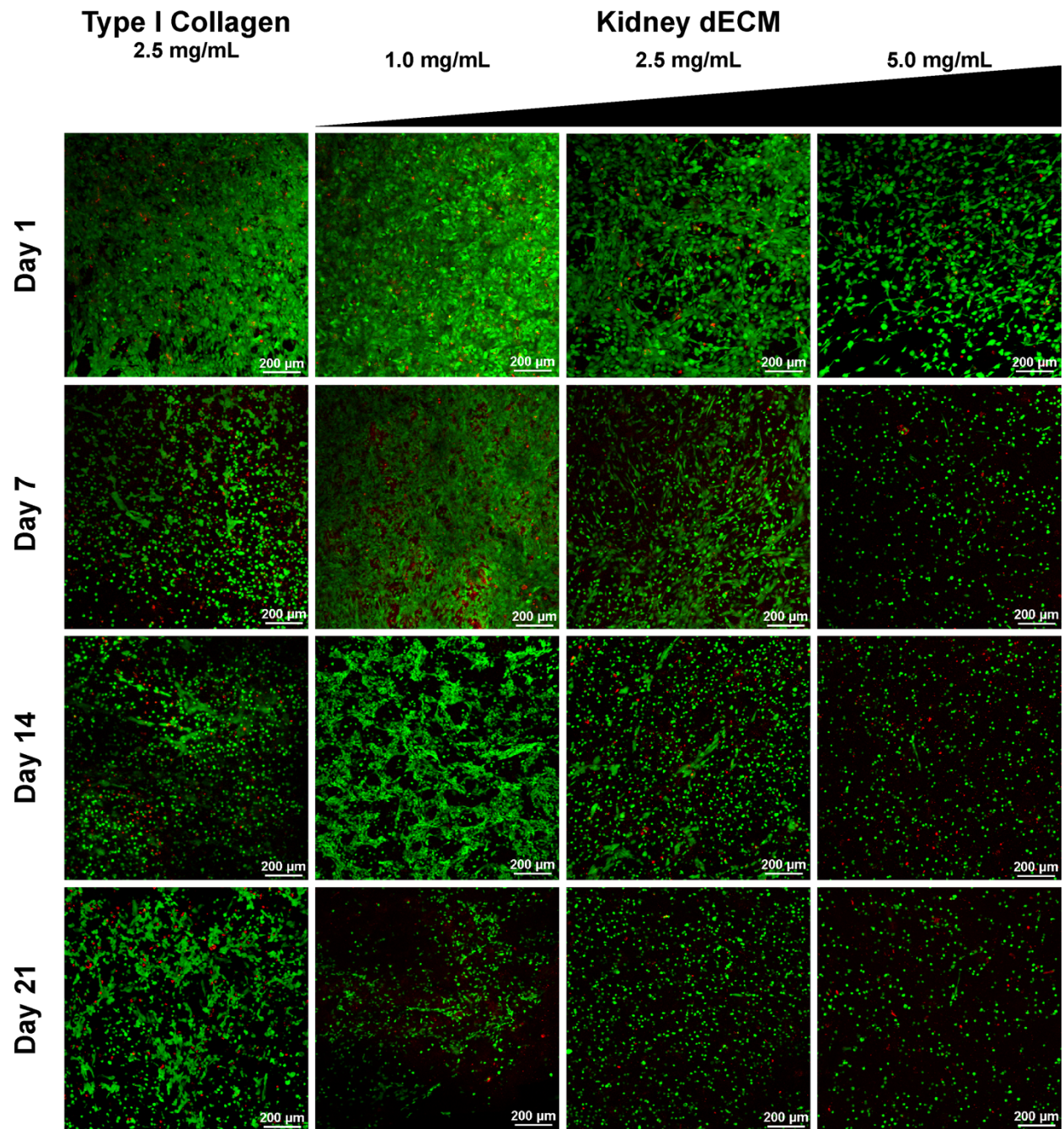


**Figure 4-3: Viability staining of podocytes encapsulated within type I collagen hydrogels or kidney dECM hydrogels of varying concentration.**

Live (green) and dead (red) viability staining and confocal imaging of podocytes at indicated time points over a 21-day culture period. Cells were thermoswitched from the permissive to the non-permissive temperature at day 7.

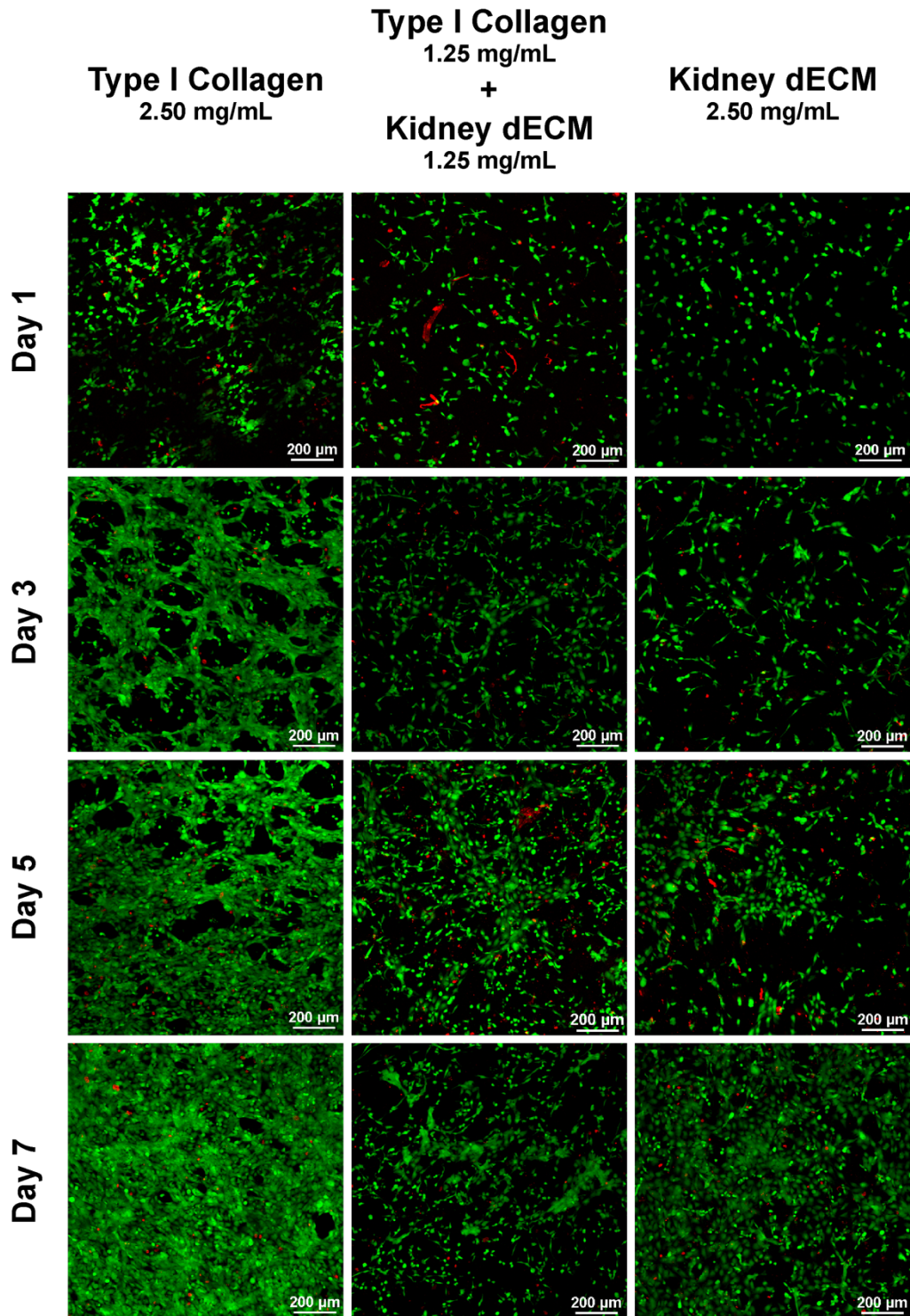


**Figure 4-4: Viability staining of podocytes encapsulated within type I collagen and kidney dECM hydrogel mixtures.**

Live (green) and dead (red) viability staining and confocal imaging of podocytes at indicated time points over a seven-day culture period at the permissive temperature.

### **4.3.3. Podocyte Culture on Matrigel and PEG-Crosslinked Gelatin Hydrogel Substrates and Gene Expression Analysis**

Podocytes cultured on Matrigel and PEG-crosslinked gelatin hydrogel substrates were immediately thermoswitched to the non-permissive temperature after seeding (**Figure 4-5**). When cultured on Matrigel, podocytes rapidly formed an interconnected network by 6 h that began to regress by 24 h and later resulted in cell aggregates. When cultured on PEG-crosslinked gelatin hydrogel substrates with no peptides, podocytes attached to the substrate and eventually began to form cord-like structures by day 7 with these structures more apparent at day 14, and cells did not form a confluent monolayer on the substrate at any point. Similar to podocytes cultured on hydrogels with no peptides, podocytes cultured on QK hydrogels resulted in cord-like formation, although clusters of cells on QK hydrogels appeared more distinct than those on hydrogels with no peptides.

Gene expression by podocytes cultured on Matrigel and PEG-crosslinked gelatin hydrogel substrates were analyzed, and genes of interest included those previously tested for with podocytes cultured on tissue culture polystyrene as well as additional genes encoding ECM proteins and cell receptors (**Figure 4-6**). In general, culture of podocytes on these hydrogel substrates resulted in an upregulation of genes of interest in comparison to culture on conventional tissue culture polystyrene; however, no clear trends were discernible from the results that signified one hydrogel substrate as superior over the others. For example, podocytes cultured on Matrigel resulted in the greatest upregulation of *SYNPO* and *COL4A4* at day 7, but podocytes cultured on hydrogels with no peptides resulted in the greatest upregulation of *MAFB*, *VEGFA*, and *KIRREL1* at day 1, whereas podocytes cultured on QK hydrogels resulted in the greatest upregulation of *PODXL* and *LAMB2* at day 1 and *CD2AP* at days 1 and 7. Notably, gene expression of important podocyte-specific markers *WT1*, *NPHS1*, and *NPHS2* were not detected from any samples. Interestingly, although differences in podocyte gene expression were observed between cells cultured on hydrogels with no peptides and QK hydrogel substrates, gene expression of the prototypical vascular endothelial growth factor receptors (*FLT1*, *KDR*, *FLT4*) was not detected from any samples.

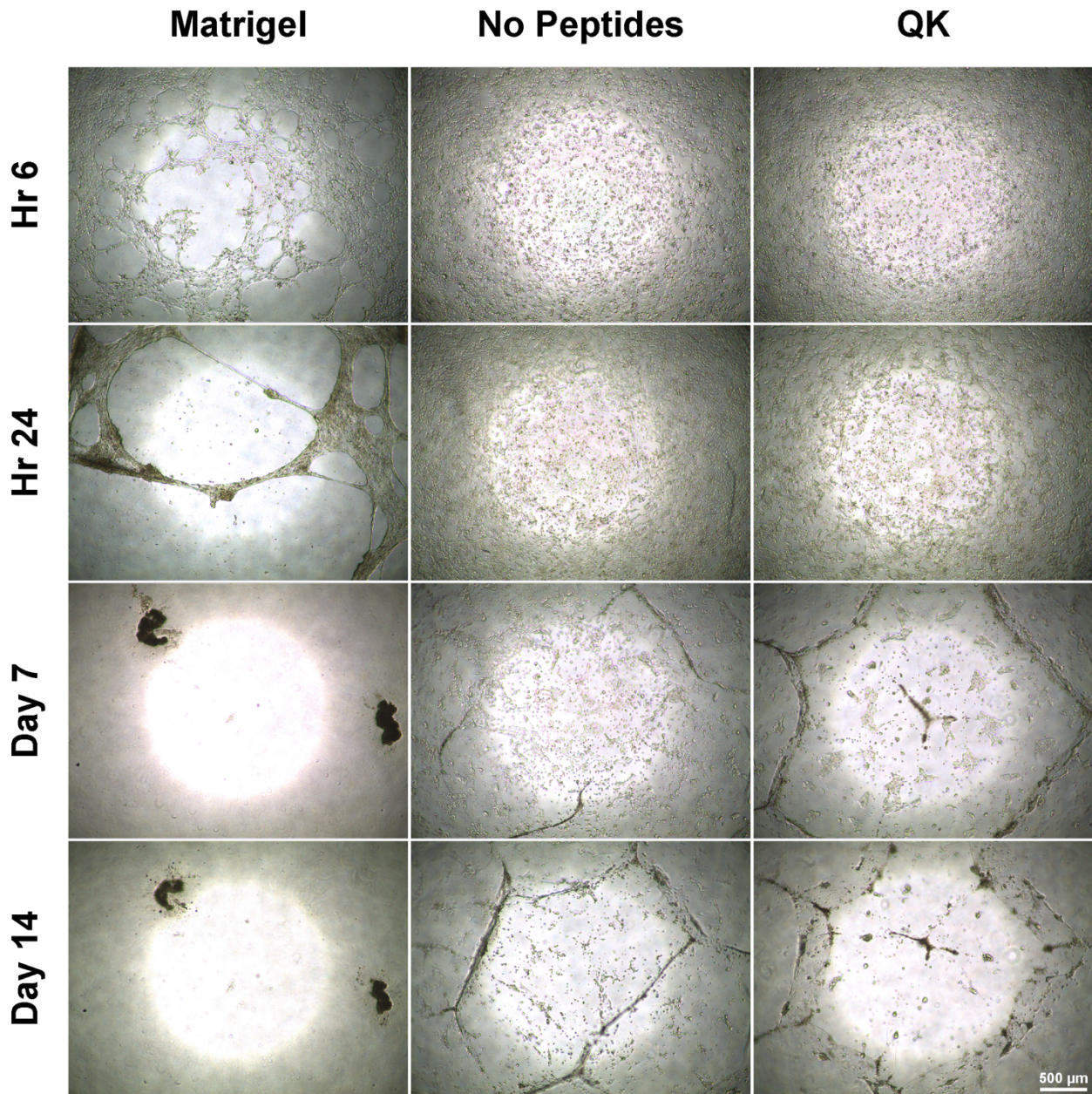


**Figure 4-5: Photomicrographs of podocytes cultured on Matrigel or PEG-crosslinked gelatin hydrogel substrates.**

Podocytes cultured on Matrigel ("Matrigel"), hydrogels with no peptides ("No Peptides"), or QK hydrogel ("QK") substrates. Cell cultures were thermoswitched from the permissive to the non-permissive temperature immediately after seeding onto hydrogel substrates. Photomicrographs were taken at indicated time points over a 14-day culture period.

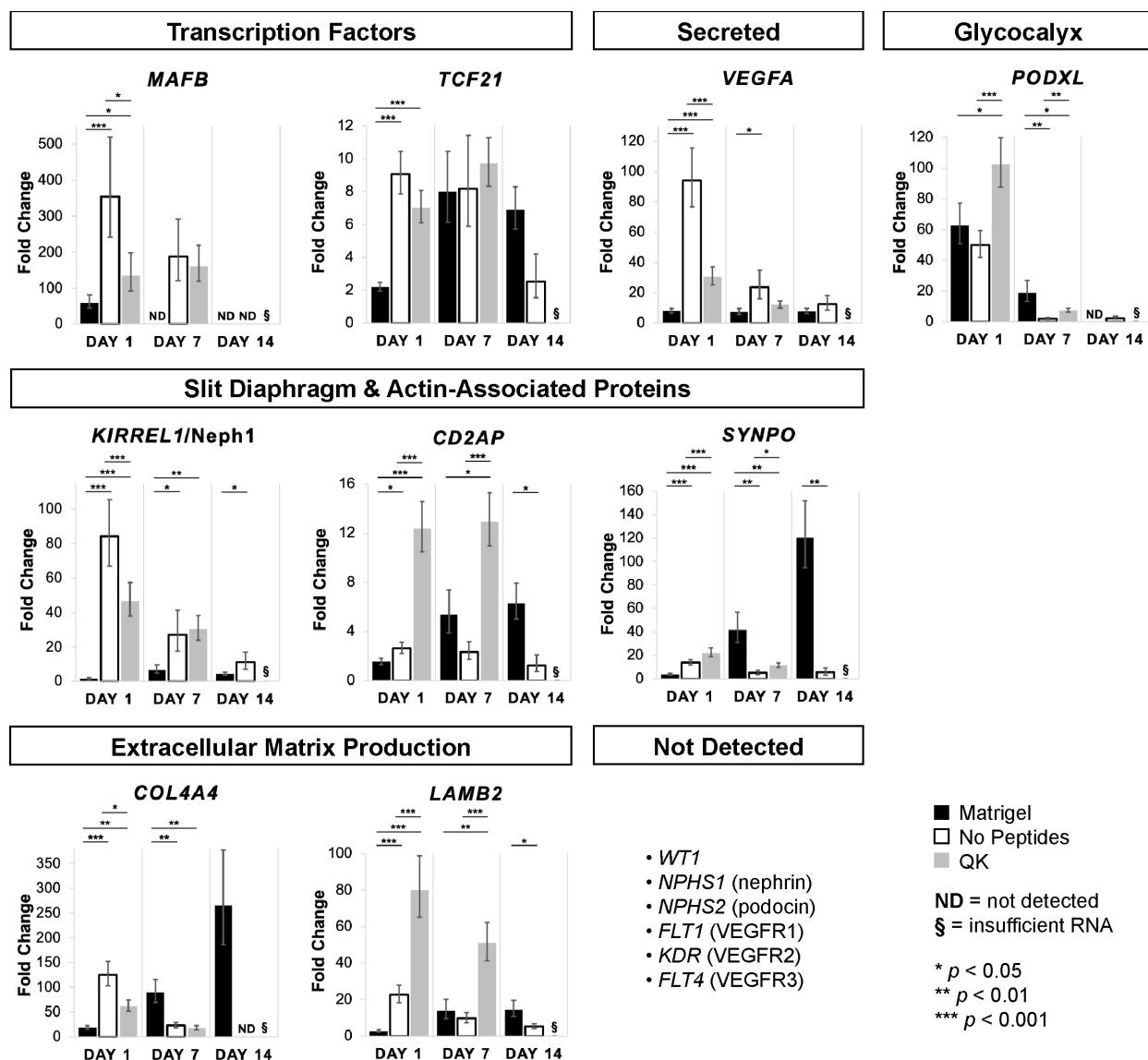


**Figure 4-6: Gene expression analysis of podocytes cultured on Matrigel or PEG-crosslinked gelatin hydrogel substrates.**

Podocytes cultured on Matrigel ("Matrigel), hydrogels with no peptides ("No Peptides), or QK hydrogel ("QK") substrates. RNA was isolated from cells cultured at the non-permissive temperature at indicated time points. Genes of interest include genes encoding transcription factors (*MAFB* for MAF bZIP transcription factor B, *TCF21* for transcription factor 21), secreted factors (*VEGFA* for vascular endothelial growth factor A), glycocalyx markers (*PODXL* for podocalyxin), slit diaphragm and actin-associated proteins (*KIRREL1* for Neph1, *CD2AP* for CD2-associated protein, *SYNPO* for synaptopodin), and extracellular matrix production (*COL4A4* for type IV collagen  $\alpha$  4 chain, *LAMB2* for laminin subunit  $\beta$  2). Additional genes of interest not detected include *WT1* (Wilms tumor protein), *NPHS1* (nephrin), *NPHS2* (podocin), *FLT1* (fms related tyrosine kinase 1 or vascular endothelial growth factor receptor 1), *KDR* (kinase insert domain receptor or vascular endothelial growth factor receptor 2), and *FLT4* (fms related tyrosine kinase 4 or vascular endothelial growth factor receptor 3). Values presented as fold-change expression normalized to gene expression of podocytes cultured on tissue culture polystyrene at day 0 ( $n = 4$ ). Statistical significance denoted by: \*  $p < 0.05$ , \*\*  $p < 0.01$ , and \*\*\*  $p < 0.001$ .

#### **4.3.4. Podocyte Culture on 3D-Printed Gelatin Scaffolds**

Podocytes were cultured on 3D-printed gelatin scaffolds and demonstrated adhesion at high cell densities regardless of pore geometry (**Figure 4-7**). When cultured at the permissive temperature for one week, cells remained attached to scaffolds lining scaffold struts. Once thermoswitched to the non-permissive temperature, cells began to adopt increasingly spread morphologies both along scaffold struts as well as rounding around scaffold pores at intersecting struts. This change in cell morphology over the culture and maturation period was also apparent from live/dead staining (**Figure 4-8**). Live/dead staining further revealed high cell viability of cells initially cultured on scaffolds that was largely preserved over the 21-day culture period. After the culture period, scaffolds with cells were additionally fixed and visualized by SEM (**Figure 4-9**). Low magnification micrographs illustrated scaffold architecture, and high magnification micrographs revealed interior pore geometries with cells lining scaffold struts and clustering within pores at strut intersections.

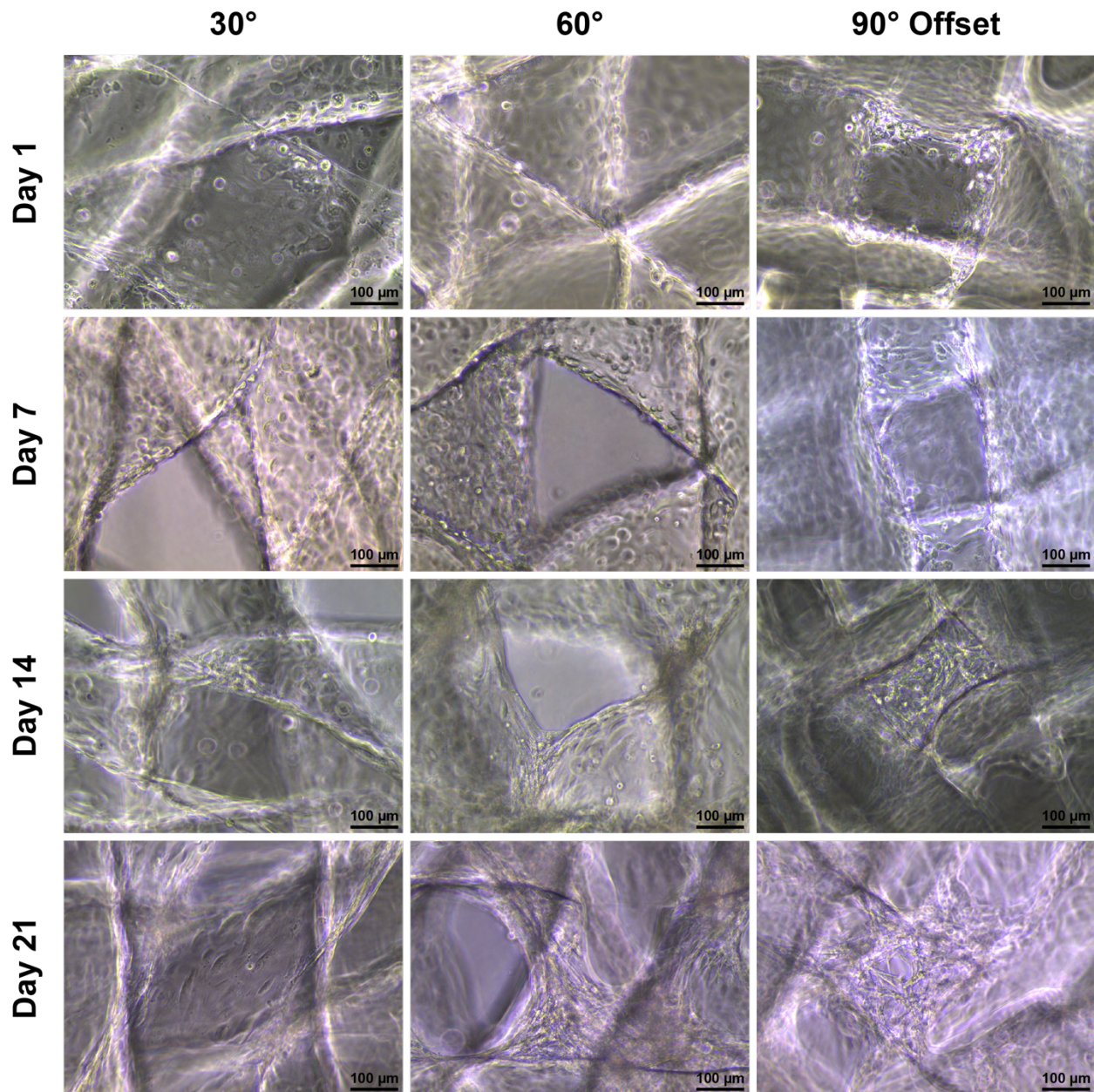


**Figure 4-7: Photomicrographs of podocytes cultured on 3D-printed gelatin scaffolds.**

Scaffolds of varying pore geometries: 30°, 60°, and 90° offset. Cells were thermoswitched from the permissive to the non-permissive temperature at day 7. Photomicrographs were taken at indicated time points over a 21-day culture period.

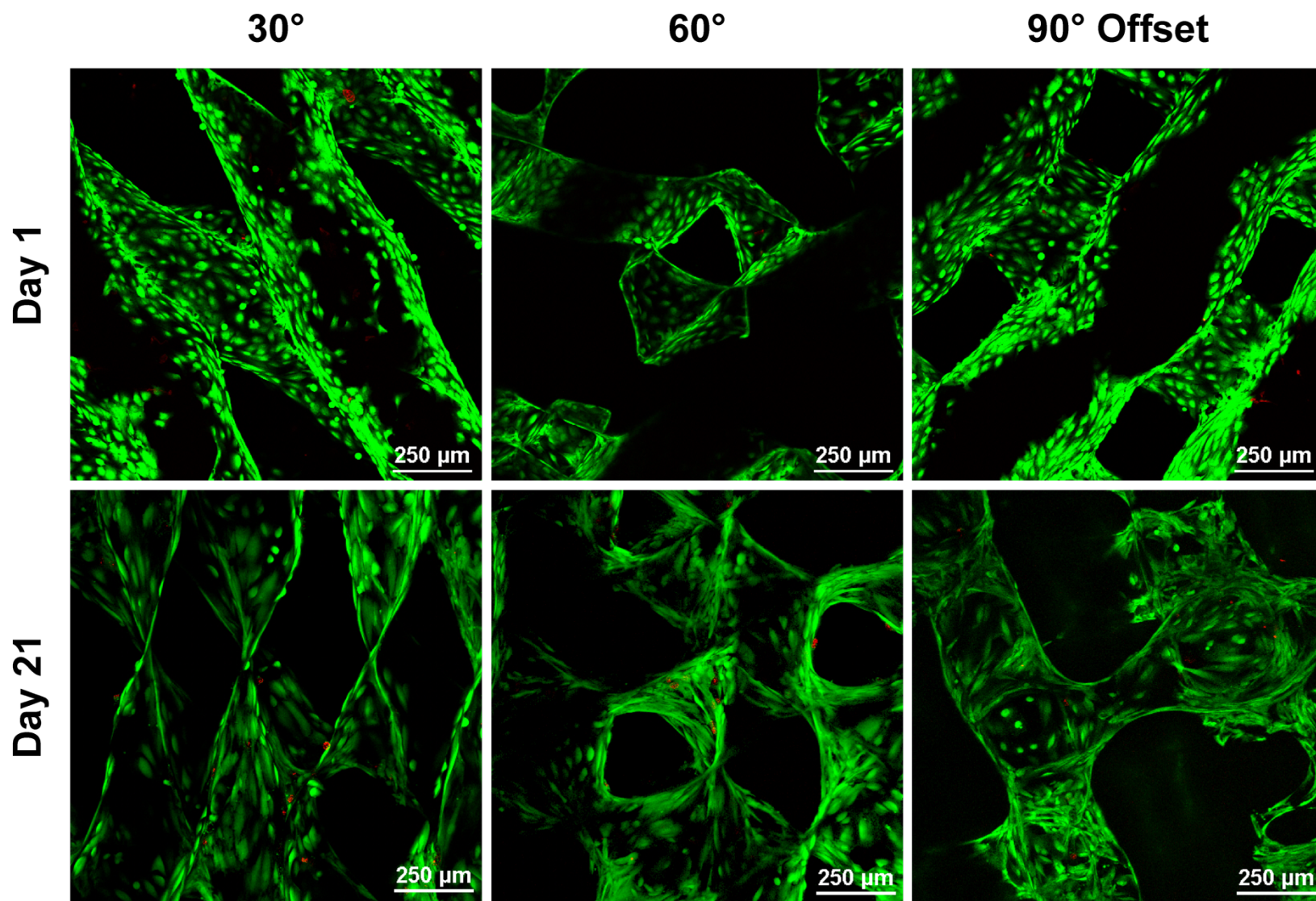


**Figure 4-8: Viability staining of podocytes cultured on 3D-printed gelatin scaffolds.**

Scaffolds of varying pore geometries: 30°, 60°, and 90° offset. Live (green) and dead (red) viability staining and confocal imaging of podocytes at days 1 and 21. Cells were thermoswitched from the permissive to the non-permissive temperature at day 7.

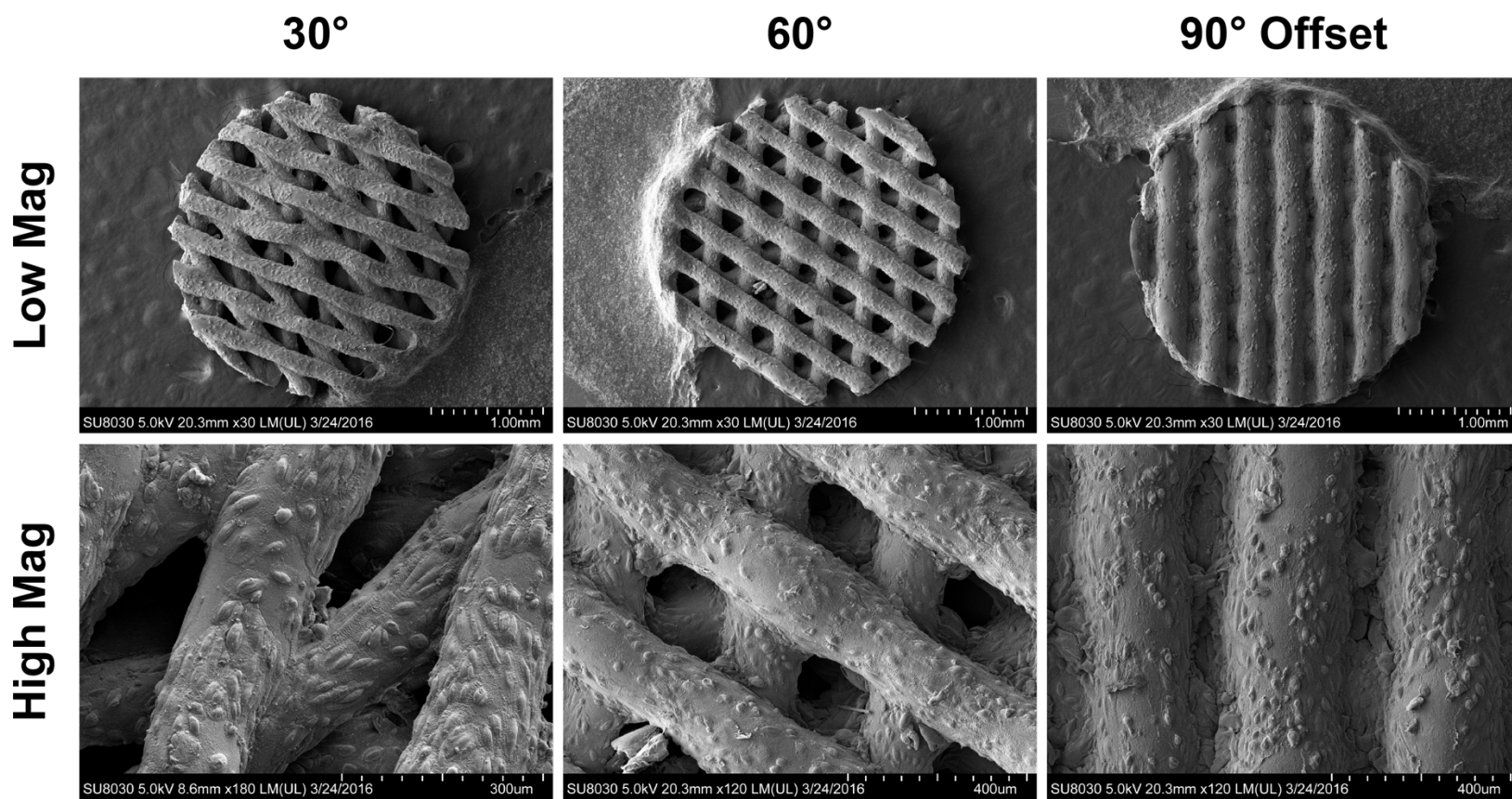


**Figure 4-9: Scanning electron micrographs of podocytes cultured on 3D-printed gelatin scaffolds.**

Scaffolds of varying pore geometries: 30°, 60°, and 90° offset. Low and high magnification micrographs of cells cultured on scaffolds for 21 days.

#### 4.4. Discussion

Podocyte cell culture *in vitro*, and especially the development of conditionally-immortalized podocyte cell lines, has enabled critical research in understanding the molecular mechanisms governing podocyte differentiation, function, and injury<sup>[391]</sup>. However, unless meticulous techniques are practiced, these cells may dedifferentiate in culture and lose their mature phenotype, resulting in misleading or misrepresented results<sup>[391]</sup>. Furthermore, conventional cell culture methods typically utilize rigid, 2D tissue culture-treated polystyrene substrates, which fail to simulate the *in vivo* microenvironment<sup>[399]</sup> and likely exacerbates these challenges. This is illustrated by the relatively low gene expression by conditionally-immortalized human podocytes cultured on tissue culture polystyrene at both the permissive and non-permissive temperatures of podocyte-specific genes of interest, including genes encoding for critical transcription factors, secreted growth factors, slit diaphragm and actin-associated proteins, and glyocalyx markers (**Figure 4-1**) by us and similar genes of interest by others<sup>[219, 398]</sup>. Here, we sought to evaluate the potential of hydrogel matrices to preserve or promote viability and a mature phenotype in conditionally-immortalized human podocytes. From these investigations, we also hoped to identify microenvironmental signaling cues and hydrogel design criteria essential for achieving these goals.

In the native microenvironment, cells produce and are surrounded by ECM responsible for imparting mechanical integrity to tissues and organs as well as presenting signaling cues to promote and maintain cell function<sup>[168, 169]</sup>. The composition of the ECM varies amongst tissues and organs within the body and even within different regions of a single tissue<sup>[169]</sup>. In many cases, tissue- and organ-specific dECM scaffolds and hydrogels have demonstrated equivalent if not superior bioactivity for regenerative engineering applications in comparison to standard controls such as collagen<sup>[264, 402]</sup>. In Chapter 2 and published elsewhere<sup>[288]</sup>, we demonstrated that porcine kidney dECM could be processed to form physically-crosslinked hydrogels capable of supporting conditionally-immortalized human glomerular endothelial cell (GEnC) viability and proliferation in culture and encapsulation studies. As another kidney-specific cell type and one that intimately interacts with GEnCs in the native microenvironment, we wanted

to evaluate podocyte response to culture on kidney dECM hydrogel substrates as well as to encapsulation within kidney dECM hydrogels for 3D culture.

Podocytes cultured on kidney dECM hydrogel substrates initially showed high cell viability as well as proliferation rates greater than those cultured on control collagen hydrogel substrates (**Figure 4-2**). These results were similar to those obtained for GEnCs; however, after extended culture past 7 days, reduced podocyte viability and increased cell death was observed for cultures on both hydrogel substrates (**Figure 4-2**). This suggests that these hydrogel substrates are missing a critical signaling cue necessary in maintaining podocyte attachment and health during maturation. Because the process of crosslinking kidney dECM hydrogels occurs under physiological conditions, these hydrogels are permissive for cell encapsulation and 3D culture. Podocytes encapsulated within kidney dECM hydrogels initially showed good cell viability at various hydrogel concentrations tested (**Figure 4-3 and 4-4**), but with continued culture periods, higher polymer or protein concentrations appeared to restrict cell spreading. It is well established in the biomaterials community that the polymer or protein concentration will influence the mesh size of the hydrogel, and increasing concentrations can limit necessary diffusion of molecules and be debilitating to cell health<sup>[233, 247, 403]</sup>. Even at lower concentrations or in collagen hydrogels (**Figure 4-3**), podocytes adopted less spread morphologies and cell viability was compromised to a greater extent than was observed for GEnCs encapsulated under similar conditions (see Chapter 2 and <sup>[288]</sup>). This suggests that perhaps podocytes are more sensitive than other cell types to encapsulation within a polymer matrix, even within a promoting hydrogel capable of undergoing remodeling by cells. This would be a reasonable conclusion given that in the mature glomerulus podocytes are only attached to the glomerular basement membrane at their foot processes and are otherwise suspended within the Bowman's space<sup>[4-6]</sup>.

To glean more information about signaling cues that may play a significant role in maintaining or promoting a mature podocyte phenotype, synthetic materials and components for hydrogels enable greater tailorability or tunability of hydrogel properties for investigating cell-material interactions. In Chapter 3 and published elsewhere<sup>[280]</sup>, we developed hydrogel substrates composed of both natural (*i.e.*, gelatin) and synthetic (*i.e.*, PEG) components with additional conjugated bioactive peptides to modulate response of

endothelial cells. Culture of GEnCs on these hydrogel substrates resulted in phosphorylation of corresponding growth factor receptors and changes in gene expression.

Podocytes cultured on control Matrigel substrates exhibited morphogenesis and subsequent regression of structures typical of most epithelial and endothelial cell types<sup>[275]</sup> (**Figure 4-5**). Podocytes cultured on PEG-crosslinked gelatin hydrogel substrates with no peptides or with conjugated QK peptides did not initially display unique responses when visualized under an optical microscope, although cell aggregation into cord-like structures was observed at later time points (**Figure 4-5**). This cord-like structure formation may have resulted from a combination of podocyte motility<sup>[20, 398]</sup> on these hydrogel substrates as well as hydrogel degradation creating an uneven surface over the two-week period.

Gene expression analysis at multiple time points revealed upregulation of detected genes of interest in podocytes cultured on hydrogel substrates in comparison to the reference population of cells cultured on conventional tissue culture polystyrene at the permissive temperature (**Figure 4-6**). These results were encouraging and further supported the hypothesis that culture of these cells on soft hydrogel substrates may indeed promote or preserve a mature phenotype; however, no specific trends could be discerned from the data with respect to the different hydrogel substrates investigated. Furthermore, the hydrogel substrates did not necessarily maintain cell survival as cell numbers appear reduced at later time points in photomicrographs (**Figure 4-5**) and, in some cases, sufficient RNA for gene expression analysis could not be isolated (**Figure 4-6**). In addition, expression of some genes was still lost over the culture period, and expression of podocyte-specific *WT1*, *NPHS1*, and *NPHS2* was not regained when podocytes were cultured on hydrogel substrates. It is particularly intriguing that differences in gene expression were observed between cells cultured on hydrogels with no peptides and QK hydrogel substrates given that gene expression for the family of vascular endothelial growth factor receptors (*FLT1*, *KDR*, *FLT4*) was not detected from any samples (**Figure 4-6**). Previous characterization of these hydrogels demonstrated similar hydrogel surface ultrastructures and stiffnesses (see Chapter 3 and <sup>[280]</sup>), therefore it is unlikely that these factors are responsible for the differences in cell response observed. It is possible that podocytes maintained protein expression of the necessary receptors at levels below the detectable limit by gene

expression analysis or that signal transduction was enhanced by the presence of co-receptors such as neuropilins<sup>[404]</sup>.

Although podocytes are not completely surrounded by ECM in the native microenvironment, neither do they lie on a completely 2D substrate as the GECs form a 3D capillary tuft that the podocytes envelop. Hydrogels are additionally versatile in that they may be manipulated and processed into specific patterns and structures. Recent advances in additive manufacturing techniques such as 3D printing and bioprinting as well as biomaterials development now enable the fabrication of complex hydrogel scaffolds and constructs with well-controlled and defined architecture<sup>[241]</sup>. In particular, researchers have demonstrated fabrication of 3D-printed gelatin hydrogel scaffolds with high-fidelity and controlled pore geometries, and the scaffold pore geometry influenced survival and function of mouse ovarian follicles<sup>[400]</sup> and gene and protein expression of human hepatocellular carcinoma cells<sup>[401]</sup>. Although using the same extrusion-based 3D printing modality it is technically challenging to replicate features of the glomerulus at the same scale, 3D-printed scaffolds nonetheless provide a means to investigate the role 3D spatial architecture may play in maintaining or promoting a mature podocyte phenotype.

Podocytes cultured on 3D-printed gelatin hydrogel scaffolds regardless of pore geometry exhibited good cell adhesion (**Figure 4-7**) and high cell viability (**Figure 4-8**) both after initial seeding on scaffolds and after extended culture for 21 days including the maturation period at the non-permissive temperature. Notably, after the maturation period at 21 days, cells adopted more spread morphologies that was especially apparent at strut intersections where cells were observed rounding the scaffold pores and adhering to multiple struts. This was also observed by SEM of samples (**Figure 4-9**). Remarkably, whereas podocytes cultured on the previous hydrogel substrates discussed often experienced cell death especially during culture at the non-permissive temperature (**Figure 4-2** and **4-5**), this was not the case for podocytes cultured on 3D-printed gelatin scaffolds (**Figure 4-7** and **4-8**). This preservation of cell health may arise from two factors that set these 3D-printed gelatin hydrogel scaffolds apart from kidney dECM hydrogel and PEG-crosslinked gelatin hydrogel substrates: hydrogel stiffness and 3D structure.

Rheological characterization was previously performed to measure the flow of hydrogels and quantify hydrogel stiffness. Complex shear moduli ( $G$ ) were measured to be in the range of 15-60 Pa for

type I collagen and kidney dECM hydrogels (see Chapter 2 and <sup>[288]</sup>) and approximately 200 Pa for PEG-crosslinked gelatin hydrogels (see Chapter 3 and <sup>[280]</sup>). Matrigel has been reported to have a complex shear modulus of 55-90 Pa<sup>[318, 369]</sup>. The complex shear modulus is related to the storage or elastic modulus ( $G'$ ) and the loss or viscous modulus ( $G''$ ) by the following equation:

$$G = \sqrt{(G')^2 + (G'')^2}$$

The relationship between the complex shear modulus and the elastic or Young's modulus ( $E$ ) is defined by the following equation:

$$E = 2G(1 + \nu)$$

where  $\nu$  represents Poisson's ratio<sup>[405]</sup>. Assuming the materials under questions are isotropic and incompressible, the above relationship simplifies to the following<sup>[406]</sup>:

$$\nu = 0.5 \text{ and } E = 3G$$

With these relationship and simplifications, it is apparent that the kidney dECM, PEG-crosslinked gelatin, and Matrigel hydrogel substrates are relatively soft with estimated Young's moduli of 600 Pa or less. On the other hand, the 3D-printed gelatin hydrogel scaffolds were previously measured to have an approximate Young's modulus of 16.8 kPa by compression testing<sup>[400]</sup>. This difference by orders of magnitude in hydrogel stiffness may account for the improved cell adhesion and spreading observed by podocytes cultured on these scaffolds as opposed to soft hydrogel substrates. These observations are additionally supported by recent results by Hu *et al.* demonstrating alterations in conditionally-immortalized human podocyte phenotype when cultured on transglutaminase-crosslinked gelatin hydrogel substrates of varying stiffness<sup>[274]</sup>. Specifically, the researchers demonstrated that podocytes exhibited upregulation of podocyte-specific gene and protein expression when cultured on gelatin hydrogel substrates of stiffnesses closest to that of healthy glomeruli (Young's moduli between 2 and 5 kPa) regardless of the extracellular matrix coatings<sup>[274]</sup>. While the hydrogel substrates and scaffolds investigated here are either less or more stiff than this optimal window, the chemical crosslinking methods employed in generating PEG-crosslinked gelatin hydrogel substrates and 3D-printed gelatin hydrogel scaffolds allow for tuning of crosslink density and thus hydrogel stiffness for future studies.

Regarding the 3D structure of printed scaffolds, Laronda *et al.* hypothesized that the open, porous structures of the scaffolds would enable ovulation and release of eggs from constructs which otherwise would be restricted in encapsulation systems<sup>[400]</sup>. Their results demonstrated that survival of mouse ovarian follicles was dependent on pore geometries that promoted multiple follicle-strut interactions to maintain the spherical shape of follicles, and that the 3D structure of scaffolds indeed allowed ovulation<sup>[400]</sup>. Lewis *et al.* additionally demonstrated that the 3D structure of scaffolds and pore geometry enhanced hepatocyte-specific functions, including albumin secretion, cytochrome P450 activity, and bile transport<sup>[401]</sup>. In a similar manner but using a different platform, recent investigations by Korolj *et al.* revealed that conditionally-immortalized mouse podocytes are sensitive to 3D surface topography and curvature, and culture on 3D topographic substrates enhanced mature podocyte gene and protein expression and foot process formation and interdigitation<sup>[407]</sup>. It would reasonably follow then that the structure of these 3D-printed gelatin hydrogel scaffolds may also influence podocyte phenotype and function, although future functional studies are necessary to confirm this otherwise speculation.

Altogether, these investigations here and those by others illustrate that hydrogel systems can be used to preserve or promote a mature or differentiated podocyte phenotype in culture; however, podocytes present a unique challenge and specific microenvironmental factors must be considered when designing these biomimetic platforms. Podocytes appear to be particularly sensitive to encapsulation within hydrogel matrices, and as a result future encapsulation studies will likely require the development of novel hydrogel systems with low polymer fractions that still maintain the necessary mechanical properties. Hydrogel substrates for podocyte culture are less technically demanding, but these substrates will still require the necessary mechanical properties (*i.e.*, optimal hydrogel stiffness) to maintain cell adhesion and may be integrated or fabricated with 3D topography and structure to promote additional maturation of cells. Continued advances in biomaterial hydrogel development and fabrication processes will enable superior *in vitro* culture platforms for understanding the exceptional biology of podocytes and their response to injury as well as engineered models of the glomerular filtration barrier.

#### 4.5. Conclusion

Podocytes are remarkable cells that are integral to the function of the glomerular filtration barrier, but their highly-differentiated state means that establishing and maintaining *in vitro* cultures of these cells representative of their *in vivo* state is notoriously challenging. As biomimetic culture platforms, hydrogels are a versatile class of biomaterials with the potential to establish a new standard for cell culture beyond traditional 2D, rigid tissue culture polystyrene. However, it has become increasingly apparent that specific microenvironmental signaling cues and subsequent hydrogel design criteria are necessary to promote and maintain podocytes in a differentiated state. Here, we provided evidence that podocytes may be particularly sensitive to encapsulation within 3D hydrogel matrices thus requiring special consideration when designing hydrogels for these types of investigations. Furthermore, podocyte morphology and maturation when cultured on hydrogel substrates is promoted by an optimal window of hydrogel stiffness as well as 3D surface topography and structure. Future investigations may explore hydrogel platforms that integrate these design criteria, such as 3D-printed hydrogel scaffolds, and critically evaluate podocyte phenotype and function through gene and protein expression. Ultimately, the establishment of superior culture systems will accelerate research and understanding of podocyte cell biology, response to injury, and possible regeneration as well as the development of *in vitro* models of the glomerular filtration barrier.

**CHAPTER V:**

**Conclusion & Future Directions**

## 5.1. Significance & Impact of Findings

Hydrogels have garnered increasing attention by the research community over the past few decades and in particular by those involved in regenerative engineering<sup>[227-229]</sup>. This is because hydrogels exhibit unique and desirable properties that arise from their structure as water-swollen, crosslinked polymer networks<sup>[226]</sup>. Specific structural parameters may be controlled during polymer synthesis or network formation to tailor or tune the necessary hydrogel properties, both biophysical and biochemical, for its intended applications. As a result, hydrogels are especially appealing as extracellular matrix (ECM) substitutes or mimics<sup>[234-236]</sup>. However, despite the clear clinical need for engineered kidney tissue models<sup>[57, 72]</sup> and the potential advances hydrogels may enable in such research, there have been relatively few investigations regarding hydrogel development and application specifically towards kidney-specific cell response and bioengineering strategies (of which have been reviewed previously in Chapter 1). The investigations presented within this dissertation thus sought to bridge this gap and examine the influence of microenvironmental signaling cues as presented by hydrogel platforms on kidney cell response with a specific focus on the components of the glomerular filtration barrier.

With this goal in mind, in Chapter 2 and published elsewhere<sup>[288]</sup>, we presented a method for generating hydrogels from kidney decellularized extracellular matrix (dECM). Researchers from numerous other groups have previously developed and characterized hydrogels from various tissues and organs<sup>[264]</sup> including the kidney<sup>[278, 279, 282]</sup>. However, although several other tissue- and organ-specific dECM hydrogels have undergone thorough characterization, this was previously not the case for dECM hydrogels derived from the entire kidney. Our results demonstrated that kidney dECM could be processed to form hydrogels with fibrillar architectures and interconnected pores similar to type I collagen hydrogels. In addition, rheological characterization revealed rapid gelation kinetics of hydrogels. Furthermore, final hydrogel stiffness could be modulated by adjusting the polymer or protein concentration of the hydrogel across several orders of magnitude, although it is important to note that changing the polymer or protein concentration for these hydrogels also alters the concentration of bioactive sites for cell interactions. Finally, these hydrogels, when employed as culture substrates, supported glomerular endothelial cell (GEnC) viability and proliferation.

Although other researchers previously evaluated response of cells cultured on kidney dECM hydrogel substrates of varying fibrillar architectures as altered by macromolecular crowding<sup>[279]</sup> or of kidney regional specificity<sup>[278, 282]</sup>, our investigation was the first to evaluate the response of cells encapsulated within kidney dECM hydrogels, and the results were unexpected. While high cell viability of GEnCs was maintained after encapsulation and after extended culture, proliferation appeared to be hindered after reaching a critical point. Histological analysis and transmission electron micrographs illustrated the occurrence of cell settling during the encapsulation process as well as the failure of fully encapsulated cells to form robust cell-cell interactions. Most surprisingly, however, GEnCs encapsulated within collagen hydrogels exhibited greater upregulation in gene expression of several genes of interest in comparison to cells encapsulated within kidney dECM hydrogels. These results were the opposite of our original hypothesis, yet additional gene expression analysis of GEnCs cultured on hydrogel substrates or encapsulated in hydrogels at greater cell densities yielded similar outcomes. Despite retention of key ECM components after decellularization, including type I collagen, type IV collagen, laminin, and sulfated glycosaminoglycans, kidney dECM hydrogels were inferior to type I collagen hydrogels in achieving the desired response by GEnCs.

The results from this investigation are in significant contrast from much of the published literature that validate dECM scaffolds<sup>[303]</sup> and hydrogels<sup>[264]</sup> for tissue- and organ-specific regenerative engineering applications. Only a few other investigations obtained similar observations, specifically in which photocrosslinked blends of cartilage, meniscus, or tendon with gelatin methacryloyl compromised maturation of encapsulated chondrocytes in comparison to cells encapsulated in gelatin methacryloyl alone<sup>[408]</sup> or physically-crosslinked or photocrosslinked cartilage or tendon hydrogels compromised chondrogenic differentiation of encapsulated human mesenchymal stem cells in comparison to cells encapsulated in gelatin methacryloyl<sup>[409]</sup>. Together, it is important to stress that ultimately these outcomes are application dependent and influenced by the experimental design, source of cells (if any), source of material, and processing procedures as there is considerable variability amongst decellularization and solubilization protocols<sup>[170, 171]</sup>.

Because dECM is inherently complex, it is difficult to precisely determine specific necessary biochemical components that may have been lost or disadvantageous components that may have been present in affecting the cell response. Therefore, in Chapter 3 and published elsewhere<sup>[280]</sup>, we presented a method for generating hydrogels with gelatin as the base material and imparting additional bioactivity through the conjugation of synthetic peptides. Employing the extremely versatile PEGX method<sup>[341]</sup>, which utilizes a reactive poly(ethylene glycol) (PEG) chemical crosslinker (PEGX), we demonstrated that natural-synthetic hydrogel substrates with tunable stiffness and presentation of bioactive signaling cues influenced endothelial cell behavior in culture. In developing and characterizing the resulting hydrogels, we identified pH as a critical parameter in regulating the crosslinking reaction and kinetics with the specific PEGX chemistry utilized—the succinimidyl valerate ester. Furthermore, as the PEG becomes part of the polymer network, increasing peptide concentrations require additional crosslinker concentrations, which ultimately influences the swelling properties of the hydrogel.

Although other researchers have previously demonstrated that conjugation of bioactive cell-binding and signaling peptides to hydrogels enhances endothelial cell morphogenesis and function<sup>[350, 351, 355, 357, 358]</sup>, this is the first investigation to utilize the PEGX method for simultaneous conjugation of peptides to a gelatin polymer network as well as the first to specifically examine the combination of laminin-derived YIGSR and vascular endothelial growth factor (VEGF)-mimetic QK peptides. Importantly, these peptides retained their bioactive signaling properties after conjugation, and we discovered that human umbilical vein endothelial cells (HUVECs) exhibited the greatest upregulation in gene expression for several genes of interest when cultured on dual peptide-conjugated gelatin hydrogel substrates at five days. These results were encouraging, however, when GEnCs were cultured under the same conditions, we observed drastically different trends. Whereas HUVECs generally tended towards upregulation of gene expression, GEnCs almost equally displayed upregulation and downregulation for the genes of interest and time points tested. Interestingly, this is the first investigation, to the best of the author's knowledge, to demonstrate enhanced signaling of these conditionally-immortalized human GEnCs in response to conjugated or tethered QK peptides in comparison to relatively little signaling to free QK peptide or human recombinant VEGF presented in solution. Together these results underscore the phenotypic heterogeneity of endothelial

cells isolated from different blood vessels and vascular beds in the body<sup>[379, 380]</sup>, which additionally influences cell response to engineered microenvironments as illustrated here and by others<sup>[154, 282, 410]</sup>.

While GEnCs form the capillary loops of the glomerulus, podocytes envelop these capillaries forming the external layer of the glomerular filtration barrier. Podocytes as a terminally differentiated cell population are particularly challenging to maintain in culture and study *in vitro* as they are typically non-proliferating and rapidly dedifferentiate under standard cell culture conditions<sup>[391, 392]</sup>. While conditional immortalization techniques have enabled more eloquent cell biology-based studies of podocytes<sup>[396]</sup>, these cultures still require careful maintenance and suffer from significant variation amongst different lines<sup>[398]</sup> or reduced or lost phenotypic expression<sup>[219]</sup>. But until recently, there have been few investigations exploring the application of hydrogel platforms for promoting or maintaining mature podocyte phenotypes in cultures.

With the knowledge that response to engineered microenvironments is often cell dependent, in Chapter 4 we presented results from investigations evaluating conditionally-immortalized human podocyte response to the hydrogel platforms discussed in Chapters 2 and 3 in addition to 3D-printed gelatin hydrogel scaffolds. In particular, it appears from viability staining and cell morphologies that podocytes are less amenable to encapsulation within hydrogels, specifically type I collagen hydrogels or kidney dECM hydrogels, than GEnCs. Although podocytes cultured on Matrigel or soft, PEG-crosslinked gelatin hydrogel substrates with or without conjugated QK peptides tended towards upregulation in gene expression of several podocyte-specific genes of interest in comparison to the reference population of cells cultured on tissue culture polystyrene, no specific trends could be distinguished amongst experimental groups. Furthermore, when cultured on these soft hydrogel substrates or on similarly soft collagen or kidney dECM hydrogel substrates, podocyte cell numbers often appeared reduced with more cells adopting rounded morphologies. In contrast, podocytes cultured on stiffer, 3D-printed gelatin scaffolds maintained good cell viability, adhesion, and larger cell morphologies after culture at the non-permissive temperature for an extended period. These results suggest that podocytes additionally may respond to substrate mechanical properties as well as 3D structure or architecture. In fact, recent investigations by others provide similar evidence for these specific microenvironmental signaling cues: Hu *et al.* demonstrated enhanced gene and protein expression by conditionally-immortalized human podocytes cultured on gelatin hydrogel substrates

of optimal stiffnesses closest to that of healthy glomeruli<sup>[274]</sup> and Korolj *et al.* demonstrated enhanced gene and protein expression by conditionally-immortalized mouse podocytes cultured on substrates with 3D topography and curvature<sup>[407]</sup>. Together, these investigations clearly illustrate the potential engineered microenvironments and hydrogels provide for improving current *in vitro* cultures towards models of more mature and functional podocytes and of the glomerular filtration barrier.

## 5.2. Future Directions

### 5.2.1. Kidney Decellularized Extracellular Matrix Hydrogels for Cell Culture and Encapsulation

Although kidney dECM hydrogels promoted cell adhesion and proliferation as a 2D substrate and permitted cell encapsulation under mild conditions, the gene expression analysis results of encapsulated GEnCs present many questions for potentially optimizing and evaluating the system. As has been mentioned numerous times throughout this dissertation, the kidney is structurally heterogeneous<sup>[1, 3]</sup>, which reasonably results in a heterogeneous distribution of ECM components throughout the organ (*i.e.*, vascular basement membrane, tubular basement membrane, stroma)<sup>[277]</sup>. However, the kidney can be broadly divided into the outer cortical region and the inner medullary region, each which contain different segments of the nephron. In particular, the glomeruli and many of the tubular structures reside in the kidney cortex whereas the remaining tubular structures and collecting ducts occupy reside in the medulla<sup>[1, 3]</sup>, and the glomeruli specifically reside in the outer cortical region of the kidney as opposed to the inner medullary region. By selectively isolating dECM from these regions, it would theoretically be possible to obtain a composition more similar or favorable towards specific kidney cell types of interest, such as GEnCs and podocytes. Others have previously demonstrated the influence of region-specific kidney dECM hydrogels on mouse kidney papilla-derived stem cell growth and metabolism<sup>[278]</sup> and developed kidney cortex dECM hydrogels that promoted maturation of human kidney peritubular microvascular cells<sup>[282]</sup>. However, a thorough characterization of region-specific kidney dECM hydrogels (*i.e.*, cortex versus medulla) with regard to biochemical composition and the resulting ultrastructure as well as rheological properties is still necessary.

Defining the biochemical composition of the ECM, both of native and decellularized tissues and organs, is technically challenging even with mass spectrometry-based proteomics<sup>[411]</sup>. Due to the inherent diversity of analytes present and the specific biochemical properties of these molecules, proteomics analysis of the ECM requires optimized workflows to avoid sample loss or bias and becomes even more difficult when quantification of analytes is desired<sup>[411]</sup>. However, researchers have published proteomics analysis using relative quantification of the ECM from the human glomerular compartment<sup>[412]</sup> as well as human kidney cortex dECM<sup>[282]</sup>. More eloquent methods have also been developed for absolute quantification of specific ECM molecules in native and decellularized rat lung<sup>[413]</sup>. To advance understanding of kidney matrix biology, define the ECM in both healthy and diseased states, and thus better inform the design of engineered microenvironments will require future investigations applying increasingly superior proteomics techniques to the kidney.

Beyond optimizing or altering the natural biochemical composition of kidney dECM hydrogels, additional studies may focus on biophysical properties of the hydrogels as well as evaluation of cell response. The results presented in this dissertation only examined relatively soft kidney dECM hydrogels ( $G \sim 1\text{-}100$  Pa) crosslinked through physical interactions, but stiffer or more robust hydrogels may be necessary to promote the desired cell phenotypes. Biophysical properties of dECM hydrogels such as hydrogel stiffness may be tuned independently of the polymer or protein concentration by employing chemical crosslinking methods<sup>[239]</sup>. Furthermore, our investigations only evaluated response by two cell types: GEnCs and podocytes, both conditionally-immortalized human cell lines. Other kidney cell types, such as tubular epithelial cells or stromal cells, or adult or pluripotent stem cells may exhibit drastically different responses when cultured on kidney dECM hydrogel substrates or encapsulated within kidney dECM hydrogels. Additional bioactive factors may also be included, whether in soluble form as media components or incorporated within the hydrogels, to enhance cell response. For example, VEGF, which has been established as an important growth factor for endothelial cell signaling<sup>[404]</sup> and specifically GEnCs<sup>[316, 377]</sup>, was purposefully omitted from the GEnC culture media in these investigations but may be a critical signaling factor in promoting formation of cell-cell interactions and mature function under these contexts. Application of pharmacologic agents and the effects on cell function may similarly be examined

for the purposes of evaluating samples as engineered kidney tissue models for toxicity or therapeutic screening<sup>[414]</sup>.

### **5.2.2. Poly(Ethylene Glycol)-Crosslinked Hydrogels With Conjugated Peptides to Enhance**

#### ***Bioactivity***

The PEGX method was originally developed as a multimaterial, cell-compatible method for 3D printing of hydrogels for scaffold fabrication as well as 3D bioprinting<sup>[341]</sup>, therefore, a variety of logical future investigations regarding additional conjugation of bioactive peptides to PEG-crosslinked hydrogels may be pursued. Specifically, for the YIGSR- and QK-conjugated PEG-crosslinked gelatin hydrogels presented in this dissertation, “soft” hydrogel formulations with ideal properties for 3D printing were identified. These partially-crosslinked hydrogel inks may be prepared and loaded into an appropriate cartridge and printhead for extrusion-based 3D printing<sup>[341]</sup>. The resulting hydrogel scaffolds may then be treated post-printing with additional PEGX as a secondary crosslinking step to both tailor hydrogel stiffness as well as stabilize scaffolds for cell culture. These 3D-printed hydrogel scaffolds with enhanced bioactivity would enable studies exploring the significance of 3D structure and architecture on endothelial cell behavior. In particular, our previous results suggest that GEnCs may actually prefer culture systems that promote cell aggregation over monolayer culture, and others have demonstrated that specific pore geometries as defined by 3D printing technologies encourage increased cell-cell interactions<sup>[400, 401]</sup>.

Researchers for several years have utilized cell-encapsulating hydrogels such as collagen and fibrin for studying endothelial cell biology and lumen formation<sup>[284]</sup>, and engineers have additionally contributed to these studies by developing superior hydrogel systems for inducing *in vitro* formation of microvasculature by endothelial cells<sup>[415]</sup>. Furthermore, 3D printing and bioprinting technologies naturally lend themselves to the engineering of vascular networks and microvasculature with controlled spatial organization and architectures<sup>[416]</sup>. The PEGX method is also amenable to cell encapsulation for 3D bioprinting of cell-laden constructs<sup>[341]</sup>. Additional investigations may then evaluate endothelial cell response to encapsulation within the YIGSR- and QK-conjugated PEG-crosslinked gelatin hydrogels presented here. Assuming positive results that provide evidence of vascular network formation, 3D

bioprinting of endothelial cell-laden constructs may explore the potential for directing network formation and fabrication of engineered vascularized tissue models. This would also be particularly interesting for a number of coculture studies including those towards modeling the glomerular filtration barrier, which will be discussed further in the proceeding section.

Although the current published PEGX chemistry and that utilized in the investigations presented here is cell compatible, because the succinimidyl valerate ester reacts with free amine groups which are also present on molecules presented by cells, it is not truly bioorthogonal. In addition, because increasing peptide concentrations requires increasing concentrations of PEGX, these formulations may be further detrimental to cell encapsulation. Therefore, future work may explore friendlier chemistries such as thiol-based reactions (*e.g.*, thiol-Michael additions) and bioorthogonal chemistries (*e.g.*, strain-promoted azide-alkyne cycloaddition, inverse-electron demand Diels-Alder reaction)<sup>[245, 246, 417]</sup>. Beyond traditional irreversible covalent interactions, application of dynamic interactions (*e.g.*, host-guest, photoswitches) would additionally enable reversible hydrogel mechanics or biofunctionalization<sup>[237, 238, 418]</sup>. However, whichever interactions employed will likely require additional characterization for optimal reaction kinetics under cell compatible conditions (*i.e.*, 37 °C and pH 7.4). Beyond chemical variants, it is also straightforward to conceptualize employing physical variants as well such as multi-arm PEG. Together, examples of PEGX variants include hetero- or homofunctional linear or multi-arm PEGs of varying lengths or molecular weights<sup>[341]</sup>. Heterofunctional PEGX would be particularly interesting in these applications as different chemistries may be exploited for crosslinking and conjugation reactions, which would enable greater control of hydrogel properties and peptide concentrations independently (**Figure 5-1**). Such versatility in the PEGX method permits experimentation with various polymers and blends, as previously described<sup>[341]</sup>, and combinations of multiple bioactive peptides for engineering hydrogels to better mimic the ECM microenvironment.

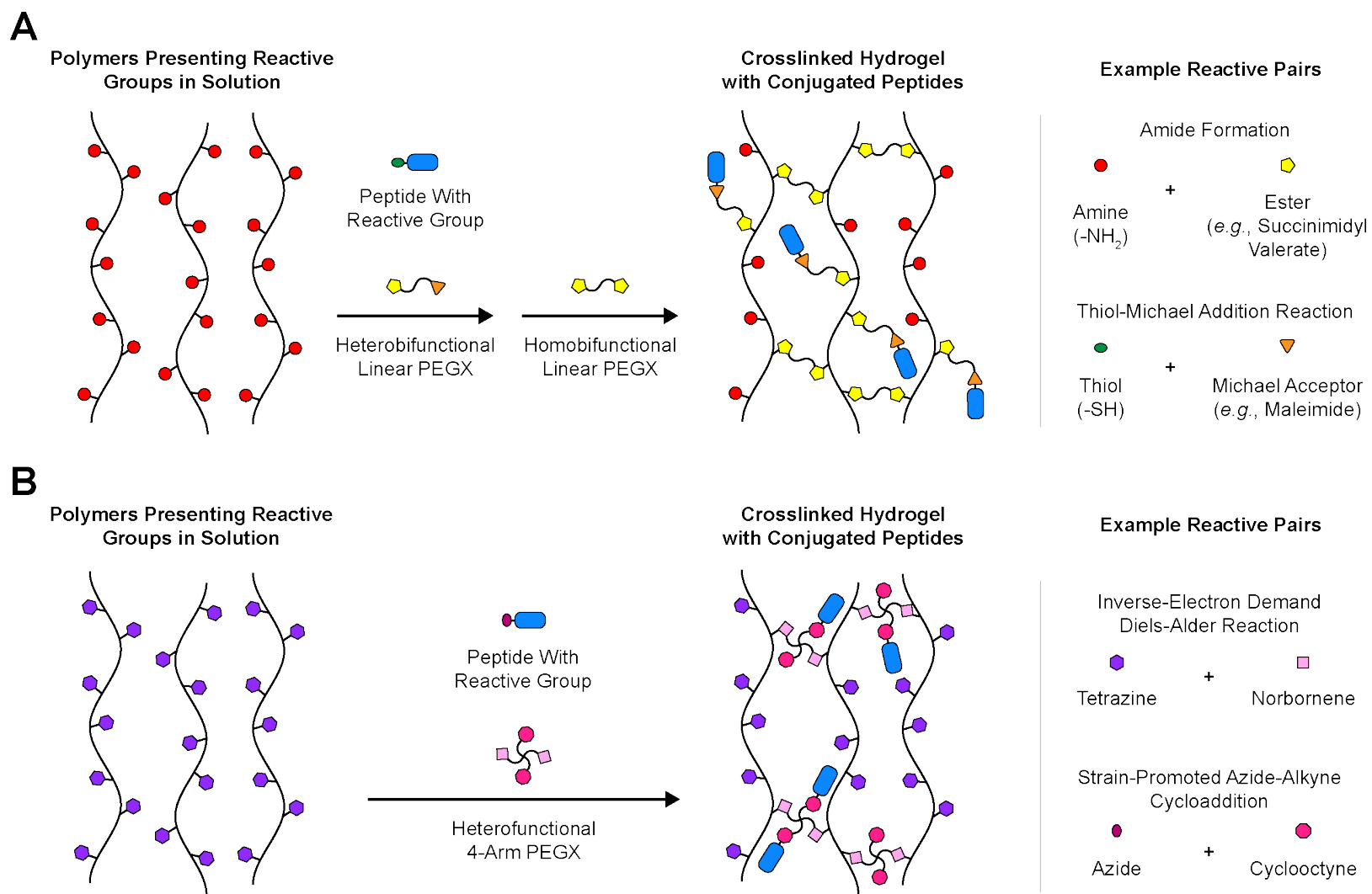


**Figure 5-1: Schematics of heterofunctional PEGX reactions for independent crosslinking of polymers and conjugation of peptides.**

(A) Peptide conjugation to polymers using heterobifunctional linear PEGX followed by polymer crosslinking and hydrogel formation using homobifunctional linear PEGX. Example chemistries include amide formation via amine and ester reactivity and thiol-Michael addition reactions. (B) Peptide conjugation to polymers and polymer crosslinking using heterofunctional 4-arm PEGX. Example chemistries include inverse-electron demand Diels-Alder reactions and strain-promoted azide-alkyne cycloadditions.

### **5.2.3. Hydrogel Platforms to Preserve or Enhance Podocyte Phenotype in In Vitro Culture Towards a Model of the Glomerular Filtration Barrier**

The investigations presented within the scope of this dissertation only provide a cursory understanding of *in vitro* microenvironmental signaling cues that preserve or enhance podocyte phenotype and function. The results discussed and published by others<sup>[274, 407]</sup> necessitate future studies evaluating the combinatorial effects of substrate stiffness and 3D structure or topography on podocyte response. Towards this end, 2D gelatin hydrogel substrates and 3D-printed gelatin hydrogel scaffolds may be prepared with varying hydrogel stiffnesses by adjusting crosslinking times or crosslinker concentrations. In addition, phenotypic or functional characterization of podocytes cultured on 3D-printed scaffolds was not previously performed and is necessary for rigorously evaluating podocyte response beyond adhesion and overall morphology. This is somewhat challenging for podocytes in particular due to their specialized nature in forming a physical barrier or sieve to regulate filtration. Measurements of gene and protein expression are useful for assessing proper transcriptional regulation, secretion of signaling factors, and ECM production<sup>[5, 17, 18]</sup>; however, these methods only provide a surrogate for true assembly of slit diaphragms and barrier function. More technically challenging techniques, often made even more challenging when applied to hydrogel-based cultures, such as electron microscopy are necessary for visualizing foot process interdigitation and normal slit diaphragms<sup>[419-421]</sup> and specialized setups are often required for measuring barrier function<sup>[145, 281, 333, 334, 407, 422]</sup>.

Ultimately, many *in vitro* podocyte investigations such as those measuring barrier function seek to establish a model of the glomerular filtration barrier, which necessitates coculture with endothelial cells such as GEnCs. As alluded to in the previous section, 3D printing and bioprinting is particularly useful for controlled spatial architectures and organization of cell populations, which is especially important for the function of the glomerular filtration barrier. Therefore, future investigations may explore 3D bioprinting of endothelial cell-laden hydrogels promoting formation of microvasculature with subsequent culture of podocytes around the exterior of printed structures (**Figure 5-2A**). This type of model would enable studies focused on the influence of podocytes on glomerular microvasculature formation and stabilization as well

as podocyte and GEnC crosstalk; however, it would not be a simple task to introduce fluid flow into this model unless special microperfusion techniques are applied<sup>[423]</sup>. Fluid flow is, of course, present in the native physiological microenvironment of the glomerulus, and researchers have illustrated that both endothelial cells<sup>[424, 425]</sup> and podocytes<sup>[145, 426]</sup> are sensitive to fluid flow and shear stress *in vitro*. Another possible coculture model may take use of unique coaxial nozzle or core-shell printing technologies for fabrication of directly-perfusable conduits<sup>[427-429]</sup>. One could imagine printing a single conduit into a simple but 3D structure through which endothelial cells would be seeded forming a lumenized vascular channel and subsequent culture of podocytes around the exterior of the printed structure (**Figure 5-2B**). This model would be organized in a manner more similar to the native glomerulus and further allows the introduction of physiologically-relevant fluid flow, although a particular challenge with coaxial nozzle printing is choosing suitable hydrogel biomaterials that are both printable and capable of maintaining this inner lumen structure without compromising the desired bioactive properties. Additional future investigations may integrate mesangial cells in a triculture model of the glomerulus.

Finally, beyond the development of targeted biomaterials and specifically hydrogel platforms, alternative sources for podocytes are currently being pursued. A number of groups have published protocols for directed differentiation of pluripotent stem cells into cells with podocyte-like characteristics<sup>[145, 146, 430, 431]</sup>, but often only a few of the known podocyte-specific markers are tested and cells are typically cultured on rigid, 2D tissue culture polystyrene. Hale *et al.* demonstrated that glomerular structures and podocytes may instead be isolated from differentiated kidney organoids, although current strategies suggest that the podocytes are still immature in nature and similar in stage to podocytes in the developing human fetal kidney<sup>[219]</sup>. Similarly, Yoshimura *et al.* demonstrated selective induction of podocytes in an organoid-like culture with evidence of interdigitating processes and formation of slit diaphragm precursors<sup>[432]</sup>, although to what degree of maturation these podocytes have reached has yet to be determined. Many researchers hypothesize that specific interactions with endothelial cells and introduction of fluid flow are necessary to enhance stem cell-derived podocyte maturation<sup>[223]</sup>. Therefore, through the strategies presented in this dissertation and investigations by others discussed here, we will likely continue

to see advances in engineered hydrogel platforms and integrated systems to promote podocyte and kidney organoid differentiation.

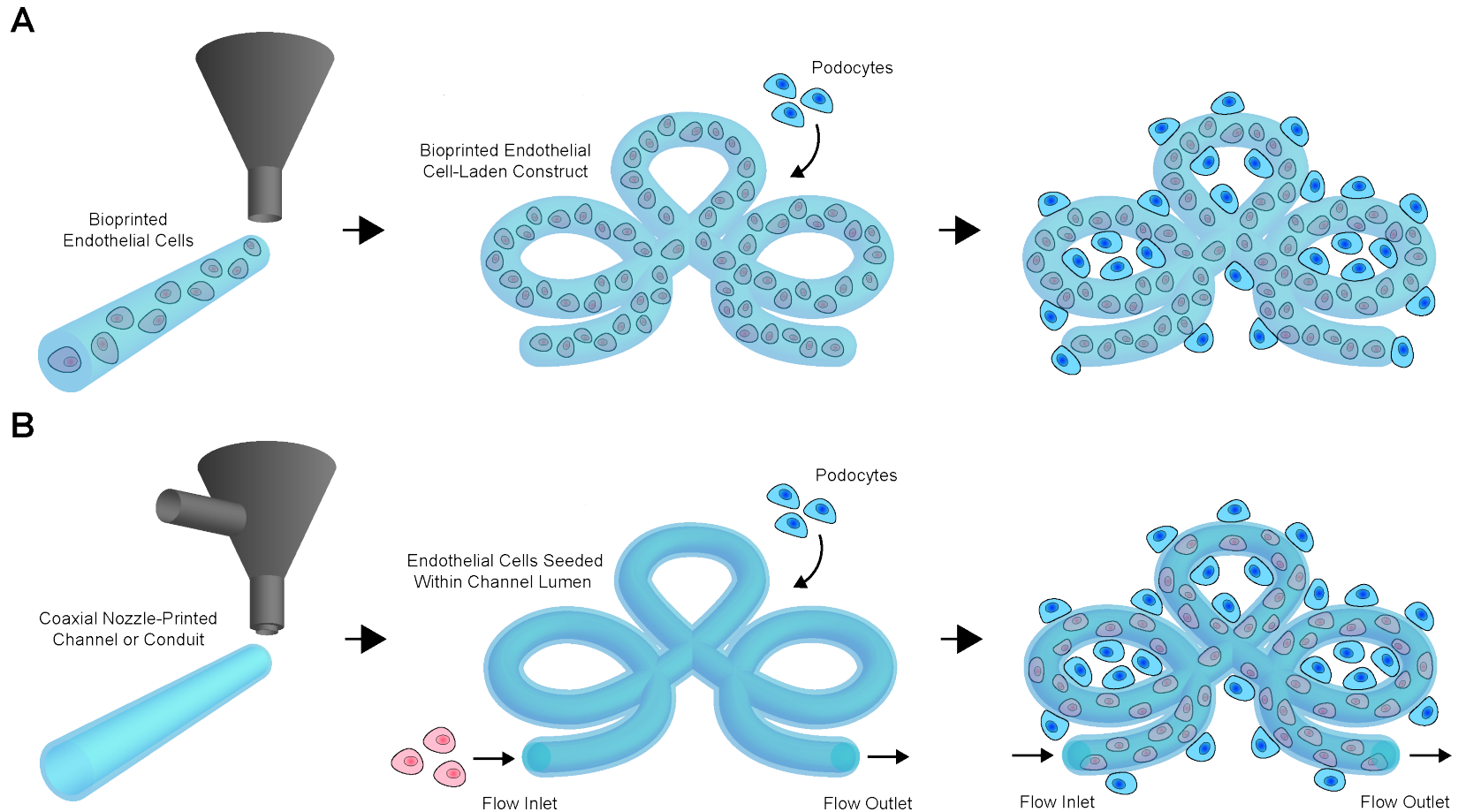


**Figure 5-2: Potential *in vitro* models of the glomerular filtration barrier enabled by 3D printing and bioprinting technologies.**

(A) Endothelial cells are bioprinted within a bioink into a 3D structure with subsequent seeding and culture of podocytes around the exterior of the printed structure. An optimal bioink would promote directed microvascular network formation by endothelial cells in a spatially-controlled manner while maintaining printing fidelity. (B) A perfusable channel or conduit is printed using a coaxial or core-shell nozzle into a 3D structure with a single flow inlet and outlet. Note that in the figure, the channel appears to intersect with itself, but this is not intended and is simply due to limitations of the schematic. Endothelial cells are perfused through and seeded within the lumen of the channel, and podocytes are cultured on the exterior of the printed structure. While more technically challenging to prepare, this model would enable fluid flow and shear stress that is physiologically similar to that of the native glomerulus.

## REFERENCES

- [1] Silverthorn DU. *Human Physiology: An Integrated Approach*. 6th Ed. Pearson Education, Inc (2013).
- [2] Bertram JF, Douglas-Denton RN, Diouf B, Hughson MD, and Hoy WE. "Human nephron number: Implications for health and disease." *Pediatric Nephrology* **26** (2011): 1529.
- [3] Kriz W, and Kaissling B. "Structural Organization of the Mammalian Kidney." *Seldin and Giebisch's The Kidney: Physiology and Pathophysiology*. 5th Ed. Academic Press (2013): 595-691.
- [4] Haraldsson B, Nyström J, and Deen WM. "Properties of the glomerular barrier and mechanisms of proteinuria." *Physiological Reviews* **88** (2008): 451-487.
- [5] Maezawa Y, Cina D, and Quaggin SE. "Glomerular Cell Biology." *Seldin and Giebisch's The Kidney: Physiology & Pathophysiology*. 5th Ed. Academic Press (2013): 721-755.
- [6] Scott RP, and Quaggin SE. "The cell biology of renal filtration." *Journal of Cell Biology* **209** (2015): 199-210.
- [7] Smith HW. *The Kidney: Structure and Function in Health and Disease*. Oxford University Press (1951).
- [8] Oliver J, and MacDowell M. *Nephrons and Kidneys: A Quantitative Study of Developmental and Evolutionary Mammalian Renal Architectonics*. Hoeber Medical Division, Harper & Row (1968).
- [9] Ellis EN, Mauer SM, Sutherland DE, and Steffes MW. "Glomerular capillary morphology in normal humans." *Laboratory Investigation* **60** (1989): 231-236.
- [10] Tisher CC, and Brenner BM. "Structure and Function of the Glomerulus." *Renal Pathology: With Clinical and Functional Correlations*. J. B. Lippincott Co. (1994): 143-161.
- [11] Satchell SC, and Braet F. "Glomerular endothelial cell fenestrations: An integral component of the glomerular filtration barrier." *American Journal of Physiology–Renal Physiology* **296** (2009): F947-F956.
- [12] Fogo AB, and Kon V. "The glomerulus—A view from the inside—The endothelial cell." *The International Journal of Biochemistry & Cell Biology* **42** (2010): 1388-1397.
- [13] Jeansson M, and Haraldsson B. "Morphological and functional evidence for an important role of the endothelial cell glycocalyx in the glomerular barrier." *American Journal of Physiology–Renal Physiology* **290** (2006): F1111-F1116.
- [14] Hjalmarsson C, Johansson BR, and Haraldsson B. "Electron microscopic evaluation of the endothelial surface layer of glomerular capillaries." *Microvascular Research* **67** (2004): 9-17.
- [15] Puelles VG, Douglas-Denton RN, Cullen-McEwen LA, Li J, Hughson MD, Hoy WE, Kerr PG, and Bertram JF. "Podocyte number in children and adults: Associations with glomerular size and

- numbers of other glomerular resident cells." *Journal of the American Society of Nephrology* **26** (2015): 2277-2288.
- [16] Puelles VG, Cullen-McEwen LA, Taylor GE, Li J, Hughson MD, Kerr PG, Hoy WE, and Bertram JF. "Human podocyte depletion in association with older age and hypertension." *American Journal of Physiology–Renal Physiology* **310** (2016): F656-F668.
- [17] Pavenstädt H, Kriz W, and Kretzler M. "Cell biology of the glomerular podocyte." *Physiological Reviews* **83** (2003): 253-307.
- [18] Greka A, and Mundel P. "Cell biology and pathology of podocytes." *Annual Review of Physiology* **74** (2012): 299-323.
- [19] Faul C, Asanuma K, Yanagida-Asanuma E, Kim K, and Mundel P. "Actin up: Regulation of podocyte structure and function by components of the actin cytoskeleton." *Trends in Cell Biology* **17** (2007): 428-437.
- [20] Welsh GI, and Saleem MA. "The podocyte cytoskeleton—Key to a functioning glomerulus in health and disease." *Nature Reviews Nephrology* **8** (2012): 14.
- [21] Wartiovaara J, Öfverstedt L-G, Khoshnoodi J, Zhang J, Mäkelä E, Sandin S, Ruotsalainen V, Cheng RH, Jalanko H, Skoglund U, and Tryggvason K. "Nephrin strands contribute to a porous slit diaphragm scaffold as revealed by electron tomography." *Journal of Clinical Investigation* **114** (2004): 1475-1483.
- [22] Grahammer F, Schell C, and Huber TB. "The podocyte slit diaphragm—From a thin grey line to a complex signalling hub." *Nature Reviews Nephrology* **9** (2013): 587.
- [23] Nielsen JS, and McNagny KM. "The role of podocalyxin in health and disease." *Journal of the American Society of Nephrology* **20** (2009): 1669-1676.
- [24] Wiggins RC. "The spectrum of podocytopathies: A unifying view of glomerular diseases." *Kidney International* **71** (2007): 1205-1214.
- [25] Kriz W, Shirato I, Nagata M, LeHir M, and Lemley KV. "The podocyte's response to stress: The enigma of foot process effacement." *American Journal of Physiology–Renal Physiology* **304** (2013): F333-F347.
- [26] Shankland SJ. "The podocyte's response to injury: Role in proteinuria and glomerulosclerosis." *Kidney International* **69** (2006): 2131-2147.
- [27] Østerby R. "Morphometric studies of the peripheral glomerular basement membrane in early juvenile diabetes I. Development of initial basement membrane thickening." *Diabetologia* **8** (1972): 84-92.
- [28] Steffes MW, Barbosa J, Basgen JM, Sutherland DE, Najarian JS, and Mauer SM. "Quantitative glomerular morphology of the normal human kidney." *Laboratory Investigation* **49** (1983): 82-86.
- [29] Suleiman H, Zhang L, Roth R, Heuser JE, Miner JH, Shaw AS, and Dani A. "Nanoscale protein architecture of the kidney glomerular basement membrane." *eLife* **2** (2013): e01149.
- [30] Simionescu M. "Ultrastructure of the microvascular wall: Functional correlations." *Handbook of Physiology* **6** (1984): 41-101.

- [31] Yurchenco PD. "Basement membranes: Cell scaffoldings and signaling platforms." *Cold Spring Harbor Perspectives in Biology* **3** (2011): a004911.
- [32] Abrahamson DR. "Glomerulogenesis in the developing kidney." *Seminars in Nephrology* **11** (1991): 375-389.
- [33] Miner JH. "Organogenesis of the kidney glomerulus: Focus on the glomerular basement membrane." *Organogenesis* **7** (2011): 75-82.
- [34] Miner JH. "Glomerular basement membrane composition and the filtration barrier." *Pediatric Nephrology* **26** (2011): 1413-1417.
- [35] Miner JH. "The glomerular basement membrane." *Experimental Cell Research* **318** (2012): 973-978.
- [36] Cruz-Acuña R, and García AJ. "Synthetic hydrogels mimicking basement membrane matrices to promote cell-matrix interactions." *Matrix Biology* **57** (2017): 324-333.
- [37] Fox JW, Mayer U, Nischt R, Aumailley M, Reinhardt D, Wiedemann H, Mann K, Timpl R, Krieg T, Engel J, and Chu M-L. "Recombinant nidogen consists of three globular domains and mediates binding of laminin to collagen type IV." *The EMBO Journal* **10** (1991): 3137-3146.
- [38] Rennke HG, Cotran RS, and Venkatachalam MA. "Role of molecular charge in glomerular permeability. Tracer studies with cationized ferritins." *Journal of Cell Biology* **67** (1975): 638-646.
- [39] Bohrer MP, Baylis C, Humes HD, Glassock RJ, Robertson CR, and Brenner BM. "Permeability of the glomerular capillary wall: Facilitated filtration of circulating polycations." *Journal of Clinical Investigation* **61** (1978): 72-78.
- [40] Iozzo RV, Zoeller JJ, and Nyström A. "Basement membrane proteoglycans: Modulators *Par Excellence* of cancer growth and angiogenesis." *Molecules and Cells* **27** (2009): 503-513.
- [41] Schlöndorff D, and Banas B. "The mesangial cell revisited: No cell is an island." *Journal of the American Society of Nephrology* **20** (2009): 1179-1187.
- [42] Vaughan MR, and Quaggin SE. "How do mesangial and endothelial cells form the glomerular tuft?" *Journal of the American Society of Nephrology* **19** (2008): 24-33.
- [43] Sakai F, and Kriz W. "The structural relationship between mesangial cells and basement membrane of the renal glomerulus." *Anatomy and Embryology* **176** (1987): 373-386.
- [44] Kriz W, Elger M, Lemley K, and Sakai T. "Structure of the glomerular mesangium: A biomechanical interpretation." *Kidney International Supplement* (1990):
- [45] Kriz W, Elger M, Mundel P, and Lemley KV. "Structure-stabilizing forces in the glomerular tuft." *Journal of the American Society of Nephrology* **5** (1995): 1731-1739.
- [46] Schlöndorff D. "The glomerular mesangial cell: An expanding role for a specialized pericyte." *The FASEB Journal* **1** (1987): 272-281.
- [47] Stockand JD, and Sansom SC. "Glomerular mesangial cells: Electrophysiology and regulation of contraction." *Physiological Reviews* **78** (1998): 723-744.

- [48] Quaggin SE, and Kreidberg JA. "Development of the renal glomerulus: Good neighbors and good fences." *Development* **135** (2008): 609-620.
- [49] Lennon R, and Hosawi S. "Glomerular cell crosstalk." *Current Opinion in Nephrology and Hypertension* **25** (2016): 187.
- [50] Little MH, and McMahon AP. "Mammalian kidney development: Principles, progress, and projections." *Cold Spring Harbor Perspectives in Biology* **4** (2012): a008300.
- [51] Shankland SJ, Smeets B, Pippin JW, and Moeller MJ. "The emergence of the glomerular parietal epithelial cell." *Nature Reviews Nephrology* **10** (2014): 158.
- [52] Ohse T, Pippin JW, Chang AM, Krofft RD, Miner JH, Vaughan MR, and Shankland SJ. "The enigmatic parietal epithelial cell is finally getting noticed: A review." *Kidney International* **76** (2009): 1225-1238.
- [53] Khanna R. "Clinical presentation & management of glomerular diseases: Hematuria, nephritic & nephrotic syndrome." *Missouri Medicine* **108** (2011): 33.
- [54] Kriz W, and Lehir M. "Pathways to nephron loss starting from glomerular diseases—Insights from animal models." *Kidney International* **67** (2005): 404-419.
- [55] Churg J, and Grishman E. "Ultrastructure of glomerular disease: A review." *Kidney International* **7** (1975): 254-270.
- [56] Chiang C-K, and Inagi R. "Glomerular diseases: Genetic causes and future therapeutics." *Nature Reviews Nephrology* **6** (2010): 539.
- [57] United States Renal Data System. "2018 USRDS Annual Data Report: Epidemiology of Kidney Disease in the United States." *National Institutes of Health, National Institute of Diabetes and Digestive and Kidney Diseases*. Bethesda, MD (2018).
- [58] Fleming GM. "Renal replacement therapy review: Past, present and future." *Organogenesis* **7** (2011): 2-12.
- [59] "The National Institute of Diabetes and Digestive and Kidney Diseases Health Information Center." National Institutes of Health, National Institute of Diabetes and Digestive and Kidney Diseases. Web Page.
- [60] Tandukar S, and Palevsky PM. "Continuous renal replacement therapy—Who, when, why and how." *Chest* **155** (2019): 626-638.
- [61] Jain AK, Blake P, Cordy P, and Garg AX. "Global trends in rates of peritoneal dialysis." *Journal of the American Society of Nephrology* **23** (2012): 533-544.
- [62] Prowle JR, and Bellomo R. "Continuous renal replacement therapy: Recent advances and future research." *Nature Reviews Nephrology* **6** (2010): 521.
- [63] Pontoriero G, Pozzoni P, Andrulli S, and Locatelli F. "The quality of dialysis water." *Nephrology Dialysis Transplantation* **18** (2003): vii21-vii25.

- [64] Boure T, and Vanholder R. "Which dialyser membrane to choose?" *Nephrology Dialysis Transplantation* **19** (2004): 293-296.
- [65] Dew MA, Switzer GE, Goycoolea JM, Allen AS, A D, Kormos RL, and Griffith BP. "Does transplantation produce quality of life benefits? A quantitative analysis of the literature." *Transplantation* **64** (1997): 1261-1273.
- [66] Wolfe RA, Ashby VB, Milford EL, Ojo AO, Ettenger RE, Agodoa LY, Held PJ, and Port FK. "Comparison of mortality in all patients on dialysis, patients on dialysis awaiting transplantation, and recipients of a first cadaveric transplant." *The New England Journal of Medicine* **341** (1999): 1725-1730.
- [67] Tonelli M, Wiebe N, Knoll G, Bello A, Browne S, Jadhav D, Klarenbach S, and Gill J. "Systematic review: Kidney transplantation compared with dialysis in clinically relevant outcomes." *American Journal of Transplantation* **11** (2011): 2093-2109.
- [68] "Organ Procurement and Transplantation Network (OPTN)." United Network for Organ Sharing. Online Database.
- [69] Kasiske BL, Cohen D, Lucey MR, and Neylan JF. "Payment for immunosuppression after organ transplantation." *JAMA: The Journal of the American Medical Association* **283** (2000): 2445-2450.
- [70] Halloran PF. "Immunosuppressive drugs for kidney transplantation." *The New England Journal of Medicine* **351** (2004): 2715-2729.
- [71] Berthiaume F, Maguire TJ, and Yarmush ML. "Tissue engineering and regenerative medicine: History, progress, and challenges." *Annual Review of Chemical and Biomolecular Engineering* **2** (2011): 403-430.
- [72] Oxburgh L, Carroll TJ, Cleaver O, Gossett DR, Hoshizaki DK, Hubbell JA, Humphreys BD, Jain S, Jensen J, Kaplan DL, Kesselman C, Ketchum CJ, Little MH, McMahon AP, Shankland SJ, Spence JR, Valerius MT, Wertheim JA, Wessely O, Zheng Y, and Drummond IA. "(Re)building a kidney." *Journal of the American Society of Nephrology* **28** (2017): 1370-1378.
- [73] Cieslinski DA, and Humes HD. "Tissue engineering of a bioartificial kidney." *Biotechnology and Bioengineering* **43** (1994): 678-681.
- [74] Song JH, and Humes HD. "The bioartificial kidney in the treatment of acute kidney injury." *Current Drug Targets* **10** (2009): 1227.
- [75] Humes HD, Buffington D, Westover AJ, Roy S, and Fissell WH. "The bioartificial kidney: Current status and future promise." *Pediatric Nephrology* **29** (2014): 343-351.
- [76] Kim S, Fissell IV WH, Humes HD, and Roy S. "Current strategies and challenges in engineering a bioartificial kidney." *Frontiers in Bioscience: Elite Edition* **7** (2015): 215.
- [77] MacKay SM, Funke AJ, Buffington DA, and Humes HD. "Tissue engineering of a bioartificial renal tubule." *ASAIO Journal* **44** (1998): 179-183.
- [78] Nikolovski J, Gulari E, and Humes HD. "Design engineering of a bioartificial renal tubule cell therapy device." *Cell Transplantation* **8** (1999): 351-364.

- [79] Humes HD, Mackay SM, Funke AJ, and Buffington DA. "Tissue engineering of a bioartificial renal tubule assist device: In vitro transport and metabolic characteristics." *Kidney International* **55** (1999): 2502-2514.
- [80] Humes HD, Buffington DA, MacKay SM, Funke AJ, and Weitzel WF. "Replacement of renal function in uremic animals with a tissue-engineered kidney." *Nature Biotechnology* **17** (1999): 451-455.
- [81] Humes HD, Fissell WH, Weitzel WF, Buffington DA, Westover AJ, MacKay SM, and Gutierrez JM. "Metabolic replacement of kidney function in uremic animals with a bioartificial kidney containing human cells." *American Journal of Kidney Diseases* **39** (2002): 1078-1087.
- [82] Fissell WH, Dyke DB, Weitzel WF, Buffington DA, Westover AJ, MacKay SM, Gutierrez JM, and Humes HD. "Bioartificial kidney alters cytokine response and hemodynamics in endotoxin-challenged uremic animals." *Blood Purification* **20** (2002): 55-60.
- [83] Fissell WH, Lou L, Abrishami S, Buffington DA, and Humes HD. "Bioartificial kidney ameliorates gram-negative bacteria-induced septic shock in uremic animals." *Journal of the American Society of Nephrology* **14** (2003): 454-461.
- [84] Humes HD, Buffington DA, Lou L, Abrishami S, Wang M, Xia J, and Fissell WH. "Cell therapy with a tissue-engineered kidney reduces the multiple-organ consequences of septic shock." *Critical Care Medicine* **31** (2003): 2421-2428.
- [85] Humes HD, Weitzel WF, Bartlett RH, Swaniker FC, Paganini EP, Luderer JR, and Sobota J. "Initial clinical results of the bioartificial kidney containing human cells in ICU patients with acute renal failure." *Kidney International* **66** (2004): 1578-1588.
- [86] Tumlin J, Wali R, Williams W, Murray P, Tolwani AJ, Vinnikova AK, Szerlip HM, Ye J, Paganini EP, Dworkin L, Finkel KW, Kraus MA, and Humes HD. "Efficacy and safety of renal tubule cell therapy for acute renal failure." *Journal of the American Society of Nephrology* **19** (2008): 1034-1040.
- [87] Humes HD, Sobota JT, Ding F, and Song JH. "A selective cytopheretic inhibitory device to treat the immunological dysregulation of acute and chronic renal failure." *Blood Purification* **29** (2010): 183-190.
- [88] Pino CJ, Yevzlin AS, Tumlin J, and Humes HD. "Cell-based strategies for the treatment of kidney dysfunction: A review." *Blood Purification* **34** (2012): 117-123.
- [89] Pino CJ, Westover AJ, Johnston KA, Buffington DA, and Humes HD. "Regenerative medicine and immunomodulatory therapy: Insights from the kidney, heart, brain, and lung." *Kidney International Reports* **3** (2018): 771-783.
- [90] Ding F, Song JH, Jung JY, Lou L, Wang M, Charles L, Westover A, Smith PL, Pino CJ, Buffington DA, and Humes HD. "A biomimetic membrane device that modulates the excessive inflammatory response to sepsis." *PLOS ONE* **6** (2011): e18584.
- [91] Pino CJ, Lou L, Smith PL, Ding F, Pagani FD, Buffington DA, and Humes HD. "A selective cytopheretic inhibitory device for use during cardiopulmonary bypass surgery." *Perfusion* **27** (2012): 311-319.
- [92] Pino CJ, Farokhrani A, Lou L, Smith PL, Johnston K, Buffington DA, and Humes HD. "Selective cytopheretic inhibitory device with regional citrate anticoagulation and portable sorbent dialysis." *Artificial Organs* **37** (2013): 203-210.

- [93] Westover AJ, Johnston KA, Buffington DA, and Humes HD. "An immunomodulatory device improves insulin resistance in obese porcine model of metabolic syndrome." *Journal of Diabetes Research* **2016** (2016):
- [94] Ding F, Yevzlin AS, Xu ZY, Zhou Y, Xie QH, Liu JF, Zheng Y, DaSilva JR, and Humes HD. "The effects of a novel therapeutic device on acute kidney injury outcomes in the intensive care unit: A pilot study." *ASAIO Journal* **57** (2011): 426-432.
- [95] Tumlin JA, Chawla L, Tolwani AJ, Mehta R, Dillon J, Finkel KW, DaSilva JR, Astor BC, Yevzlin AS, and Humes HD. "The effect of the selective cytopheretic device on acute kidney injury outcomes in the intensive care unit: A multicenter pilot study." *Seminars in Dialysis* **26** (2013): 616-623.
- [96] Tumlin JA, Galphin CM, Tolwani AJ, Chan MR, Vijayan A, Finkel K, Szamosfalvi B, Dev D, DaSilva JR, Astor BC, Yevzlin A, and Humes HD. "A multi-center, randomized, controlled, pivotal study to assess the safety and efficacy of a selective cytopheretic device in patients with acute kidney injury." *PLOS ONE* **10** (2015): e0132482.
- [97] Szamosfalvi B, Westover A, Buffington D, Yevzlin A, and Humes HD. "Immunomodulatory device promotes a shift of circulating monocytes to a less inflammatory phenotype in chronic hemodialysis patients." *ASAIO Journal* **62** (2016): 623-630.
- [98] Selewski DT, Goldstein SL, Fraser E, Plomaritas K, Mottes T, Terrell T, and Humes HD. "Immunomodulatory device therapy in a pediatric patient with acute kidney injury and multiorgan dysfunction." *Kidney International Reports* **2** (2017): 1259-1264.
- [99] Westover AJ, Buffington DA, and Humes HD. "Enhanced propagation of adult human renal epithelial progenitor cells to improve cell sourcing for tissue-engineered therapeutic devices for renal diseases." *Journal of Tissue Engineering and Regenerative Medicine* **6** (2012): 589-597.
- [100] Buffington DA, Pino CJ, Chen L, Westover AJ, Hageman G, and Humes HD. "Bioartificial renal epithelial cell system (BRECS): A compact, cryopreservable extracorporeal renal replacement device." *Cell Medicine* **4** (2012): 33-43.
- [101] Westover AJ, Buffington DA, Johnston KA, Smith PL, Pino CJ, and Humes HD. "A bio-artificial renal epithelial cell system conveys survival advantage in a porcine model of septic shock." *Journal of Tissue Engineering and Regenerative Medicine* **11** (2017): 649-657.
- [102] Johnston KA, Westover AJ, Rojas-Pena A, Buffington DA, Pino CJ, Smith PL, and Humes HD. "Development of a wearable bioartificial kidney using the Bioartificial Renal Epithelial Cell System (BRECS)." *Journal of Tissue Engineering and Regenerative Medicine* **11** (2017): 3048-3055.
- [103] Pino CJ, Westover AJ, Buffington DA, and Humes HD. "Bioengineered renal cell therapy device for clinical translation." *ASAIO Journal* **63** (2017): 305.
- [104] Ueda H, Watanabe J, Konno T, Takai M, Saito A, and Ishihara K. "Asymmetrically functional surface properties on biocompatible phospholipid polymer membrane for bioartificial kidney." *Journal of Biomedical Materials Research Part A* **77** (2006): 19-27.
- [105] Dankers PYW, Boomker JM, der Vlag AHv, Smedts FMM, Harmsen MC, and van Luyn MJA. "The use of fibrous, supramolecular membranes and human tubular cells for renal epithelial tissue engineering: Towards a suitable membrane for a bioartificial kidney." *Macromolecular Bioscience* **10** (2010): 1345-1354.

- [106] Mollet BB, Bogaerts ILJ, van Almen GC, and Dankers PYW. "A bioartificial environment for kidney epithelial cells based on a supramolecular polymer basement membrane mimic and an organotypical culture system." *Journal of Tissue Engineering and Regenerative Medicine* **11** (2017): 1820-1834.
- [107] Ni M, Teo JCM, bin Ibrahim MS, Zhang K, Tasnim F, Chow P-Y, Zink D, and Ying JY. "Characterization of membrane materials and membrane coatings for bioreactor units of bioartificial kidneys." *Biomaterials* **32** (2011): 1465-1476.
- [108] Zhang H, Tasnim F, Ying JY, and Zink D. "The impact of extracellular matrix coatings on the performance of human renal cells applied in bioartificial kidneys." *Biomaterials* **30** (2009): 2899-2911.
- [109] Oo ZY, Deng R, Hu M, Ni M, Kandasamy K, bin Ibrahim MS, Ying JY, and Zink D. "The performance of primary human renal cells in hollow fiber bioreactors for bioartificial kidneys." *Biomaterials* **32** (2011): 8806-8815.
- [110] Schophuizen CMS, De Napoli IE, Jansen J, Teixeira S, Wilmer MJ, Hoenderop JGJ, Van den Heuvel LPW, Masereeuw R, and Stamatialis D. "Development of a living membrane comprising a functional human renal proximal tubule cell monolayer on polyethersulfone polymeric membrane." *Acta Biomaterialia* **14** (2015): 22-32.
- [111] Fissell WH, Fleischman AJ, Humes HD, and Roy S. "Development of continuous implantable renal replacement: Past and future." *Translational Research* **150** (2007): 327-336.
- [112] Fissell WH, Roy S, and Davenport A. "Achieving more frequent and longer dialysis for the majority: Wearable dialysis and implantable artificial kidney devices." *Kidney International* **84** (2013): 256-264.
- [113] Salani M, Roy S, and Fissell IV WH. "Innovations in wearable and implantable artificial kidneys." *American Journal of Kidney Diseases* **72** (2018): 745-751.
- [114] Fissell WH, Dubnisheva A, Eldridge AN, Fleischman AJ, Zydney AL, and Roy S. "High-performance silicon nanopore hemofiltration membranes." *Journal of Membrane Science* **326** (2009): 58-63.
- [115] Melvin ME, Fissell WH, Roy S, and Brown DL. "Silicon induces minimal thromboinflammatory response during 28-day intravascular implant testing." *ASAIO Journal* **56** (2010): 344.
- [116] Li L, Marchant RE, Dubnisheva A, Roy S, and Fissell IV WH. "Anti-biofouling sulfobetaine polymer thin films on silicon and silicon nanopore membranes." *Journal of Biomaterials Science, Polymer Edition* **22** (2011): 91-106.
- [117] Muthusubramaniam L, Lowe R, Fissell WH, Li L, Marchant RE, Desai TA, and Roy S. "Hemocompatibility of silicon-based substrates for biomedical implant applications." *Annals of Biomedical Engineering* **39** (2011): 1296-1305.
- [118] Kensinger C, Karp S, Kant R, Chui BW, Goldman K, Yeager T, Gould ER, Buck A, Laneve DC, Groszek JJ, Roy S, and Fissell IV WH. "First implantation of silicon nanopore membrane hemofilters." *ASAIO Journal* **62** (2016): 491.

- [119] Iqbal Z, Moses W, Kim S, Kim EJ, Fissell WH, and Roy S. "Sterilization effects on ultrathin film polymer coatings for silicon-based implantable medical devices." *Journal of Biomedical Materials Research Part B: Applied Biomaterials* **106** (2018): 2327-2336.
- [120] Iqbal Z, Kim S, Moyer J, Moses W, Abada E, Wright N, Kim EJ, Park J, Fissell WH, Vartanian S, and Roy S. "In vitro and in vivo hemocompatibility assessment of ultrathin sulfobetaine polymer coatings for silicon-based implants." *Journal of Biomaterials Applications* (2019): 0885328219831044.
- [121] Kanani DM, Fissell WH, Roy S, Dubnisheva A, Fleischman A, and Zydney AL. "Permeability-selectivity analysis for ultrafiltration: Effect of pore geometry." *Journal of Membrane Science* **349** (2010): 405-410.
- [122] Feinberg BJ, Hsiao JC, Park J, Zydney AL, Fissell WH, and Roy S. "Silicon nanoporous membranes as a rigorous platform for validation of biomolecular transport models." *Journal of Membrane Science* **536** (2017): 44-51.
- [123] Feinberg BJ, Hsiao JC, Park J, Zydney AL, Fissell WH, and Roy S. "Slit pores preferred over cylindrical pores for high selectivity in biomolecular filtration." *Journal of Colloid and Interface Science* **517** (2018): 176-181.
- [124] Kim S, Feinberg B, Kant R, Chui B, Goldman K, Park J, Moses W, Blaha C, Iqbal Z, Chow C, Wright N, Fissell IV WH, Zydney AL, and Roy S. "Diffusive silicon nanopore membranes for hemodialysis applications." *PLOS ONE* **11** (2016): e0159526.
- [125] Kim S, Heller J, Iqbal Z, Kant R, Kim EJ, Durack J, Saeed M, Do L, Hetts S, Wilson M, Brakeman P, Fissell IV WH, and Roy S. "Preliminary diffusive clearance of silicon nanopore membranes in a parallel plate configuration for renal replacement therapy." *ASAIO Journal* **62** (2016): 169.
- [126] Fissell WH, Manley S, Westover A, Humes HD, Fleischman AJ, and Roy S. "Differentiated growth of human renal tubule cells on thin-film and nanostructured materials." *ASAIO Journal* **52** (2006): 221-227.
- [127] Ferrell N, Desai RR, Fleischman AJ, Roy S, Humes HD, and Fissell IV WH. "A microfluidic bioreactor with integrated transepithelial electrical resistance (TEER) measurement electrodes for evaluation of renal epithelial cells." *Biotechnology and Bioengineering* **107** (2010): 707-716.
- [128] Ferrell N, Ricci KB, Groszek J, Marmorstein JT, and Fissell WH. "Albumin handling by renal tubular epithelial cells in a microfluidic bioreactor." *Biotechnology and Bioengineering* **109** (2012): 797-803.
- [129] Brakeman P, Miao S, Cheng J, Lee C-Z, Roy S, Fissell IV WH, and Ferrell N. "A modular microfluidic bioreactor with improved throughput for evaluation of polarized renal epithelial cells." *Biomicrofluidics* **10** (2016): 064106.
- [130] Judy JW. "Microelectromechanical systems (MEMS): Fabrication, design and applications." *Smart Materials and Structures* **10** (2001): 1115.
- [131] Grayson ACR, Shawgo RS, Johnson AM, Flynn NT, Li Y, Cima MJ, and Langer R. "A BioMEMS review: MEMS technology for physiologically integrated devices." *Proceedings of the IEEE* **92** (2004): 6-21.
- [132] Bashir R. "BioMEMS: State-of-the-art in detection, opportunities and prospects." *Advanced Drug Delivery Reviews* **56** (2004): 1565-1586.

- [133] Verpoorte E, and De Rooij NF. "Microfluidics meets MEMS." *Proceedings of the IEEE* **91** (2003): 930-953.
- [134] Reyes DR, Iossifidis D, Auroux P-A, and Manz A. "Micro total analysis systems. 1. Introduction, theory, and technology." *Analytical Chemistry* **74** (2002): 2623-2636.
- [135] Stone HA, Stroock AD, and Ajdari A. "Engineering flows in small devices: Microfluidics toward a lab-on-a-chip." *Annual Review of Fluid Mechanics* **36** (2004): 381-411.
- [136] Bhatia SN, and Ingber DE. "Microfluidic organs-on-chips." *Nature Biotechnology* **32** (2014): 760.
- [137] Wikswo JP. "The relevance and potential roles of microphysiological systems in biology and medicine." *Experimental Biology and Medicine* **239** (2014): 1061-1072.
- [138] Weinberg E, Kaazempur-Mofrad M, and Borenstein J. "Concept and computational design for a bioartificial nephron-on-a-chip." *The International Journal of Artificial Organs* **31** (2008): 508-514.
- [139] Nissenson AR, Ronco C, Pergamit G, Edelstein M, and Watts R. "The human nephron filter: Toward a continuously functioning, implantable artificial nephron system." *Blood Purification* **23** (2005): 269-274.
- [140] Lee S-J, and Choi B-K. "The artificial glomerulus design using diffusion in microchannels." *International Journal of Precision Engineering and Manufacturing* **13** (2012): 307-310.
- [141] Kim S, and Takayama S. "Organ-on-a-chip and the kidney." *Kidney Research and Clinical Practice* **34** (2015): 165-169.
- [142] Wilmer MJ, Ng CP, Lanz HL, Vulto P, Suter-Dick L, and Masereeuw R. "Kidney-on-a-chip technology for drug-induced nephrotoxicity screening." *Trends in Biotechnology* **34** (2016): 156-170.
- [143] Ashammakhi N, Wesseling-Perry K, Hasan A, Elkhammas E, and Zhang YS. "Kidney-on-a-chip: Untapped opportunities." *Kidney International* (2018):
- [144] Yeung CK, and Himmelfarb J. "Kidneys on chips: Emerging technology for preclinical drug development." *Clinical Journal of the American Society of Nephrology* **14** (2019): 144-146.
- [145] Musah S, Mammoto A, Ferrante TC, Jeanty SS, Hirano-Kobayashi M, Mammoto T, Roberts K, Chung S, Novak R, Ingram M, Fatanat-Didar T, Koshy S, Weaver JC, Church GM, and Ingber DE. "Mature induced-pluripotent-stem-cell-derived human podocytes reconstitute kidney glomerular-capillary-wall function on a chip." *Nature Biomedical Engineering* **1** (2017): 0069.
- [146] Musah S, Dimitrakakis N, Camacho DM, Church GM, and Ingber DE. "Directed differentiation of human induced pluripotent stem cells into mature kidney podocytes and establishment of a Glomerulus Chip." *Nature Protocols* **13** (2018): 1662-1685.
- [147] Jang K-J, Mehr AP, Hamilton GA, McPartlin LA, Chung S, Suh K-Y, and Ingber DE. "Human kidney proximal tubule-on-a-chip for drug transport and nephrotoxicity assessment." *Integrative Biology* **5** (2013): 1119-1129.

- [148] Sciancalepore AG, Sallustio F, Girardo S, Passione LG, Camposeo A, Mele E, Di Lorenzo M, Costantino V, Schena FP, and Pisignano D. "A bioartificial renal tubule device embedding human renal stem/progenitor cells." *PLOS ONE* **9** (2014): e87496.
- [149] Weber EJ, Chapron A, Chapron BD, Voellinger JL, Lidberg KA, Yeung CK, Wang Z, Yamaura Y, Hailey DW, Neumann T, Shen DD, Thummel KE, Muczynski KA, Himmelfarb J, and Kelly EJ. "Development of a microphysiological model of human kidney proximal tubule function." *Kidney International* **90** (2016): 627-637.
- [150] Sakolish C, Weber EJ, Kelly EJ, Himmelfarb J, Mouneimne R, Grimm FA, House JS, Wade T, Han A, Chiu WA, and Rusyn I. "Technology transfer of the microphysiological systems: A case study of the human proximal tubule tissue chip." *Scientific Reports* **8** (2018): 14882.
- [151] Maass C, Sorensen NB, Himmelfarb J, Kelly EJ, Stokes CL, and Cirit M. "Translational assessment of drug-induced proximal tubule injury using a kidney microphysiological system." *CPT: Pharmacometrics & Systems Pharmacology* (2019):
- [152] Nieskens TTG, and Wilmer MJ. "Kidney-on-a-chip technology for renal proximal tubule tissue reconstruction." *European Journal of Pharmacology* **790** (2016): 46-56.
- [153] Mu X, Zheng W, Xiao L, Zhang W, and Jiang X. "Engineering a 3D vascular network in hydrogel for mimicking a nephron." *Lab on a Chip* **13** (2013): 1612-1618.
- [154] Ligresti G, Nagao RJ, Xue J, Choi YJ, Xu J, Ren S, Aburatani T, Anderson SK, MacDonald JW, Bammler TK, Schwartz SM, Muczynski K, Duffield JS, Himmelfarb J, and Zheng Y. "A novel three-dimensional human peritubular microvascular system." *Journal of the American Society of Nephrology* **27** (2016): 2370-2381.
- [155] Sakolish CM, and Mahler GJ. "A novel microfluidic device to model the human proximal tubule and glomerulus." *RSC Advances* **7** (2017): 4216-4225.
- [156] Rayner SG, Phong KT, Xue J, Lih D, Shankland SJ, Kelly EJ, Himmelfarb J, and Zheng Y. "Reconstructing the human renal vascular-tubular unit in vitro." *Advanced Healthcare Materials* **7** (2018): 1801120.
- [157] Maschmeyer I, Lorenz AK, Schimek K, Hasenberg T, Ramme AP, Hübner J, Lindner M, Drewell C, Bauer S, Thomas A, Sambo NS, Sonntag F, Lauster R, and Marx U. "A four-organ-chip for interconnected long-term co-culture of human intestine, liver, skin and kidney equivalents." *Lab on a Chip* **15** (2015): 2688-2699.
- [158] Chang S-Y, Weber EJ, Sidorenko VS, Chapron A, Yeung CK, Gao C, Mao Q, Shen D, Wang J, Rosenquist TA, Dickman KG, Neumann T, Grollman AP, Kelly EJ, Himmelfarb J, and Eaton DL. "Human liver-kidney model elucidates the mechanisms of aristolochic acid nephrotoxicity." *JCI Insight* **2** (2017):
- [159] Verneti L, Gough A, Baetz N, Blutt S, Broughman JR, Brown JA, Foulke-Abel J, Hasan N, In J, Kelly E, Kovbasnjuk O, Repper J, Senutovitch N, Stabb J, Yeung CK, Zachos NC, Donowitz M, Estes M, Himmelfarb J, Truskey G, Wikswo JP, and Taylor DL. "Functional coupling of human microphysiology systems: Intestine, liver, kidney proximal tubule, blood-brain barrier and skeletal muscle." *Scientific Reports* **7** (2017): 42296.
- [160] Vaezi M, Seitz H, and Yang S. "A review on 3D micro-additive manufacturing technologies." *The International Journal of Advanced Manufacturing Technology* **67** (2013): 1721-1754.

- [161] Sochol RD, Gupta NR, and Bonventre JV. "A role for 3D printing in kidney-on-a-chip platforms." *Current Transplantation Reports* **3** (2016): 82-92.
- [162] Homan KA, Kolesky DB, Skylar-Scott MA, Herrmann J, Obuobi H, Moisan A, and Lewis JA. "Bioprinting of 3D convoluted renal proximal tubules on perfusable chips." *Scientific Reports* **6** (2016): 34845.
- [163] Lin NYC, Homan KA, Robinson SS, Kolesky DB, Duarte N, Moisan A, and Lewis JA. "Renal reabsorption in 3D vascularized proximal tubule models." *Proceedings of the National Academy of Sciences of the United States of America* **116** (2019): 5399-5404.
- [164] Mohammed MI, Haswell S, and Gibson I. "Lab-on-a-chip or chip-in-a-lab: Challenges of commercialization lost in translation." *Procedia Technology* **20** (2015): 54-59.
- [165] Badylak SF, Taylor D, and Uygun K. "Whole-organ tissue engineering: Decellularization and recellularization of three-dimensional matrix scaffolds." *Annual Review of Biomedical Engineering* **13** (2011): 27-53.
- [166] Song JJ, and Ott HC. "Organ engineering based on decellularized matrix scaffolds." *Trends in Molecular Medicine* **17** (2011): 424-432.
- [167] Soto-Gutierrez A, Wertheim JA, Ott HC, and Gilbert TW. "Perspectives on whole-organ assembly: Moving toward transplantation on demand." *The Journal of Clinical Investigation* **122** (2012): 3817-3823.
- [168] Hynes RO. "The extracellular matrix: Not just pretty fibrils." *Science* **326** (2009): 1216-1219.
- [169] Frantz C, Stewart KM, and Weaver VM. "The extracellular matrix at a glance." *Journal of Cell Science* **123** (2010): 4195-4200.
- [170] Gilbert TW, Sellaro TL, and Badylak SF. "Decellularization of tissues and organs." *Biomaterials* **27** (2006): 3675-3683.
- [171] Crapo PM, Gilbert TW, and Badylak SF. "An overview of tissue and whole organ decellularization processes." *Biomaterials* **32** (2011): 3233-3243.
- [172] Keane TJ, Swinehart IT, and Badylak SF. "Methods of tissue decellularization used for preparation of biologic scaffolds and in vivo relevance." *Methods* **84** (2015): 25-34.
- [173] Ott HC, Matthiesen TS, Goh S-K, Black LD, Kren SM, Netoff TI, and Taylor DA. "Perfusion-decellularized matrix: Using nature's platform to engineer a bioartificial heart." *Nature Medicine* **14** (2008): 213.
- [174] Kitahara H, Yagi H, Tajima K, Okamoto K, Yoshitake A, Aeba R, Kudo M, Kashima I, Kawaguchi S, Hirano A, Kasai M, Akamatsu Y, Oka H, Kitagawa Y, and Shimizu H. "Heterotopic transplantation of a decellularized and recellularized whole porcine heart." *Interactive Cardiovascular and Thoracic Surgery* **22** (2016): 571-579.
- [175] Uygun BE, Soto-Gutierrez A, Yagi H, Izamis M-L, Guzzardi MA, Shulman C, Milwid J, Kobayashi N, Tilles A, Berthiaume F, Hertl M, Nahmias Y, Yarmush ML, and Uygun K. "Organ reengineering through development of a transplantable recellularized liver graft using decellularized liver matrix." *Nature Medicine* **16** (2010): 814.

- [176] Soto-Gutierrez A, Zhang L, Medberry C, Fukumitsu K, Faulk D, Jiang H, Reing J, Gramignoli R, Komori J, Ross M, Nagaya M, Lagasse E, Stolz D, Strom SC, Fox IJ, and Badylak SF. "A whole-organ regenerative medicine approach for liver replacement." *Tissue Engineering Part C: Methods* **17** (2011): 677-686.
- [177] Barakat O, Abbasi S, Rodriguez G, Rios J, Wood RP, Ozaki C, Holley LS, and Gauthier PK. "Use of decellularized porcine liver for engineering humanized liver organ." *Journal of Surgical Research* **173** (2012): e11-e25.
- [178] Ott HC, Clippinger B, Conrad C, Schuetz C, Pomerantseva I, Ikononou L, Kotton D, and Vacanti JP. "Regeneration and orthotopic transplantation of a bioartificial lung." *Nature Medicine* **16** (2010): 927.
- [179] Petersen TH, Calle EA, Zhao L, Lee EJ, Gui L, Raredon MB, Gavrilov K, Yi T, Zhuang ZW, Breuer C, Herzog E, and Niklason LE. "Tissue-engineered lungs for in vivo implantation." *Science* **329** (2010): 538-541.
- [180] Gilpin SE, Guyette JP, Gonzalez G, Ren X, Asara JM, Mathisen DJ, Vacanti JP, and Ott HC. "Perfusion decellularization of human and porcine lungs: Bringing the matrix to clinical scale." *The Journal of Heart and Lung Transplantation* **33** (2014): 298-308.
- [181] Uzarski JS, Xia Y, Belmonte JCI, and Wertheim JA. "New strategies in kidney regeneration and tissue engineering." *Current Opinion in Nephrology and Hypertension* **23** (2014): 399-405.
- [182] Caralt M, Uzarski JS, Iacob S, Obergfell KP, Berg N, Bijonowski BM, Kiefer KM, Ward HH, Wandinger-Ness A, Miller WM, Zhang ZJ, Abecassis MM, and Wertheim JA. "Optimization and critical evaluation of decellularization strategies to develop renal extracellular matrix scaffolds as biological templates for organ engineering and transplantation." *American Journal of Transplantation* **15** (2015): 64-75.
- [183] He M, Callanan A, Lagaras K, Steele JAM, and Stevens MM. "Optimization of SDS exposure on preservation of ECM characteristics in whole organ decellularization of rat kidneys." *Journal of Biomedical Materials Research Part B: Applied Biomaterials* **105** (2017): 1352-1360.
- [184] Sullivan DC, Mirmalek-Sani S-H, Deegan DB, Baptista PM, AbouShwareb T, Atala A, and Yoo JJ. "Decellularization methods of porcine kidneys for whole organ engineering using a high-throughput system." *Biomaterials* **33** (2012): 7756-7764.
- [185] Orlando G, Farney AC, Iskandar SS, Mirmalek-Sani S-H, Sullivan DC, Moran E, AbouShwareb T, De Coppi P, Wood KJ, Stratta RJ, Atala A, Yoo JJ, and Soker S. "Production and implantation of renal extracellular matrix scaffolds from porcine kidneys as a platform for renal bioengineering investigations." *Annals of Surgery* **256** (2012): 363-370.
- [186] Wang Y, Bao J, Wu Q, Zhou Y, Li Y, Wu X, Shi Y, Li L, and Bu H. "Method for perfusion decellularization of porcine whole liver and kidney for use as a scaffold for clinical-scale bioengineering engrafts." *Xenotransplantation* **22** (2015): 48-61.
- [187] Guan Y, Liu S, Liu Y, Sun C, Cheng G, Luan Y, Li K, Wang J, Xie X, and Zhao S. "Porcine kidneys as a source of ECM scaffold for kidney regeneration." *Materials Science and Engineering: C* **56** (2015): 451-456.

- [188] Poornejad N, Momtahan N, Salehi AS, Scott DR, Fronk CA, Roeder BL, Reynolds PR, Bundy BC, and Cook AD. "Efficient decellularization of whole porcine kidneys improves reseeded cell behavior." *Biomedical Materials* **11** (2016): 025003.
- [189] Orlando G, Booth C, Wang Z, Totonelli G, Ross CL, Moran E, Salvatori M, Maghsoudlou P, Turmaine M, Delario G, Al-Shraideh Y, Farooq U, Farney AC, Rogers J, Iskandar SS, Burns A, Marini FC, De Coppi P, Stratta RJ, and Soker S. "Discarded human kidneys as a source of ECM scaffold for kidney regeneration technologies." *Biomaterials* **34** (2013): 5915-5925.
- [190] Peloso A, Petrosyan A, Da Sacco S, Booth C, Zambon JP, O'Brien T, Aardema C, Robertson J, De Filippo RE, Soker S, Stratta RJ, Perin L, and Orlando G. "Renal extracellular matrix scaffolds from discarded kidneys maintain glomerular morphometry and vascular resilience and retains critical growth factors." *Transplantation* **99** (2015): 1807-1816.
- [191] Song JJ, Guyette JP, Gilpin SE, Gonzalez G, Vacanti JP, and Ott HC. "Regeneration and experimental orthotopic transplantation of a bioengineered kidney." *Nature Medicine* **19** (2013): 646-651.
- [192] Abolbashari M, Agcaoili SM, Lee M-K, Ko IK, Aboushwareb T, Jackson JD, Yoo JJ, and Atala A. "Repopulation of porcine kidney scaffold using porcine primary renal cells." *Acta Biomaterialia* **29** (2016): 52-61.
- [193] Ross EA, Williams MJ, Hamazaki T, Terada N, Clapp WL, Adin C, Ellison GW, Jorgensen M, and Batich CD. "Embryonic stem cells proliferate and differentiate when seeded into kidney scaffolds." *Journal of the American Society of Nephrology* **20** (2009): 2338-2347.
- [194] Ross EA, Abrahamson DR, St. John P, Clapp WL, Williams MJ, Terada N, Hamazaki T, Ellison GW, and Batich CD. "Mouse stem cells seeded into decellularized rat kidney scaffolds endothelialize and remodel basement membranes." *Organogenesis* **8** (2012): 49-55.
- [195] Bonandrini B, Figliuzzi M, Papadimou E, Morigi M, Perico N, Casiraghi F, Dipl C, Sangalli F, Conti S, Benigni A, Remuzzi A, and Remuzzi G. "Recellularization of well-preserved acellular kidney scaffold using embryonic stem cells." *Tissue Engineering Part A* **20** (2014): 1486-1498.
- [196] Guan Y, Liu S, Sun C, Cheng G, Kong F, Luan Y, Xie X, Zhao S, Zhang D, Wang J, Li K, and Liu Y. "The effective bioengineering method of implantation decellularized renal extracellular matrix scaffolds." *Oncotarget* **6** (2015): 36126.
- [197] Du C, Narayanan K, Leong MF, Ibrahim MS, Chua YP, Khoo VMH, and Wan ACA. "Functional kidney bioengineering with pluripotent stem-cell-derived renal progenitor cells and decellularized kidney scaffolds." *Advanced Healthcare Materials* **5** (2016): 2080-2091.
- [198] Clevers H. "Modeling development and disease with organoids." *Cell* **165** (2016): 1586-1597.
- [199] Lancaster MA, and Knoblich JA. "Organogenesis in a dish: Modeling development and disease using organoid technologies." *Science* **345** (2014): 1247125.
- [200] Fatehullah A, Tan SH, and Barker N. "Organoids as an in vitro model of human development and disease." *Nature Cell Biology* **18** (2016): 246-254.
- [201] Jaenisch R, and Young R. "Stem cells, the molecular circuitry of pluripotency and nuclear reprogramming." *Cell* **132** (2008): 567-582.

- [202] Sato T, Vries RG, Snippert HJ, van De Wetering M, Barker N, Stange DE, van Es JH, Abo A, Kujala P, Peters PJ, and Clevers H. "Single Lgr5 stem cells build crypt-villus structures in vitro without a mesenchymal niche." *Nature* **459** (2009): 262.
- [203] Spence JR, Mayhew CN, Rankin SA, Kuhar MF, Vallance JE, Tolle K, Hoskins EE, Kalinichenko VV, Wells SI, Zorn AM, Shroyer NF, and Wells JM. "Directed differentiation of human pluripotent stem cells into intestinal tissue in vitro." *Nature* **470** (2011): 105.
- [204] Lancaster MA, Renner M, Martin C-A, Wenzel D, Bicknell LS, Hurles ME, Homfray T, Penninger JM, Jackson AP, and Knoblich JA. "Cerebral organoids model human brain development and microcephaly." *Nature* **501** (2013): 373.
- [205] Eiraku M, Takata N, Ishibashi H, Kawada M, Sakakura E, Okuda S, Sekiguchi K, Adachi T, and Sasai Y. "Self-organizing optic-cup morphogenesis in three-dimensional culture." *Nature* **472** (2011): 51.
- [206] Nakano T, Ando S, Takata N, Kawada M, Muguruma K, Sekiguchi K, Saito K, Yonemura S, Eiraku M, and Sasai Y. "Self-formation of optic cups and storable stratified neural retina from human ESCs." *Cell Stem Cell* **10** (2012): 771-785.
- [207] Lam AQ, Freedman BS, Morizane R, Lerou PH, Valerius MT, and Bonventre JV. "Rapid and efficient differentiation of human pluripotent stem cells into intermediate mesoderm that forms tubules expressing kidney proximal tubular markers." *Journal of the American Society of Nephrology* **25** (2014): 1211-1225.
- [208] Taguchi A, Kaku Y, Ohmori T, Sharmin S, Ogawa M, Sasaki H, and Nishinakamura R. "Redefining the in vivo origin of metanephric nephron progenitors enables generation of complex kidney structures from pluripotent stem cells." *Cell Stem Cell* **14** (2014): 53-67.
- [209] Xia Y, Nivet E, Sancho-Martinez I, Gallegos T, Suzuki K, Okamura D, Wu M-Z, Dubova I, Esteban CR, Montserrat N, Campistol JM, and Izpisua Belmonte JC. "Directed differentiation of human pluripotent cells to ureteric bud kidney progenitor-like cells." *Nature Cell Biology* **15** (2013): 1507.
- [210] Takasato M, Er PX, Becroft M, Vanslambrouck JM, Stanley EG, Elefanty AG, and Little MH. "Directing human embryonic stem cell differentiation towards a renal lineage generates a self-organizing kidney." *Nature Cell Biology* **16** (2014): 118-126.
- [211] Takasato M, Pei XE, Chiu HS, Maier B, Baillie GJ, Ferguson C, Parton RG, Wolvetang EJ, Roost MS, de Sousa Lopes SMC, and Little MH. "Kidney organoids from human iPS cells contain multiple lineages and model human nephrogenesis." *Nature* **526** (2015): 564-568.
- [212] Takasato M, Er PX, Chiu HS, and Little MH. "Generation of kidney organoids from human pluripotent stem cells." *Nature Protocols* **11** (2016): 1681.
- [213] Morizane R, Lam AQ, Freedman BS, Kishi S, Valerius MT, and Bonventre JV. "Nephron organoids derived from human pluripotent stem cells model kidney development and injury." *Nature Biotechnology* **33** (2015): 1193-1200.
- [214] Morizane R, and Bonventre JV. "Generation of nephron progenitor cells and kidney organoids from human pluripotent stem cells." *Nature Protocols* **12** (2017): 195.
- [215] Taguchi A, and Nishinakamura R. "Higher-order kidney organogenesis from pluripotent stem cells." *Cell Stem Cell* **21** (2017): 730-746. e736.

- [216] Freedman BS, Brooks CR, Lam AQ, Fu H, Morizane R, Agrawal V, Saad AF, Li MK, Hughes MR, Vander Werff R, Peters DT, Lu J, Baccei A, Siedlecki AM, Valerius MT, Musunuru K, McNagny KM, Steinman TI, Zhou J, Lerou PH, and Bonventre JV. "Modelling kidney disease with CRISPR-mutant kidney organoids derived from human pluripotent epiblast spheroids." *Nature Communications* **6** (2015): 8715.
- [217] Kim YK, Refaeli I, Brooks CR, Jing P, Gulieva RE, Hughes MR, Cruz NM, Liu Y, Churchill AJ, Wang Y, Fu H, Pippin JW, Lin LY, Shankland SJ, Vogl AW, McNagny KM, and Freedman BS. "Gene-edited human kidney organoids reveal mechanisms of disease in podocyte development." *Stem Cells* **35** (2017): 2366-2378.
- [218] Cruz NM, Song X, Czerniecki SM, Gulieva RE, Churchill AJ, Kim YK, Winston K, Tran LM, Diaz MA, Fu H, Finn LS, Pei Y, Himmelfarb J, and Freedman BS. "Organoid cystogenesis reveals a critical role of microenvironment in human polycystic kidney disease." *Nature Materials* **16** (2017): 1112.
- [219] Hale LJ, Howden SE, Phipson B, Lonsdale A, Pei XE, Ghobrial I, Hosawi S, Wilson S, Lawlor KT, Khan S, Oshlack A, Quinlan C, Lennon R, and Little MH. "3D organoid-derived human glomeruli for personalised podocyte disease modelling and drug screening." *Nature Communications* **9** (2018): 5167.
- [220] Czerniecki SM, Cruz NM, Harder JL, Menon R, Annis J, Otto EA, Gulieva RE, Islas LV, Kim YK, Tran LM, Martins TJ, Pippin JW, Fu H, Kretzler M, Shankland SJ, Himmelfarb J, Moon RT, Paragas N, and Freedman BS. "High-throughput screening enhances kidney organoid differentiation from human pluripotent stem cells and enables automated multidimensional phenotyping." *Cell Stem Cell* **22** (2018): 929-940. e924.
- [221] Kumar SV, Pei XE, Lawlor KT, Motazedian A, Scurr M, Ghobrial I, Combes AN, Zappia L, Oshlack A, Stanley EG, and Little MH. "Kidney micro-organoids in suspension culture as a scalable source of human pluripotent stem cell-derived kidney cells." *Development* **146** (2019): dev172361.
- [222] Takasato M, and Little MH. "A strategy for generating kidney organoids: Recapitulating the development in human pluripotent stem cells." *Developmental Biology* **420** (2016): 210-220.
- [223] Sharmin S, Taguchi A, Kaku Y, Yoshimura Y, Ohmori T, Sakuma T, Mukoyama M, Yamamoto T, Kurihara H, and Nishinakamura R. "Human induced pluripotent stem cell-derived podocytes mature into vascularized glomeruli upon experimental transplantation." *Journal of the American Society of Nephrology* **27** (2016): 1778-1791.
- [224] Garreta E, Prado P, Tarantino C, Oriá R, Fanlo L, Martí E, Zalvidea D, Trepát X, Roca-Cusachs P, Gavaldà-Navarro A, Cozzuto L, Campistol JM, Izpisua Belmonte JC, del Pozo CH, and Montserrat N. "Fine tuning the extracellular environment accelerates the derivation of kidney organoids from human pluripotent stem cells." *Nature Materials* **18** (2019): 397.
- [225] Homan KA, Gupta N, Kroll KT, Kolesky DB, Skylar-Scott M, Miyoshi T, Mau D, Valerius MT, Ferrante T, Bonventre JV, Lewis JA, and Morizane R. "Flow-enhanced vascularization and maturation of kidney organoids in vitro." *Nature Methods* **16** (2019): 255.
- [226] Hoffman AS. "Hydrogels for biomedical applications." *Advanced Drug Delivery Reviews* **64** (2012): 18-23.

- [227] Lee KY, and Mooney DJ. "Hydrogels for tissue engineering." *Chemical Reviews* **101** (2001): 1869-1880.
- [228] Drury JL, and Mooney DJ. "Hydrogels for tissue engineering: Scaffold design variables and applications." *Biomaterials* **24** (2003): 4337-4351.
- [229] Slaughter BV, Khurshid SS, Fisher OZ, Khademhosseini A, and Peppas NA. "Hydrogels in regenerative medicine." *Advanced Materials* **21** (2009): 3307-3329.
- [230] Peppas NA, Bures P, Leobandung WS, and Ichikawa H. "Hydrogels in pharmaceutical formulations." *European Journal of Pharmaceutics and Biopharmaceutics* **50** (2000): 27-46.
- [231] Hoare TR, and Kohane DS. "Hydrogels in drug delivery: Progress and challenges." *Polymer* **49** (2008): 1993-2007.
- [232] Peppas NA, Huang Y, Torres-Lugo M, Ward JH, and Zhang J. "Physicochemical foundations and structural design of hydrogels in medicine and biology." *Annual Review of Biomedical Engineering* **2** (2000): 9-29.
- [233] Nicodemus GD, and Bryant SJ. "Cell encapsulation in biodegradable hydrogels for tissue engineering applications." *Tissue Engineering Part B: Reviews* **14** (2008): 149-165.
- [234] Lutolf MP, and Hubbell JA. "Synthetic biomaterials as instructive extracellular microenvironments for morphogenesis in tissue engineering." *Nature Biotechnology* **23** (2005): 47.
- [235] Tibbitt MW, and Anseth KS. "Hydrogels as extracellular matrix mimics for 3D cell culture." *Biotechnology and Bioengineering* **103** (2009): 655-663.
- [236] Geckil H, Xu F, Zhang X, Moon S, and Demirci U. "Engineering hydrogels as extracellular matrix mimics." *Nanomedicine* **5** (2010): 469-484.
- [237] Burdick JA, and Murphy WL. "Moving from static to dynamic complexity in hydrogel design." *Nature Communications* **3** (2012): 1269.
- [238] Rosales AM, and Anseth KS. "The design of reversible hydrogels to capture extracellular matrix dynamics." *Nature Reviews Materials* **1** (2016): 15012.
- [239] Hennink WE, and van Nostrum CF. "Novel crosslinking methods to design hydrogels." *Advanced Drug Delivery Reviews* **64** (2012): 223-236.
- [240] Guvendiren M, Lu HD, and Burdick JA. "Shear-thinning hydrogels for biomedical applications." *Soft Matter* **8** (2012): 260-272.
- [241] Malda J, Visser J, Melchels FP, Jüngst T, Hennink WE, Dhert WJ, Groll J, and Huttmacher DW. "25th anniversary article: Engineering hydrogels for biofabrication." *Advanced Materials* **25** (2013): 5011-5028.
- [242] Rutz AL, Lewis PL, and Shah RN. "Toward next-generation bioinks: Tuning material properties pre- and post-printing to optimize cell viability." *MRS Bulletin* **42** (2017): 563-570.
- [243] Nimmo CM, and Shoichet MS. "Regenerative biomaterials that "click": Simple, aqueous-based protocols for hydrogel synthesis, surface immobilization, and 3D patterning." *Bioconjugate Chemistry* **22** (2011): 2199-2209.

- [244] Azagarsamy MA, and Anseth KS. "Bioorthogonal click chemistry: An indispensable tool to create multifaceted cell culture scaffolds." **2** (2013): 5-9.
- [245] Jiang Y, Chen J, Deng C, Suuronen EJ, and Zhong Z. "Click hydrogels, microgels and nanogels: Emerging platforms for drug delivery and tissue engineering." *Biomaterials* **35** (2014): 4969-4985.
- [246] Madl CM, and Heilshorn SC. "Bioorthogonal strategies for engineering extracellular matrices." *Advanced Functional Materials* **28** (2018): 1706046.
- [247] Thiele J, Ma Y, Bruekers SMC, Ma S, and Huck WTS. "25th anniversary article: Designer hydrogels for cell cultures: A materials selection guide." *Advanced Materials* **26** (2014): 125-148.
- [248] Wallace DG, and Rosenblatt J. "Collagen gel systems for sustained delivery and tissue engineering." *Advanced Drug Delivery Reviews* **55** (2003): 1631-1649.
- [249] Young S, Wong M, Tabata Y, and Mikos AG. "Gelatin as a delivery vehicle for the controlled release of bioactive molecules." *Journal of Controlled Release* **109** (2005): 256-274.
- [250] Ahmed TAE, Dare EV, and Hincke M. "Fibrin: A versatile scaffold for tissue engineering applications." *Tissue Engineering Part B: Reviews* **14** (2008): 199-215.
- [251] Daamen WF, Veerkamp JH, Van Hest JCM, and Van Kuppevelt TH. "Elastin as a biomaterial for tissue engineering." *Biomaterials* **28** (2007): 4378-4398.
- [252] Lee H, Noh K, Lee SC, Kwon I-K, Han D-W, Lee I-S, and Hwang Y-S. "Human hair keratin and its-based biomaterials for biomedical applications." *Tissue Engineering and Regenerative Medicine* **11** (2014): 255-265.
- [253] Vepari C, and Kaplan DL. "Silk as a biomaterial." *Progress in Polymer Science* **32** (2007): 991-1007.
- [254] Abaee A, Mohammadian M, and Jafari SM. "Whey and soy protein-based hydrogels and nano-hydrogels as bioactive delivery systems." *Trends in Food Science & Technology* **70** (2017): 69-81.
- [255] Reddy N, and Yang Y. "Potential of plant proteins for medical applications." *Trends in Biotechnology* **29** (2011): 490-498.
- [256] Rowley JA, Madlambayan G, and Mooney DJ. "Alginate hydrogels as synthetic extracellular matrix materials." *Biomaterials* **20** (1999): 45-53.
- [257] Zarrintaj P, Manouchehri S, Ahmadi Z, Saeb MR, Urbanska AM, Kaplan DL, and Mozafari M. "Agarose-based biomaterials for tissue engineering." *Carbohydrate Polymers* **187** (2018): 66-84.
- [258] Bhattarai N, Gunn J, and Zhang M. "Chitosan-based hydrogels for controlled, localized drug delivery." *Advanced Drug Delivery Reviews* **62** (2010): 83-99.
- [259] Sun G, and Mao JJ. "Engineering dextran-based scaffolds for drug delivery and tissue repair." *Nanomedicine* **7** (2012): 1771-1784.
- [260] Burdick JA, and Prestwich GD. "Hyaluronic acid hydrogels for biomedical applications." *Advanced Materials* **23** (2011): H41-H56.

- [261] Freudenberg U, Liang Y, Kiick KL, and Werner C. "Glycosaminoglycan-based biohybrid hydrogels: A sweet and smart choice for multifunctional biomaterials." *Advanced Materials* **28** (2016): 8861-8891.
- [262] Chang C, and Zhang L. "Cellulose-based hydrogels: Present status and application prospects." *Carbohydrate Polymers* **84** (2011): 40-53.
- [263] Ismail H, Irani M, and Ahmad Z. "Starch-based hydrogels: Present status and applications." *International Journal of Polymeric Materials and Polymeric Biomaterials* **62** (2013): 411-420.
- [264] Saldin LT, Cramer MC, Velankar SS, White LJ, and Badylak SF. "Extracellular matrix hydrogels from decellularized tissues: Structure and function." *Acta Biomaterialia* **49** (2017): 1-15.
- [265] Dasgupta A, Mondal JH, and Das D. "Peptide hydrogels." *RSC Advances* **3** (2013): 9117-9149.
- [266] Cui H, Webber MJ, and Stupp SI. "Self-assembly of peptide amphiphiles: From molecules to nanostructures to biomaterials." *Peptide Science* **94** (2010): 1-18.
- [267] Li J, Mo L, Lu C-H, Fu T, Yang H-H, and Tan W. "Functional nucleic acid-based hydrogels for bioanalytical and biomedical applications." *Chemical Society Reviews* **45** (2016): 1410-1431.
- [268] Sionkowska A. "Current research on the blends of natural and synthetic polymers as new biomaterials." *Progress in Polymer Science* **36** (2011): 1254-1276.
- [269] White JA, and Deen WM. "Agarose-dextran gels as synthetic analogs of glomerular basement membrane: Water permeability." *Biophysical Journal* **82** (2002): 2081-2089.
- [270] Discher DE, Janmey P, and Wang Y-I. "Tissue cells feel and respond to the stiffness of their substrate." *Science* **310** (2005): 1139-1143.
- [271] Discher DE, Mooney DJ, and Zandstra PW. "Growth factors, matrices, and forces combine and control stem cells." *Science* **324** (2009): 1673-1677.
- [272] Beamish JA, Chen E, and Putnam AJ. "Engineered extracellular matrices with controlled mechanics modulate renal proximal tubular cell epithelialization." *PLOS ONE* **12** (2017): e0181085.
- [273] Love HD, Ao M, Jorgensen S, Swearingen L, Ferrell N, Evans R, Gewin L, Harris RC, Zent R, Roy S, and Fissell IV WH. "Substrate elasticity governs differentiation of renal tubule cells in prolonged culture." *Tissue Engineering Part A* (2019):
- [274] Hu M, Azeloglu EU, Ron A, Tran-Ba K-H, Calizo RC, Tavassoly I, Bhattacharya S, Jayaraman G, Chen Y, Rabinovich V, Iyengar R, Hone JC, He JC, and Kaufman LJ. "A biomimetic gelatin-based platform elicits a pro-differentiation effect on podocytes through mechanotransduction." *Scientific Reports* **7** (2017): 43934.
- [275] Kleinman HK, and Martin GR. "Matrigel: Basement membrane matrix with biological activity." *Seminars in Cancer Biology* **15** (2005): 378-386.
- [276] Kitahara T, Hiromura K, Ikeuchi H, Yamashita S, Kobayashi S, Kuroiwa T, Kaneko Y, Ueki K, and Nojima Y. "Mesangial cells stimulate differentiation of endothelial cells to form capillary-like networks in a three-dimensional culture system." *Nephrology Dialysis Transplantation* **20** (2005): 42-49.

- [277] van Genderen AM, Jansen J, Cheng C, Vermonden T, and Masereeuw R. "Renal tubular- and vascular basement membranes and their mimicry in engineering vascularized kidney tubules." *Advanced Healthcare Materials* **7** (2018): 1800529.
- [278] O'Neill JD, Freytes DO, Anandappa AJ, Oliver JA, and Vunjak-Novakovic GV. "The regulation of growth and metabolism of kidney stem cells with regional specificity using extracellular matrix derived from kidney." *Biomaterials* **34** (2013): 9830-9841.
- [279] Magno V, Friedrichs J, Weber HM, Prewitz MC, Tsurkan MV, and Werner C. "Macromolecular crowding for tailoring tissue-derived fibrillated matrices." *Acta Biomaterialia* **55** (2017): 109-119.
- [280] Su J, Satchell SC, Wertheim JA, and Shah RN. "Poly(ethylene glycol)-crosslinked gelatin hydrogel substrates with conjugated bioactive peptides influence endothelial cell behavior." *Biomaterials* **201** (2019): 99-112.
- [281] Bruggeman LA, Doan RP, Loftis J, Darr A, and Calabro A. "A cell culture system for the structure and hydrogel properties of basement membranes: Application to capillary walls." *Cellular and Molecular Bioengineering* **5** (2012): 194-204.
- [282] Nagao RJ, Xu J, Luo P, Xue J, Wang Y, Kotha S, Zeng W, Fu X, Himmelfarb J, and Zheng Y. "Decellularized human kidney cortex hydrogels enhance kidney microvascular endothelial cell maturation and quiescence." *Tissue Engineering Part A* **22** (2016): 1140-1150.
- [283] O'Brien LE, Zegers MMP, and Mostov KE. "Building epithelial architecture: Insights from three-dimensional culture models." *Nature Reviews Molecular Cell Biology* **3** (2002): 531.
- [284] Koh W, Stratman AN, Sacharidou A, and Davis GE. "In vitro three dimensional collagen matrix models of endothelial lumen formation during vasculogenesis and angiogenesis." *Methods in Enzymology* **443** (2008): 83-101.
- [285] Astashkina AI, Mann BK, Prestwich GD, and Grainger DW. "A 3-D organoid kidney culture model engineered for high-throughput nephrotoxicity assays." *Biomaterials* **33** (2012): 4700-4711.
- [286] Astashkina AI, Jones CF, Thiagarajan G, Kurtzborn K, Ghandehari H, Brooks BD, and Grainger DW. "Nanoparticle toxicity assessment using an in vitro 3-D kidney organoid culture model." *Biomaterials* **35** (2014): 6323-6331.
- [287] DesRochers TM, Suter L, Roth A, and Kaplan DL. "Bioengineered 3D human kidney tissue, a platform for the determination of nephrotoxicity." *PLOS ONE* **8** (2013): e59219.
- [288] Su J, Satchell SC, Shah RN, and Wertheim JA. "Kidney decellularized extracellular matrix hydrogels: Rheological characterization and human glomerular endothelial cell response to encapsulation." *Journal of Biomedical Materials Research Part A* **106A** (2018): 2448-2462.
- [289] Waters JP, Richards YC, Skepper JN, Southwood M, Upton PD, Morrell NW, Pober JS, and Bradley JR. "A 3D tri-culture system reveals that activin receptor-like kinase 5 and connective tissue growth factor drive human glomerulosclerosis." *The Journal of Pathology* **243** (2017): 390-400.
- [290] United States Renal Data System. "2015 Annual Data Report: Epidemiology of Kidney Disease in the United States." *National Institutes of Health, National Institutes of Diabetes and Digestive and Kidney Disease*. Bethesda, MD (2015).

- [291] Jha V, Garcia-Garcia G, Iseki K, Li Z, Naicker S, Plattner B, Saran R, Wang AY-M, and Yang C-W. "Chronic kidney disease: Global dimension and perspectives." *The Lancet* **382** (2013): 260-272.
- [292] Pampaloni F, Reynaud EG, and Stelzer EHK. "The third dimension bridges the gap between cell culture and live tissue." *Nature Reviews Molecular Cell Biology* **8** (2007): 839-845.
- [293] Antoni D, Burckel H, Josset E, and Noel G. "Three-dimensional cell culture: A breakthrough in vivo." *International Journal of Molecular Sciences* **16** (2015): 5517-5527.
- [294] Ly JP, Onay T, and Quaggin SE. "Mouse models to study kidney development, function and disease." *Current Opinion in Nephrology and Hypertension* **20** (2011): 382-390.
- [295] Eddy AA, López-Guisa JM, Okamura DM, and Yamaguchi I. "Investigating mechanisms of chronic kidney disease in mouse models." *Pediatric Nephrology* **27** (2012): 1233-1247.
- [296] O'Sullivan ED, Hughes J, and Ferenbach DA. "Renal aging: Causes and consequences." *Journal of the American Society of Nephrology* (2016): ASN. 2015121308.
- [297] Van der Worp HB, Howells DW, Sena ES, Porritt MJ, Rewell S, O'Collins V, and Macleod MR. "Can animal models of disease reliably inform human studies?" *PLOS Medicine* **7** (2010): e1000245.
- [298] Langer R, and Vacanti JP. "Tissue engineering." *Science* **260** (1993): 920-926.
- [299] Vacanti JP, and Langer R. "Tissue engineering: The design and fabrication of living replacement devices for surgical reconstruction and transplantation." *The Lancet* **354** (1999): S32-S34.
- [300] Lanza R, Langer R, and Vacanti JP. *Principles of Tissue Engineering*. Academic Press (2011).
- [301] Yang S, Leong K-F, Du Z, and Chua C-K. "The design of scaffolds for use in tissue engineering. Part I. Traditional factors." *Tissue Engineering* **7** (2001): 679-689.
- [302] Bissell MJ, Hall HG, and Parry G. "How does the extracellular matrix direct gene expression?" *Journal of Theoretical Biology* **99** (1982): 31-68.
- [303] Badylak SF, Freytes DO, and Gilbert TW. "Extracellular matrix as a biological scaffold material: Structure and function." *Acta Biomaterialia* **5** (2009): 1-13.
- [304] Jonker AM, Löwik DWPM, and van Hest JCM. "Peptide-and protein-based hydrogels." *Chemistry of Materials* **24** (2012): 759-773.
- [305] Rutz AL, and Shah RN. "Protein-Based Hydrogels." *Polymeric Hydrogels as Smart Biomaterials*. Springer (2016): 73-104.
- [306] Singelyn JM, DeQuach JA, Seif-Naraghi SB, Littlefield RB, Schup-Magoffin PJ, and Christman KL. "Naturally derived myocardial matrix as an injectable scaffold for cardiac tissue engineering." *Biomaterials* **30** (2009): 5409-5416.
- [307] Singelyn JM, and Christman KL. "Modulation of material properties of a decellularized myocardial matrix scaffold." *Macromolecular Bioscience* **11** (2011): 731-738.
- [308] Ungerleider JL, Johnson TD, Rao N, and Christman KL. "Fabrication and characterization of injectable hydrogels derived from decellularized skeletal and cardiac muscle." *Methods* **84** (2015): 53-59.

- [309] Wassenaar JW, Gaetani R, Garcia JJ, Braden RL, Luo CG, Huang D, DeMaria AN, Omens JH, and Christman KL. "Evidence for mechanisms underlying the functional benefits of a myocardial matrix hydrogel for post-MI treatment." *Journal of the American College of Cardiology* **67** (2016): 1074-1086.
- [310] Sellaro TL, Ranade A, Faulk DM, McCabe GP, Dorko K, Badylak SF, and Strom SC. "Maintenance of human hepatocyte function in vitro by liver-derived extracellular matrix gels." *Tissue Engineering Part A* **16** (2009): 1075-1082.
- [311] Lee JS, Shin J, Park H-M, Kim Y-G, Kim B-G, Oh J-W, and Cho S-W. "Liver extracellular matrix providing dual functions of two-dimensional substrate coating and three-dimensional injectable hydrogel platform for liver tissue engineering." *Biomacromolecules* **15** (2013): 206-218.
- [312] Loneker AE, Faulk DM, Hussey GS, D'Amore A, and Badylak SF. "Solubilized liver extracellular matrix maintains primary rat hepatocyte phenotype *in-vitro*." *Journal of Biomedical Materials Research Part A* **104** (2016): 957-965.
- [313] DeQuach JA, Lin JE, Cam C, Hu D, Salvatore MA, Sheikh F, and Christman KL. "Injectable skeletal muscle matrix hydrogel promotes neovascularization and muscle cell infiltration in a hindlimb ischemia model." *European Cells & Materials* **23** (2012): 400.
- [314] Fu Y, Fan X, Tian C, Luo J, Zhang Y, Deng L, Qin T, and Lv Q. "Decellularization of porcine skeletal muscle extracellular matrix for the formulation of a matrix hydrogel: A preliminary study." *Journal of Cellular and Molecular Medicine* (2016):
- [315] Ungerleider JL, Johnson TD, Hernandez MJ, Elhag DI, Braden RL, Dzieciatkowska M, Osborn KG, Hansen KC, Mahmud E, and Christman KL. "Extracellular matrix hydrogel promotes tissue remodeling, arteriogenesis, and perfusion in a rat hindlimb ischemia model." *JACC: Basic to Translational Science* **1** (2016): 32-44.
- [316] Satchell SC, Tasman CH, Singh A, Ni L, Geelen J, von Ruhland CJ, O'Hare MJ, Saleem MA, van den Heuvel LP, and Mathieson PW. "Conditionally immortalized human glomerular endothelial cells expressing fenestrations in response to VEGF." *International Society of Nephrology* **69** (2006): 1633-1640.
- [317] Freytes DO, Martin J, Velankar SS, Lee AS, and Badylak SF. "Preparation and rheological characterization of a gel form of the porcine urinary bladder matrix." *Biomaterials* **29** (2008): 1630-1637.
- [318] Zuidema JM, Rivet CJ, Gilbert RJ, and Morrison FA. "A protocol for rheological characterization of hydrogels for tissue engineering strategies." *Journal of Biomedical Materials Research Part B: Applied Biomaterials* **102** (2014): 1063-1073.
- [319] Ali SH, and DeCaprio JA. "Cellular transformation by SV40 large T antigen: Interaction with host proteins." *Seminars in Cancer Biology* **11** (2001): 15-22.
- [320] Kuroda Y, Wakao S, Kitada M, Murakami T, Nojima M, and Dezawa M. "Isolation, culture and evaluation of multilineage-differentiating stress-enduring (Muse) cells." *Nature Protocols* **8** (2013): 1391-1415.
- [321] Sun Q, and Overholtzer M. "Methods for the Study of Entosis." *Necrosis: Methods and Protocols*. Humana Press (2013): 59-66.

- [322] Elliot Jr. RA, and Hoehn JG. "Use of commercial porcine skin for wound dressings." *Plastic and Reconstructive Surgery* **52** (1973): 401-405.
- [323] Zhang Y, He Y, Bharadwaj S, Hammam N, Carnagey K, Myers R, Atala A, and Van Dyke M. "Tissue-specific extracellular matrix coatings for the promotion of cell proliferation and maintenance of cell phenotype." *Biomaterials* **30** (2009): 4021-4028.
- [324] DeQuach JA, Mezzano V, Miglani A, Lange S, Keller GM, Sheikh F, and Christman KL. "Simple and high yielding method for preparing tissue specific extracellular matrix coatings for cell culture." *PLOS ONE* **5** (2010): e13039.
- [325] Hulmes DJS. "Collagen Diversity, Synthesis and Assembly." *Collagen*. Springer (2008): 15-47.
- [326] Parkinson J, Kadler KE, and Brass A. "Simple physical model of collagen fibrillogenesis based on diffusion limited aggregation." *Journal of Molecular Biology* **247** (1995): 823-831.
- [327] Brightman AO, Rajwa BP, Sturgis JE, McCallister ME, Robinson JP, and Voytik-Harbin SL. "Time-lapse confocal reflection microscopy of collagen fibrillogenesis and extracellular matrix assembly in vitro." *Biopolymers* **54** (2000): 222-234.
- [328] Storm C, Pastore JJ, MacKintosh FC, Lubensky TC, and Janmey PA. "Nonlinear elasticity in biological gels." *Nature* **435** (2005): 191-194.
- [329] Erk KA, Henderson KJ, and Shull KR. "Strain stiffening in synthetic and biopolymer networks." *Biomacromolecules* **11** (2010): 1358-1363.
- [330] Levental I, Georges PC, and Janmey PA. "Soft biological materials and their impact on cell function." *Soft Matter* **3** (2007): 299-306.
- [331] Wells RG. "The role of matrix stiffness in regulating cell behavior." *Hepatology* **47** (2008): 1394-1400.
- [332] De Smet F, Segura I, De Bock K, Hohensinner PJ, and Carmeliet P. "Mechanisms of vessel branching." *Arteriosclerosis, Thrombosis, and Vascular Biology* **29** (2009): 639-649.
- [333] Slater SC, Beachley V, Hayes T, Zhang D, Welsh GI, Saleem MA, Mathieson PW, Wen X, Su B, and Satchell SC. "An in vitro model of the glomerular capillary wall using electrospun collagen nanofibres in a bioartificial composite basement membrane." *PLOS ONE* **6** (2011): e20802.
- [334] Slater SC, Ramnath RD, Uttridge K, Saleem MA, Cahill PA, Mathieson PW, Welsh GI, and Satchell SC. "Chronic exposure to laminar shear stress induces Kruppel-like factor 2 in glomerular endothelial cells and modulates interactions with co-cultured podocytes." *The International Journal of Biochemistry & Cell Biology* **44** (2012): 1482-1490.
- [335] Oliver JA, Maarouf O, Cheema FH, Martens TP, and Al-Awqati Q. "The renal papilla is a niche for adult kidney stem cells." *Journal of Clinical Investigation* **114** (2004): 795-804.
- [336] Al-Awqati Q, and Oliver JA. "The kidney papilla is a stem cells niche." *Stem Cell Reviews* **2** (2006): 181-184.

- [337] Mozes MM, Böttinger EP, Jacot TA, and Kopp JB. "Renal expression of fibrotic matrix proteins and of transforming growth factor- $\beta$  (TGF- $\beta$ ) isoforms in TGF- $\beta$  transgenic mice." *Journal of the American Society of Nephrology* **10** (1999): 271-280.
- [338] Zeisberg M, Bonner G, Maeshima Y, Colorado P, Müller GA, Strutz F, and Kalluri R. "Renal fibrosis: Collagen composition and assembly regulates epithelial-mesenchymal transdifferentiation." *The American Journal of Pathology* **159** (2001): 1313-1321.
- [339] Ruiz-Torres MP, Lopez-Ongil S, Griera M, Diez-Marques ML, Rodriguez-Puyol M, and Rodriguez-Puyol D. "The accumulation of extracellular matrix in the kidney: Consequences on cellular function." *Journal of Nephrology* **18** (2005): 334.
- [340] Dewavrin J-Y, Hamzavi N, Shim VPW, and Raghunath M. "Tuning the architecture of three-dimensional collagen hydrogels by physiological macromolecular crowding." *Acta Biomaterialia* **10** (2014): 4351-4359.
- [341] Rutz AL, Hyland KE, Jakus AE, Burghardt WR, and Shah RN. "A multimaterial bioink method for 3D printing tunable, cell-compatible hydrogels." *Advanced Materials* **27** (2015): 1607-1614.
- [342] Tabata Y, and Ikada Y. "Protein release from gelatin matrices." *Advanced Drug Delivery Reviews* **31** (1998): 287-301.
- [343] Van Vlierberghe S, Dubrue P, and Schacht E. "Biopolymer-based hydrogels as scaffolds for tissue engineering applications: A review." *Biomacromolecules* **12** (2011): 1387-1408.
- [344] Graf J, Iwamoto Y, Sasaki M, Martin GR, Kleinman HK, Robey FA, and Yamada Y. "Identification of an amino acid sequence in laminin mediating cell attachment, chemotaxis, and receptor binding." *Cell* **48** (1987): 989-996.
- [345] Graf J, Ogle RC, Robey FA, Sasaki M, Martin GR, Yamada Y, and Kleinman HK. "A pentapeptide from the laminin B1 chain mediates cell adhesion and binds to 67000 laminin receptor." *Biochemistry* **26** (1987): 6896-6900.
- [346] Jun H-W, and West J. "Development of a YIGSR-peptide-modified polyurethaneurea to enhance endothelialization." *Journal of Biomaterials Science, Polymer Edition* **15** (2004): 73-94.
- [347] Jun HW, and West JL. "Modification of polyurethaneurea with PEG and YIGSR peptide to enhance endothelialization without platelet adhesion." *Journal of Biomedical Materials Research Part B: Applied Biomaterials* **72** (2005): 131-139.
- [348] Jun H-W, and West JL. "Endothelialization of microporous YIGSR/PEG-modified polyurethaneurea." *Tissue Engineering* **11** (2005): 1133-1140.
- [349] Jung JP, Moyano JV, and Collier JH. "Multifactorial optimization of endothelial cell growth using modular synthetic extracellular matrices." *Integrative Biology* **3** (2011): 185-196.
- [350] Fittkau MH, Zilla P, Bezuidenhout D, Lutolf MP, Human P, Hubbell JA, and Davies N. "The selective modulation of endothelial cell mobility on RGD peptide containing surfaces by YIGSR peptides." *Biomaterials* **26** (2005): 167-174.
- [351] Ali S, Saik JE, Gould DJ, Dickinson ME, and West JL. "Immobilization of cell-adhesive laminin peptides in degradable PEGDA hydrogels influences endothelial cell tubulogenesis." *BioResearch Open Access* **2** (2013): 241-249.

- [352] D'Andrea LD, Iaccarino G, Fattorusso R, Sorriento D, Carannante C, Capasso D, Trimarco B, and Pedone C. "Targeting angiogenesis: Structural characterization and biological properties of a de novo engineered VEGF mimicking peptide." *Proceedings of the National Academy of Sciences of the United States of America* **102** (2005): 14215-14220.
- [353] Olsson A-K, Dimberg A, Kreuger J, and Claesson-Welsh L. "VEGF receptor signalling? In control of vascular function." *Nature Reviews Molecular Cell Biology* **7** (2006): 359-371.
- [354] Vlieghe P, Lisowski V, Martinez J, and Khrestchatisky M. "Synthetic therapeutic peptides: Science and market." *Drug Discovery Today* **15** (2010): 40-56.
- [355] Cai L, Dinh CB, and Heilshorn SC. "One-pot synthesis of elastin-like polypeptide hydrogels with grafted VEGF-mimetic peptides." *Biomaterials Science* **2** (2014): 757-765.
- [356] Chan TR, Stahl PJ, and Yu SM. "Matrix-bound VEGF mimetic peptides: Design and endothelial-cell activation in collagen scaffolds." *Advanced Functional Materials* **21** (2011): 4252-4262.
- [357] Leslie-Barbick JE, Saik JE, Gould DJ, Dickinson ME, and West JL. "The promotion of microvasculature formation in poly(ethylene glycol) diacrylate hydrogels by an immobilized VEGF-mimetic peptide." *Biomaterials* **32** (2011): 5782-5789.
- [358] Parthiban SP, Rana D, Jabbari E, Benkirane-Jessel N, and Ramalingam M. "Covalently immobilized VEGF-mimicking peptide with gelatin methacrylate enhances microvascularization of endothelial cells." *Acta Biomaterialia* **51** (2017): 330-340.
- [359] Habeeb AFSA. "Determination of free amino groups in proteins by trinitrobenzenesulfonic acid." *Analytical Biochemistry* **14** (1966): 328-336.
- [360] Kuijpers AJ, Engbers GHM, Krijgsveld J, Zaat SAJ, Dankert J, and Feijen J. "Cross-linking and characterisation of gelatin matrices for biomedical applications." *Journal of Biomaterials Science, Polymer Edition* **11** (2000): 225-243.
- [361] Arnaoutova I, George J, Kleinman HK, and Benton G. "The endothelial cell tube formation assay on basement membrane turns 20: State of the science and the art." *Angiogenesis* **12** (2009): 267-274.
- [362] Arnaoutova I, and Kleinman HK. "In vitro angiogenesis: Endothelial cell tube formation on gelled basement membrane extract." *Nature Protocols* **5** (2010): 628-635.
- [363] Sieminski AL, Hebbel RP, and Gooch KJ. "The relative magnitudes of endothelial force generation and matrix stiffness modulate capillary morphogenesis in vitro." *Experimental Cell Research* **297** (2004): 574-584.
- [364] Byfield FJ, Reen RK, Shentu T-P, Levitan I, and Gooch KJ. "Endothelial actin and cell stiffness is modulated by substrate stiffness in 2D and 3D." *Journal of Biomechanics* **42** (2009): 1114-1119.
- [365] Santos L, Fuhrmann G, Juenet M, Amdursky N, Horejs CM, Campagnolo P, and Stevens MM. "Extracellular stiffness modulates the expression of functional proteins and growth factors in endothelial cells." *Advanced Healthcare Materials* **4** (2015): 2056-2063.

- [366] Davis GE, and Camarillo CW. "Regulation of endothelial cell morphogenesis by integrins, mechanical forces, and matrix guidance pathways." *Experimental Cell Research* **216** (1995): 113-123.
- [367] Califano JP, and Reinhart-King CA. "A balance of substrate mechanics and matrix chemistry regulates endothelial cell network assembly." *Cellular and Molecular Bioengineering* **1** (2008): 122.
- [368] Sun J, Jamilpour N, Wang F-Y, and Wong PK. "Geometric control of capillary architecture via cell-matrix mechanical interactions." *Biomaterials* **35** (2014): 3273-3280.
- [369] Zaman MH, Trapani LM, Sieminski AL, MacKellar D, Gong H, Kamm RD, Wells A, Lauffenburger DA, and Matsudaira P. "Migration of tumor cells in 3D matrices is governed by matrix stiffness along with cell-matrix adhesion and proteolysis." *Proceedings of the National Academy of Sciences of the United States of America* **103** (2006): 10889-10894.
- [370] Finetti F, Basile A, Capasso D, Di Gaetano S, Di Stasi R, Pascale M, Turco CM, Ziche M, Morbidelli L, and D'Andrea LD. "Functional and pharmacological characterization of a VEGF mimetic peptide on reparative angiogenesis." *Biochemical Pharmacology* **84** (2012): 303-311.
- [371] Holmes K, Roberts OL, Thomas AM, and Cross MJ. "Vascular endothelial growth factor receptor-2: Structure, function, intracellular signalling and therapeutic inhibition." *Cellular Signalling* **19** (2007): 2003-2012.
- [372] Koch S, Tugues S, Li X, Gualandi L, and Claesson-Welsh L. "Signal transduction by vascular endothelial growth factor receptors." *Biochemical Journal* **437** (2011): 169-183.
- [373] Anderson SM, Shergill B, Barry ZT, Manousiouthakis E, Chen TT, Botvinick E, Platt MO, Iruela-Arispe ML, and Segura T. "VEGF internalization is not required for VEGFR-2 phosphorylation in bioengineered surfaces with covalently linked VEGF." *Integrative Biology* **3** (2011): 887-896.
- [374] Chen TT, Luque A, Lee S, Anderson SM, Segura T, and Iruela-Arispe ML. "Anchorage of VEGF to the extracellular matrix conveys differential signaling responses to endothelial cells." *The Journal of Cell Biology* **188** (2010): 595-609.
- [375] Lee S, Jilani SM, Nikolova GV, Carpizo D, and Iruela-Arispe ML. "Processing of VEGF-A by matrix metalloproteinases regulates bioavailability and vascular patterning in tumors." *Journal of Cell Biology* **169** (2005): 681-691.
- [376] Ferrara N. "Vascular endothelial growth factor: Basic science and clinical progress." *Endocrine Reviews* **25** (2004): 581-611.
- [377] Eremina V, Baelde HJ, and Quaggin SE. "Role of the VEGF-A signaling pathway in the glomerulus: Evidence for crosstalk between components of the glomerular filtration barrier." *Nephron Physiology* **206** (2007): 32-37.
- [378] Kretzler M, Schröppel B, Merkle M, Huber S, Mundel P, Horster M, and Schlöndorff D. "Detection of multiple vascular endothelial growth factor splice isoforms in single glomerular podocytes." *Kidney International* **54** (1998): S159-S161.
- [379] Aird WC. "Phenotypic heterogeneity of the endothelium: I. Structure, function, and mechanisms." *Circulation Research* **100** (2007): 158-173.

- [380] Aird WC. "Phenotypic heterogeneity of the endothelium: II. Representative vascular beds." *Circulation Research* **100** (2007): 174-190.
- [381] Salinas CN, and Anseth KS. "Mixed mode thiol-acrylate photopolymerizations for the synthesis of PEG-peptide hydrogels." *Macromolecules* **41** (2008): 6019-6026.
- [382] Moon JJ, Saik JE, Poche RA, Leslie-Barbick JE, Lee S-H, Smith AA, Dickinson ME, and West JL. "Biomimetic hydrogels with pro-angiogenic properties." *Biomaterials* **31** (2010): 3840-3847.
- [383] Miller JS, Shen CJ, Legant WR, Baranski JD, Blakely BL, and Chen CS. "Bioactive hydrogels made from step-growth derived PEG-peptide macromers." *Biomaterials* **31** (2010): 3736-3743.
- [384] Van Hove AH, Beltejar M-JG, and Benoit DS. "Development and in vitro assessment of enzymatically-responsive poly(ethylene glycol) hydrogels for the delivery of therapeutic peptides." *Biomaterials* **35** (2014): 9719-9730.
- [385] Van Hove AH, Antonienko E, Burke K, Brown III E, and Benoit DSW. "Temporally tunable, enzymatically responsive delivery of proangiogenic peptides from poly(ethylene glycol) hydrogels." *Advanced Healthcare Materials* **4** (2015): 2002-2011.
- [386] Goktas M, Cinar G, Orujalipour I, Ide S, Tekinay AB, and Guler MO. "Self-assembled peptide amphiphile nanofibers and PEG composite hydrogels as tunable ECM mimetic microenvironment." *Biomacromolecules* **16** (2015): 1247-1258.
- [387] Griffin SV, Petermann AT, Durvasula RV, and Shankland SJ. "Podocyte proliferation and differentiation in glomerular disease: Role of cell-cycle regulatory proteins." *Nephrology Dialysis Transplantation* **18** (2003): vi8-vi13.
- [388] Burlington H, and Cronkite EP. "Characteristics of cell cultures derived from renal glomeruli." *Proceedings of the Society for Experimental Biology and Medicine* **142** (1973): 143-149.
- [389] Fish AJ, Michael AF, Vernier RL, and Brown DM. "Human glomerular cells in tissue culture." *Laboratory Investigation* **33** (1975): 330-341.
- [390] Striker GE, Killen PD, and Farin FM. "Human glomerular cells in vitro: Isolation and characterization." *Transplantation Proceedings* **12** (1980): 88-99.
- [391] Shankland SJ, Pippin JW, Reiser J, and Mundel P. "Podocytes in culture: Past, present, and future." *Kidney International* **72** (2007): 26-36.
- [392] Krtil J, Platenik J, Kazderova M, Tesaf V, and Zima T. "Culture methods of glomerular podocytes." *Kidney and Blood Pressure Research* **30** (2007): 162-174.
- [393] Delarue F, Virone A, Hagege J, Lacave R, Peraldi M-N, Adida C, Rondeau E, Feunteun J, and Sraer J-D. "Stable cell line of T-SV40 immortalized human glomerular visceral epithelial cells." *Kidney International* **40** (1991): 906-912.
- [394] Jat PS, Noble MD, Ataliotis P, Tanaka Y, Yannoutsos N, Larsen L, and Kioussis D. "Direct derivation of conditionally immortal cell lines from an H-2Kb-tsA58 transgenic mouse." *Proceedings of the National Academy of Sciences of the United States of America* **88** (1991): 5096-5100.
- [395] Mundel P, Reiser J, Mejía Borja AZ, Pavenstädt H, Davidson GR, Kriz W, and Zeller R. "Rearrangements of the cytoskeleton and cell contacts induce process formation during

- differentiation of conditionally immortalized mouse podocyte cell lines." *Experimental Cell Research* **236** (1997): 248-258.
- [396] Saleem MA, O'Hare MJ, Reiser J, Coward RJ, Inward CD, Farren T, Xing CY, Ni L, Mathieson PW, and Mundel P. "A conditionally immortalized human podocyte cell demonstrating nephrin and podocin expression." *Journal of the American Society of Nephrology* **13** (2002): 630-638.
- [397] Ni L, Saleem M, and Mathieson PW. "Podocyte culture: Tricks of the trade." *Nephrology* **17** (2012): 525-531.
- [398] Chittiprol S, Chen P, Petrovic-Djergovic D, Eichler T, and Ransom RF. "Marker expression, behaviors, and responses vary in different lines of conditionally immortalized cultured podocytes." *American Journal of Physiology–Renal Physiology* **301** (2011): F660-F671.
- [399] Lee J, Cuddihy MJ, and Kotov NA. "Three-dimensional cell culture matrices: State of the art." *Tissue Engineering Part B: Reviews* **14** (2008): 61-86.
- [400] Laronda MM, Rutz AL, Xiao S, Whelan KA, Duncan FE, Roth EW, Woodruff TK, and Shah RN. "A bioprosthetic ovary created using 3D printed microporous scaffolds restores ovarian function in sterilized mice." *Nature Communications* **8** (2017): 15261.
- [401] Lewis PL, Green RM, and Shah RN. "3D-printed gelatin scaffolds of differing pore geometry modulate hepatocyte function and gene expression." *Acta Biomaterialia* **69** (2018): 63-70.
- [402] Brown BN, and Badylak SF. "Extracellular matrix as an inductive scaffold for functional tissue reconstruction." *Translational Research* **163** (2014): 268-285.
- [403] Seliktar D. "Designing cell-compatible hydrogels for biomedical applications." *Science* **336** (2012): 1124-1128.
- [404] Ferrara N, Gerber H-P, and LeCouter J. "The biology of VEGF and its receptors." *Nature Medicine* **9** (2003): 669.
- [405] Roylance D. *Mechanics of Materials*. Wiley (1996).
- [406] Janmey PA, Georges PC, and Hvidt S. "Basic rheology for biologists." *Methods in Cell Biology* **83** (2007): 1-27.
- [407] Korolj A, Laschinger C, James C, Hu E, Velikonja C, Smith N, Gu I, Ahadian S, Willette R, Radisic M, and Zhang B. "Curvature facilitates podocyte culture in a biomimetic platform." *Lab on a Chip* **18** (2018): 3112-3128.
- [408] Visser J, Levett PA, te Moller NCR, Besems J, Boere KWM, van Rijen MHP, de Grauw JC, Dhert WJA, van Weeren PR, and Malda J. "Crosslinkable hydrogels derived from cartilage, meniscus, and tendon tissue." *Tissue Engineering Part A* **21** (2015): 1195-1206.
- [409] Rothrauff BB, Coluccino L, Gottardi R, Ceseracciu L, Scaglione S, Goldoni L, and Tuan RS. "Efficacy of thermoresponsive, photocrosslinkable hydrogels derived from decellularized tendon and cartilage extracellular matrix for cartilage tissue engineering." *Journal of Tissue Engineering and Regenerative Medicine* **12** (2018): e159-e170.

- [410] Marcu R, Choi YJ, Xue J, Fortin CL, Wang Y, Nagao RJ, Xu J, MacDonald JW, Bammler TK, Murry CE, Muczynski K, Stevens KR, Himmelfarb J, Schwartz SM, and Zheng Y. "Human organ-specific endothelial cell heterogeneity." *iScience* **4** (2018): 20-35.
- [411] Byron A, Humphries JD, and Humphries MJ. "Defining the extracellular matrix using proteomics." *International Journal of Experimental Pathology* **94** (2013): 75-92.
- [412] Lennon R, Byron A, Humphries JD, Randles MJ, Carisey A, Murphy S, Knight D, Brenchley PE, Zent R, and Humphries MJ. "Global analysis reveals the complexity of the human glomerular extracellular matrix." *Journal of the American Society of Nephrology* **25** (2014): 939-951.
- [413] Hill RC, Calle EA, Dzieciatkowska M, Niklason LE, and Hansen KC. "Quantification of extracellular matrix proteins from a rat lung scaffold to provide a molecular readout for tissue engineering." *Molecular & Cellular Proteomics* **14** (2015): 961-973.
- [414] Breslin S, and O'Driscoll L. "Three-dimensional cell culture: The missing link in drug discovery." *Drug Discovery Today* **18** (2013): 240-249.
- [415] Bae H, Puranik AS, Gauvin R, Edalat F, Carrillo-Conde B, Peppas NA, and Khademhosseini A. "Building vascular networks." *Science Translational Medicine* **4** (2012): 160ps123-160ps123.
- [416] Datta P, Ayan B, and Ozbolat IT. "Bioprinting for vascular and vascularized tissue biofabrication." *Acta Biomaterialia* **51** (2017): 1-20.
- [417] Sletten EM, and Bertozzi CR. "Bioorthogonal chemistry: Fishing for selectivity in a sea of functionality." *Angewandte Chemie International Edition* **48** (2009): 6974-6998.
- [418] Kirschner CM, and Anseth KS. "Hydrogels in healthcare: From static to dynamic material microenvironments." *Acta Materialia* **61** (2013): 931-944.
- [419] Gagliardini E, Conti S, Benigni A, Remuzzi G, and Remuzzi A. "Imaging of the porous ultrastructure of the glomerular epithelial filtration slit." *Journal of the American Society of Nephrology* **21** (2010): 2081-2089.
- [420] Burghardt T, Hochapfel F, Salecker B, Meese C, Gröne H-J, Rachel R, Wanner G, Krahn MP, and Witzgall R. "Advanced electron microscopic techniques provide a deeper insight into the peculiar features of podocytes." *American Journal of Physiology-Renal Physiology* **309** (2015): F1082-F1089.
- [421] Ichimura K, Miyazaki N, Sadayama S, Murata K, Koike M, Nakamura K-i, Ohta K, and Sakai T. "Three-dimensional architecture of podocytes revealed by block-face scanning electron microscopy." *Scientific Reports* **5** (2015): 8993.
- [422] Li M, Corbelli A, Watanabe S, Armelloni S, Ikehata M, Parazzi V, Pignatari C, Giardino L, Mattinzoli D, Lazzari L, Puliti A, Cellesi F, Zennaro C, Messa P, and Rastaldi MP. "Three-dimensional podocyte-endothelial cell co-cultures: Assembly, validation, and application to drug testing and intercellular signaling studies." *European Journal of Pharmaceutical Sciences* **86** (2016): 1-12.
- [423] Burg MB. "Introduction: Background and development of microperfusion technique." *Kidney International* **22** (1982): 417-424.
- [424] Dewey CF, Bussolari SR, Gimbrone MA, and Davies PF. "The dynamic response of vascular endothelial cells to fluid shear stress." *Journal of Biomechanical Engineering* **103** (1981): 177-185.

- [425] Davies PF. "Flow-mediated endothelial mechanotransduction." *Physiological Reviews* **75** (1995): 519-560.
- [426] Friedrich C, Endlich N, Kriz W, and Endlich K. "Podocytes are sensitive to fluid shear stress in vitro." *American Journal of Physiology–Renal Physiology* **291** (2006): F856-F865.
- [427] Zhang Y, Yu Y, Chen H, and Ozbolat IT. "Characterization of printable cellular micro-fluidic channels for tissue engineering." *Biofabrication* **5** (2013): 025004.
- [428] Zhang Y, Yu Y, Akkouch A, Dababneh A, Dolati F, and Ozbolat IT. "In vitro study of directly bioprinted perfusable vasculature conduits." *Biomaterials Science* **3** (2015): 134-143.
- [429] Jia W, Gungor-Ozkerim PS, Zhang YS, Yue K, Zhu K, Liu W, Pi Q, Byambaa B, Dokmeci MR, Shin SR, and Khademhosseini A. "Direct 3D bioprinting of perfusable vascular constructs using a blend bioink." *Biomaterials* **106** (2016): 58-68.
- [430] Song B, Smink AM, Jones CV, Callaghan JM, Firth SD, Bernard CA, Laslett AL, Kerr PG, and Ricardo SD. "The directed differentiation of human iPS cells into kidney podocytes." *PLOS ONE* **7** (2012): e46453.
- [431] Ciampi O, Iacone R, Longaretti L, Benedetti V, Graf M, Magnone MC, Patsch C, Xinaris C, Remuzzi G, Benigni A, and Tomasoni S. "Generation of functional podocytes from human induced pluripotent stem cells." *Stem Cell Research* **17** (2016): 130-139.
- [432] Yoshimura Y, Taguchi A, Tanigawa S, Yatsuda J, Kamba T, Takahashi S, Kurihara H, Mukoyama M, and Nishinakamura R. "Manipulation of nephron-patterning signals enables selective induction of podocytes from human pluripotent stem cells." *Journal of the American Society of Nephrology* **30** (2019): 304-321.
- [433] Mehta RL, Pascual MT, Soroko S, Savage BR, Himmelfarb J, Ikizler TA, Paganini EP, and Chertow GM. "Spectrum of acute renal failure in the intensive care unit: The PICARD experience." *Kidney International* **66** (2004): 1613-1621.
- [434] Pannu N, and Nadim MK. "An overview of drug-induced acute kidney injury." *Critical Care Medicine* **36** (2008): S216-S223.
- [435] Naughton CA. "Drug-induced nephrotoxicity." *American Family Physician* **78** (2008):
- [436] Dahlgren JG, Anderson ET, and Hewitt WL. "Gentamicin blood levels: A guide to nephrotoxicity." *Antimicrobial Agents and Chemotherapy* **8** (1975): 58-62.
- [437] Pabla N, and Dong Z. "Cisplatin nephrotoxicity: Mechanisms and renoprotective strategies." *Kidney International* **73** (2008): 994-1007.
- [438] Irvine JD, Takahashi L, Lockhart K, Cheong J, Tolan JW, Selick H, and Grove JR. "MDCK (Madin-Darby canine kidney) cells: A tool for membrane permeability screening." *Journal of Pharmaceutical Sciences* **88** (1999): 28-33.
- [439] Uzarski JS, Bijonowski BM, Wang B, Ward HH, Wandinger-Ness A, Miller WM, and Wertheim JA. "Dual-purpose bioreactors to monitor noninvasive physical and biochemical markers of kidney and liver scaffold recellularization." *Tissue Engineering Part C: Methods* **21** (2015): 1032-1043.

- [440] Uzarski JS, Su J, Xie Y, Zhang ZJ, Ward HH, Wandinger-Ness A, Miller WM, and Wertheim JA. "Epithelial cell repopulation and preparation of rodent extracellular matrix scaffolds for renal tissue development." *Journal of Visualized Experiments* (2015): e53271.
- [441] Reiser J, Gupta V, and Kistler AD. "Toward the development of podocyte-specific drugs." *Kidney International* **77** (2010): 662-668.
- [442] Montesano R, Schaller G, and Orci L. "Induction of epithelial tubular morphogenesis in vitro by fibroblast-derived soluble factors." *Cell* **66** (1991): 697-711.
- [443] Montesano R, Matsumoto K, Nakamura T, and Orci L. "Identification of a fibroblast-derived epithelial morphogen as hepatocyte growth factor." *Cell* **67** (1991): 901-908.
- [444] Lewis PL, Su J, Yan M, Meng F, Glaser SS, Alpini GD, Green RM, Sosa-Pineda B, and Shah RN. "Complex bile duct network formation within liver decellularized extracellular matrix hydrogels." *Scientific Reports* **8** (2018): 12220.
- [445] Lewis PL, Yan M, Su J, and Shah RN. "Directing the growth and alignment of biliary epithelium within extracellular matrix hydrogels." *Acta Biomaterialia* **85** (2019): 84-93.

**CHAPTER VI:**

**Appendices**

## **6.1. Appendix A: Dose-Dependent Cytotoxicity of Gentamicin and Cisplatin on Madin-Darby Canine Kidney (MDCK) Cells Measured by the Resazurin Reduction Assay**

### **6.1.1. Introduction**

It is estimated that the nephrotoxic, or kidney damaging, side effects of drugs cause 20-30% of acute kidney injury cases for hospitalized patients in intensive care units<sup>[433]</sup>. The mechanisms by which nephrotoxicity occurs varies considerably, but in many instances, drugs must pass through the kidneys in order to be excreted and thus exert direct toxic effects on the kidney tubules<sup>[434]</sup>. Several drugs have been identified that may potentially cause patient nephrotoxic side effects<sup>[435]</sup>, including the aminoglycoside antibiotic gentamicin<sup>[436]</sup> and the chemotherapeutic cisplatin<sup>[437]</sup>. Towards developing superior *in vitro* models for understanding and evaluating nephrotoxicity, it is necessary to establish baseline toxicity of known nephrotoxic agents on kidney cells. Here, we investigated the dose-dependent cytotoxic effects of gentamicin and cisplatin on distal tubule-derived Madin-Darby canine kidney (MDCK) cell<sup>[438]</sup> number in culture via a metabolic activity assay.

### **6.1.2. Materials & Methods**

*Madin-Darby Canine Kidney Cell Culture.* MDCK cells were maintained in a 1:1 mixture of Dulbecco's Modified Eagle Medium and Ham's F-12 (Gibco, #11320) supplemented with 10% fetal bovine serum (Gibco, #16000), and 1% penicillin-streptomycin (Gibco, #15140) at 37 °C and 5% CO<sub>2</sub>. Media was exchanged every two to three days, and cells were used at passage 45 or below for experimental studies. Cells were plated in tissue culture-treated 24-well plates (Corning, #3527) or 96-well plates (Corning #3585) at an approximate density of 15,500 cells/cm<sup>2</sup> one day prior to treatment. To dissociate cells, cells were rinsed once with 1× Dulbecco's phosphate-buffered saline (DPBS, Mediatech, #21-030) and incubated with TrypLE Express (Gibco, #12605) at 37 °C for 10-15 min. TrypLE Express was deactivated with excess cell culture media, and detached cells were collected and counted via the trypan blue exclusion method using Trypan Blue solution (Sigma-Aldrich, #T8154). Cells were centrifuged at 1100 RPM for 5 min and resuspended in complete media at the desired cell concentration.

*Treatments and Evaluation of Cell Metabolic Activity as a Surrogate for Cell Number.* Cells were treated with gentamicin (Gibco, #15750) at the following concentrations: 0.00, 0.25, 0.50, 1.00, 2.50, 5.00, 10.00, and 20.00 mM for up to 10 days. Cisplatin (Sigma-Aldrich, #1134357) was prepared as a 1.0 mM stock solution in DPBS, and cells were treated with cisplatin at the following concentrations: 0.00, 0.01, 0.10, 1.00, 10.00, and 100.00  $\mu$ M for up to 14 days. Cell metabolic activity as a surrogate for cell number was measured by the resazurin reduction assay. A 10 $\times$  (4400  $\mu$ M) resazurin stock solution was first prepared by dissolving resazurin sodium salt (Sigma-Aldrich, #R7017) in DPBS. The 10 $\times$  stock solution was then sterile filtered through a polyethersulfone mesh with a pore size of 0.22  $\mu$ m (EMD Millipore, #SCGP00525) and used to prepare a 1 $\times$  stock solution in DPBS. Both 10 $\times$  and 1 $\times$  stock solutions were stored at 4 °C protected from light for up to two weeks. Resazurin working solutions (44  $\mu$ M) were prepared fresh by diluting 1 $\times$  resazurin stock solution in complete media (1:10 dilution). Culture media was aspirated from wells and replaced with resazurin working solution for 1 h at 37 °C and 5% CO<sub>2</sub>, after which the reduced resazurin was collected and replaced with fresh medium. Reduced resazurin was transferred to black, opaque 96-well plates (Corning, #3915), and fluorescence intensity was measured on a BioTek Cytation 3 Cell-Imaging Multi-Mode Reader at an excitation wavelength of 540 nm and an emission wavelength of 590 nm. Gain was determined automatically by including a completely reduced, positive control of resorufin solution prepared by autoclaving resazurin working solution at 121 °C for 30 min. Fluorescence intensities were normalized to unreduced, negative controls, and correlated to cell number using a standard curve of separately plated cells established on day 1. Biological samples were tested in triplicate ( $n = 3$ ). All data is presented as the mean  $\pm$  standard error of the mean.

### 6.1.3. Results & Discussion

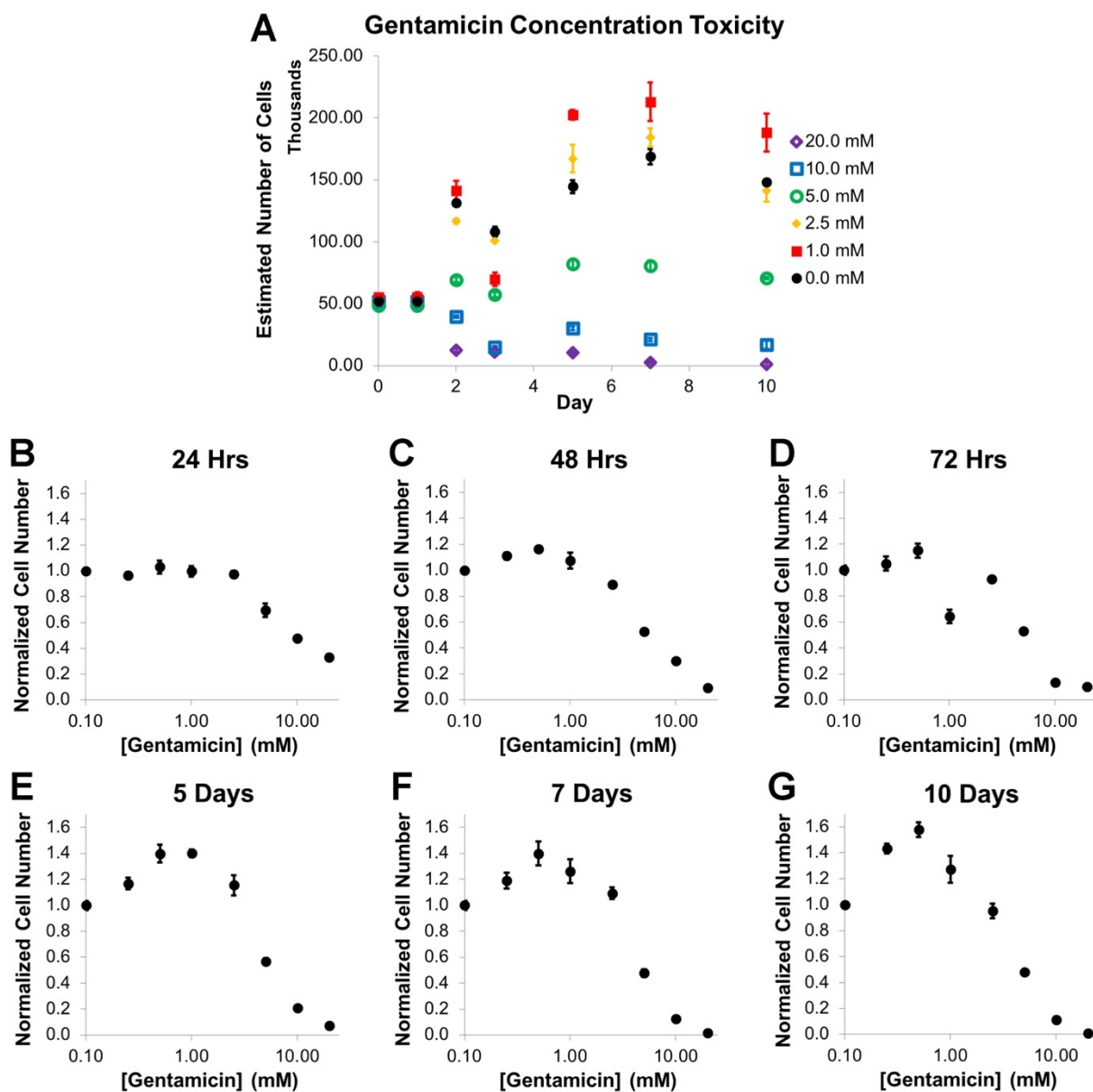


**Figure 6-1: Estimated MDCK cell number after continuous treatment with gentamicin.**

(A) Cell number plotted against time for varying concentrations of gentamicin. Semi-log plots of dose-response relationships between normalized cell number and gentamicin concentration after (B) 24 h, (C) 48 h, (D) 72 h, (E) 5 days, (F) 7 days, and (G) 10 days of continuous treatment.

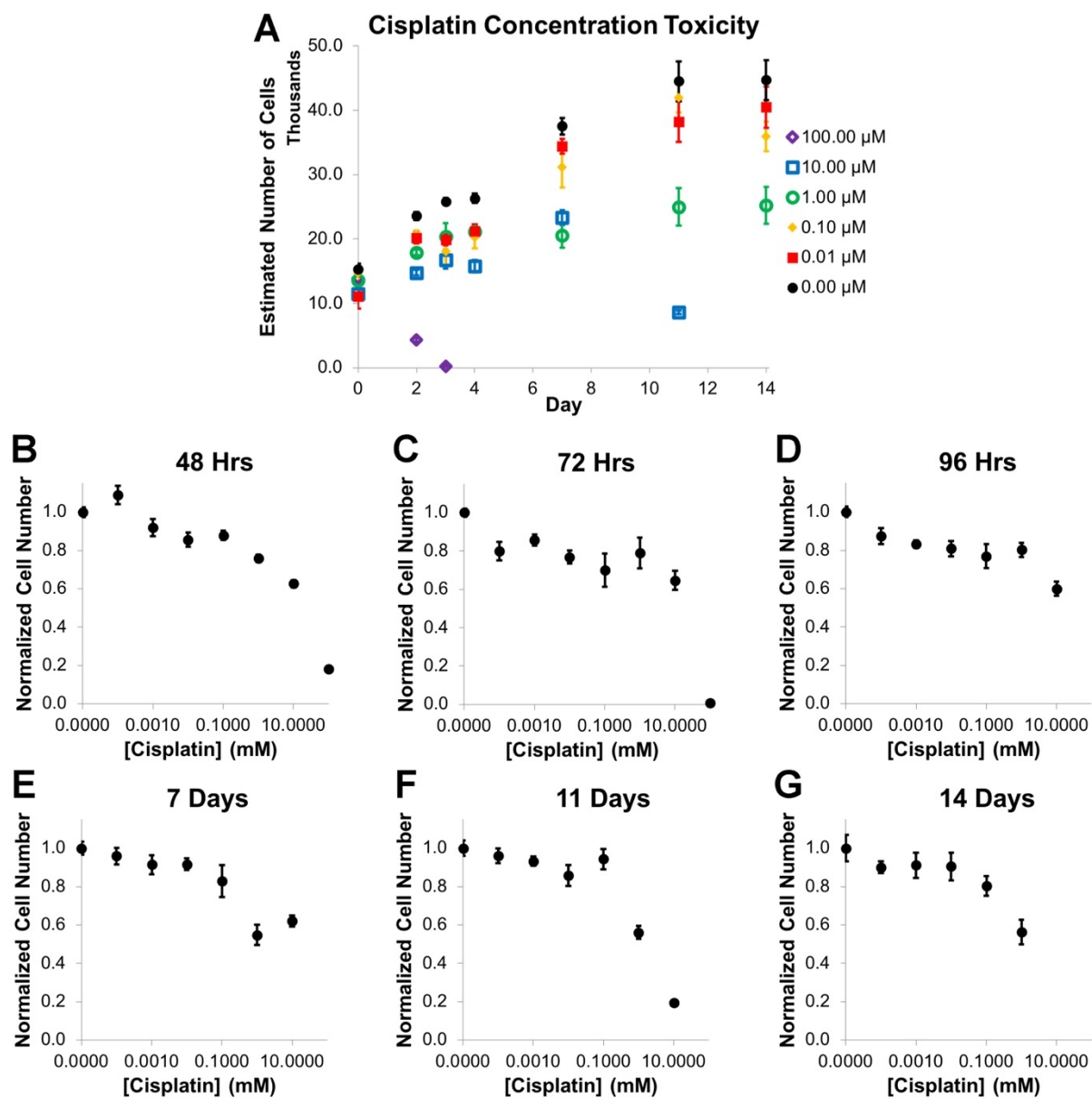


**Figure 6-2: Estimated MDCK cell number after continuous treatment with cisplatin.**

(A) Cell number plotted against time for varying concentrations of cisplatin. Semi-log plots of dose-response relationships between normalized cell number and cisplatin concentration after (B) 48 h, (C) 72 h, (D) 96 h, (E) 7 days, (F) 11 days, and (G) 14 days of continuous treatment. Biological samples were tested in triplicate ( $n = 3$ ).

Treatment of MDCK cells with gentamicin resulted in dose-dependent reductions in estimated cell numbers. Gentamicin concentrations of 2.5 mM and lower did not appear detrimental to cell health as estimated cell numbers were similar to if not somewhat higher than untreated controls at all time points

**(Figure 6-1 A)**. Cytotoxic effects of gentamicin were observed at concentrations of 5.0 mM and higher, and sigmoidal dose-response relationships were visualized on semi-log plots (**Figure 6-1 B-G**) with the relationships becoming more distinct with extended treatment times. Similarly, treatment of MDCK cells with cisplatin resulted in dose-dependent reductions in estimated cell numbers. Cisplatin concentrations of 0.10  $\mu$ M and lower did not appear detrimental to cell health (**Figure 6-2 A**). Cytotoxic effects of cisplatin were observed at concentrations of 1.00  $\mu$ M and higher with complete cell death by day 4 for cells exposed to 100.00  $\mu$ M and by day 14 for cells exposed to 10.00  $\mu$ M cisplatin. Sigmoidal dose-response relationships were again visualized on semi-log plots (**Figure 6-2 B-G**). These results demonstrate that MDCK cells, a distal tubular epithelial cell line, are sensitive to exposure by the known nephrotoxic agents gentamicin and cisplatin in a dose-dependent manner. With this knowledge and the concentrations established here, future investigations may explore susceptibility of bioengineered kidney tissues to injury by these agents towards developing superior models for drug screening and nephrotoxicity testing.

## **6.2. Appendix B: Evaluation of Madin-Darby Canine Kidney (MDCK) Cells Cultured on Kidney Decellularized Extracellular Matrix Scaffolds**

### **6.2.1. Introduction**

Kidney decellularized extracellular matrix (dECM) scaffolds have received increasing attention as a platform for developing bioengineered, transplantable kidneys<sup>[181]</sup>. The extracellular matrix acts as a natural scaffold material with tissue- and organ-specific compositions and structural architectures to support cell growth and maturation<sup>[303]</sup>. Previous research has demonstrated that rat kidney dECM scaffolds support attachment and proliferation of the distal tubule-derived Madin-Darby canine kidney (MDCK) epithelial cell line, and that cells lined and formed tubule-like structures<sup>[182, 439, 440]</sup>. Beyond the clinical need of bioengineered kidneys for transplantation, there is a broader need for bioengineered kidney tissues as *in vitro* models for drug development and nephrotoxicity testing. Here, we investigated the ability of rat kidney dECM scaffold disks in supporting MDCK cell adhesion and promoting formation of epithelial structures towards potential applications in higher throughput screens and assays.

### **6.2.2. Materials & Methods**

*Rat Kidney Recovery.* Rat kidney recovery and decellularization were performed as described previously<sup>[182, 440]</sup>. Kidneys were recovered from male Sprague Dawley rats (200-250 g) by the Northwestern University Comprehensive Transplant Center Microsurgery Core following guidelines approved by the Northwestern Institutional Animal Care and Use Committee (IACUC) as described previously. Rats were anesthetized using intraperitoneal injection of pentobarbital (50 mg/kg), and a longitudinal midline incision was performed to open the abdomen. The abdominal aorta and the inferior vena cava were dissected from above the right renal hilum to the iliac bifurcation, and the ureter was dissected at the urinary bladder. Two hundred units of heparin were injected through the penile vein. The abdominal aorta was ligated above the renal arteries, followed by cannulation of both infrarenal abdominal aorta with a 18G catheter (BD Biosciences, #381447). Both kidneys were perfused with cold saline through the infrarenal cannula. After perfusion, renal arteries and veins were transected and the kidneys were removed. Kidney renal arteries

were cannulated with 24G catheters (BD Biosciences, #381412) and frozen in 1× Dulbecco's phosphate-buffered saline (DPBS, Corning, #21-030) and stored at -20 or -80 °C until decellularization.

*Rat Kidney Decellularization.* Rat kidneys were thawed and decellularized by sequential perfusion of the following solutions using a Cole-Parmer MasterFlex L/S peristaltic pump: 500 mL deionized H<sub>2</sub>O (1 mL/min), 1000 mL 1% (v/v) Triton X-100 (Amresco, #0694) in deionized H<sub>2</sub>O (5 mL/min), 1000 mL 1% (v/v) Triton X-100 in deionized H<sub>2</sub>O (1 mL/min), 1000 mL 0.1% (v/v) sodium dodecyl sulfate (Sigma-Aldrich, #05030) in deionized H<sub>2</sub>O (5 mL/min), and 500 mL deionized H<sub>2</sub>O (1 mL/min). Decellularized kidneys were stored in DPBS at 4 °C for up to two weeks before embedding in Tissue-Tek Optimal Cutting Temperature Compound (Sakura, 4583) with Peel-A-Way disposable embedding molds (Polysciences, #18646B-1) using a bath of liquid N<sub>2</sub>-chilled 2-methylbutane (EMD Millipore, #MX0760) and stored at -20 or -80 °C. Frozen kidney dECM sections, ~1 mm thick, were prepared on a Thermo Scientific HM525 NX Cryostat, and kidney dECM disks were punched from sections with an 8-mm biopsy punch (Integra Miltex, #33-37) and stored in DPBS at 4 °C for up to one week. Prior to seeding, disk scaffolds were sterilized in 0.1% (v/v) peracetic acid (Sigma-Aldrich, #269336) and 4% (v/v) ethanol (Decon Laboratories, #2701) in deionized H<sub>2</sub>O for 1 h, rinsed three times with excess sterile DPBS for 1 h each, and conditioned in complete culture medium for 1 h.

*Madin-Darby Canine Kidney (MDCK) Cell Culture and Scaffold Seeding.* MDCK cells were maintained in a 1:1 mixture of Dulbecco's Modified Eagle Medium and Ham's F-12 (Gibco, #11320) supplemented with 10% fetal bovine serum (Gibco, #16000), and 1% penicillin-streptomycin (Gibco, #15140) at 37 °C and 5% CO<sub>2</sub>. Media was exchanged every two to three days, and cells were used at passage 45 or below for experimental studies. To prepare cells for seeding, cells were rinsed once with DPBS and incubated with TrypLE Express (Gibco, #12605) at 37 °C for 10-15 min to dissociate cells. TrypLE Express was deactivated with excess cell culture media, and detached cells were collected and counted via the trypan blue exclusion method using Trypan Blue solution (Sigma-Aldrich, #T8154). Cells were centrifuged at 1100 RPM for 5 min and resuspended in complete media at the desired cell concentration. Cells were then seeded onto scaffolds under static or dynamic conditions. For static conditions, concentrated cell suspensions of 2.5, 5.0, or 10.0 × 10<sup>5</sup> cells in 200 µL were added to scaffolds

placed in 96-well, clear, round-bottom plates (Corning, #3879), and cells were allowed to attach for at least 5 h before being transferred to larger well plates. For dynamic conditions, concentrated cell suspensions of  $2.5 \times 10^5$  cells in 500  $\mu$ L and two scaffolds placed in 50 mL Mini Bioreactor centrifuge tubes with vent caps (Corning, #431720) and rotated at an angle on a SCILOGEX MX-RL-E Analog Rotisserie Tube Rotator.

*Sample Processing and Imaging.* Samples were fixed in 10% neutral-buffered formalin (Thermo Scientific, #5701) for at least 48 h before paraffin embedding and sectioning. For histological analysis, sections were deparaffinized in xylene (Fisher Scientific, #X3P) and rehydrated prior to staining with Mayer's hematoxylin solution (Sigma-Aldrich, #MHS) and eosin Y solution (Sigma-Aldrich, #HT110132). After staining, #1 glass coverslips (Fisher Scientific, #12-542B or #12-545D) were mounted with Richard-Allan Scientific Cytoseal XYL (Thermo Scientific, #8312-4), and slides were imaged on a Zeiss Axioskop upright microscope mounted with an AxioCam MRc5 camera using AxioVision 4.8.3 software. For immunofluorescence, sections were deparaffinized in xylene and rehydrated prior to antigen retrieval in a BioCare Medical Decloaking Chamber NxGen (model no. DC2012) at 110 °C for 15 min with antigen retrieval buffer (Abcam, #ab94674). Sections were then outlined with an Aqua-Hold2 Pap Pen (Scientific Device Laboratory, #2886909), rinsed with 1 $\times$  phosphate-buffered saline (PBS, Mediatech, #21-040), permeabilized with 0.05% (v/v) TWEEN-20 (Sigma-Aldrich, #P9416) in PBS for 10 min, and then blocked with SEA BLOCK Blocking Buffer (Thermo Scientific, #37527) for 30 min. Primary antibodies were diluted in blocking buffer as follows: goat anti-E-cadherin at 1:20 (R&D Systems, #AF648) and mouse anti-acetylated  $\alpha$  tubulin at 1:1000 (Sigma-Aldrich, #T7451). Sections were incubated with primary antibodies at 4 °C overnight in a humidified chamber, rinsed with PBS, and then incubated with secondary antibodies for 1 h at 37 °C in a humidified chamber. Secondary antibodies were diluted 1:300 in blocking buffer: donkey anti-goat Alexa Fluor 488 (Invitrogen, #A-11055) and donkey anti-mouse Alexa Fluor 555 (Invitrogen, #A-31570). After secondary antibody incubation, sections were rinsed with PBS, cell nuclei were stained with 300 nM 4',6'-diamidino-2-phenylindole (DAPI, Invitrogen, #D1306) in PBS for 2 min, and sections were rinsed again. Coverslips were mounted with Mowiol mounting medium containing Mowiol 4-88 Reagent (Calbiochem, #475904), glycerol (EMD Millipore, #137028), and 0.2 M Tris buffer (pH 8.5, Fisher Scientific, #BP152). Slides were imaged on a Nikon C2+ confocal microscope.

### 6.2.3. Results & Discussion

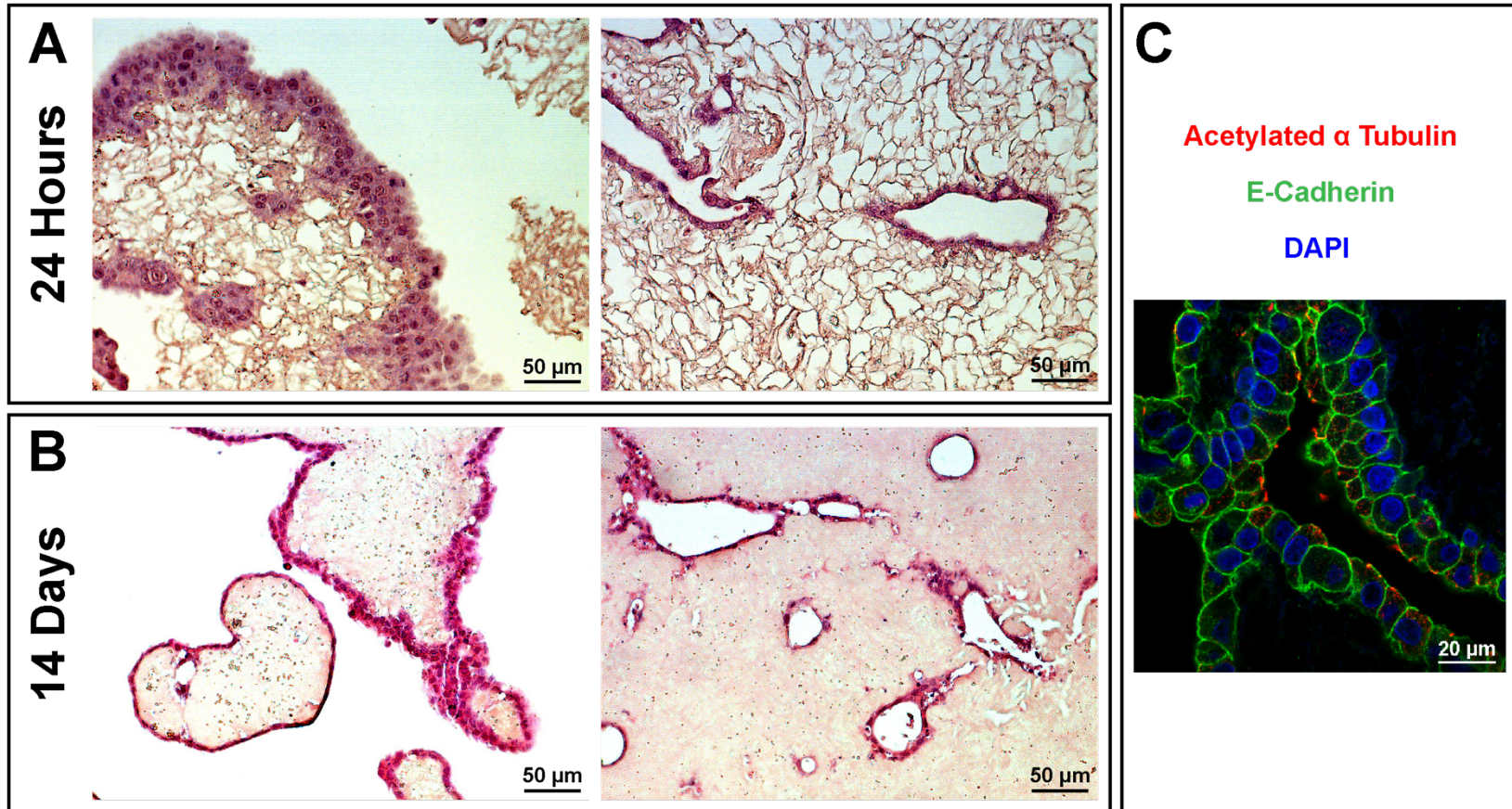


**Figure 6-3: Histological analysis and immunofluorescence staining of MDCK cells cultured on kidney dECM scaffold disks.** Histological analysis via hematoxylin and eosin staining of samples cultured for (A) 24 h and (B) 14 days. (C) Immunofluorescence staining for acetylated  $\alpha$  tubulin (red), E-cadherin (green), and cell nuclei via DAPI (blue) of sample after 24 h in culture.

Kidney dECM scaffold disks promoted adhesion of MDCK cells seeded under static or dynamic conditions. At early time points, cells appeared to form multi-layered structures lining the outer perimeter and inner tube-like structures of scaffolds (**Figure 6-3 A**). After extended culture, these multi-layered structures appeared to thin as cells adopted a flatter, more epithelial-like morphology (**Figure 6-3 B**). In addition, the inner structure of scaffolds appeared more compact and denser. No infiltration of cells was observed at either early or late time points. Immunofluorescence staining of samples culture for 24 h revealed strong expression of the cell adhesion molecule E-cadherin as well as expression of cilia labeled by acetylated  $\alpha$  tubulin (**Figure 6-3 C**); however, staining also revealed the lack of a distinct, well-defined columnar morphology that is typical of epithelial structures.

These results demonstrate that rat kidney dECM scaffold disks promote MDCK cell attachment and functional protein expression, but additional investigations are necessary to optimize conditions that promote maturation of epithelial structures. For example, immunofluorescence staining of samples cultured for longer durations may demonstrate the need for a maturation period before a well-defined columnar morphology is adopted. Further functional characterization may include visualization of apical-basal polarity of cells and evaluation of appropriate ion or molecule transport. Future studies may explore modifications to the dECM scaffold disk preparation or dECM itself to promote specific cell-matrix interactions or enable cell infiltration.

### **6.3. Appendix C: Evaluation of Conditionally-Immortalized Human Podocytes Cultured on Kidney Decellularized Extracellular Matrix Scaffolds**

#### **6.3.1. Introduction**

Between 2012 and 2016, glomerular disease was the leading cause of end-stage renal disease in pediatric patients<sup>[57]</sup>. While glomerular diseases may result from a variety of genetic or environmental factors, it is believed that podocytes, and specifically injury to podocytes, play a central role in the progression of glomerular diseases<sup>[24]</sup>. For decades, researchers have investigated the unique characteristics of podocytes through both animal models<sup>[294]</sup> and *in vitro* culture of human podocytes<sup>[391]</sup> with applications toward the development of drugs specifically targeting this exceptional cell population<sup>[441]</sup>. However, animal models do not always emulate human physiology and disease<sup>[297]</sup> whereas traditional cell culture techniques rely on rigid, 2D substrates that are quite dissimilar to native microenvironment<sup>[399]</sup>. In physiological contexts, the extracellular matrix acts as a natural scaffold material with tissue- and organ-specific compositions and structural architectures to support cell growth and maturation<sup>[303]</sup>. Therefore, here we aimed to investigate kidney decellularized extracellular matrix (dECM) scaffold disks as culture platforms to support human podocyte attachment and viability.

#### **6.3.2. Materials & Methods**

*Rat Kidney Recovery.* Rat kidney recovery and decellularization were performed as described previously<sup>[182, 440]</sup>. Kidneys were recovered from male Sprague Dawley rats (200-250 g) by the Northwestern University Comprehensive Transplant Center Microsurgery Core following guidelines approved by the Northwestern Institutional Animal Care and Use Committee (IACUC) as described previously. Rats were anesthetized using intraperitoneal injection of pentobarbital (50 mg/kg), and a longitudinal midline incision was performed to open the abdomen. The abdominal aorta and the inferior vena cava were dissected from above the right renal hilum to the iliac bifurcation, and the ureter was dissected at the urinary bladder. Two hundred units of heparin were injected through the penile vein. The abdominal aorta was ligated above the renal arteries, followed by cannulation of both infrarenal abdominal aorta with a 18G catheter (BD Biosciences, #381447). Both kidneys were perfused with cold saline through the infrarenal cannula. After

perfusion, renal arteries and veins were transected and the kidneys were removed. Kidney renal arteries were cannulated with 24G catheters (BD Biosciences, #381412) and frozen in 1× Dulbecco's phosphate-buffered saline (DPBS, Corning, #21-030) and stored at -20 or -80 °C until decellularization.

*Rat Kidney Decellularization.* Rat kidneys were thawed and decellularized by sequential perfusion of the following solutions using a Cole-Parmer MasterFlex L/S peristaltic pump: 500 mL deionized H<sub>2</sub>O (1 mL/min), 1000 mL 1% (v/v) Triton X-100 (Amresco, #0694) in deionized H<sub>2</sub>O (5 mL/min), 1000 mL 1% (v/v) Triton X-100 in deionized H<sub>2</sub>O (1 mL/min), 1000 mL 0.1% (v/v) sodium dodecyl sulfate (Sigma-Aldrich, #05030) in deionized H<sub>2</sub>O (5 mL/min), and 500 mL deionized H<sub>2</sub>O (1 mL/min). Decellularized kidneys were stored in DPBS at 4 °C for up to two weeks before embedding in Tissue-Tek Optimal Cutting Temperature Compound (Sakura, 4583) with Peel-A-Way disposable embedding molds (Polysciences, #18646B-1) using a bath of liquid N<sub>2</sub>-chilled 2-methylbutane (EMD Millipore, #MX0760) and stored at -20 or -80 °C. Frozen kidney dECM sections, ~1 mm thick, were prepared on a Thermo Scientific HM525 NX Cryostat, and kidney dECM disks were punched from sections with an 8-mm biopsy punch (Integra Miltex, #33-37) and stored in DPBS at 4 °C for up to one week. Prior to seeding, disk scaffolds were sterilized in 0.1% (v/v) peracetic acid (Sigma-Aldrich, #269336) and 4% (v/v) ethanol (Decon Laboratories, #2701) in deionized H<sub>2</sub>O for 1 h, rinsed three times with excess sterile DPBS for 1 h each, and conditioned in complete culture medium for 1 h.

*Podocyte Culture.* Conditionally-immortalized human podocytes were cultured as described previously<sup>[396]</sup>. These are primary cells that have been transfected with a temperature-sensitive *SV40-T* antigen and the essential catalytic subunit of human telomerase (*hTERT*) to prevent replicative senescence<sup>[319, 396]</sup>. Culture at the permissive temperature of 33 °C results in active expression of the transgenes to maintain an immature cell state and allow proliferation of the cells. Thermoswitching to the non-permissive temperature of 37 °C results in inactivation of the transgenes, causing the cells to become quiescent and adopt a more mature phenotype [2002 Saleem]. Podocytes were expanded in RPMI 1640 (Gibco, #11875) supplemented with 10% fetal bovine serum (FBS, Gibco, #16000), 1% penicillin-streptomycin (Gibco, #15140), and 1% insulin-transferrin-sodium selenite (ITS Liquid Media Supplement, Sigma-Aldrich, #13146) at 33 °C and 5% CO<sub>2</sub>. During experimental studies, cells were thermoswitched as

indicated to 37 °C and 5% CO<sub>2</sub> in RPMI 1640 supplemented with 10% FBS and 1% penicillin-streptomycin. Media was exchanged every two to three days, and cells were used at passage 21 for experimental studies.

*Scaffold Seeding.* To prepare cells for seeding, cells were rinsed once with DPBS and incubated with TrypLE Express (Gibco, #12605) at 33 °C for 5 min to dissociate cells. TrypLE Express was deactivated with excess cell culture media, and detached cells were collected and counted via the trypan blue exclusion method using Trypan Blue solution (Sigma-Aldrich, #T8154). Cells were centrifuged at 1200 RPM for 5 min and resuspended in complete media at the desired cell concentration. Cells were then seeded onto scaffolds as concentrated cell suspensions of  $1.0 \times 10^5$  cells in 300  $\mu$ L were added to scaffolds placed in 96-well, clear, round-bottom plates (Corning, #3879), and cells were allowed to attach for at least 5 h before being transferred to tissue culture-treated 24-well plates (Corning, #3527). Cells were thermoswitched from the permissive to the non-permissive temperature after 7 days in culture.

*Sample Processing and Imaging.* Cell viability was evaluated using the LIVE/DEAD Assay Viability/Cytotoxicity Kit for Mammalian Cells (Invitrogen, #L3224) following the manufacturer's protocol. Briefly, samples were transferred to glass-bottom microwell dishes (MatTek, #P35G-1.0-14-C), rinsed once with DPBS, incubated with 4  $\mu$ M ethidium homodimer and 2  $\mu$ M calcein in DPBS for 30 min at 37 °C, and then rinsed once more with DPBS before imaging on a Nikon C2+ confocal microscope. For histological analysis, samples were fixed in 10% neutral-buffered formalin (Thermo Scientific, #5701) for at least 48 h before paraffin embedding and sectioning. Sections were deparaffinized in xylene (Fisher Scientific, #X3P) and rehydrated prior to staining with Mayer's hematoxylin solution (Sigma-Aldrich, #MHS) and eosin Y solution (Sigma-Aldrich, #HT110132). After staining, #1 glass coverslips (Fisher Scientific, #12-542B or #12-545F) were mounted with Richard-Allan Scientific Cytoseal XYL (Thermo Scientific, #8312-4), and slides were imaged on a Zeiss Axioskop upright microscope mounted with an AxioCam MRc5 camera using AxioVision 4.8.3 software. For transmission electron microscopy (TEM), samples were fixed in 2.5% (v/v) glutaraldehyde (Sigma-Aldrich, #G7776) and 3% (m/v) sucrose (J. T. Baker, #4072-01) for 1 h at room temperature, post-fixed with 1% osmium tetroxide for 1 h then 1% uranyl acetate in maleate buffer for an additional hour, dehydrated in a graded ethanol and propylene oxide series, and embedded in Epon (polymerized at 60 °C for 48 h). Ultrathin sections were visualized with an FEI Tecnai Spirit G2 TEM.

### **6.3.3. Results & Discussion**

Podocytes cultured on kidney dECM scaffold disks exhibited good cell viability over the extended 21-day culture period (**Figure 6-4**), however, cells appeared inhomogeneously distributed across scaffolds. Sectioning of samples and histological analysis suggested some cell infiltration of scaffolds but relatively low cell densities and, again, an inhomogeneous distribution of cells (**Figure 6-4**). TEM of samples demonstrated close podocyte-matrix interactions with scaffolds, but prototypical podocyte morphologies (*i.e.*, main cell body and processes) were not observed (**Figure 6-4**). Therefore, kidney dECM scaffold disks supported podocyte attachment and preserved cell viability; however, additional investigations evaluating podocyte-specific response in comparison to controls is necessary. Although prototypical podocyte morphologies were not observed, gene and protein expression analysis for relevant cell-matrix and slit diaphragm components may reveal an enhanced podocyte phenotype when cultured on kidney dECM scaffolds. Future studies may also explore the possibility of isolating glomerular-specific dECM, including the glomerular basement membrane, or targeting cells to glomerular regions in scaffolds for investigating podocyte-matrix interactions.

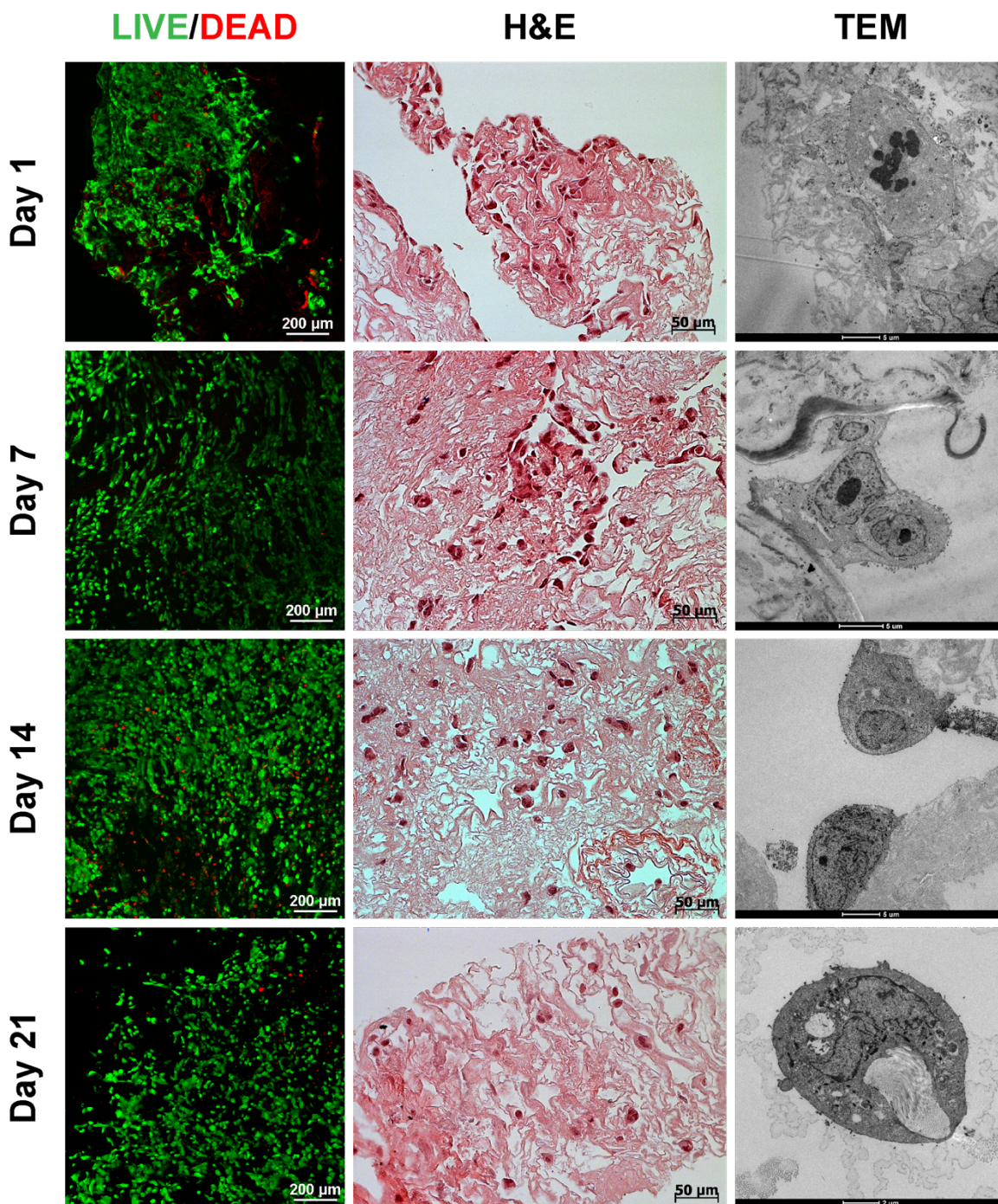


**Figure 6-4: Viability staining, histological analysis, and transmission electron micrographs of human podocytes cultured on kidney dECM scaffold disks.**

LIVE/DEAD viability staining and confocal imaging of samples at indicated time points where live or viable cells are labeled in green and dead cell nuclei are labeled in red. Histological analysis via hematoxylin and eosin (H&E) staining of samples at indicated time points. Transmission electron micrographs (TEM) of samples at indicated time points. Podocytes were cultured at the permissive temperature for the first 7 days and thermoswitched thereafter to the non-permissive temperature.

## **6.4. Appendix D: Viability Staining of Madin-Darby Canine Kidney (MDCK) Cells Encapsulated Within Kidney Decellularized Extracellular Matrix (dECM) Hydrogels**

### **6.4.1. Introduction**

Madin-Darby canine kidney (MDCK) cells are distal tubule-derived epithelial cells that have been utilized in a variety of cell biology investigations<sup>[438]</sup>. When encapsulated and cultured in a 3D extracellular matrix microenvironment such as type I collagen hydrogels, MDCK cells reproducibly form cyst structures and exhibit basolateral polarization<sup>[283]</sup>. Such systems have advanced understanding of epithelial development and morphogenesis. To induce the formation of branching tubules from cysts, MDCK cells must be exposed to additional signaling factors typically provided exogenously<sup>[442, 443]</sup>. In Chapter 2 and published elsewhere<sup>[288]</sup>, we described the development and characterization of kidney decellularized extracellular matrix (dECM) hydrogels suitable for cell culture and encapsulation. These hydrogels are formulated from a complex mixture of kidney-specific proteins, polysaccharides, and other components retained after decellularization. Here, we investigated the capacity of these kidney dECM hydrogels to promote epithelial morphogenesis by encapsulated MDCK cells through viability staining and confocal imaging of samples.

### **6.4.2. Materials & Methods**

*Kidney Decellularization.* Porcine kidneys were decellularized as described previously in Chapter 2 and published elsewhere<sup>[288]</sup>. Female Yorkshire pig (3-4 months in age) kidneys were obtained fresh from Northwestern Simulation (Northwestern University Feinberg School of Medicine) following approval by the Northwestern Institutional Animal Care and Use Committee (IACUC) and stored at -80 °C until decellularization. Prior to decellularization, kidneys were thawed for several hours in warm water and then minced into pieces approximately 0.5 × 0.5 × 0.25 cm in size with a clean razor blade. During this process, the majority of the renal pelvis and perirenal fat was removed. Kidney tissue pieces were then rinsed with deionized H<sub>2</sub>O under constant stirring for one day at room temperature with intermittent H<sub>2</sub>O changes. After rinsing, kidney pieces were treated with 0.1% (m/v) sodium dodecyl sulfate (Sigma-Aldrich, #L3771) under constant stirring for two days. Afterwards, decellularized kidney pieces were rinsed with deionized H<sub>2</sub>O

under constant stirring for one day with intermittent H<sub>2</sub>O changes to ensure removal of residual detergent from the tissue. The resulting kidney dECM was frozen at -80 °C until further processing.

*Preparation of Kidney Decellularized Extracellular Matrix Hydrogels.* Kidney dECM hydrogels were prepared as described previously in Chapter 2 and published elsewhere<sup>[288, 444]</sup> following previously described protocols for other dECM<sup>[317]</sup>. Briefly, frozen kidney dECM was lyophilized for two days using a Labconco FreeZone 6 Plus, snap frozen in liquid N<sub>2</sub>, and milled with a Thomas Wiley Mini-Mill Cutting Mill. Milled dECM was enzymatically digested at 10 mg/mL kidney dECM in 1 mg/mL pepsin (Sigma-Aldrich, #P7000) and 0.01 M HCl (Sigma-Aldrich, #H9892) for 48 h. The resulting pepsin digest was aliquoted and frozen at -80 °C. Aliquots were thawed overnight at 4 °C as needed for experiments. Hydrogel precursor polymer solutions were prepared by neutralizing the pepsin digest with one-hundredth the volume of 1.0 M NaOH (Sigma-Aldrich, #S2770), adding one-tenth of the total volume desired of 10× PBS (Mediatech, #46-013) to achieve a final concentration of 1×, and diluting the mixture with sterile MilliQ H<sub>2</sub>O. Hydrogels were formed after incubation of precursor polymer solutions at 37 °C for at least 1 h. Type I collagen hydrogels were prepared similarly from purified porcine type I atelo-collagen (Advanced BioMatrix, #5169-100ML).

*Preparation of Well Plates for Experimental Studies.* Well plates were coated with poly(2-hydroxyethylmethacrylate) [poly(2-HEMA)] at least one day prior to cell encapsulation within hydrogels to prevent cell attachment to well plate surfaces following established protocols<sup>[320, 321]</sup>. Briefly, poly(2-HEMA) (Sigma-Aldrich, #P3932) was dissolved in 95% (v/v) ethanol at a concentration of 30 mg/mL under constant stirring at 40-60 °C and then sterile filtered through a polyethersulfone mesh with a pore size of 0.22 μm (EMD Millipore, #SCGP00525). Sufficient volume of the poly(2-HEMA) solution was added to each well to cover the well surface, and the solution was allowed to evaporate overnight in a biosafety cabinet.

*Madin-Darby Canine Kidney (MDCK) Cell Culture and Encapsulation.* MDCK cells were maintained in a 1:1 mixture of Dulbecco's Modified Eagle Medium and Ham's F-12 (Gibco, #11320) supplemented with 10% fetal bovine serum (Gibco, #16000), and 1% penicillin-streptomycin (Gibco, #15140) at 37 °C and 5% CO<sub>2</sub>. Media was exchanged every two to three days, and cells were used at passage 27 for experimental studies. To prepare cells for encapsulation, cells were rinsed once with 1× Dulbecco's phosphate-buffered saline (DPBS, Mediatech, #21-030) and incubated with TrypLE Express (Gibco, #12605) at 37 °C for 10-

15 min. TrypLE Express was deactivated with excess cell culture media, and detached cells were collected and counted via the trypan blue exclusion method using Trypan Blue solution (Sigma-Aldrich, #T8154). Counted cells were aliquoted to obtain the necessary number of cells for encapsulation at the desired concentration of 1 million cells/mL. The cell suspension was centrifuged at 1100 RPM for 5 min, and pellets were resuspended in a minimal volume of complete media. Concentrated cell suspensions were added to hydrogel precursor polymer solutions, gently pipetted to mix, and cast into wells (200  $\mu\text{L}/\text{cm}^2$ ). Hydrogel precursor polymer solutions with cells were incubated at 37 °C for at least 1 h to ensure hydrogel formation and cell encapsulation before complete media was added to wells and plates were transferred to 37 °C and 5% CO<sub>2</sub>.

*Cell Viability Imaging.* Cell viability was evaluated using the LIVE/DEAD Assay Viability/Cytotoxicity Kit for Mammalian Cells (Invitrogen, #L3224) following the manufacturer's protocol. Briefly, samples were transferred to glass-bottom microwell dishes (MatTek, #P35G-1.0-14-C), rinsed once with DPBS, incubated with 4  $\mu\text{M}$  ethidium homodimer and 2  $\mu\text{M}$  calcein in DPBS for 30 min at 37 °C, and then rinsed once more with DPBS before imaging on a Nikon C2+ confocal microscope.

### **6.4.3. Results & Discussion**

MDCK cell viability appeared compromised the day after encapsulation regardless of the hydrogel protein or polymer concentration (**Figure 6-5**). However, the method of crosslinking and hydrogel formation for type I collagen and dECM hydrogel relies on physical interactions and the formation of collagen fibrils<sup>[325-327]</sup>, which is generally mild enough to enable cell encapsulation without detriment to cell health. Therefore, it is likely that cells were not handled with the proper care during preparation of the cells and encapsulation (e.g., cell passaging, mixing of cells with the hydrogel precursor polymer solution). At lower hydrogel concentrations, cell settling was more apparent by the presence of monolayer-like cell colonies. After one week in culture, formation of cysts was observed by the appearance of hollow, spherical structures in all samples with cysts appearing in greater numbers when encapsulated in kidney dECM hydrogels of higher concentrations in comparison to kidney dECM hydrogels of lower concentrations or collagen hydrogels (**Figure 6-5**). After two weeks in cultures, cyst structures persisted in all samples, although cysts in kidney

dECM hydrogels at 2.5 mg/mL appeared the greatest in size and number compared to other conditions (**Figure 6-5**). Note that the cell monolayer present in the sample image is likely a result of sample handling and transfer to the appropriate dish for imaging.

These results demonstrate that kidney dECM hydrogels enable cyst formation by encapsulated MDCK cells as collagen hydrogels do; however, additional investigations are necessary to further characterize these cyst-like structures, including evidence of apical-basal polarity and formation of a continuous basement membrane. Furthermore, from these initial studies, it does not appear that these kidney dECM hydrogels contain the necessary signaling factors (*i.e.*, hepatocyte growth factor<sup>[443]</sup>) to induce complex morphogenesis of branching structures. An interesting future investigation may be a comparison of morphogenesis by encapsulated MDCK cells within liver dECM hydrogels, which have been previously shown to support complex network formation by cholangiocytes or biliary epithelial cells<sup>[444, 445]</sup>. Beyond biochemical signaling cues, biophysical cues may also influence cell morphogenesis, and additional studies may explore the role of hydrogel stiffness in promoting or restricting cyst- and tubule-like structure formation by encapsulated MDCK cells independently of polymer or protein concentration by employing other crosslinking methods such as chemical crosslinkers<sup>[239]</sup>.

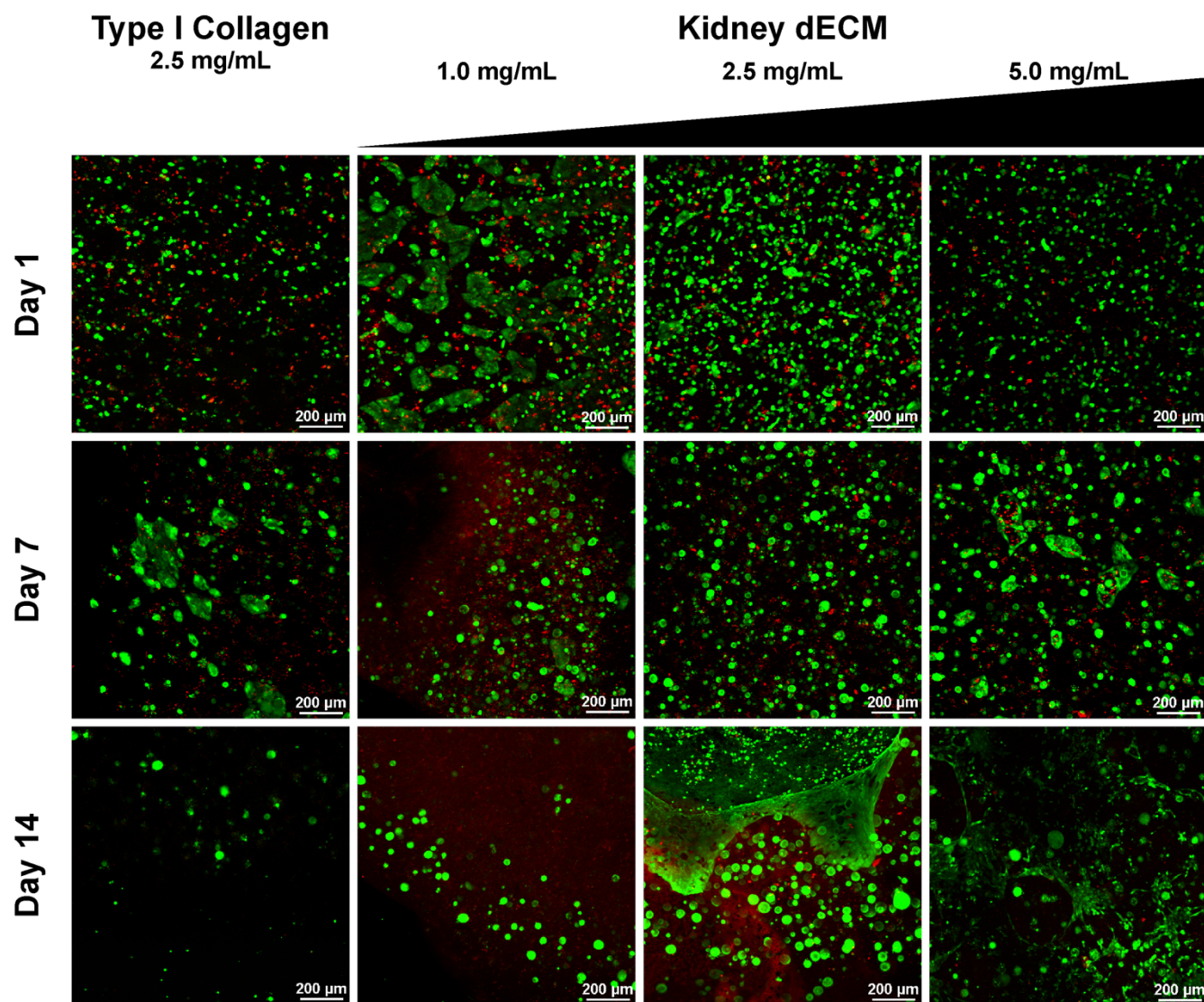


**Figure 6-5: Viability staining of MDCK cells encapsulated within type I collagen hydrogels or kidney dECM hydrogels of varying concentrations.**

Live (green) and dead (red) viability staining and confocal imaging of MDCK cells at indicated time points over a 14-day culture period.

## **6.5. Appendix E: Rheological Characterization of Various Tissue- and Organ-Specific**

### **Decellularized Extracellular Matrix Hydrogels**

In collaboration with other members of the Shah TEAM Laboratory: Emma S. Gargus, Adam E. Jakus, PhD, and Phillip L. Lewis, PhD, who provided the bovine ovary, porcine muscle, and porcine liver dECM digests, respectively.

#### **6.5.1. Introduction**

Decellularized extracellular matrix (dECM) derived from tissues and organs is thought to retain many of the biochemical signaling factors from the original tissue or organ, which will vary based on the source of the material<sup>[303]</sup>. Therefore, researchers continue to investigate these inherently bioactive and complex materials for tissue- or organ-specific applications. dECM may be processed into a variety of forms, but hydrogels in particular are versatile and suitable as platforms for cell culture or as injectable materials<sup>[264]</sup>. A variety of studies have been published detailing the development, characterization, and application of dECM hydrogels derived from different tissues and organs as well as different species<sup>[264]</sup>. However, methods of characterization vary from study to study, making direct comparisons amongst different dECM sources challenging. Here, we investigated the rheological properties of several different dECM hydrogels developed in the laboratory demonstrating unique tissue- and organ-specific characteristics despite similar processing and measuring procedures.

#### **6.5.2. Materials & Methods**

*Tissue and Organ Decellularization.* Porcine kidneys and livers were obtained fresh from female Yorkshire pigs (3-4 months in age) at Northwestern Simulation (Northwestern University Feinberg School of Medicine) following approval by the Northwestern Institutional Animal Care and Use Committee (IACUC). Porcine muscle was obtained from a local butcher's market (Chicago, IL). Bovine ovaries from young cows were collected from Aurora Packing Company (Aurora, IL). Tissues and organs were stored at -80 °C until decellularization. Prior to decellularization, tissues and organs were thawed for several hours in warm water and then cut into pieces approximately 0.5 × 0.5 × 0.25 cm in size with a clean razor blade. During this

process, excess fat was removed. Tissue pieces were then rinsed with deionized H<sub>2</sub>O under constant stirring for at least one day at room temperature or 4°C with intermittent H<sub>2</sub>O changes. After rinsing, kidney pieces were treated with 0.1% (m/v) sodium dodecyl sulfate (Sigma-Aldrich, #L3771) under constant stirring for at least two days. Afterwards, decellularized tissue pieces were rinsed with deionized H<sub>2</sub>O under constant stirring for at least one day with intermittent H<sub>2</sub>O changes to ensure removal of residual detergent from the tissue. The resulting tissue- and organ-specific dECM was frozen at -80 °C until further processing.

*Rat Kidney Recovery and Decellularization.* Rat kidney recovery and decellularization were performed as described previously<sup>[182, 440]</sup>. Kidneys were recovered from male Sprague Dawley rats (200-250 g) by the Northwestern University Comprehensive Transplant Center Microsurgery Core following guidelines approved by the Northwestern Institutional Animal Care and Use Committee (IACUC) as described previously. Rats were anesthetized using intraperitoneal injection of pentobarbital (50 mg/kg), and a longitudinal midline incision was performed to open the abdomen. The abdominal aorta and the inferior vena cava were dissected from above the right renal hilum to the iliac bifurcation, and the ureter was dissected at the urinary bladder. Two hundred units of heparin were injected through the penile vein. The abdominal aorta was ligated above the renal arteries, followed by cannulation of both infrarenal abdominal aorta with a 18G catheter (BD Biosciences, #381447). Both kidneys were perfused with cold saline through the infrarenal cannula. After perfusion, renal arteries and veins were transected and the kidneys were removed. Kidney renal arteries were cannulated with 24G catheters (BD Biosciences, #381412) and frozen in 1× Dulbecco's phosphate-buffered saline (DPBS, Corning, #21-030) and stored at -20 or -80 °C until decellularization. Rat kidneys were thawed and decellularized by sequential perfusion of the following solutions using a Cole-Parmer MasterFlex L/S peristaltic pump: 500 mL deionized H<sub>2</sub>O (1 mL/min), 1000 mL 1% (v/v) Triton X-100 (Amresco, #0694) in deionized H<sub>2</sub>O (5 mL/min), 1000 mL 1% (v/v) Triton X-100 in deionized H<sub>2</sub>O (1 mL/min), 1000 mL 0.1% (v/v) sodium dodecyl sulfate (Sigma-Aldrich, #05030) in deionized H<sub>2</sub>O (5 mL/min), and 500 mL deionized H<sub>2</sub>O (1 mL/min). Decellularized rat kidneys were frozen at -80 °C until further processing.

*Preparation of Decellularized Extracellular Matrix Hydrogels.* Hydrogels were prepared from dECM as described previously in Chapter 2 and published elsewhere<sup>[288, 444]</sup> following previously described

protocols for other dECM<sup>[317]</sup>. Briefly, frozen dECM was lyophilized for at least two days using a VirTis adVantage Plus EL-85, snap frozen in liquid N<sub>2</sub>, and milled with a Thomas Wiley Mini-Mill Cutting Mill. Milled dECM was enzymatically digested at 10 mg/mL dECM in 1 mg/mL pepsin (Sigma-Aldrich, #P7000) and 0.01 M HCl (Sigma-Aldrich, #H9892) for 48 h. The resulting pepsin digest was aliquoted and frozen at -80 °C. Aliquots were thawed overnight at 4 °C as needed for experiments. Hydrogel precursor polymer solutions were prepared by neutralizing the pepsin digest with one-hundredth the volume of 1.0 M NaOH (Sigma-Aldrich, #S2770), adding one-tenth of the total volume desired of 10× PBS (Mediatech, #46-013) to achieve a final concentration of 1×, and diluting the mixture with sterile MilliQ H<sub>2</sub>O to achieve the desired final concentration (5.0 mg/mL). Hydrogels were formed after incubation of precursor polymer solutions at 37 °C for at least 1 h.

*Rheology.* Rheological characterization was performed following a recommended protocol for hydrogels for tissue engineering applications<sup>[318]</sup>. Testing was performed using an Anton Paar MCR 302 with a 25-mm parallel-plate fixture under strain-controlled conditions. All samples were prepared fresh, and the lower Peltier cell was set to 4 °C for sample loading. After lowering the measuring system, mineral oil (Amresco, #J217) was applied to the edges of the sample and fixture, and the system was enclosed within a solvent trap to prevent sample dehydration. Time sweeps were performed for 120 min. at 37 °C, 0.1% strain, and 10 rad/s. Frequency and strain sweeps were performed immediately following under the same conditions. All sweeps were performed in triplicate ( $n = 3$ ). Data is presented as the mean  $\pm$  standard error of the mean.

### **6.5.3. Results & Discussion**

All dECM hydrogel formulations exhibited rapid gelation as demonstrated by the initial rise of shear storage moduli ( $G'$ ) above shear loss moduli ( $G''$ ) (**Figure 6-6**). All formulations also displayed relatively short times until stabilization of shear moduli as demonstrated by the onset of the plateau regions, typically within 10 min or less. Interestingly, equilibrium complex shear moduli ( $G$ ) and shear storage moduli, a gauge of hydrogel stiffness, varied amongst dECM sources. In order of decreasing stiffness: porcine kidney, bovine ovary, porcine liver, porcine kidney cortex, porcine muscle, and rat kidney. After hydrogel formation,

shear moduli of formulations were relatively independent of frequency, especially below 25 rad/s (**Figure 6-7**). Rat kidney dECM hydrogels were the exception in this case likely due to the extremely soft hydrogels formed relative to other formulations. Similarly, all formulations were relatively independent of strain with a linear viscoelastic region up to approximately 10% strain after which strain-stiffening followed by catastrophic failure occurred (**Figure 6-8**).

It is unsurprising that differences in rheological properties of the presented dECM hydrogels were observed. Although the various dECM was processed similarly in that the material was digested in pepsin, which cleaves telopeptide bonds and disrupts collagen fibril aggregates<sup>[325]</sup>, and hydrogel formation subsequently occurred by entropy-driven self-assembly of matrix components<sup>[325-327]</sup>, the exact biochemical compositions and the ratios of these components is unique to each. And it has been demonstrated by others that additional components such as proteoglycans and glycosaminoglycans alters the rate of self-assembly and network structure<sup>[327]</sup>. Even regional differences within the same organ (whole kidney versus kidney cortex) and species differences (porcine kidney versus rat kidney) result in significant differences in rheological properties likely due to differences in dECM composition. This alters the resulting dECM hydrogel stiffness and simultaneously the amount of strain-stiffening the hydrogel can undergo before rupture of the network.

The results presented here highlight the influence of material source on the resulting dECM hydrogel rheological properties. Future investigations may explore dECM hydrogels from other sources not explored here as well as the effects of different processing procedures on the resulting properties. In addition to rheological characterization, a number of additional studies are necessary to well-characterize dECM hydrogels in a manner that is comparable across multiple tissues and organs, species, and processing procedures. Examples include thorough biochemical characterization (such as quantitative mass spectrometry-based proteomics) and ultrastructural characterization and quantification. Ultimately these investigations will not only advance understanding of dECM hydrogel properties and applications but also encourage informed design of synthetic and natural-synthetic hydrogels as engineered extracellular matrix microenvironments.

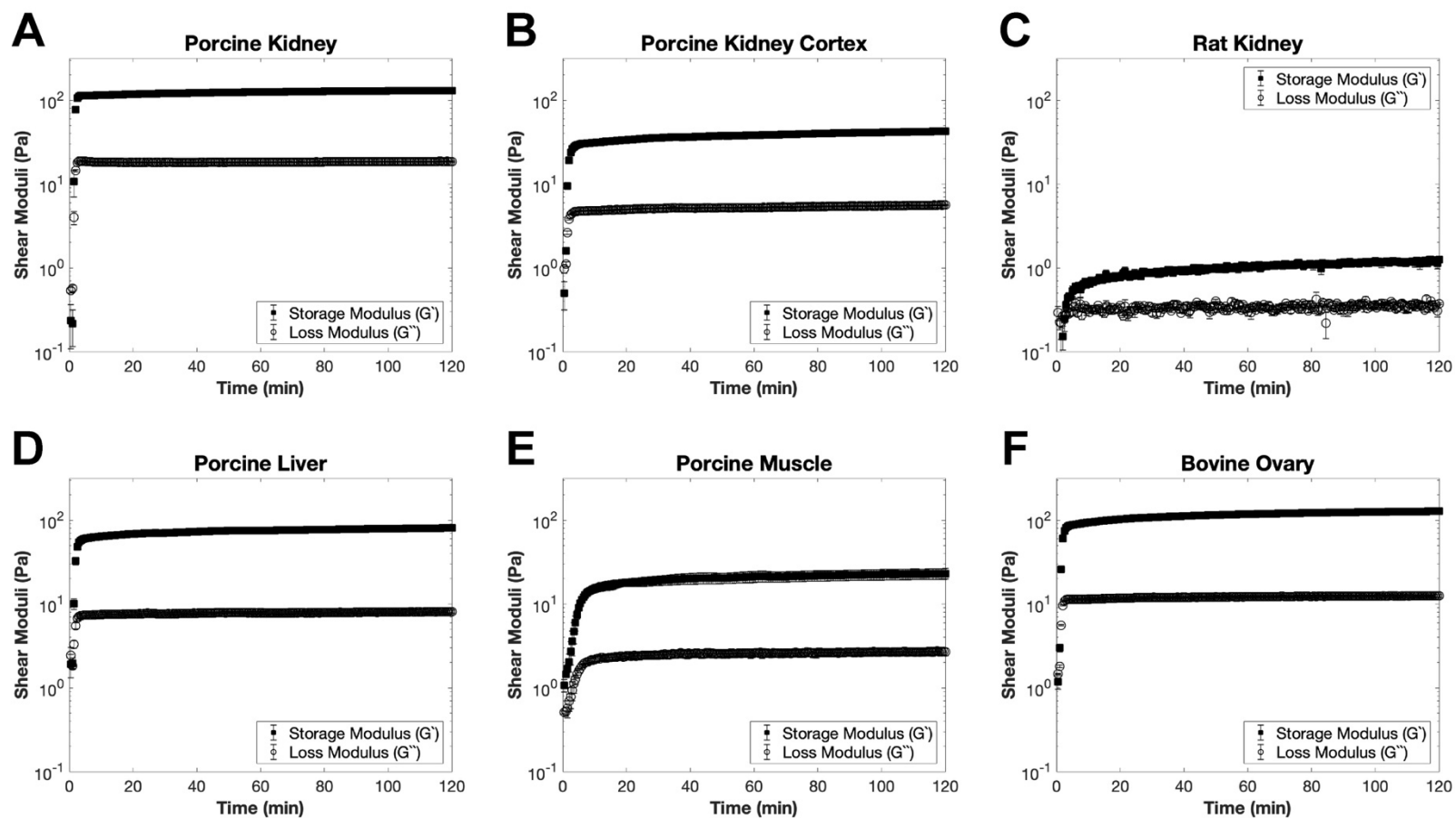


**Figure 6-6: Rheological time sweeps of tissue and organ dECM hydrogels.**

Rheological characterization of hydrogel formation over time with shear storage ( $G'$ ) and loss ( $G''$ ) moduli plotted on semi-log plots: (A) porcine kidney, (B) porcine kidney cortex, (C) rat kidney, (D) porcine liver, (E) porcine muscle, and (F) bovine ovary dECM hydrogels. All sweeps were performed in triplicate ( $n = 3$ ).

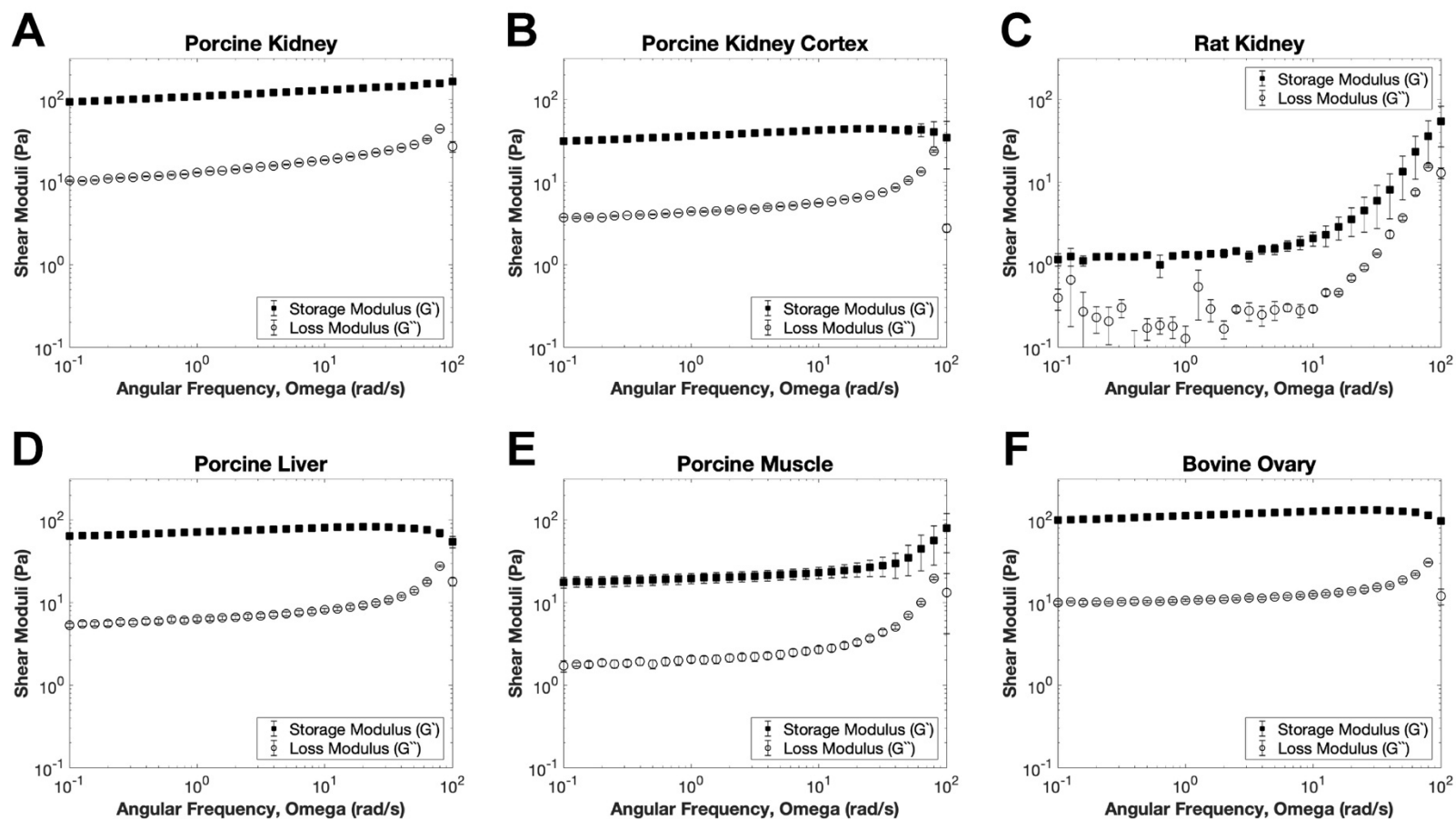


**Figure 6-7: Rheological frequency sweeps of tissue and organ dECM hydrogels.**

Shear storage ( $G'$ ) and loss ( $G''$ ) moduli plotted against angular frequency on log-log plots: (A) porcine kidney, (B) porcine kidney cortex, (C) rat kidney, (D) porcine liver, (E) porcine muscle, and (F) bovine ovary dECM hydrogels. All sweeps were performed in triplicate ( $n = 3$ ).

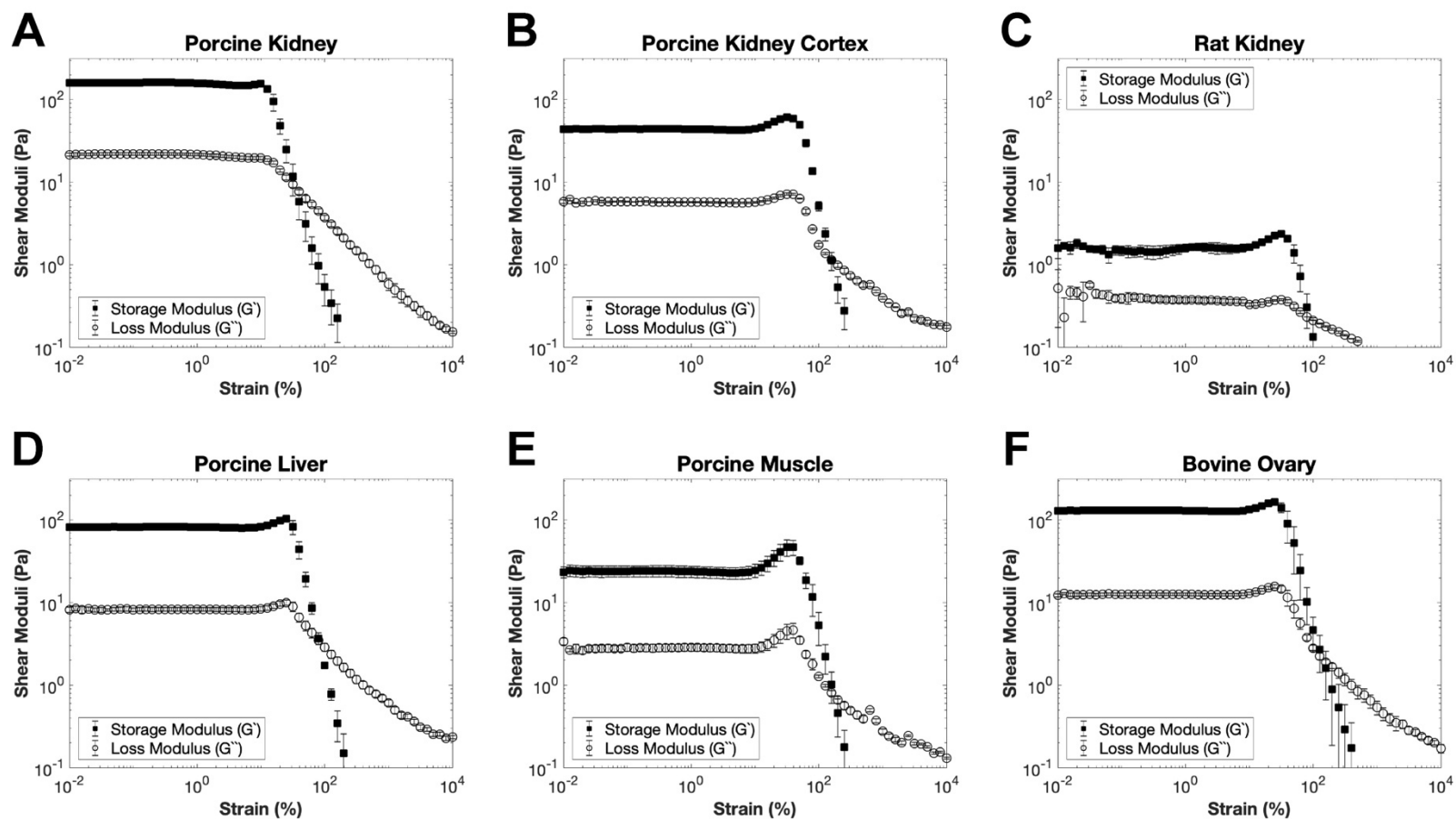


**Figure 6-8: Rheological strain or amplitude sweeps of tissue and organ dECM hydrogels.**

Shear storage ( $G'$ ) and loss ( $G''$ ) moduli plotted against strain on log-log plots: (A) porcine kidney, (B) porcine kidney cortex, (C) rat kidney, (D) porcine liver, (E) porcine muscle, and (F) bovine ovary dECM hydrogels. All sweeps were performed in triplicate ( $n = 3$ ).

**CURRICULUM VITAE**

**Jimmy Su**

Pronouns: he/him/his • [linkedin.com/in/JimmySu15](https://www.linkedin.com/in/JimmySu15)  
[JimmySu2020@u.northwestern.edu](mailto:JimmySu2020@u.northwestern.edu) • [Jimmy.Su15@gmail.com](mailto:Jimmy.Su15@gmail.com) • Cell: 848-459-3014  
 Current Mailing Address: 548 W. Briar Place • Apt. 3E • Chicago, IL 60657 • USA

**EDUCATION**

---

<b>Northwestern University</b> Doctor of Philosophy in Biomedical Engineering (Regenerative Medicine and Engineering) Certificate in Biotechnology	Evanston, IL September 2019
<b>Northwestern University</b> Master of Science in Biomedical Engineering (Regenerative Medicine and Engineering) Cumulative GPA: 3.89 / 4.00	Evanston, IL September 2017
<b>The Johns Hopkins University</b> Bachelor of Science in Biomedical Engineering (Cell and Tissue Engineering) Cumulative GPA: 3.95 / 4.00	Baltimore, MD December 2013

**CERTIFICATIONS**

---

<b>Machine Learning by Stanford University on Coursera</b> License Number: 6FLC3KHURVNW	March 2019
--	------------

**RESEARCH EXPERIENCE**

---

**Graduate Student Research Assistant at Northwestern University.**

Chicago, IL. January 2015 to August 2019.

Co-PI: Jason A. Wertheim, MD, PhD – Surgery (Organ Transplantation).

Co-PI: Ramille N. Shah, PhD – Materials Science & Engineering and Surgery.

- Engineered biomaterial hydrogels as platforms for cell culture (2D) and encapsulation (3D).
- Applied analytical and experimental methods to characterize hydrogel material properties.
- Investigated cell-material interactions through molecular biology techniques and assays to understand how material properties influence cell behavior towards engineering functional kidney tissues.
- Facilitated productive and multidisciplinary collaborations resulting in co-authored publications.

**Bioink Engineer Intern at CELLINK.**

Blacksburg, VA & Gothenburg, Sweden. June 2017 to August 2017.

Supervisors: Héctor Martínez, PhD – Chief Technology and Scientific Officer.

Patrick Thayer, PhD – Bioink Officer.

- Characterized rheological properties and printability of bioinks for 3D printing and bioprinting.
- Performed cell-based experiments to evaluate cell health and function in bioprinted constructs.
- Collaborated with sales and applications teams to facilitate more informed client interactions.

**Microfluidics Intern at Euveda Biosciences, Inc.**

Baltimore, MD. January 2014 to July 2014.

Supervisor: Zhizhong Yin, PhD – Chief Executive Officer.

- Designed and constructed microfluidic devices via photo- and soft lithography in the microfabrication laboratory.
- Collaborated with laboratories at Johns Hopkins Medicine for device and applications testing.

**Jimmy Su****Research Intern at the Lieber Institute for Brain Development.**

Baltimore, MD. January 2014 to July 2014.

PI: Thomas M. Hyde, MD, PhD – Basic Sciences Division and Chief Operating Officer.

- Assisted in expression vector testing for validation of alternative splice variant protein expression.
- Helped with genotyping and transcript analysis of apolipoprotein E isoforms in brain bank samples.

**Amgen Scholars Research Assistant at Columbia University.**

New York City, NY. May 2013 to August 2013.

PI: Jung-Chi Liao, PhD – Mechanical Engineering.

Performed immunofluorescence and stimulated emission depletion (STED) superresolution microscopy to investigate the molecular architecture of the primary ciliary transition zone.

**Undergraduate Research Assistant at the Johns Hopkins University.**

Baltimore, MD. October 2011 to October 2012.

PI: Sharon Gerecht, PhD – Chemical and Biomolecular Engineering, Institute for NanoBioTechnology.

Investigated differences in extracellular matrix deposited by breast cancer cells versus normal fibroblasts and how the extracellular matrix composition influenced the formation of vasculature by endothelial cells.

**Summer Undergraduate Research Assistant at Columbia University Medical Center.**

New York City, NY. June 2011 to August 2011.

PI: Timothy C. Wang, MD – Medicine (Gastroenterology), Irving Cancer Research Center.

Investigated the growth of pancreatic cancer cell lines, measured their invasiveness and tumorigenicity through various assays, and analyzed their response to the drug cisplatin.

**TEACHING EXPERIENCE****Quantitative Systems Physiology (BMD\_ENG 303/403) Teaching Assistant.**

Department of Biomedical Engineering, Northwestern University, Evanston IL.

April 2018 to June 2018.

Instructor: Robert A. Linsenmeier, PhD – Biomedical Engineering, Neurobiology, and Ophthalmology.

**Introduction to Programming for Scientists & Engineers (EN.600.112) Teaching Assistant.**

Department of Computer Science, The Johns Hopkins University, Baltimore, MD.

September 2013 to December 2013, July 2012 to December 2012.

Instructors: Joanne Selinski, PhD – Computer Science.

Peter H Fröhlich, PhD – Computer Science.

**FELLOWSHIPS****Ruth L. Kirschstein National Research Service Award (NRSA) Individual Predoctoral Fellowship (F31).**

National Institute of Diabetes and Digestive and Kidney Diseases (NIDDK),

Fed. Award ID No.: F31 DK108544.

September 2017 to August 2020.

“Microenvironmental Signaling Cues to Model Glomerular Endothelial Cell and Podocyte Interactions.”

**Predoectional Biotechnology Training Program (BTP) Trainee.**

Northwestern University. September 2015 to August 2017.

Funded by National Institute of General Medical Sciences (NIGMS),

Fed. Award ID No.: T32 GM008449.

**Walter P. Murphy Fellowship.** Northwestern University. September 2014 to December 2014.**GEM Ph.D. Associate Fellowship.**

The National GEM Consortium & Northwestern University. September 2014 to August 2019.

**Amgen Scholar.** Amgen Foundation & Columbia University/Barnard College. May 2013 to August 2013.

**Jimmy Su****Wake Forest Institute for Regenerative Medicine Summer Scholar (Declined).**

Wake Forest University School of Medicine. May 2013 to August 2013.

**John R. Laidig Memorial Engineering Scholarship.** Holmdel High School. June 2010.**HONORS & AWARDS**

---

**Scientific Images Contest, 5<sup>th</sup> Place.** Northwestern University Science in Society. December 11<sup>th</sup>, 2018.**Richard W. Jones Research Progress Award in Biomaterials and Regenerative Medicine.**Department of Biomedical Engineering, Northwestern University. May 17<sup>th</sup>, 2018.**Honorable Mention, National Science Foundation Graduate Research Fellowship Program.**

April 2015.

**Richard J. Johns Award for Outstanding Academic Achievement.**Department of Biomedical Engineering, the Johns Hopkins University. May 5<sup>th</sup>, 2014.**General and Departmental Honors.** The Johns Hopkins University. May 2014.**The Johns Hopkins University Freshman Essay Contest, 1<sup>st</sup> Place.** August 2010.**College Board AP Scholars with Distinction.** College Board. July 2010.**National Merit Finalist.** National Merit Scholarship Program. April 2010.**PUBLICATIONS**

---

- [7] **Su J**, Satchell SC, Wertheim JA, and Shah RN. "Poly(ethylene glycol)-crosslinked gelatin hydrogel substrates with conjugated bioactive peptides influence endothelial cell behavior." *Biomaterials* **102** (2019): 99-112. DOI: [10.1016/j.biomaterials.2019.02.001](https://doi.org/10.1016/j.biomaterials.2019.02.001)
- [6] Lewis PL, Yan M, **Su J**, and Shah RN. "Directing the growth and alignment of biliary epithelium within extracellular matrix hydrogels." *Acta Biomaterialia* **85** (2019): 84-93. DOI: [10.1016/j.actbio.2018.12.039](https://doi.org/10.1016/j.actbio.2018.12.039)
- [5] Lewis PL, **Su J**, Yan M, Meng F, Glaser SS, Alpini GD, Green RM, Sosa-Pineda B, and Shah RN. "Complex bile duct network formation within liver decellularized extracellular matrix hydrogels." *Scientific Reports* **8** (2018): 12220. DOI: [10.1038/s41598-018-30433-6](https://doi.org/10.1038/s41598-018-30433-6)
- [4] **Su J**, Satchell SC, Shah RN, and Wertheim JA. "Kidney decellularized extracellular matrix hydrogels: Rheological characterization and human glomerular endothelial cell response to encapsulation." *Journal of Biomedical Materials Research Part A* **106** (2018): 2448-2462. DOI: [10.1002/jbm.a.36439](https://doi.org/10.1002/jbm.a.36439)
- [3] Zhou J, **Su J**, Fu X, Zheng L, and Yin Z. "Microfluidic device for primary tumor spheroid isolation." *Experimental Hematology & Oncology* **6** (2017): 22. DOI: [10.1186/s40164-017-0084-3](https://doi.org/10.1186/s40164-017-0084-3)
- [2] Yang TT, **Su J**, Wang W-J, Craige B, Witman GB, Tsou M-FB, and Liao J-C. "Superresolution pattern recognition reveals the architectural map of the ciliary transition zone." *Scientific Reports* **5** (2015): 14096. DOI: [10.1038/srep14096](https://doi.org/10.1038/srep14096)
- [1] Uzarski JS, **Su J**, Xie Y, Zhang ZJ, Ward HH, Wandinger-Ness A, Miller WM, and Wertheim JA. "Epithelial cell repopulation and preparation of rodent extracellular matrix scaffolds for renal tissue development." *Journal of Visualized Experiments* **102** (2015): e53271. DOI: [10.3791/53271](https://doi.org/10.3791/53271)

**INTELLECTUAL PROPERTY**

---

- [1] Nguyen H, LeMoel J, Bhasin BJ, **Su J**, Hubbard R, Reeder S, and Ackley L. "System for Preventing Instrument Retention." U.S. Patent Application No. 14/889,323, filed 2016 December 22. U.S. Publication No. 2016/0371574 A1. PCT No. PCT/US2014/036973. International Application No. WO 2014/182701 A1, filed 2014 November 13.

**Jimmy Su****NATIONAL CONFERENCE ABSTRACTS & PRESENTATIONS**

- [5] **Su J**, Satchell SC, Wertheim JA, and Shah RN. "Poly(ethylene glycol)-crosslinked gelatin hydrogel substrates with conjugated bioactive peptides as a basement membrane mimic for endothelial cell culture." Conference Abstract: *Society for Biomaterials 2019 Annual Meeting & Exposition* (oral presentation). April 4<sup>th</sup>, 2019.
- [4] **Lewis PL**, **Su J**, Venter J, Meng F, Glaser S, Green RM, Alpini G, Sosa-Pineda B, and Shah RN. "In vitro formation of three-dimensional biliary trees within decellularized liver extracellular matrix hydrogels." *Gastroenterology* **154** (2018): S-1078-S-1079. Conference Abstract: *Digestive Disease Week* (oral presentation). June 3<sup>rd</sup>, 2018. DOI: [10.1016/S0016-5085\(18\)33594-7](https://doi.org/10.1016/S0016-5085(18)33594-7)
- [3] **Su J**, **Thayer P**, and Martínez H. "3D bioprinting of vascular networks and incorporation of growth factor mimetic peptides." Conference Abstract: *Biofabrication* (poster). October 17<sup>th</sup>, 2017.
- [2] **Su J**, **Thayer P**, and Martínez H. "Incorporation of growth factor mimetic peptides into GelMA bioinks." Conference Abstract: *Biomedical Engineering Society Annual Meeting* (poster). October 12<sup>th</sup>, 2017.
- [1] **Su J**, Wertheim JA, and Shah RN. "Renal extracellular matrix-derived hydrogels for cell culture." *Frontiers in Bioengineering and Biotechnology*. Conference Abstract: *10th World Biomaterials Congress* (oral presentation). May 22<sup>nd</sup>, 2016. DOI: [10.3389/conf.FBIOE.2016.01.00712](https://doi.org/10.3389/conf.FBIOE.2016.01.00712)

**SEMINARS & POSTER SESSIONS**

- [14] **Su J**, Satchell SC, Wertheim JA, and Shah RN. "Poly(ethylene glycol)-crosslinked gelatin hydrogel substrates with conjugated bioactive peptides as a basement membrane mimic for endothelial cell culture." *Northwestern University Biomedical Engineering Research Day* (poster presentation). Chicago, IL. May 17<sup>th</sup>, 2019.
- [13] **Su J**, Shah RN, and Wertheim JA. "Hydrogel substrates for modulating cell response towards the development of engineered kidney tissues." *Northwestern University Feinberg Cardiovascular and Renal Research Institute Research Project Updates* (oral presentation). Chicago, IL. April 15<sup>th</sup>, 2019.
- [12] **Su J**, Satchell SC, Wertheim JA, and Shah RN. "Poly(ethylene glycol)-crosslinked gelatin hydrogel substrates with conjugated bioactive peptides as a basement membrane mimic for endothelial cell culture." *Northwestern University Biomedical Career Development Forum* (poster presentation and flash talk). Evanston, IL. March 28<sup>th</sup> & 29<sup>th</sup>, 2019.
- [11] **Su J**, Satchell SC, Wertheim JA, and Shah RN. "Poly(ethylene glycol)-crosslinked gelatin hydrogel substrates with conjugated bioactive peptides as a basement membrane mimic for endothelial cell culture." *Northwestern University Collaborative in Transplant-Related Immunology and Biomedical Engineering Seminar* (oral presentation). Chicago, IL. December 19<sup>th</sup>, 2018.
- [10] **Su J**, Satchell SC, Wertheim JA, and Shah RN. "Hydrogel platforms for investigating kidney cell-material and cell-cell interactions." *Northwestern University Department of Biomedical Engineering Research Day* (oral presentation). May 17<sup>th</sup>, 2018.
- [9] **Su J**, Thayer P, and Martínez H. "My internship at CELLINK: Bioprinters and bioinks for 3D bioprinting." *Northwestern University Collaborative in Transplant-Related Immunology and Biomedical Engineering Seminar* (oral presentation). Chicago, IL. October 4<sup>th</sup>, 2017.
- [8] **Lewis PL**, Yan M, **Su J**, Alpini G, Green R, and Shah RN. "In vitro assembly of 3D bile duct networks within decellularized extracellular matrix hydrogels." *Micro Additive Manufacturing Smart Manufacturing Seminar Series* (oral presentation). Evanston, IL. October 3<sup>rd</sup>, 2017.
- [7] **Su J**, Shah RN, and Wertheim JA. "Investigating glomerular endothelial cell & podocyte interactions within 3D extracellular matrix microenvironments." *Northwestern University Department of Surgery Research Conference* (oral presentation). Chicago, IL. January 11<sup>th</sup>, 2017.
- [6] **Su J**, Shah RN, and Wertheim JA. "Investigating glomerular endothelial cell & podocyte interactions within 3D extracellular matrix microenvironments." *Northwestern University Collaborative in Transplant-Related Immunology and Biomedical Engineering Seminar* (oral presentation). Chicago, IL. November 2<sup>nd</sup>, 2016.

## Jimmy Su

- [5] Lewis PL, **Su J**, and Shah RN. "Towards 3D printing functional livers & kidneys." Rising Stars of SQI, Simpson Querrey Institute for BioNanotechnology, Northwestern University (poster). Chicago, IL. January 21<sup>st</sup>, 2016.
- [4] **Su J**, Shah RN, and Wertheim JA. "Engineering 3D culture environments to study podocyte & endothelial cell interactions." *Northwestern University Department of Surgery Research Conference* (oral presentation). Chicago, IL. March 22<sup>nd</sup>, 2016.
- [3] **Su J**, Yang TT, Wang W-J, Tsou M-FB, and Liao J-C. "Molecular architecture of the transition zone of primary cilia." *Amgen Scholars Program at Columbia University & Barnard College* (oral presentation). New York City, NY. July 30<sup>th</sup>, 2013.
- [2] Bhasin B, Hubbard R, LeMoel J, Reeder S, **Su J**, Kitchen G, Lam I, Mao A, and Nguyen HT. "Haptact: Preventing OR Sponge Retention." *The Johns Hopkins University Center for Bioengineering Innovation & Design Spring Design Day 2013* (poster). Baltimore, MD. May 7<sup>th</sup>, 2013.
- [1] Bhasin B, Hubbard R, LeMoel L, Reeder S, **Su J**, and Nguyen HT. "Instrument Tracking in the Operating Room." *The Johns Hopkins University Center for Bioengineering Innovation & Design Fall Design Day 2012* (poster). Baltimore, MD. December 11<sup>th</sup>, 2012.

### MENTORSHIP

**Melis Ozkan**, Maine South High School Student, Park Ridge, IL. August 2015 to May 2016.

Ozkan M, **Su J**, Wertheim JA, and Shah RN. "The effect of ECM concentration on the metabolic activity/estimated cell number and morphology of RCTE cells."

*Illinois Junior Academy of Science, Regionals and State Competitions – Gold Medalist.*

### SKILLS

**Molecular Biology:** Mammalian cell culture (2D and 3D, immortalized, primary, stem cells), histology, assay development (biochemical, cell-based), absorption and fluorescence spectroscopy, nucleic acid extraction and quantitation, polymerase chain reaction (PCR), quantitative real-time PCR (qPCR), immunofluorescence staining, fluorescence and confocal microscopy.

**Materials & Engineering:** Electron microscopy, oscillatory rheology, hydrogel synthesis and characterization, 3D printing and bioprinting, microfabrication (photolithography, soft lithography), microfluidics.

**Computers:** Experienced with PCs and Macintosh computers, Microsoft Office (Word, Excel, PowerPoint).

**Image Analysis & Design:** ImageJ, Adobe Illustrator and Photoshop.

**Coding & Engineering:** Python, MATLAB, computer-aided design (CAD), G-code.

### ACADEMIC EXTRACURRICULARS

**Graduates Mentoring Undergraduates (GMU)**, Executive Board Member.

Northwestern University, April 2017 to February 2018.

**Biomedical Engineering Graduate Students (BMEGS)**, Ambassador.

Northwestern University, October 2014 to October 2017.

**Chicago Graduate Students Association (CGSA)**, Student Life and Advocacy Representative.

Northwestern University, June 2015 to June 2016.

**Library Student Advisory Council**, Committee Member.

The Johns Hopkins University, October 2010 to December 2013.

### VOLUNTEER WORK

**QAAA Oral Histories Timecoding Volunteer.**

Queer Asian American Archive (QAAA), University of Illinois at Chicago.

August 2018 to August 2019.

**Jimmy Su****2018 SASE National Conference Volunteer,****Attendance Sub-Committee & SASEhack Event Volunteer.**

Society of Asian Scientists and Engineers (SASE). February 2018 to October 2018.  
Schaumburg, IL. Conference Dates: October 4<sup>th</sup>-6<sup>th</sup>, 2018.

**2017 7<sup>th</sup> Annual oSTEM Conference, Volunteer Panelist.**

Out in Science, Technology, Engineering, and Mathematics (oSTEM).

Dear White People: Intersection of Race/Ethnicity & LGBTQIA Identity Panel.

Chicago, IL. November 11<sup>th</sup>, 2017.

**2017 SASE National Conference & STEM Career Fair, SASEhack Event Volunteer.**

Society of Asian Scientists and Engineers (SASE).

Schaumburg, IL. October 14<sup>th</sup>-15<sup>th</sup>, 2017.

**2016 Northwestern University Biotechnology Day, Event Volunteer.** Evanston, IL. November 10<sup>th</sup>, 2016.**2016 Creating Change Conference, Conference Volunteer.**

National LGBTQ Task Force.

Chicago, IL. January 20<sup>th</sup>-24<sup>th</sup>, 2016.

**2015 National Queer Asian Pacific Islander Alliance Conference, Conference Volunteer.**

National Queer Asian Pacific Islander Conference (NQAPIA).

Chicago, IL. August 6<sup>th</sup>-8<sup>th</sup>, 2016.